Microstructural Evolution of a Multiphase Steel Microalloyed with Vanadium

By

Jorge Zuno-Silva

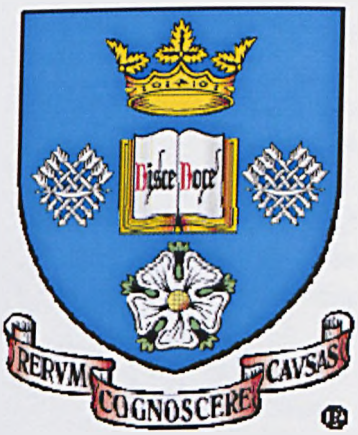

Thesis submitted for the degree of Doctor of Philosophy

Department of Engineering Materials

The University of Sheffield

February of 2009

Abstract

Multiphase steels have improved mechanical properties and enhanced ductility compared to conventional high strength steels and therefore have the potential for contributing to automotive mass reduction and crashworthiness requirements. The mechanical properties of multiphase steels are strongly dependent of the amount, size and morphology of retained austenite, bainite and martensite. The high work hardening and uniform deformation is a consequence of the Transformation Induced Plasticity (TRIP) effect of the retained austenite during straining. Further improvements in mechanical properties (>1000 MPa UTS) can be produced by precipitation, thus, vanadium additions are being considered. In this work a detailed study of the microstructural and complex precipitation evolution during the intercritical annealing of a multiphase steel microalloyed with vanadium was undertaken. Steels samples of a base composition and two vanadium (0.06% and 0.12%) microalloyed multiphase steels were supplied by Corus at the end of the commercial production route, from two different hot mill coiling temperatures. The microstructure of these five steels was examined in detail and compared to the tensile properties. The addition of vanadium increased the amount of austenite retained at the end of the process in an almost linear fashion. The lower coiling temperature (550°C) gave higher UTS than the higher coiling temperature (640°C), as expected. The expected tensile strength (UTS) increment was produced by vanadium additions but in all cases there was a reduction in ductility. The increase in UTS appeared to be mainly a result of grain size refinement, with some contribution from precipitation hardening in the 0.12%V steel, rather than the effect of the additional retained austenite content. A laboratory based simulation of the commercial intercritical anneal and bainite transformation was constructed, comprising 7 stages, including the intercritical anneal 795 °C (20 seconds), and an isothermal bainitic transformation at 460°C for 5 seconds. Steels identical to those produced by the commercial process, but in the hot and cold rolled condition were investigated. The vanadium carbide precipitation, transformation/dissolution and overall microstructural change at each stage of the annealing process were investigated. The majority of precipitation of VC occurred during hot coiling, with the lower coiling temperature leading to a smaller VC size distribution. The VC strongly controlled the rate of ferrite recrystallisation and final ferrite grain size on heating to the intercritical anneal following the cold rolling stage. Some further precipitation occurred during heating, but the extent was small compared to that which occurred on coiling. At the end of the intercritical anneal, the vanadium addition was found to have three main effects, namely, a reduction in microstructural scale, an increase in the retained austenite content and a reduction in the carbon content in the retained austenite. A subsequent intermediate cool resulted in a reduction in retained austenite for all materials, with this mainly resulting in transformation to martensite, but also bainite for the base alloy only. The isothermal bainite transformation resulted in bainite formation, but no enhancement of the carbon content in the remaining austenite. The amount of bainite decreased with increase in vanadium addition. The final total volume fraction second phases was similar for all materials, demonstrating that the vanadium addition had altered the proportion of phases only, namely increasing austenite content and decreasing bainite content. The final vanadium carbide size distribution was determined more by the vanadium content than the coiling temperature. The carbon content of the final austenite varied with vanadium addition in the same way as the commercial alloys. The principal role of the vanadium addition is discussed.

Acknowledgements

I would like to express my sincere gratitude to my supervisor Professor W. Mark Rainforth for his valuable guidance, support and encouragement throughout this thesis work.

I would like to acknowledge to the Mexican Government through the Consejo Nacional de Ciencia y Tecnologia (CONACyT) for financial support of this project. I would also like to thank to Corus – IJmuiden for the provision of the research materials.

Thank you to the technical staff of the Department of Engineering Materials: Dave Manvell, P. Staton, Dr Peter Korgul, C. Shields and in particular to Dr. Heath Bagshaw for his support and training in the microscopes.

I would like to thank to my parents Manuel Zuno and Guadalupe Silva and also to my fathers in law Guillermo Torres and Teresa Gonzales for their support and good wishes. I am speciality grateful with my wife Lety Torres and my little son Jethro Zuno for their patience, love and energy to conclude this thesis

I am very grateful with my excellent friends Axel Becerra and Mariela Pedraza for all their extraordinary support and for provide me all the necessary to complete my work and also my special grateful to my friend Catherine Grange for her help and professional dedication to review the english grammar of this work, thank you very much. Also thanks to my best friend Dr. Arnoldo Bedolla for his support and positive attitude. A personal thank to my friends Omar Jimenez and Oliver Hernandez who helped me with the EBSD on the Jeol 6400.

Also, thanks to my friends in office H6, Akemi, Amit, Vishwa and Sam who have made my time so pleasurable. Many thanks to Dr. Maria Magdalena for the help and assistance with the Sirion FEG-SEM microscope and for sharing hers experience. Also, thanks to Dr. Ruth Poths for her help and training with the TEM samples preparation. Thank you very much to Vanessa Dalton for her kind attention.

Contents

Nomenclature and abbreviations

γ	Austenite
α	Ferrite
µm	Microns
γ_r	Retained austenite
nm	nanometre
TRIP	Transformation induced plasticity
Ac_1	Austenite formation start temperature on heating (°C)
Ac_3	Austenite formation completion temperature on heating (°C)
A_{r3}	Transformation start temperature (°C)
M_S	Martensite-start temperature (°C)
M_F	Martensite-finish temperature (°C)
UTS	Ultimate tensile strength (MPa)
YS	Yield strength (MPa)
XRD	X-ray Diffraction
SEM	Scanning electron microscopy
TEM	Transmission Electron Microscopy
EELS	Electron Energy Loss Spectroscopy
EDS	Energy Dispersive X-ray Spectroscopy
h	Hour
T	Temperature (°C)
s	second
HSLA	High Strength Low Alloy steel
Wt %	Weight percent

DP	Dual phase steel
AHSS	Advanced high strength steels
T_R	Recrystallisation temperature (°C)
CCR	Conventional control rolling
P_z	Pinning pressure exerted by particles on unit area of the boundary
Fv	Volume fraction spherical particles of radius r
R	Radius of the matrix grains as sphere
γ	Specific energy of the boundary on the Zener pinning relationship
σ_y	Yield strength on the Hall - Petch relationship
$\bar{r}$	Ratio of strain in the width direction to that in the thickness direction during tensile plastic forming
CR	Cooling rate (Ks^{-1})
Vol.	Volume
n	Strain hardening exponent
El	Elongation (%)
$C\gamma_R$	Carbon content in retained austenite (%)
$V\gamma_R$	Volume fraction of retained austenite (%)
l	Long (mm)
w	Wide (mm)
t	Thickness (mm)
TMC	Thermomechanical compression
Å	Angstroms
V	Voltage
Kv	Kilo voltage
bcc	Body centre cubic

fcc	Face centre cubic
DP	Dual phase steel
pp	Precipitate
CT	Coiling temperature (°C)
FEGSEM	Field emission gun - scanning electron microscopy
MA	Martensite – austenite constituent
A_g	Uniform elongation (%)
R_m	Ultimate tensile strength (MPa)

List of Figures

Page

List of Tables

Page

Chapter 1 Introduction

The drive for increasingly high strength steels in the automotive industry is motivated through the need to decrease fuel consumption (and therefore to be more lightweight) but also to increase safety. Thin and stiff sections are needed to achieve a mass reduction in the car's structure but at the same time the crashworthiness (i.e. front barrier, front offset barrier, side impact, roof of crush and rear impact) requirements must be satisfied. Multiphase steels have the potential for a step forward in the production of light – weight car components with improved mechanical properties and enhanced ductility.

The extraordinary mechanical properties of multiphase steels over HSLA and Dual Phase steels arise from their complex microstructure which consists of a ferrite matrix (ductile phase), martensite (hard phase), bainite and dispersed grains of retained austenite. Austenite is metastable at room temperature at which the carbon content plays a key role in its stabilization. Furthermore, the martensite and the bainite transformation are influenced by the chemical composition and grain size of the retained austenite. The retained austenite transforms to martensite during straining as a consequence of the so-called TRIP (TRansformation Induced Plasticity) effect. Several research works have demonstrated that this phenomenon improves the balance between strength and ductility. Thus, it is desirable to retain considerable fractions of retained austenite. C – Si – Mn multiphase steels can achieve 800 MPa UTS, however, future developments will require higher strengths (>1000 MPa UTS and >20% elongation) than can be offered by conventional C-Si-Mn multiphase steel, and this will require the additional strength provided by precipitation. Niobium, titanium and vanadium have been successfully applied as microalloying additions in the HSLA steels. It is well known that vanadium is highly soluble in the austenite phase at lower temperatures than niobium and titanium.

However, vanadium is much less effective in refining grain size than Nb and Ti. While multiphase steels can be made to high strength in the laboratory, it is a completely different matter to reproduce these values in the plant, where the strength levels tend to be lower. Therefore, V additions are being considered to provide an additional increment in strength.

Initial processing of multiphase steels is by hot rolling followed by a cold reduction (typically ~50%) to provide the required surface finish and gauge tolerance. Following the cold roll, the steel is intercritically annealed, and then goes through a controlled cooling sequence to the isothermal bainite transformation region. The microstructure changes throughout this complex process. The hot roll coiling temperature determines the extent of precipitation prior to the intercritical anneal. Most of the current research on multiphase steels has been mainly focused on C – Si – Mn steels with limited investigation into microalloyed (Nb, V or Ti) multiphase steels, and particularly limited on the role of V additions.

The general aim of this research project was to study the microstructural and precipitation evolution during the intercritical annealing in the different stages of the process of a multiphase steel microalloyed with vanadium, in particular to know whether or not the vanadium content affects the microstructure transformation, compared to an equivalent base composition multiphase steel. The intercritical annealing process applied by Corus was adapted to the laboratory to simulate the conditions in plant. Samples of the base composition and two vanadium (0.06 wt. % and 0.12 wt. %) microalloyed multiphase steels were intercritically annealed at 795 °C in the $\alpha + \gamma$ area and held for a short time (20 seconds), followed by a controlled cooling to the isothermal bainitic transformation and cooling down to room temperature. Also a through-process route investigation was undertaken in order to understand the origins of the hot–rolled microstructure. The location and type of precipitates was determined using advanced electron optical techniques; in particular the exact composition and location of precipitate species were determined using TEM with associated electron energy loss spectroscopy (EELS). In addition, the composition of the residual austenite was determined as a function of thermal history.

The research work was conducted under the following specific objectives:

1. To study a vanadium microalloyed multiphase steel with V contents of 0.06 and 0.12 wt. %. Specifically, to quantify the microstructure in terms of ferrite, bainite, martensite and retained austenite as a function of V content and coiling temperature.

2. Following cold rolling, to understand the effect of restoration processes during the heating stage to the intercritical anneal. Determine the extent of precipitation during this heating stage.

3. Determine the extent of precipitate transformation/dissolution and solute re-distribution within the austenite during the intercritical anneal. To quantify the size and distribution of V-based precipitates as a function of thermal history.

4. Determine the austenite to ferrite re-transformation and bainite formation during subsequent cooling. Thereby, to correlate microstructure with tensile properties and make recommendations for process optimisation.

Chapter 2 Literature review

2.1 Advanced high strength steels (AHSS)

2.1.1 Introduction

Cars are mostly made of steel because it is the benchmark material for designing safe vehicles in high volume production. According to King [1] "Steel is a material with a unique, inherent capacity to absorb impact and thus diffuse crash energy". Steel can be engineered to collapse in a controlled manner. Steel also hardens when crushed, which means it becomes stronger on impact, allowing the steel to absorb more energy.

The initial challenge for advanced high strength steels was to make the popular midsize family car lighter and as comfortable and safe as larger cars. The early 1990s' vehicle was primarily composed of low carbon steel, which constituted about 78% of the vehicle, and high strength steels (forming just 22%). Nowadays the need to improve the lightweighting and crashworthiness, i.e. front barrier, front offset barrier, side impact, and roof of crush and rear impact has resulted in the use of high strength steels for 90% of the body mass and low carbon steels for the remaining 10% as can be seen in Figure 2.1 that shown the DP steel application [2, 7].

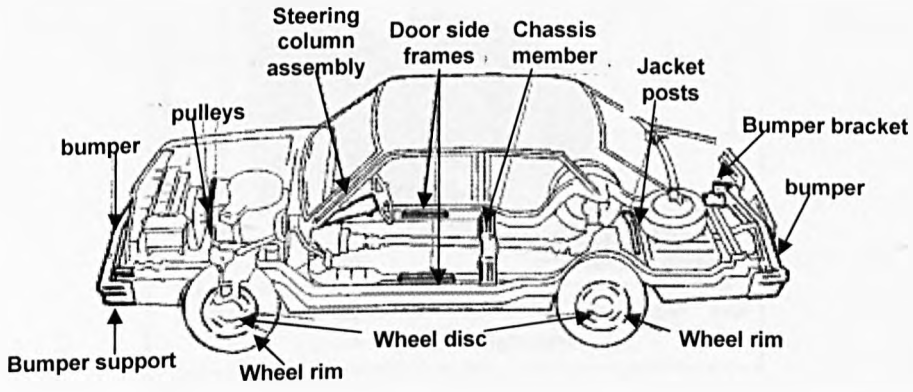

Figure 2.1 Automotive components formed with dual phase steels [7].

The carbon–manganese (C-Mn) and high strength low alloy (HSLA) steels are classified as conventional high strength (HSS) steels, see Figure 2.2. The chemical composition of the C-Mn steels is similar to that of low carbon mild steels, but the C-Mn steels have more carbon and manganese in order to increase the strength. This carbon increment is not practical for yield strengths higher than 350 MPa because there is a decrease in elongation and weldability [3, 4]. The HSLA steels have higher strength but generally lower ductility than the C-Mn steels. This family of steels usually has a ferritic microstructure of finer grain size that has been strengthened with carbides or carbonitrides formed by niobium, titanium or vanadium. Their lower formability is one of the drawbacks of these steels [3, 5].

Thin and stiff sections are required to achieve a weight reduction in the car's structure. In this context, advanced high strength steels (AHSS) have improved strength and enhanced formability, which allows for a reduction in the thickness of sheet steel. The dual phase (DP) steels, transformation induced plasticity (TRIP) steels, and martensitic steels are within the AHSS classification, Figure 2.2 [2].

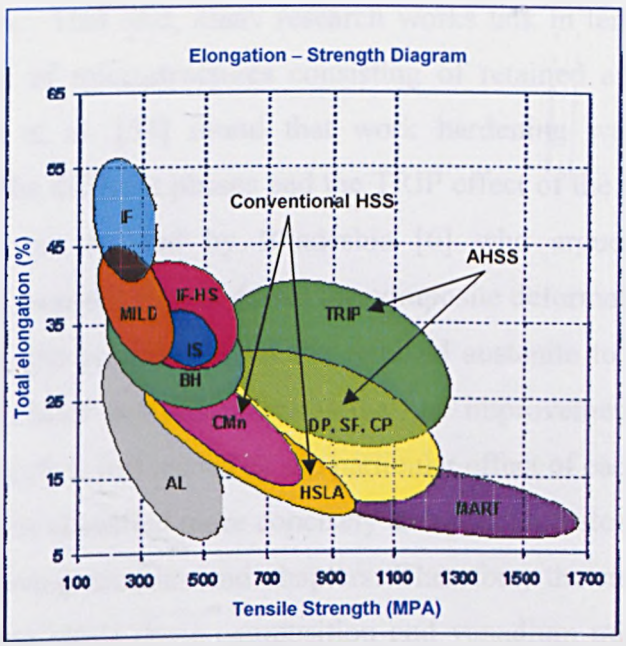

Fig. 2.2 Conventional high strength (HSS) and advanced high strength (AHSS) steels [2].

Martensitic steels have a microstructure comprised of only martensite. The car parts that can be manufactured using the martensitic steels are door intrusion beams, bumper reinforcement beams, side sill reinforcements, and belt line reinforcements [3]. Dual phase (DP) steels have a microstructure consisting mainly of soft ferrite, with grains of martensite spread in the ferritic matrix. The strength level of the dual phase steels is correlated to the amount of martensite in the microstructure [3]. Similar to the dual phase steels, the microstructure of the so-called transformation induced plasticity (TRIP) steels is based on a ferritic matrix. In addition to the martensite phase, TRIP steels have bainite and retained austenite, which enhance the strength and work-hardening respectively [3].

In reference to the "TRIP steels" denomination, it is important to make clear that a true TRIP steel is fully austenitic and that its chemical composition includes an expensive austenite stabiliser, such as nickel [47]. Some studies refer to these steels as "TRIP – assisted steels" because in the overall microstructure the retained austenite ranged between 5 and 10 %. That said, many research works talk in terms of "TRIP steels" despite their reports of microstructures consisting of retained austenite, bainite and martensite. Jacques et al. [54] found that work hardening was improved by the composite effect of the different phases and the TRIP effect of the retained austenite. A similar conclusion was reached by Bhadeshia [6] who argues that the uniform elongation of TRIP – assisted steel is due to the composite deformation behaviour of the major phases; where the contribution of the retained austenite to the total elongation was of 2.25 %. This brief analysis indicates that the improvement of the mechanical properties of these steels is influenced by the particular effect of each phase. Thus, these sorts of steels could be classified more concisely as multiphase steels and this term will be used in the following sections and chapters. Therefore, the materials used in this project are multiphase steels (base composition and vanadium microalloyed) because their microstructure consists of a ferritic matrix, retained austenite, bainite and martensite.

AHSS steels have the potential to reduce the costs of production. For instance, some car components consist of two or more pieces but the improved formability of the AHSS steels allows the manufacture of these components with just one piece even with complex shapes. The use of only one piece reduces the manufacturing costs, i.e. a reduced amount of parts signifies less welding and the weld flanges are eliminated (mass reduction) [3]. The higher strength brings with it better mechanical properties and crash performance, whilst keeping, or even reducing, thickness of sections. Thus, the manufacture of the elements used in the car's structure depends on the AHSS steel's ductility [3]. At the same time the ductility is linked to the work hardening behaviour during plastic straining, see Figure 2.3.

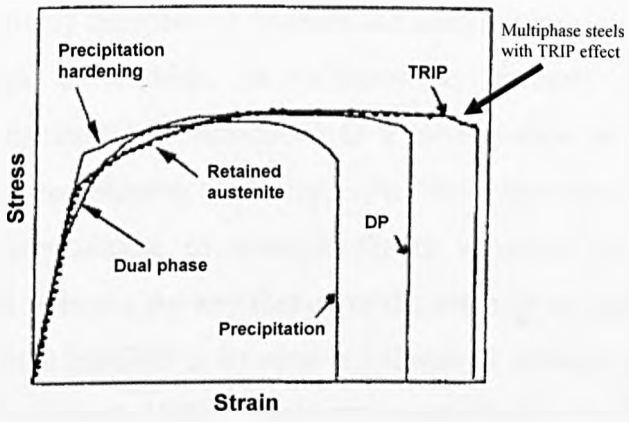

Fig. 2.3 Stress – strain curve for the HSLA, DP and multiphase steels [7].

The retained austenite in multiphase steels transforms into martensite during plastic straining. New dislocations are created and as a consequence the work-hardening is increased resulting in enhanced ductility [7]. In multiphase steels the high work hardening rates continue at higher plastic strains, whereas with dual phase (DP) steels, the work hardening rate decreases. However, ductility remains superior to conventional HSLA steels. Therefore, the work hardening rate is one of the main reasons for the enhanced formability of multiphase steels and to a lesser extent, DP steels over HSLA steels [3, 7]. The following sections provide details of the individual steels briefly introduced so far.

2.1.2 High strength low alloy steel (HSLA)

Sellars [8] classified High Strength Low Alloy (HSLA) steels as those containing niobium, titanium, vanadium, aluminium or a combination of any of these elements. The elements are added to form carbides or carbonitrides that inhibit recrystallisation of the austenite and result in fine ferrite grain sizes, which promote high strength. Cohen and Hansen [9] describe HSLA steels as a successful metallurgical innovation in which alloying additions and thermomechanical processing have been brought together effectively to attain improved combinations of engineering properties through microstructural control.

This practice is relatively inexpensive because the alloying elements are needed only in small concentrations as carbide, or carbonitride, formers and the associated thermomechanical processing is introduced as a modification of the final hot rolling operation. Although precipitation hardening with fine carbonitrides and sub-structural changes due to warm rolling of austenite/ferrite mixtures can contribute to the strengthening of HSLA steels, the key feature of the ultimate microstructure is the small ferritic grain size which provides a favourable balance of strength and toughness in the as-rolled steel. Microalloyed HSLA steels are successfully used as strip, plate, bar, structural section and forged bar products [10]; they find applications in several diverse fields such as in oil and gas pipelines, agricultural, and pressure vessel industries, as off-shore structures and platforms; and in the construction of cranes, bridges, ships, buildings, railroad tank cars, power transmission and TV towers. When the weight of an automobile is reduced by using HSLA steel in such parts as bumpers, bumper supports, motor mounts, door guard rails and suspension parts, additional mass can be saved because a lighter car will permit the use of lighter wheels, brakes and suspension system [11].

2.1.2.1 Controlled rolling of the HSLA steels

The purpose of the controlled-rolling operation in HSLA steels is to refine the relatively coarse, as-reheated austenitic microstructure by a series of high-temperature rolling/recrystallisation steps, and then to impose a heavy reduction in a temperature regime where austenite recrystallisation is inhibited between rolling passes (below the T_R temperature). This gives austenite grains that remain pancake-shaped and subsequent transformation after rolling to low temperature transformation products results in a fine grain size and associated improved mechanical properties [11]. The conventional controlled rolling (CCR) process involves the following five steps, as shown in a schematic temperature/time profile in Fig. 2.4 for the rolling of HSLA steel:

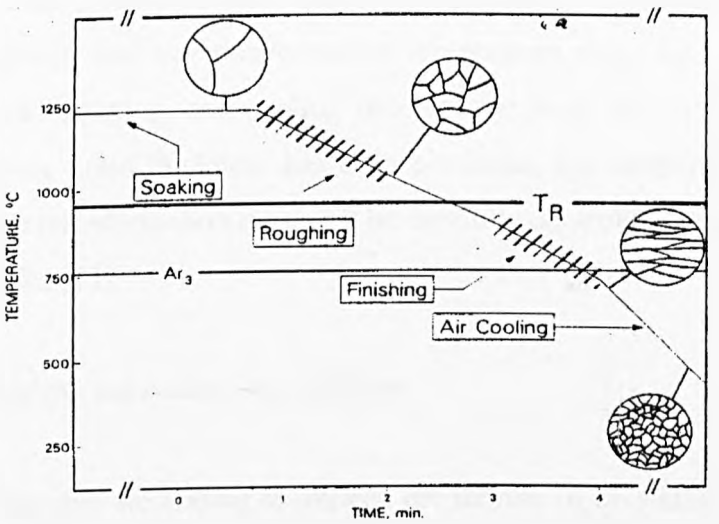

Fig. 2.4 Schematic temperature / time profile for controlled rolling [11].

1. Reheating the steel plate or slab to the austenitizing temperature and soaking it at this temperature to produce uniform γ grains.

2. A series of high temperature rolling (roughing) passes to continually refine the γ grains by sequential recrystallization (in the γ recrystallization temperature range).

3. A time delay during the processing is applied to the steel components to reduce the temperature to allow the strain-induced precipitation of e.g. NbC.

4. Incorporating a series of low temperature finish-rolling passes in the austenite non-recrystallization region to break–up and flatten (or pancake) the recrystallised γ grains, completed above or below Ar_3 temperature in the two phase austenite-ferrite region.

5. Finally controlled cooling to form ultra-fine ferrite grains from such deformed (pan-caked) γ - grains [11].

The subsequent transformation of the conditioned austenite into ferritic microstructures determines the final grain size and associated mechanical properties. The effects of austenitic morphology and the transformation-temperature range (as governed by alloy content, rolling deformation, and cooling rate) are the most important. Even after the minimum austenitic grain thickness has been produced, the temperature range of the austenite to-ferrite transformation must still be carefully controlled, thereby determining the reaction kinetics [11].

2.1.2.2 The role of the microalloying additions

Microalloying elements are known to impede the motion of crystalline defects such as grain boundaries, recrystallisation boundaries and dislocations when the microalloying elements are present either as solute (weak pinning) or as precipitate (strong pinning) [12]. Hence the microalloy elements can suppress grain coarsening, static recrystallization and the motion of dislocations. When they are in solid solution in austenite, these elements can also increase hardenability, therefore leading to lower transformation temperatures. The suppression of both grain coarsening and recrystallization contributes to the control of the austenite microstructure (i.e. conventional controlled rolling or recrystallisation).

The purpose of the addition of microalloy elements in steels is two fold:

(a) To produce precipitation strengthening and
(b) Grain refinement.

During controlled rolling, both of these phenomena are caused by the precipitation of extremely fine dispersion of very small and stable microalloy carbides (NbC, VC, TiC), nitrides (NbN, VN, TiN) and/or carbonitrides (NbCN, VCN, TiCN, (Nb,V)CN, (Nb,Ti)CN) [12].

The precipitation of these carbides or carbonitrides on low or high angle boundaries will delay recovery and recrystallisation; consequently dislocations will promote the heterogeneous nucleation of precipitates. The recrystallisation performance as a function of time and temperature is present in Figure 2.5. The temperature T_1 corresponds to the solvus temperature, above which no precipitation takes place and as a result, recrystallisation would start at times given by the line A-C. The curve B-D shows the commencement of recrystallisation with the existence of precipitated particles [13]. The dotted curves indicate the beginning of precipitation both in a deformed or un-deformed microstructure. The recrystallisation behaviour is expected to take place in accordance with the bold line A-B-D from which can be identified three stages [13].

Stage I. $T > T_1$
There is no precipitation, thus the recrystallisation behaviour is that of a solute-containing alloy.

Stage II. $T_1 > T > T_2$
Recrystallisation takes place before precipitation; therefore the recrystallisation is similar to stage I.

Stage III. $T < T_2$

Precipitation takes place before recrystallisation. The precipitated particles control the recovery rate. In due course recrystallisation may occur. Eventually, discontinuous precipitation may occur on mobile high angle grain boundaries [13].

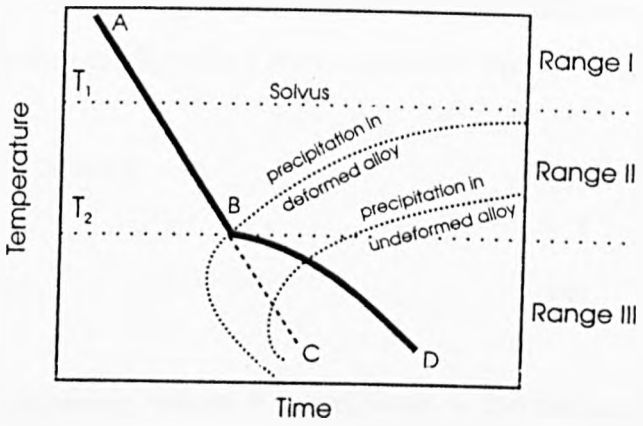

Fig. 2.5 Recrystallisation – precipitation – temperature – time diagram [13].

Gladman [14] proposed that the small precipitates interact with the grain boundaries because of the elimination of that part of the grain boundary that it is occupied by the particle. However, the exact origin of retardation of recrystallization is a subject of controversy, with various additional theories proposed, based on solute drag and precipitate pinning of dislocations and grain boundaries. The boundary will be pinned by the particle by Zener pinning:

$$P_z = 3 F_v \gamma / 2 r \qquad (1)$$

Where, P_z is the pinning pressure exerted by the particles on unit area of the boundary, F_v is the volume fraction of randomly distributed spherical particles of radius r and γ is the specific energy of the boundary [15]. On the other hand, considering the driving force for boundary movement and expressing this as the force per unit area, F, gives:

$$F = 2\gamma / R \qquad (2)$$

Where R is the radius of the matrix grains considered as sphere.

Thus, the pinning force, P_z, will be in opposition to the movement of the grain boundary; thus, if the pinning force, P_z is greater than the force boundary movement, the boundary will be pinned, but if the pinning force P_z is smaller than the force boundary movement, the grain boundary will be mobile. The equality between the pinning force P_z and the driving force for the boundary movement will provides the balance between pinning and boundary movement, this equality is given as follow [15]:

$$3 F_v \gamma / 2 r = 2\gamma / R \quad (3)$$

Or

$$R = 4r / 3F_v \quad (4)$$

This is the Zener relationship, where, R corresponds to the radius of the grains, r is the mean radius of the dispersed particles and F_v is the volume fraction of the spherical particles [15].

Cuddy [16] proposed that solute drag is important, since the temperature where the entire recrystallization stops during multipass deformation of microalloyed steels increases with an increase in the amount of solute present in the alloy at the start of deformation. He also observed that inhibition of recrystallization resulted from pinning by carbonitrides of size between 0.5 and 10 nm. Yamamoto et al. [17] mention that retardation of recovery and recrystallization can occur by two mechanisms: the pinning effect by strain-induced precipitates and the solute drag effect by solute atoms. These researchers concluded that Nb, V and Ti in solution retard recovery in deformed austenite and consequently delay the onset of recrystallization, but do not greatly influence the rate of recrystallization once initiated. Among the alloy elements, Nb has the strongest effect, Figure 2.6.

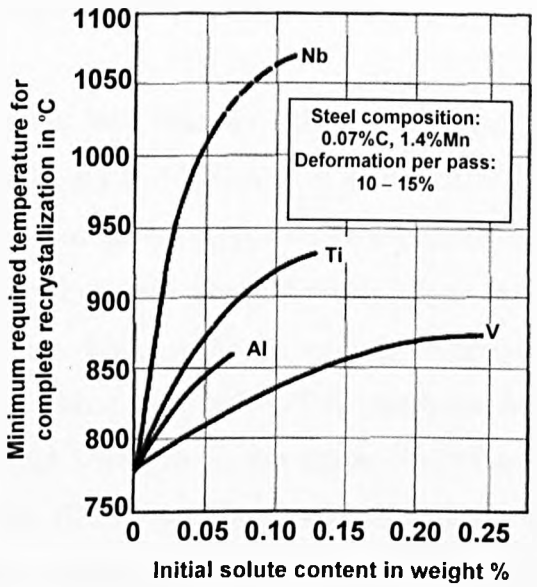

Fig. 2.6 Effect of the Nb, Ti, Al and V on recrystallisation [16].

Rainforth et al. [18] point out that the study of the formation of NbC in microalloyed steels is difficult, for instance, among other factors, the transformation of the austenite to ferrite and other low temperature transformation products removes the prior dislocation structure on which the precipitates had nucleated. Attempts to avoid changes to the precipitate distribution during cooling using a quench leads to the formation of martensite which obscures the location of the fine precipitates. In order to find one answer to this issue, they showed that the use of a Fe-30 Ni-0.1 C-0.1Nb microalloyed steel, precipitation occurs entirely on dislocations, present principally as microband walls but also as a rudimentary subgrain structure.

The role of microalloying elements in controlled plate steel is different from that in hot rolled strip steel. For example, in plate steel, Nb is employed to stop or significantly delay the recrystallization of γ in the early stage and allow further deformation to produce fine austenite 'pancakes' that transform to very fine ferrite grains. Therefore, lower reheat temperature is beneficial. In hot strip rolling, Nb is used to stop γ recrystallization late in the rolling process and to permit water cooling to produce very fine grains which can be precipitation strengthened at lower temperature by Nb after the steel has been coiled [12].

2.1.2.3 Mechanical properties of the HSLA steels

Typical stress-strain curves for C-Mn or mild steel, HSLA steel and Dual Phase steel in Fig. 2.7 show that yield strength of HSLA steel in the 350-700 MPa range is double that of C-Mn steel [10]. The mechanical properties of microalloyed HSLA steels result from several factors including fine grain size and precipitation, which depend in turn on the complex effects of alloy design and the rolling techniques. Grain refinement by austenite conditioning with controlled rolling methods has resulted in improved toughness and high yield strengths in the range of 345 to 620 MPa. Many of the proprietary microalloyed HSLA steels have carbon contents as low as 0.06% or even lower, but are still able to develop yield strengths of 485 MPa [12].

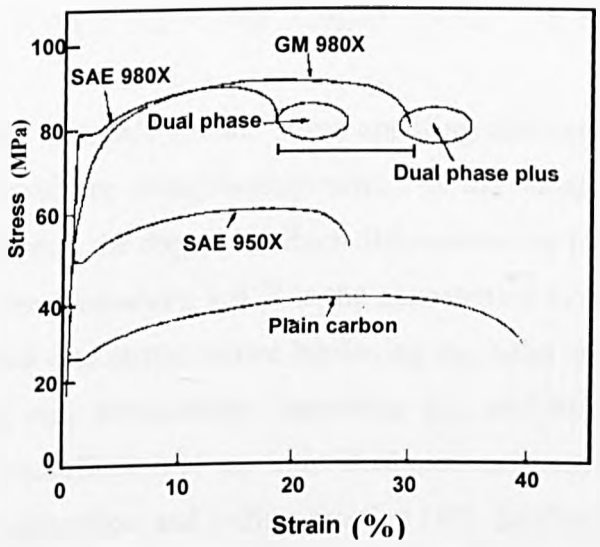

Fig. 2.7 Stress (MPa) – strain curve for plain carbon, HSLA (SAE 950X) and Dual Phase steels [10].

The microalloying influence the microstructure and hence the properties of steel through [19]:

a. Precipitation of carbonitrides

b. Solid solution

c. The removal of nitrogen from solid solution through the formation of nitrides

The major strengthening mechanisms in controlled microalloyed HSLA steels include: grain refinement; precipitation hardening by strain-enhanced inter-phase precipitation of microalloyed carbides and carbonitrides at semi-coherent and incoherent **γ/α** interfaces; solid solution strengthening from Mn, Si, and un-combined N; dislocation substructure (including dislocation tangles and cell walls) strengthening; and texture hardening. The observed lower yield stress of a polycrystalline controlled rolled microalloyed HSLA steel can be expressed by the following Hall - Petch relationship:

$$\sigma_y = \sigma_o + K_y d^{-1/2} \qquad (5)$$

The yield strength in these alloys can be expressed as [10]:

$$\sigma_y = (\sigma_{lh} + \sigma_{sh} + \sigma_{dh} + \sigma_{ph} + \sigma_{texh}) + Ck_s l^{-1/2} + K_y d^{-1/2} \qquad (6)$$

where σ_o is the internal or lattice friction stress opposing dislocation motion; $Ck_s l^{-1/2}$ is the sub-grain or substructure strengthening term, l is the subgrain diameter; k_y is a pinning constant measuring the degree to which dislocations are piled up at the barriers; d is the mean grain size (diameter); $k_y d^{-1/2}$ is the contribution to strength by the ferrite grain size σ_o is divided into terms: lattice hardening σ_{lh}, solid solution hardening σ_{sh}, dislocation hardening σ_{dh}, precipitation hardening σ_{ph}, and texture hardening σ_{texh}. However, the relative contribution of any individual mechanism presumably varies with the change in steel composition and rolling practice [10]. Studies have shown that the spring-back is greater as the strength of HSLA steel increases. This constitutes one of the major concerns in using HSLA steels in formed parts, especially in the automotive industry. HSLA steels of 550 MPa yield strength are thought to be unsuitable for automobile outer body panel applications because of inadequate formability and excessive spring-back that cannot be reduced sufficiently with die modifications. However, HSLA steels of 275 to 345 MPa yield strength have proved suitable in these body panels. Proper part and die design, combined with suitable material selection, can help to reduce the spring-back problem [11].

2.1.3 Dual phase steels

Dual phase (DP) steels, whose microstructure consists mainly of ferrite and martensite, are an excellent choice for applications where low yield strength, high tensile strength, continuous yielding and good uniform elongation are required [20]. Figure 2.1 shows the location in an automobile where they are used. DP is similar to microalloyed HSLA steels in that they have a fine grain size. However, the main strengthening mechanism in DP steels comes from the martensite (obtained from the transformed austenite) which acts as the load carrying element in a relatively soft ferrite matrix which provides the indispensable element of ductility [21]. Depending on the volume fraction of martensite in the microstructure, several grades of DP steels with different strength levels can be produced. DP steels containing 10 – 20% of martensite typically have an ultimate tensile strength of around 600 MPa, yield strength from 300 to 400 MPa, and a relatively high ductility (24 – 30 % of total elongation) [22].

Dual phase steels are conventionally produced by partial austenitization of low carbon steel within the ($\alpha + \gamma$) phase field, followed by accelerated cooling to transform the austenite to martensite. In addition to martensite, the resulting microstructures may consist of epitaxial ferrite, pearlite, bainite or retained austenite depending on cooling rates and intercritical annealing temperatures used [22].

2.1.3.1 Stress – strain curve

Mintz [7] compared the stress-strain curves for precipitation hardened, DP and multiphase steels, Figure 2.8. It can be seen that the DP steels, although having the lowest yield strengths, work harden very rapidly. However their $\bar{r}$ values (ratio of strain in the width direction to that in the thickness direction during tensile plastic forming) are poor and consequently deep drawability suffers. By contrast, multiphase steels have higher yield strengths but still exhibit greater elongations than DP steels and also have good deep drawability.

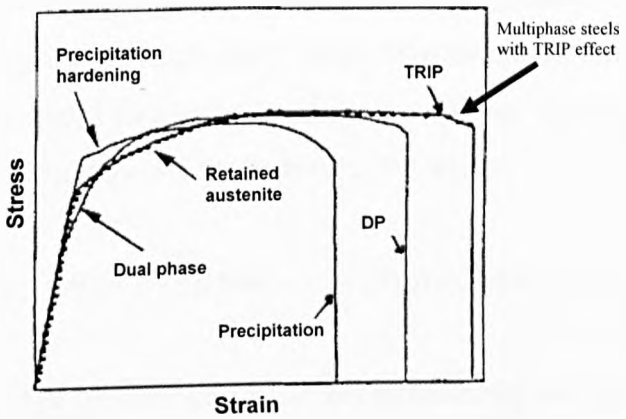

Fig. 2.8 Stress – strain curve for precipitation hardening, DP and multiphase steels [7].

In DP steels the transformation from γ to martensite during cooling causes pre-yielding in the adjacent ferrite grains, leading to continuous yielding in the stress strain curve. More importantly, this transformation results in rapid sustained work hardening; it is this feature that leads to high values of the work hardening exponent *n*, high elongations and excellent stretch formability. To obtain continuous yielding a minimum amount (>5%) of martensite is required. The largest elongations and highest *n* values often correspond to about 10-15% second phase (by volume), where the second phase includes retained austenite as well as martensite [7].

2.1.3.2 Martensite in Dual – Phase steels

It has been shown that the morphology (size, shape, and distribution) of martensite has a marked effect on the tensile fracture behaviour and ductility of DP steels; fine discontinuous, randomly orientated martensite particles in a continuous ferrite matrix giving optimum mechanical properties [7]. Martensite formation is favoured by higher alloying additions or higher cooling rates. The effect of alloying elements on the martensite start temperature M_s can be expressed as [20]:

$$M_s = 539 - 423(\%C) - 17.7\,(\%Ni) - 12.1(\%Cr) - 7.5\,(\%Mo) \qquad (7)$$

Carbon has the greatest effect on hardenability but the C addition required can be reduced by adding Ni, Cr, and Mo. Alternatively, alloying additions can be replaced by increasing the cooling rate through the $\gamma \rightarrow \alpha$ transformation temperature range [20]. Mintz [7] has also reported an equation which is useful for calculating the cooling rate (CR, Ks^{-1}) required to produce 5% martensite in DP steels:

$$Log_{10}(CR) = 4.93 - 1.7(\%Mn) - 1.34(\%Si) - 5.86(\%C) \quad (8)$$

After the C content, Mn has the greatest effect in reducing the cooling rate required to produce martensite and so is a favoured addition. Silicon accelerates the formation of polygonal ferrite and, in amounts of ~2%, promotes the fine fibrous distribution of martensite in a continuous ferrite matrix. Silicon also increases the activity of C in ferrite and may promote a more ductile ferrite [7].

Sun and Pugh [23] found that tensile strength and elongation of as-rolled DP steels depend not only on the martensite volume fraction and any work hardening but also on the morphology of the second phase or martensite. The as-rolled DP steel with long martensite 'fibres' has low ductility and high strength and the short martensite 'fibres' DP steel has the best combination of strength and ductility.

Similarly Bayran et al. [24] argues that the fine fibrous martensite is the reason for high ductility and continuous yielding. Continuous yielding in DP steels can be due to: (1) the transformation of austenite to the hard martensite, introducing a high density of mobile dislocations in the adjacent ferrite matrix; and (2) residual stresses from the martensite grains. Su and Gurlan [25] conclude that the apparent linearity of the yield strength variation with volume fraction of martensite is attributed to the dominant effect of martensite content on the microstructural spacings which control slip in ferrite. Jena and Chaturvedi [26] believe that the strength of martensite is primarily due to two factors. The structural contribution is from the fine substructure and is largely dependent of the carbon content.

The second contribution is due to the interactions between the dislocations and the strain fields of the interstitial carbon atoms. Martensite forms from high-temperature austenite and retains all the carbon which partitions to the austenite at the intercritical annealing temperature. Therefore, the variation of the carbon content of martensite caused by changes in the intercritical annealing temperature is the most important factor which controls the strength of martensite. However, other considerations (e.g. formability and weldability) mean that the carbon content is limited to ~0.1 wt. % maximum. The change in the carbon content alters solid-solution hardening, carbon rearrangement and work hardening. Carbon content also affects precipitation hardening which might take place during quenching.

2.1.3.3 Ferrite in Dual – Phase steels

The strength of ferrite in DP steel depends upon its grain size, substitutional and interstitial solute contents and dislocation density and morphology. It has been shown that the grain size of ferrite in a dual-phase structure is insensitive to the volume fraction of the second phase [26]. Changes in the solute content of ferrite caused by changes in the intercritical annealing temperature would have very little effect on the strength of ferrite. For example, interstitial solutes such as carbon have maximum effect on the strength of ferrite. The change in the carbon content of ferrite caused by variations in the intercritical annealing temperature is of the order of 0.01%. This has the effect of altering the strength of ferrite by only about 15 MPa.

The density and distribution of dislocations in ferrite present in DP structures are governed by the stresses associated with the martensitic transformation. Thus, changes in the strength of ferrite caused by changes in the intercritical annealing temperature could arise primarily from changes in the dislocation substructure. However, these changes in the strength of ferrite would be very small compared with those in the strength of martensite [26].

In agreement with this observation, Deb and Chaturvedi [27] reported that the partitioning of the alloying elements across the ferrite-austenite interface depends on the intercritical annealing temperature and also has an influence on the overall properties of the material. Such partitioning across the ferrite-austenite interface can result in a local inhomogeneity which may be responsible for the variation in micro-hardness within a ferrite grain. They concluded that overall improvement in mechanical properties is mainly attributed to the refinement of dynamically recrystallised ferrite grains, the change in number density of dislocations and the volume fraction of second-phase islands, nevertheless, the intricate interaction of these variables does not allow a quantitative evaluation of the contribution of each individual factor on the improvement of strength and ductility.

2.1.3.4 Annealing

Speich [28] pointed out that, in the continuous-annealing technique, the steel sheet is heated for a short time (~2 min) into the intercritical temperature range to form ferrite-austenite mixtures, followed by accelerated cooling (~10 °C/s) to transform the austenite phase into martensite. The actual cooling rate is dependent on sheet thickness and quench conditions. As a result, steel compositions must be adjusted to obtain the hardenability needed for the cooling rate (sheet thickness). For hot-rolled grades, thickness greater than 17.8 mm; 1.5Mn-Si-V or 1.2Mn-Si-Mo-Cr steels have been proposed. For thinner, cold-rolled grades, simpler 1.2Mn steels have been proposed. The carbon content of these steels is generally below 0.15 wt. % to be sure that the sheet steels are weldable. Rocha et al. [20] concluded that the volume fraction of phases present in the microstructure depend on the processing parameters, such as heating rate, soaking temperature, and soaking time, and the duration and slow cooling final temperature process. During heating to the annealing temperature, the austenite islands form at the completely recrystallised ferrite grain boundaries and at spherical cementite particles. During soaking and slow cooling, the microstructure becomes more homogeneous while the volume fraction of ferrite and carbides decrease.

2.1.3.5 Formation of austenite during intercritical annealing

Speich et al. [28] have shown that the formation of austenite during intercritical annealing can be separated into several steps: (1) almost instantaneous nucleation of austenite at pearlite or grain-boundary cementite particles, followed by very rapid growth of austenite until the carbide phase is dissolved; (2) slower growth of austenite into ferrite at a rate that is controlled by carbon diffusion in austenite at high temperatures (~850 °C) and by manganese diffusion in ferrite (or along grain boundaries) at low temperatures (~750 °C); and (3) a move towards equilibrium volume fractions and composition of ferrite and austenite at a rate that is controlled by manganese diffusion in austenite.

2.1.3.6 Transformation of austenite after intercritical annealing

The carbon content of the austenite is fixed by the time and temperature of the intercritical annealing; the hardenability of the austenite phase varies with intercritical temperature. Thus, at low temperatures where the carbon content of the austenite is high, the hardenability of the austenite is high. Similarly, at high temperatures where the carbon content of the austenite is low, the hardenability of the austenite is low and because ferrite already pre-exists, transformation of the austenite can proceed by epitaxial growth of this "old" ferrite into austenite with no nucleation step required [28].

The transformation of the austenite phase into martensite in DP steels occurs at low temperatures so that the ferrite phase must plastically deform to accommodate the volume expansion (~2 to 4%) arising from the austenite-to-martensite transformation. As a result, both a high dislocation density and residual stresses are generated in the ferrite phase immediately surrounding the martensite particle. The austenite - martensite transformation substructure in DP steels can vary from the lath martensite substructure, typical of low-carbon, to internally twinned substructures typical of high-carbon content.

These changes in morphology reflect the effect of intercritical annealing temperature on the carbon content of the austenite phase and in turn its effect on the M_s temperature [28]. As the transformation of the austenite phase to martensite is not complete, retained austenite is also generally present in dual-phase steels in amounts varying from 2 to 9%. The retained austenite is generally believed to be contained within the martensite particles [28].

2.1.3.7 Work hardening and yield behaviour

Ferrite-martensite steels, in general, do not show a yield point because the combination of high residual stresses and a high mobile dislocation density causes plastic flow to occur easily at low plastic strains as shown in Figure 2.6. Because plastic flow begins simultaneously at many sites throughout the specimen, discontinuous yielding is suppressed. Hansen and Pradhan [29] identified the factors required for continuous yielding which included a sufficiently fast cooling to ensure that the austenite-to-martensite transformation produces a high dislocation density in the ferrite phase. The lack of yield point in these steels eliminates Lüders band formation and assures a good surface finish after drawing [28].

The work-hardening processes in DP steels are complex but can be separated into three stages. In the first stage (strain of 0.1 to 0.5%), rapid work hardening is present because of the elimination of residual stresses and the rapid buildup of back stresses in the ferrite caused by the plastic incompatibility of the two phases, martensite and ferrite. The work-hardening behaviour of DP steels is complex in these initial stages. However, the higher initial work-hardening rate is believed to contribute to the good formability of these steels. In the second stage (strain of 0.5 to 4%), the work-hardening rate of the ferrite is reduced as the plastic flow of the ferrite is constrained by the hard, un-deforming martensite particles and transformation of retained austenite may also occur during this stage. Finally, in the third stage (strain of 4 to 18%), dislocation cell structures are formed and further deformation in the ferrite is governed by dynamic recovery and cross slip and eventual yielding of the martensite phase [28].

2.1.3.8 Effect of alloying elements

Fallahi [30] reported the role of important alloying elements on the dual phase structure and properties are as follows:

Carbon is necessary in amounts greater than 0.04 wt. % in order to secure the strength of steel and to form martensite. Good ductility and toughness requires an initial C content of about 0.1 wt. % or less so that the carbon content of the final ferrite and martensite phases can be controlled. For strong tough martensite it is about ~ 0.3-0.4 wt. % C depending on the total alloy content.

Silicon promotes the ferrite transformation and enriches C in γ enhancing martensite transformation. It reduces the solubility of carbon and hence promotes ductility of ferrite. It inhibits carbide formation, particularly Fe_3C at the ferrite – martensite interface and increases the slope of the A_3 line, thus allowing more flexibility in heat treatment. Silicon also raises transformation temperature, refines microstructure, and may also contribute to solid solution strengthening.

Manganese is required in quantities greater than 0.6 wt. % in order to enhance the stability of austenite and to finally form at least 5 wt % martensite. However, when more than 1.8 wt. % of Mn is used, the ferrite transformation is suppressed and the bainite transformation is promoted, and hence it is difficult to finally form at least 70% ferrite and obtain a value not higher than 0.7 of the ratio for the (YS / UTS), and therefore Mn% is limited to 0.6-1.8 wt. %.

Phosphorus is an important element when the cooling rate is high (C.R. > 50 °C/s) to form at least 70% ferrite and allow YS / UTS < 0.70. It has been reported that at least 0.04 wt. % P is necessary to avoid a large amount of bainite being formed. However, the upper limit of P must be 0.2 wt. % because of brittle fracture on forming and (YS / UTS) > 0.70 due to excessive ferrite strengthening.

Chromium stabilizes ferrite to increase hardenability and it increases connectivity of martensite. Chromium decreases the dissolved C content in ferrite by promoting the C partitioning between austenite and ferrite, so improves ductility of ferrite and hardenability of austenite. Chromium also depresses ferrite and pearlite formation, promoting granular and high C martensite. The ratio of the maximum to minimum acceptable cooling rates increases from (CR max / CR min) = 10 to16 for 0.5 wt. % Cr.

Molybdenum increases the slope of the A_3 line, allowing more flexibility in heat treatment. It increases hardenability and the pearlite reaction is delayed much more strongly than the polygonal ferrite reaction (the pearlite nose shifts markedly to the right).

Aluminium is used as a deoxidant, requiring at least 0.01 wt. % Al, but more than 0.1 wt. % Al results in an increases of inclusion content, and is not desirable. The influence of Al is similar to that of Si, with Al forming AlN in ferrite in the presence of nitrogen.

Sulphur in quantities greater than 0.008 wt. % results in very poor formability due to the development of elongated inclusions of MnS during hot rolling.

These additional alloying elements may lead to more complex effects on austenite formation than previously discussed. For instance, vanadium and niobium interact strongly with carbon and nitrogen to form a fine dispersion of VCN or NbCN. Upon intercritical annealing this dispersion may be dissolved as the austenite phase grows into the ferrite. Also, silicon widens the $\alpha + \gamma$ phase field and permits a wider range of intercritical temperatures to be used.

2.1.4 Multiphase steels

2.1.4.1 Introduction

As was previously analysed in the section of advanced high strength steels (AHSS) of Chapter 2, the multiphase steels are those whose microstructure consist of a ferritic matrix having bainite, martensite and important amounts (5 -10%) of retained austenite. The multiphase microstructure is formed through the use of an intercritical anneal and subsequent isothermal annealing in the bainitic transformation region, called austempering [31].

Multiphase steels have the potential for a step forward in the production of low mass car components with improved mechanical properties [32]. The varying contents of bainite, martensite and retained austenite affect the multiphase steels balance between strength and ductility. The formability of multiphase steels is superior to conventional high strength steels such as HSLA steels allowing automotive engineers more freedom in part design to optimize weight and structural performance [33]. Retained austenite is responsible for the high work hardening and uniform deformation as a consequence of the "TRIP" effect during the straining. This combination of strength and formability has potential application in the automotive industry, especially for the manufacture of crash parts such as side impact protection and bumpers and also in structural parts i.e. reinforcements or cross members [34]. Most of the current literature reports the relationship between mechanical properties and microstructure in terms of the volume fraction of the retained austenite as reported by Mintz [7] in Table 2.1, for different multiphase steels compositions. Bhadeshia [6] on his work argue that multiphase steels with a chemical composition of Fe – 0.15C – 1.5Mn – 1.5Si wt %, the final microstructure contains 20 % bainitic ferrite with 10 % retained austenite in a ferritic matrix, however, mechanical properties are not reported.

Table 2.1 Composition, mechanical properties and retained austenite content of cold reduced and intercritically annealed multiphase steels.

	Chemical composition (wt %)							
Steel	C	Mn	Si	Al	Nb	γ_R vol. %	YS (MPa)	TS (MPa)
1	0.28	1.50	1.41	0.66	---	16	489	813
2	0.19	1.42	0.55	0.92	---	21	421	620
3	0.12	1.50	1.10	0.40	---	15	460	645
4	0.20	1.49	----	1.99	---	11	363	658
5	0.16	1.30	0.40	---	0.01	8	365	810

Wasilkowska et al. [39] argue that the correlations between processing parameters, chemical composition, microstructure and mechanical properties of multiphase steels imply to deal with the complexity of the microstructure (variability of morphology, size and composition). In addition the structural phases surrounding retained austenite can decisively contribute to its stability.

2.1.4.2 Transformation – induced plasticity (TRIP) concept and multiphase steels classification

The transformation – induced plasticity (TRIP) phenomenon has significantly improved the strength of C-Mn-Si steels while retaining the ductility required for forming automotive body. The term transformation – induced plasticity (TRIP) is attributed to Zackay et al. [35] who developed high alloy steels that remained fully austenitic at room temperature. The elongation was substantially improved due to the deformation-induced austenite to martensite transformation. In the 1980s the TRIP effect was demonstrated in low alloy steels (0.2C, 1-2Mn, and 1-2Si (wt %)). "TRIP-assisted multiphase steels" are hereafter referred to as “multiphase steels” due to the small volume fractions of other phases namely bainite and martensite as well as the retained austenite in a ferrite-matrix.

This denomination was made with the aim to distinguish the TRIP-assisted multiphase steels from the fully austenitic TRIP steels [36]. Despite observation that Dual Phase steels regularly contain noticeable quantities of retained austenite and may give a small TRIP-like effect, the multiphase steels classification is properly applied to steels where the heat treatment cycle is constructed to deliberately retain a fraction of austenite in sufficient quantity that its presence can be seen in the flow curves from tensile tests [37].

2.1.4.3 Intercritical annealing process

The microstructure of multiphase steels (ferrite, bainite and retained austenite) is primarily obtained through an intercritical annealing and a subsequent isothermal annealing in the bainitic region, also called austempering. The intercritical annealing process of cold rolled multiphase steels generally consists of five stages. However, the current literature has been studied in the different stages because of the complexity of the phase transformations that occurs in each one of the five stages [38]. These five stages are described below and Figure 2.9 shows the thermomechanical schedule for the multiphase steels:

Stage 1 - Fast heating

The changes produced on the cold rolled microstructure are the partial ferrite recrystallisation and the beginning of the pearlite dissolution.

Stage 2 - Intercritical annealing region

Once the temperature is above of the A_1 temperature, the austenite starts to form. This first austenite formed has more carbon than the equilibrium carbon content of austenite in the intercritical range. However, even for small annealing times, the carbon partitions between the ferrite and austenite.

Stage 3 - Fast cooling

Rapid cooling is applied from the annealing temperature to the isothermal bainitic transformation also called austempering. This fast cooling produces the so called "new" ferrite which grows from the existing intercritical ferrite.

Stage 4 – Isothermal bainitic transformation (austempering)

This stage is governed by the bainite transformation but is the most critical stage for the austenite retention, which depends on its carbon content, volume fraction and grain size.

Stage 5 - Final cooling

After the bainitic transformation the multiphase steel is relatively slow cooled or goes to the hot dip galvanising stage. At this point some of the retained austenite transform to martensite which often happens to the Si-free multiphase steels due to their high Al content [38].

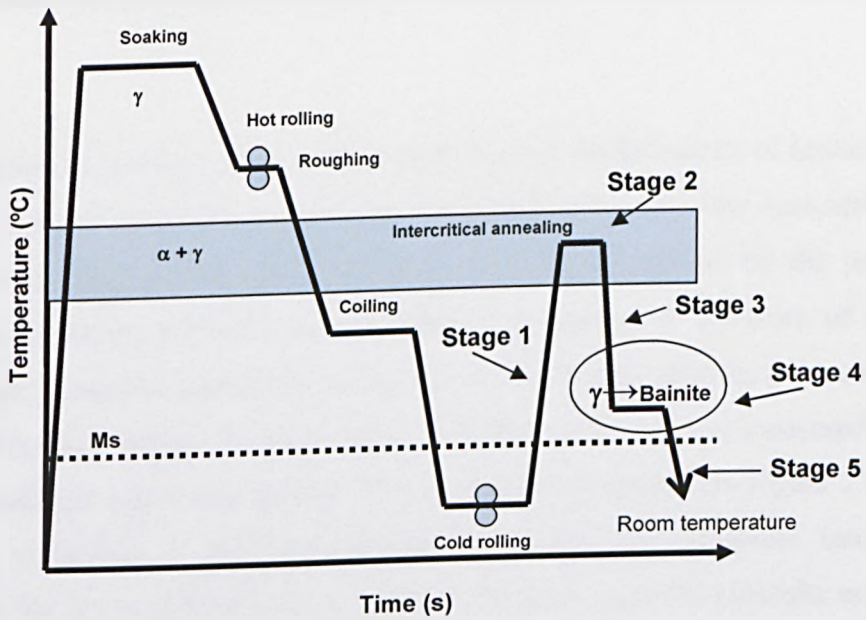

Fig. 2.9 Conventional thermomechanical process for the multiphase steels.

2.1.4.3.1 Microstructure in cold rolled multiphase steels

In the cold rolled condition the microstructure consists of ferrite, pearlite and possibly some traces of martensite. Wasilkowska et al. [39] employed a TRIP-assisted-700 multiphase steel. The cold rolled microstructure before the intercritical annealing consisted of ferrite + cementite.

In a similar way, Saleh and Priestner [40] report that the cold rolled microstructure steel used in their work was composed of ferrite and dispersed carbide located within ferrite grains, and in elongated ferrite grain boundaries. The material processing was as follows: a cast ingot of 80 – 120 mm length, 15 mm thickness and 75 mm width was hot rolled at 1150 °C to reduce its thickness from 15 to 11 mm and after this, the steel was cold rolled to a final thickness of 5 mm which was produced in 13 passes. However, the previous grain size of the phases and its content are not reported.

2.1.4.3.2 Austenite formation during heating and the initial stages of intercritical anneal

The dissolution of pearlite, other carbide particles and the formation of austenite occurs in the first stage of intercritical annealing. The transformation of the austenite from the pearlite is controlled mainly by C diffusion and may be slowed by the presence of substitutional alloying elements such as Mn [7]. According to the work of Jeong and Kim [41] the austenite formation during the intercritically annealing process can be separated into four stages in accordance with the trends of the measured hardness values of austenite and ferrite phases. This correlation is plotted in Figure 2.10, which shows the variations of the microhardness of ferrite and austenite intercritically annealed at 780 °C for different times where at the final stage the austenite content was of 26 %. The austenite content evolution is also presented.

Stage 1.- When the steel is heated to just above the transformation temperature A_1, pearlite dissolution occurs slowly, but a small increase in temperature can cause a marked increase in the dissolution rate [6]. When the cementite starts dissolving, the carbon diffuses into the growing austenite. As a result, the growth rate of austenite is controlled by the rate of carbon diffusion in austenite [41].

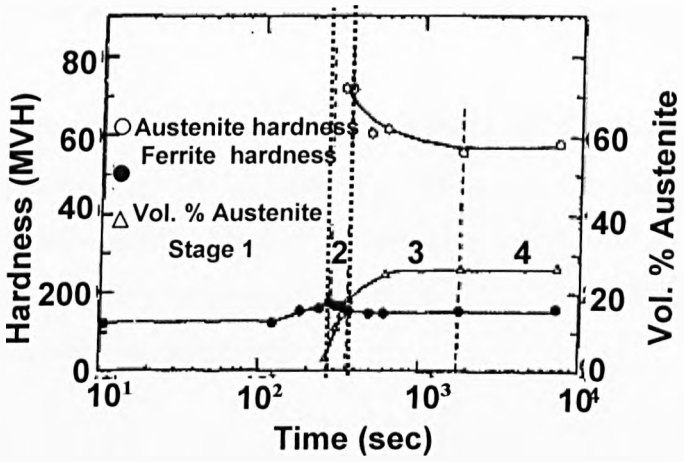

Figure 2.10 Hardness values of ferrite and austenite and volume (%) of austenite [41].

Stage 2.- The ferrite hardness decreases, see Figure 2.10. In this stage the growth of austenite is considered to be developed in two ways: Firstly, the austenite growing in the pearlite region which is controlled by the carbon diffusion from the adjacent dissolving pearlitic cementite. Secondly, the formation of thin films of austenite at ferrite grain boundaries. These thin films are produced due to the supersaturation of carbon in the ferrite adjacent to the pearlite.

Stage 3.- The subsequent growth of the austenite into ferrite constitutes a third stage. Another characteristic is that the hardness of the austenite begins to decrease whilst ferrite remains at a constant value, Figure 2.10.

Stage 4.- In this stage the hardness values of the ferrite and austenite are constant and the austenite fraction also remains constant. This suggests that any further growth of the austenite may not be controlled by the carbon diffusion at all, but substitutional alloying element can control the austenite growth. However, it was observed that as a result of the very slow diffusion of substitutional alloying elements, the volume fraction of austenite was kept constant even at long annealing times [41].

2.1.4.3.3 Temperature and holding time effect on the austenite formation

The amount of austenite in the steel is determined by the annealing time which determines the partitioning of the alloying elements towards equilibrium. The redistribution of substitutional alloying elements is much slower than that of the interstitial elements, i.e. carbon diffusivity is about 10^5 - 10^6 times larger than those of the substitutional alloying elements [42].

Silva et al. [43] found that the beginning of the ferrite recrystallization of the cold rolled steel is shown by an inflection in the hardness curve versus annealing temperature at approximately 670 °C, Figure 2.11. The hardness increment shown in this curve is because of the austenite to martensite transformation after quenching which starts on cooling from 700 °C. This gives the expected change from elongated to equiaxed grains for temperatures between 600 and 700 °C, Figures 2.12.

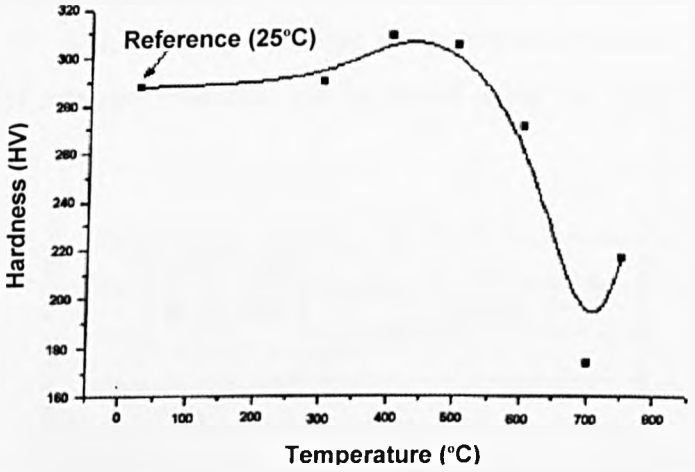

Fig. 2.11 Effect of annealing temperature on Vickers microhardness [43].

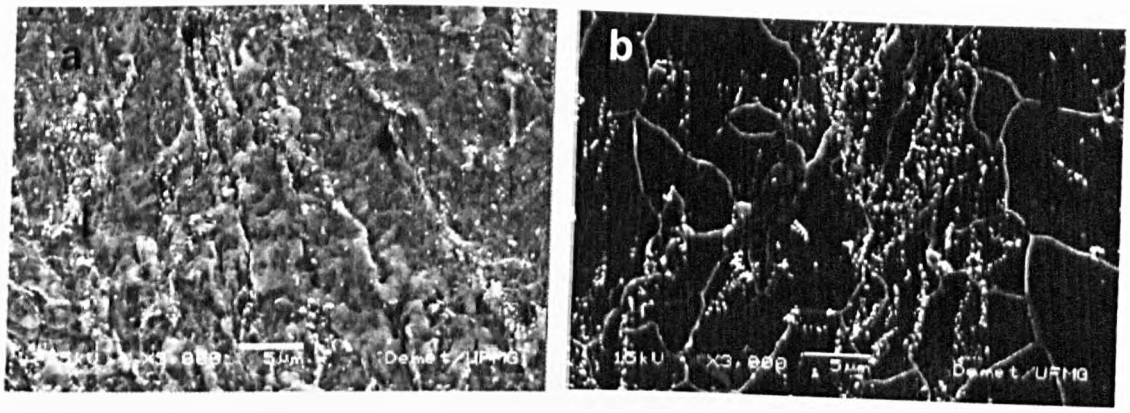

Fig. 2.12 Microstructural changes from elongated to equiaxed grains between 600°C and 700°C [43].

Emadoddin et al. [44] found that the most favourable intercritical annealing temperature to achieve the maximum amount of retained austenite is 860 °C in the case of Al-TRIP-assisted multiphase steel, (0.12-C, 1.6-Mn, Si-1.28, 0.05-Al, all in wt %), meanwhile for the Si-TRIP-assisted steel (0.27-C, 1.48-Mn, Si-0.28, 1.08-Al, all in wt %) it is 810 °C, see Figure 2.13. Also they reported that the optimum condition for increasing the volume fraction of retained austenite can be found using the $(Ac_1+Ac_3)/2 + 20$ °C relationship.

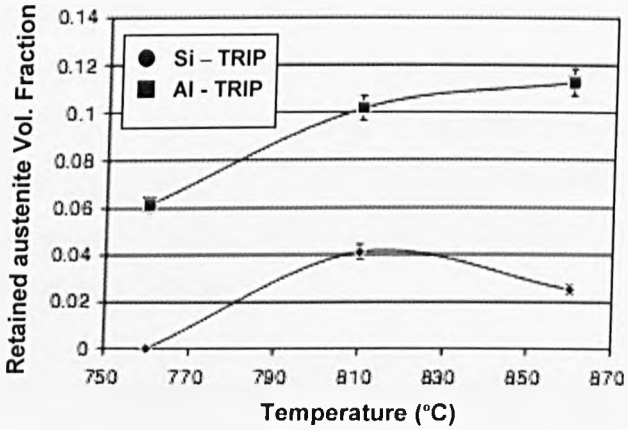

Fig. 2.13 Volume fraction of retained austenite for Al and Si – TRIP assisted steels at different annealing temperatures [44].

Similar effects were found by Shi et al. [45], as shown in Figure 2.14 which shows that as the intercritical annealing temperature is increased the volume fraction of ferrite is decreased, whereas the volume fraction of retained austenite changes randomly. Nevertheless, the retained austenite content in all the studied samples was higher than 10 vol. %, and the highest values are approximately 18 vol. %.

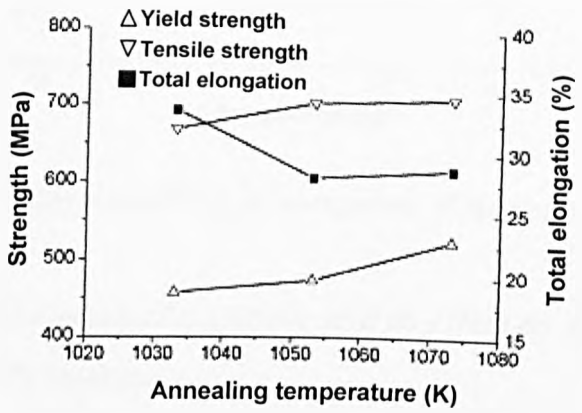

Fig. 2.14 Annealing temperature effect on elongation, yield and tensile strength [45].

Rocha et al. [20] found that the yield strength (YS) increases as the soaking temperature is increased, whereas the ultimate tensile strength (UTS) decreases. Total elongation does not change considerably, though it is slightly higher at the intermediate intercritical soaking temperature of 780 °C, see Figure 2.15. This behaviour was attributed to the changes in phase proportion produced at different annealing temperatures. A decrease in the soaking temperature results in the formation of less austenite and therefore less bainite is formed on quenching, because the austenite is richer in hardening elements, leading to an increase in the UTS and a decrease in the YS, which results in a lower yield ratio.

The formation of carbides inside the martensite during the overaging also contributes to a decrease in strength. The ductility increases with an increase in the volume fraction of ferrite and decreases when the martensite content is increased [20].

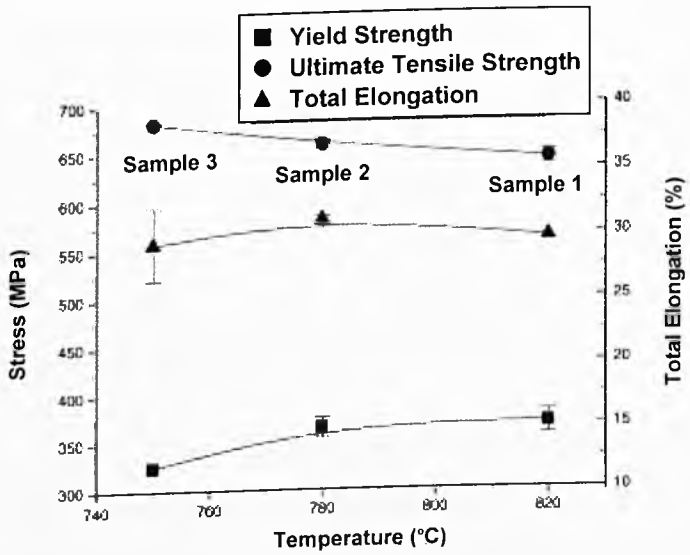

Fig. 2.15 Annealing temperature effect on elongation, yield and tensile strength [20].

2.1.4.3.4 Stability of the retained austenite and its effect on the strain hardening exponent "n" values

As shown before, elongation is substantially improved by the retained austenite content, having a positive effect on the strain hardening exponent "n" value of the multiphase steels. In this context, the retained austenite content is determined by the heat treatment conditions. Thus the "n" value will depend on the annealing process. A multiphase steel with chemical composition: 0.27C – 1.6Mn – 2.0Si wt. %, was studied by Srivastava et al. [46], who found that the strain-hardening exponent, "n", varied with heat-treatment conditions. Table 2.2 shows the results obtained with different heat treatments. According to this table, samples A and B showed somewhat higher "n" values of 0.224 and 0.213, respectively, compared with the "n" values of 0.199 and 0.168 for samples C and D, respectively. Even though the total elongation was approximately constant for all intercritical annealing (IA) and isothermal bainitic transformation (IBT) times, the "n"-value for samples A and B increased with the higher IA time (10 min). The time variation in the IBT area did not show any effect on "n"-values. Figure 2.16 shows the influence of heat-treatment conditions on the strength and elongation for the different samples [46].

Table 2.2 Heat treatment effect on n-values for multiphase steel [46]

Sample code	Heat treatment details	YS (MPa)	UTS (MPa)	YS/UTS	EL (%)	n-value	UTS×EL (MPa*%)
A	IA-800°C-10min	386	679	0.57	31	0.224	21,049
C	IBT-400°C-3min IA-800°C-5min	381	652	0.58	31	0.208	20,212
B	IBT-400°C-3min IA-800°C-10min	404	681	0.59	32	0.213	21,792
D	IBT-400°C-5min IA-800°C-5min IBT-400°C-5min	438	661	0.66	31	0.198	20,491

According to Table 2.2 and Figure 2.16, samples A and B have excellent formability and good mechanical properties. This formability improvement is attributed to the fact that specimens A and B have higher strain-hardening index ("n" value) and elongation than conventional high-formability cold-rolled sheet steels.

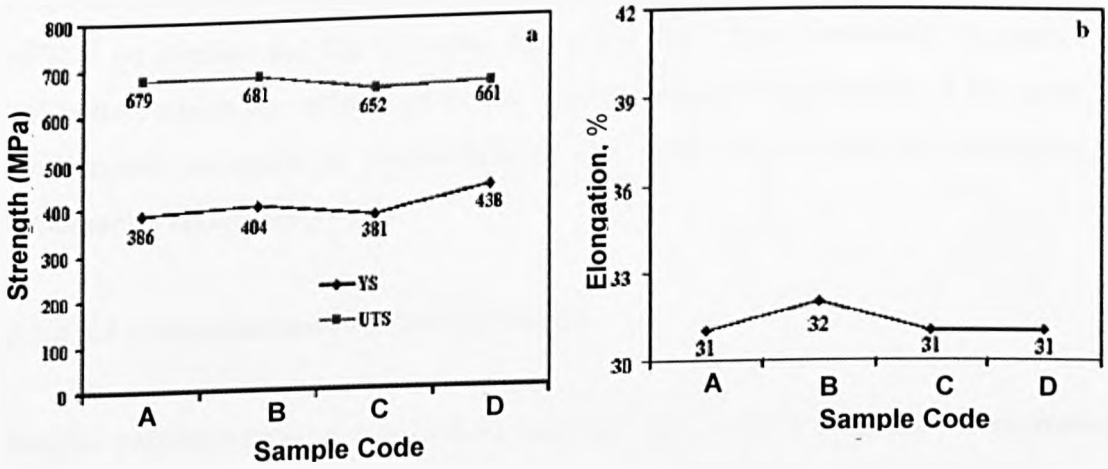

Fig. 2.16 Influence of the heat treatment in the strength and elongation for a 0.27C – 1.6Mn – 2.0Si wt. % multiphase steel [46].

Samples C and D did not show good formability even with high elongation, Table 2.2 and Figure 2.16, attributed to the lower austenite content from the shorter intercritical anneal. It is well known that during isothermal treatment the carbon content in retained austenite increases as the amount of retained austenite reduces, leading to an extremely high stability of retained austenite. This kind of retained austenite does not transform to martensite even at high strains and as a result poor formability is obtained.

It is clear, therefore, that the carbon content of the retained austenite is a critical variable for the stability of the retained austenite and therefore the formability, and consequently the time and temperature of the intercritical anneal [46]. In a similar manner, Srivastava et al. [47] worked with a cold-rolled multiphase steel with Si-Al - 0.21 wt% C. Their major finding was that the formability and the amount of retained austenite decrease when the intercritical annealing holding time is increased. The multiphase steel was intercritically annealed at 900 °C for 5 min. The amount of retained austenite was 7.89% and the elongation was 30%. Under the same intercritical temperature but with a holding time of 10 min the retained austenite content was of 6.75% and the elongation obtained was of 26%. The isothermal bainitic transformation was the same in both cases. The carbon concentration in the retained austenite was 0.82% producing the higher stability in the latter heat treatment. The tensile strength result obtained under these heat treatment conditions was 600 MPa with an elongation of 31% on average and the "n" value was of 0.2 [47]. Thus, formability depends of the "n" values which are influenced by the retained austenite content but at the same time the retained austenite is determined by the intercritical annealing conditions, i.e. temperature and holding time.

2.1.4.3.5 Isothermal bainitic transformation

Bainite transformation of intercritical austenite has become of primary importance in the processing of these high strength formable steels. Indeed, bainite transformation during thermal processing of the multiphase steels allows carbon enrichment of a substantial amount of austenite so that the austenite remains stable after quenching to room temperature. Previous studies have shown that austenite can be retained by partial bainite transformation in steels containing rather large amounts of silicon from 1.5 to 2.5 wt% [48]. At temperatures between 350 °C and 550 °C, bainite consists of needles or laths of ferrite with cementite precipitates between the laths and this is known as upper bainite. The ferrite laths grow into partially transformed austenite, as illustrated schematically in Figure 2.17.

The ferrite laths grow into the austenite in a similar way to Widmanstätten side-plates. The ferrite nucleates on a grain boundary with orientation relationship with one of the austenite grains, γ_2. Since the undercooling is very large the nucleus grows most rapidly into the γ_2 grain forming ferrite laths with low energy semicoherent interfaces. This takes place at several sites along boundary so that a group of finely spaced laths develops. For carbon levels below about 0.5wt% the transition temperature increases, with increasing carbon from 0.5-0.7wt% C the transition temperature decreases and above approximately 0.7wt% C it is constant at about 350°C. [49].

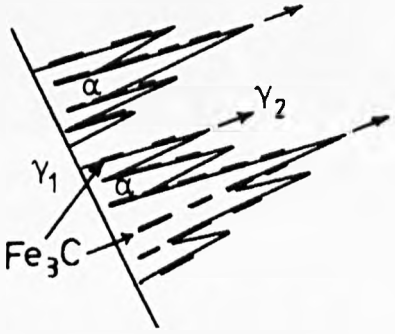

Fig. 2.17 Schematic illustration of the bainite development [49].

Hulka [48] argued that the bainite transformation takes place during isothermal holding and this transformation ceases before the complete consumption of the residual austenite has occurred. However, the overall rate at which bainite forms has been found to depend on transformation temperature. This transformation process causes a build-up of carbon in the austenite near the interface, which significantly persists at low temperature and hinders the progress of the reaction. The microstructure reported by Zaefferer et al. [50] from their experimental multiphase steel is shown in Figure 2.18. The material was cold rolled with an average reduction of 65% and annealed at 803 °C for 3 min. The controlled cooling was carried out using gas stream and the cooling rate was 20 °C/s. Bainite transformation was undertaken isothermally followed by cooling down to room temperature.

The microstructure consisted of retained austenite, bainite and martensite in a ferrite matrix. Figure 2.18(a) shows a bainite grain mixed with retained austenite, while it is difficult to differentiate the phases when viewed in the SEM, Figure 2.18(b).

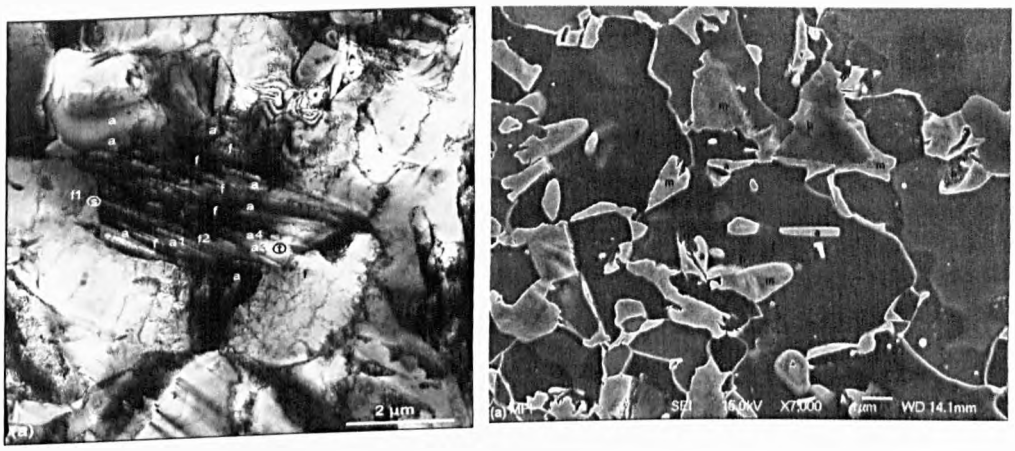

Fig. 2.18 Microstructure obtained by Zaefferer et al. [50], (a) Bright field TEM image showing bainite (b) SEM microstructure.

Singh et al. [51] explained that growing bainite cannot cross grain boundaries, as the growth of each platelet is accompanied by a change in shape of the transformed region, defined as an invariant plane strain (IPS) with a large shear component. The IPS, which occurs at relatively high temperatures, will plastically deform the adjacent austenite. This results in a local increase in dislocation density, which hinders the growth of the bainite plate so that each plate only achieves a limited size that is much smaller than the size of the residual austenite grain. Similarly, Shipway et al. [52] explained that the growth of bainite by a displacive mechanism is retarded by deformation debris in the residual austenite. This means that displacive transformation can be suppressed by prior deformation of the parent phase, and this effect is known as mechanical stabilization. It should be noted that during transformation of γ into bainite C is rejected from the bainite and retained austenite is once again enriched with C and further chemically stabilised. Thus, the plastic deformation in the intercritical region produce defects that accelerate the bainite nucleation rate but at the same time decreases its growth rate, resulting in a smaller size of the colonies, shorter plates and a smaller volume fraction of bainite [53].

Jacques [54] compares the bainite morphology as a function of the size of the austenite grain in which it occurs. The classical bainite sheaf structure can be clearly seen in Figure 2.19(a). The first bainitic ferrite sub-units nucleate at the austenite grain boundary and grow towards the interior of the austenite grain. New sub-units then nucleate and grow from the tip of the previous ones, bringing about the sheaf structure. This process is valid as long as tip nucleation is possible, i.e. as long as the austenite grains are larger than the platelet length. By contrast, the bainite morphology is completely different when the austenite grain size is only a few micrometers as in the case of the intercritical austenite shown in Figure 2.19(b). The bainite that forms in very small austenite grains comprises adjacent platelets that completely cross the austenite grain.

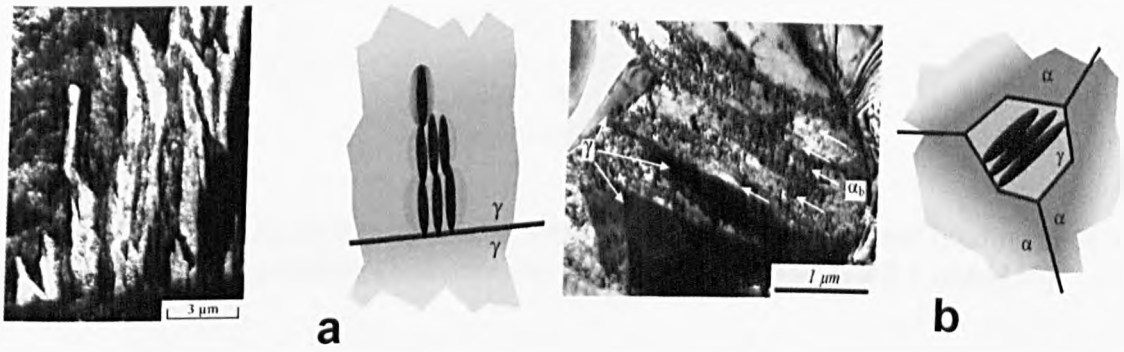

Fig. 2.19 Bainite comparison by Jacques [54], (a) typical bainite sheaf, (b) bainite obtained in a thermomechanical processing of TRIP steels.

Not surprisingly, the temperature and holding time affects the bainitic transformation in the isothermal region during the annealing process of the TRIP-assisted steels. Figure 2.20, presents the evolution of the volume fraction of bainite as a function of the holding time in the bainitic transformation area at 360 °C and 410 °C for high silicon multiphase steel. The graph clearly shows how the bainite transformation kinetics is faster at 410 °C. In addition, bainite transformation stops before the initial intercritical austenite has completely transformed. This transformation produces carbon enrichment of the residual austenite up to a maximum level attained at the transformation motionless state, Figure 2.20.

This behaviour is explained by considering (1) the displacive mechanism of bainite formation, (2) the carbon partitioning between bainitic ferrite and residual austenite and (3) the inhibition of cementite precipitation from austenite. The bainite transformation level is lower when the holding temperature is higher [55].

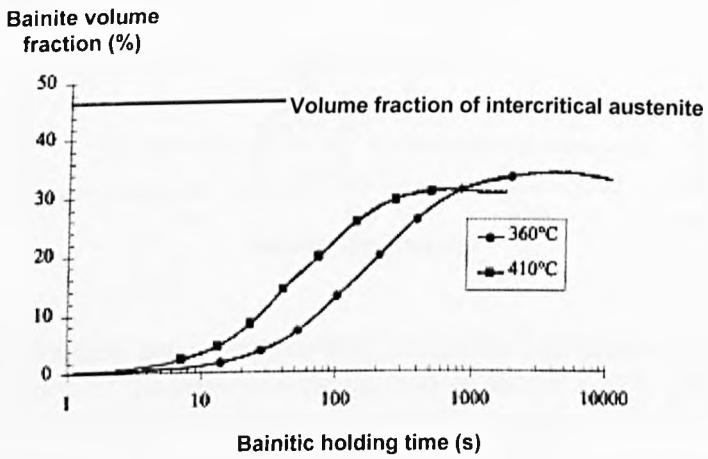

Fig. 2.20 Volume fraction of bainite in high Si steel during isothermal holding at 360 and 410 °C (intercritical annealing was carried out at 760 °C for 6 min) [55].

Fig. 2.21 shows, for high Si steel, the variations of the volume fraction and carbon content of the retained austenite as a function of the bainite transformation time at 360 °C and 410 °C. For the two different temperatures, these curves show a first stage during which the bainitic holding time is accompanied by a carbon enrichment of residual austenite in such a way that the austenite stabilizer effect of carbon allows the retention of a greater amount of austenite (16-18%) at room temperature. For longer bainitic holding times, the amount of retained austenite and the carbon content does not change during the transformation as was shown in Figure 2.20 [55].

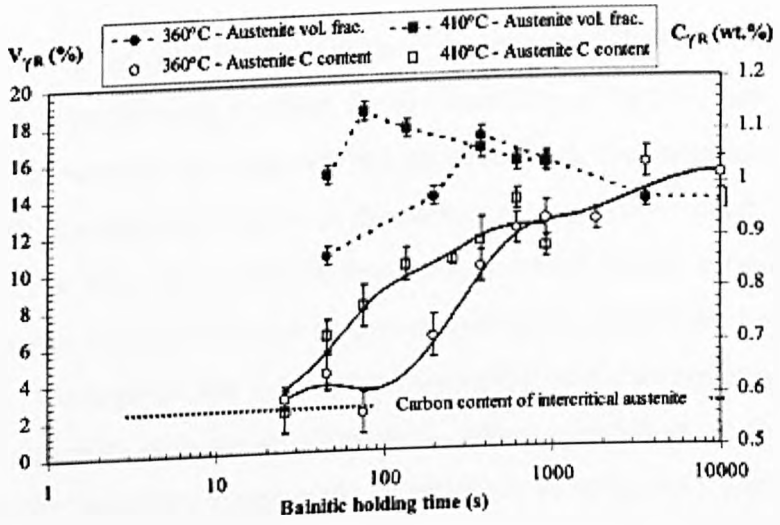

Fig. 2.21 Volume fraction and carbon content of retained austenite in high Si steel as a function of the bainitic holding time at 360 or 410°C [55].

2.1.4.4 Alloy Elements Effect

To achieve the required microstructure and mechanical properties of thermally treated multiphase steels, Hosseini [56] suggests having a good metallurgical knowledge of all the different parameters involved in their processing and the obvious one is chemical composition. Since the 1990s, numerous studies have been carried out on low-alloyed Si-Mn TRIP-assisted multiphase steels, which have been developed based on addition of up to 2 wt % silicon, the aim of this high content of silicon is to prevent carbide precipitation during transformation of austenite to bainite. For low alloyed multiphase steels, austenite is stabilized mainly by C but also by Mn. The total C-content of these grades should be as low as possible with a maximum carbon equivalent of percent allowed; in order to carry out the essential welding of the steel [57].

2.1.4.4.1 Carbon

The carbon has a fundamental function in the composition of the multiphase steels. It is well known that its partitioning between the different phases (ferrite, bainite, martensite and austenite) is essential to improve the properties of the material. However, in multiphase steels, the specific purpose of the carbon is to enrich as much as possible the austenite in order to have the lowest M_s temperature, which allows enough austenite to be retained at room temperature and as a consequence to obtain the best mechanical properties [38]. Throughout the intercritical annealing and austempering, the carbon content in the austenite is increased. The first carbon enrichment of the austenite is produced after the pearlite or cementite dissolution at annealing temperatures and secondly, during the austempering the austenite is carbon enriched as a result of the suppression of the formation of carbides during the bainitic transformation, due to the presence of the alloying elements such as silicon and aluminium. The enhancement of carbon in the austenite increases its thermal stability and consequently the austenite can be retained upon cooling to room temperature [31]. Whereas the multiphase steels produced at laboratory scale have a carbon content up to 0.4 wt %, current multiphase steels are manufactured with a carbon content range from 0.20 wt % to 0.25 wt. % and even less (0.15 wt % C) for reasons of weldability [38].

2.1.4.4.2 Manganese

Manganese is the principal strengthening element in plain carbon high – strength structural steels when it is present in amounts over 1wt %. It functions mainly as a mild solid – solution strengthener in ferrite, but it also provides a marked decrease in the austenite to ferrite transformation temperature. In addition, manganese can enhance the precipitation strengthening of vanadium steels and to a lesser extent, niobium steels [58]. Lis [59] observed that multiphase steels only work where the formation of pearlite is avoided, this make the addition of certain alloys essential, particularly Si and Mn. The Mn has two functions in multiphase steels: on one hand Mn has a stabilizing effect on austenite; on the other hand Mn delays the formation of pearlite during cooling.

The temperature level in the bainite range controls the transformation and consequently C-enrichment in austenite and the volume fraction as well as the stability retained austenite [21]. There is a thin spike of the alloying element in front of the migrating interface. Increasing annealing time below A_{C1} increases the concentration of Mn in cementite and thus in newly-formed austenite during the next annealing in the $(\alpha + \gamma)$ temperature range [59].

2.1.4.4.3 Silicon

Traditionally silicon is present in fully deoxidized structural steels in amounts up to 0.35 wt %, which ensures the production of sound ingots. Silicon has a strengthening effect in low-alloy structural steels, i.e. it has a significant effect on yield strength enhancement by solid – solution strengthening [58]. Figure 2.22 shows the silicon effect on the ferrite hardness. The values correspond to low silicon (LSi - 0.39 wt. %) and high silicon (HSi – 1.5 wt. %) steels. According to the figure below, the hardness of the ferrite is significantly smaller in LSi than in HSi steels. This difference of the ferrite hardness is a result from the higher silicon content of HSi steel. Previous work has reported that the tensile strength of ferrite increases by about 100 MPa per weight percent of silicon [60].

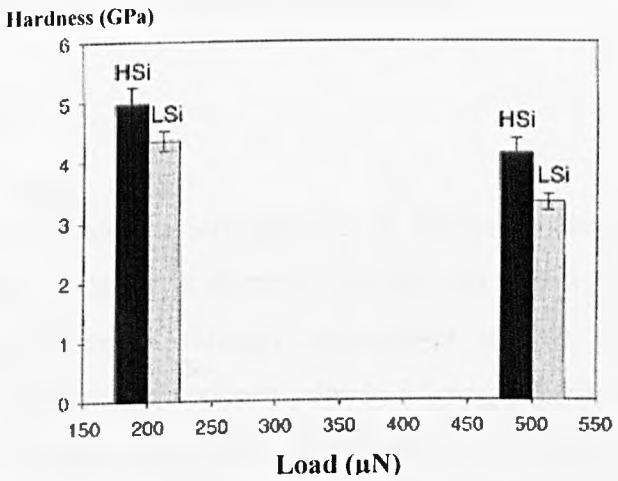

Fig. 2.22 Ferrite hardness values for low silicon (LSi – 0.39 wt. %) and high silicon (HSi – 1.5 wt. %) for two different maximum indentation loads [60].

The most significant characteristic of silicon is that it favours the carbon rejection from the bainitic ferrite to the remaining austenite without producing precipitation of Fe_3C in the bainite. The exact mechanism for the suppression of iron carbide is not fully clear. Some work has suggested that because silicon is insoluble in Fe_3C, in order for Fe_3C to nucleate and grow the silicon must diffuse away from the particle, which takes time [7]. Normally between 1–2 wt % of silicon is added to steels but unfortunately if silicon levels are >0·5 wt % it can cause problems during the galvanising process. It has been found that a silicon content of about ~0·8 wt % produces a reasonable amount of retained austenite. A drawback is that silicon preferentially oxidises during hot rolling and the resultant scale is too difficult to remove, leading to bare spots after galvanising [7]. Mn and Si form a very stable Mn_2SiO_4 oxide film on the surface during the annealing process. The surface tension properties of this oxide when in contact with liquid Zn inhibit the ability to galvanise the steel [61]. As a consequence, studies have been initiated with other elements, such as Cu, Ni, Al, Mo and P as a replacement for Si but these additions are not popular with steel makers. It has been shown that a silicon concentration of 1.5 wt % is sufficient to inhibit cementite precipitation from austenite during bainite transformation conducted around 350-400 °C. However, for the low silicon steel (0.38 wt % of silicon) to be isothermally held in the same temperature range, austenite decomposition by cementite precipitation occurs simultaneously with the formation of bainitic ferrite so that carbon enrichment of austenite is reduced and no incomplete reaction phenomenon can be observed [55].

2.1.4.4.4 Phosphorus

P is an effective solid solution strengthener in ferrite. It also enhances corrosion resistance but causes a decrease in ductility. Phosphorus at low levels (<0.05 wt %P) can also cause embrittlement through segregation to the prior–austenite grain boundaries. On the other hand, phosphorus, due to it being a ferrite former and delaying the precipitation of carbides could be an alternative to take into account in the composition of multiphase steel, although phosphorus slows down Zn–Fe reactions during galvannealing processes [7].

2.1.4.4.5 Aluminium

Al is generally used as deoxidizer and was the first element used to control austenite grain growth during reheating [58]. The effect of aluminium in the multiphase steel processing is similar to that of silicon, i.e. it is a ferrite former and increases the activity of carbon in ferrite, and as a result carbon is rejected from the ferrite into the austenite producing a softer ferrite. Also, aluminium, like silicon, is not soluble in Fe_3C and delays the precipitation of iron carbide [7].

2.1.4.4.6 Vanadium

V shows such a high level of solubility that, within the range of carbon and vanadium levels found in microalloyed vanadium steels, the solubility limit imposes no restriction on the level of dissolved vanadium that can exist in equilibrium with high dissolved carbon levels in the austenite at 1200 °C. Consequently, it does not limit the dispersion strengthening that can be attained from vanadium carbide (or carbo-nitride) precipitation [62]. The significant levels of dispersion strengthening in vanadium microalloyed medium carbon steels noted earlier have been exploited in the development of medium carbon forging steels for a wide range of applications, such as connecting rods, steering linkages and stub axles, all requiring an adequate level of strength and fatigue resistance [62].

2.1.4.4.7 Niobium

Many works have showed that small additions between 0.03 to 0.05 wt % of niobium increase yield strength by a combination effect of precipitation strengthening and grain refinement. Niobium has a stronger effect than vanadium due to niobium carbide being more stable in austenite than vanadium carbide at typical rolling temperatures. The lower solubility of niobium carbide in austenite provides more stable precipitate particles, which pin the austenite grain boundaries and thus retard austenite grain growth [58].

Sugimoto et al. [63] working with a multiphase steel microalloyed with niobium found that niobium additions in a range of 0.02–0.11 wt % decrease carbon content of the retained austenite, except at high austempering temperatures, Figure 2.23. On the other hand in a narrow range between 0.05–0.08 wt % of niobium, it was observed that it brings about little increase in retained austenite volume fraction at low austempering temperatures, although its volume fraction decreases at high austempering temperatures.

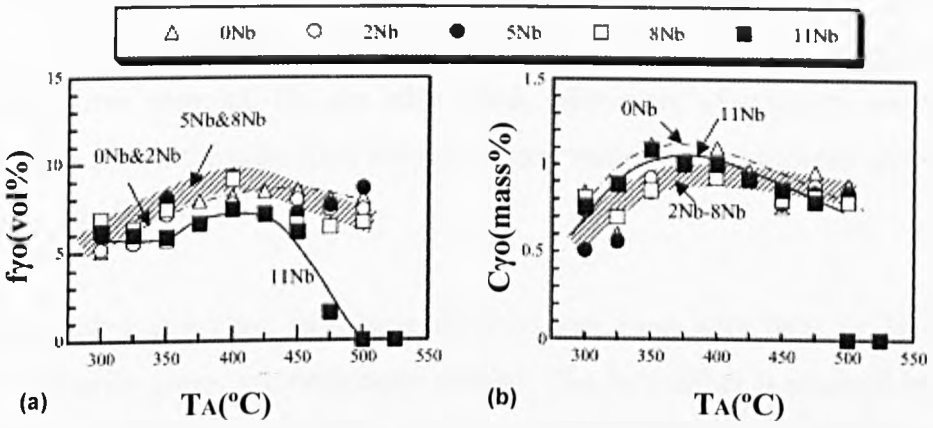

Fig. 2.23 (a) Volume fraction and (b) carbon concentration of retained austenite as a function of austempering temperature and niobium content [63].

It has been reported that niobium has the following roles in conventional multiphase steels [64].

(1) Niobium in solid solution lowers the martensite start temperature. Additionally, in dissolved form it suppresses carbide precipitation in the temperature range of isothermal bainite formation leading to an increment in the residual austenite content and its carbon content.

(2) Niobium precipitation as carbides, nitrides or carbonitrides has a grain refining effect, increasing the tensile strength. Also, niobium suppresses pearlite formation in the TRIP-assisted multiphase steels [64].

Thus, it is expected that high retained austenite volume fraction at low austempering temperatures of steel samples of 0.05 wt % Nb (labelled 5Nb) and 0.08 wt % Nb (labelled 8Nb) may be caused by the niobium in dissolved form which suppresses cementite precipitation in the temperature range of bainite formation, as was explained before, see Figure 2.23. When multiphase steel was austempered at 400–500 °C, niobium addition of 0.05–0.11 wt % changed the grain morphology of the ferritic matrix and retained austenite. These grain morphology changes may suppress a decrease in carbon concentration of retained austenite due to niobium in solid solution as a ferrite former element. On the other hand, refinement of retained austenite and matrix (ferrite) grains through prior austenite grain refining is considered to be caused by niobium carbides [63].

In addition, Heller and Nuss [65] have reported that even with 0.03 wt % niobium addition, the ferrite grains are noticeably refined. The best effect is attained by adding quantities of niobium between 0.025 and 0.05 wt %. Alternatively, using titanium or a combined addition of titanium and niobium also causes the same grain refinement effect, with the resultant improvement in mechanical properties, Figure 2.24. The residual austenite grain size produced was between 1.6 and 1.9 μm, this size is considered optimum to transform into martensite during the deformation process and consequently contribute to the TRIP effect. For Nb and Nb + Ti multiphase steels, carbon content in the retained austenite was of ~1wt %. In contrast to microalloy-free steel, microalloyed (Nb and Ti) steels show much higher residual austenite contents, i.e. the highest value was produced with 0.042 wt % niobium.

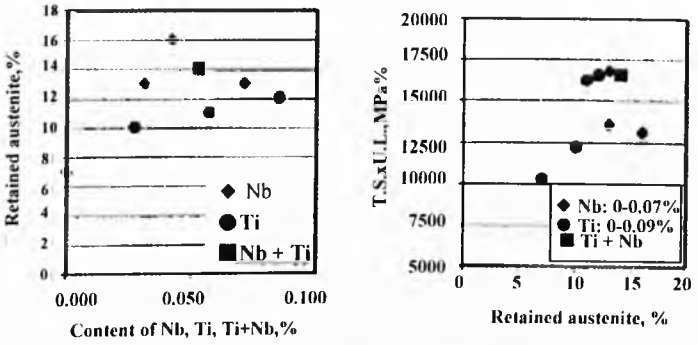

Fig. 2.24 Influence of Ti and Nb on retained austenite content and mechanical properties: U.L. is uniform elongation [65].

As a result of the grain refinement effect, the yield strength and the tensile strength in Nb–Ti microalloyed steels increased by ~100 MPa, Figure 2.25. If the product of tensile strength and elongation is applied as a criterion to evaluate the quality of retained austenite, the positive influence can be observed when the microalloying element contents are increased. The best values are produced with high titanium contents [65].

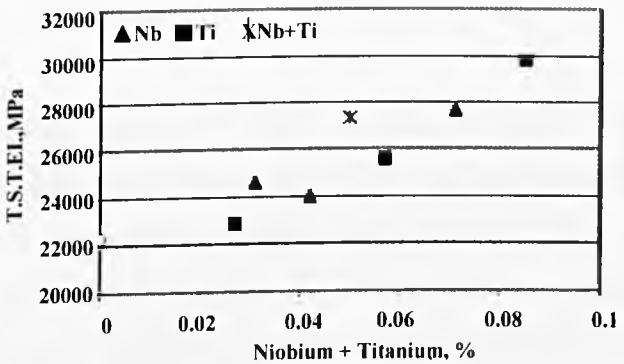

Fig. 2.25 Influence of microalloying elements on formability or retained austenite steels: T.El. is the total elongation [65].

Table 2.3 Mechanical properties of steels for automotive applications [3]

Steel Grade	YS (MPa)	UTS (MPa)	Total EL (%)	n Value (5-15%)	r Bar
DP 280/600	280	600	30-34	0.21	1
DP 300/500	300	500	30-34	0.16	1
HSLA 350/450	**350**	**450**	**23-27**	**0.14**	**1.1**
DP 350/600	350	600	24-30	0.14	1
DP 400/700	400	700	19-25	0.14	1
TRIP 450/800	**450**	**800**	**26-32**	**0.24**	**0.9**
DP 500/800	500	800	14-20	0.14	1
DP 700/1000	**700**	**1,000**	**12-17**	**0.09**	**0.9**

2.1.4.5 Mechanical performance

Comparative mechanical properties of high strength low alloy (HSLA), TRIP-assisted multiphase and several grades of dual phase (DP) steels are reported by Schaeffler [3] in Table 2.3. The DP steels have excellent yield strength (280 – 700 MPa) and high UTS (1000 MPa). However the higher "n" value (0.24) corresponds to the TRIP-assisted multiphase steels, which simultaneously have high strengths (700 MPa) and enhanced elongation (26 - 32 %). Despite the HSLA has very close values of YS (350 MPa) and UTS (450 MPa) to the DP grade 300/500, its elongation range (23 - 27%) is relatively lower than DP 300/500 (30 – 34 %).

2.1.4.5.1 Stress – strain curve behaviour of multiphase steels

The low yield strength exhibited by TRIP-assisted multiphase steels is attributed to the interaction of high residual stresses and a high mobile dislocation density, Figure 2.26(a), [66].

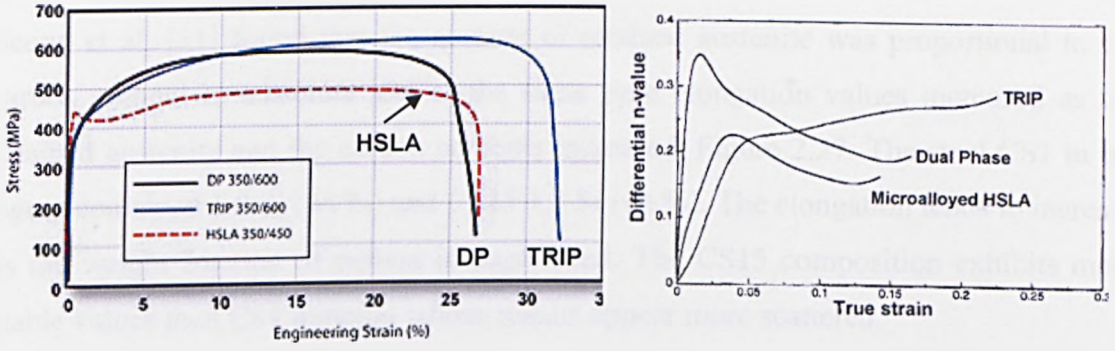

a b

Fig. 2.26 a) Stress – strain behaviour and b) differential strain hardening n-value for HSLA, DP and TRIP-assisted multiphase steels [66].

Besides the improved strength and enhanced ductility, the flow behaviour of DP steels and TRIP-assisted multiphase steels is different to high strength low alloy (HSLA) steels. While HSLA exhibit a higher yield point, DP steels have continuous yielding (as discussed earlier in part 2.1.3.1 of dual phase steels section) and TRIP-assisted multiphase steels present high uniform elongation and relatively low necking elongation, see Figure 2.26(a). In addition, the HSLA steels have lower ductility and exhibit Lüder's bands. Figure 2.26(b) gives the work hardening behaviour of the steels, which makes the differences far more obvious. It is clear that the DP steels exhibit rapid initial work hardening, but this falls with strain, whereas multiphase steels uniquely exhibit a higher work hardening exponent "n" that continues to increase with strain [48]. This enhancement of the differential "n" can be attributed to the generation of additional stresses and dislocations in the ferrite grains and at the ferrite/bainite interface as retained austenite transforms to martensite during straining [66].

The austenite to martensite transformation is accompanied by a volume expansion which in multiphase steels deforms the ferrite structure and new dislocations are created. This results in a localised increment of the strain hardening coefficient, which delays the onset of necking and ultimately leads to a higher uniform and total elongation. Not surprisingly, the amount of retained austenite, its size, shape and distribution affect the mechanical properties of multiphase steels [67].

Seong et al. [31] found that the amount of retained austenite was proportional to the carbon content in austenite and at the same time elongation values increased as the retained austenite and the carbon contents increased, Figure 2.27. The steel CS1 in the figure contained 1.0 Si (wt %) and CS15 1.5 Si (wt %). The elongation tends to increase as the weight fraction of carbon is augmented. The CS15 composition exhibits more stable values than CS1 material whose results appear more scattered.

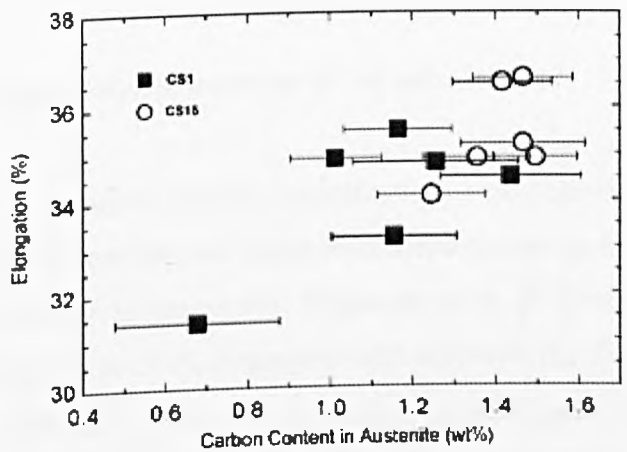

Fig. 2.27 Carbon content in retained austenite effect on elongation [31].

It is not only the retained austenite that plays a key role in the mechanical properties of multiphase steels. Clearly, the ferrite and bainite phases also affect the shape of the flow curve. De Cooman [38] suggests that it is appropriate to test each phase individually in order to evaluate their particular contribution to the mechanical properties. Clearly, the problem is that retained austenite cannot be produced in bulk as easily as ferrite or bainite. Figure 2.28 shows the results of the stress – strain test for ferritic and bainitic steels.

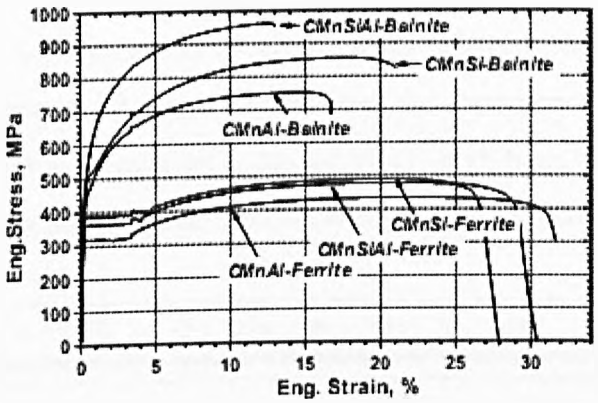

Fig. 2.28 Stress – strain curves for individual ferrite and bainite phases [38].

Figure 2.28 clearly shows the relatively large Lüders strain associated with the ferritic steels. In the case of bainitic steels, the bainite is associated with the absence or a very limited Lüder's strain, a pronounced work hardening and a very low yield – to tensile strength ratio [38].

2.1.4.5.2 Tensile properties improvement by Nb microalloy

In addition to the annealing process optimization, microalloying elements such as niobium, titanium and vanadium are being considered for use in the multiphase steels in order to improve mechanical properties. Sugimoto et al. [63] worked with a C-Mn-Si TRIP-assisted multiphase steel microalloyed with niobium: the chemical composition is presented in the Table 2.4. They found that the yield stresses of 5Nb–11Nb steels increased by about 50 MPa, when the steels was austempered at temperatures higher than 400 °C. However, tensile strength was not influenced by niobium addition, Figure 2.29.

Table 2.4 Chemical composition (mass %) and estimated martensite – start temperature (M_s, °C) for the steels used by Sugimoto et al. [63].

Steel	C	Si	Mn	P	S	Al	Nb	N	M_s
0 Nb	0.20	1.50	1.50	<0.02	0.005	0.040	–	0.0060	421
2 Nb	0.20	1.50	1.50	<0.02	0.005	0.040	0.020	0.0060	421
5 Nb	0.20	1.54	1.52	0.005	0.002	0.030	0.048	0.0074	420
8 Nb	0.20	1.48	1.51	0.005	0.003	0.024	0.078	0.0068	420
11 Nb	0.20	1.48	1.44	0.004	0.003	0.040	0.109	0.0113	423

Total elongation was enhanced by niobium additions of 0.05–0.08 mass% when the multiphase steel was austempered between 450–500 °C, the temperature used for hot-dip galvanizing, Figure 2.30. It is considered in accordance with the previous investigation that the large elongation is caused by (1) high long range internal stress in matrix and (2) relatively high volume fraction and stability of retained austenite.

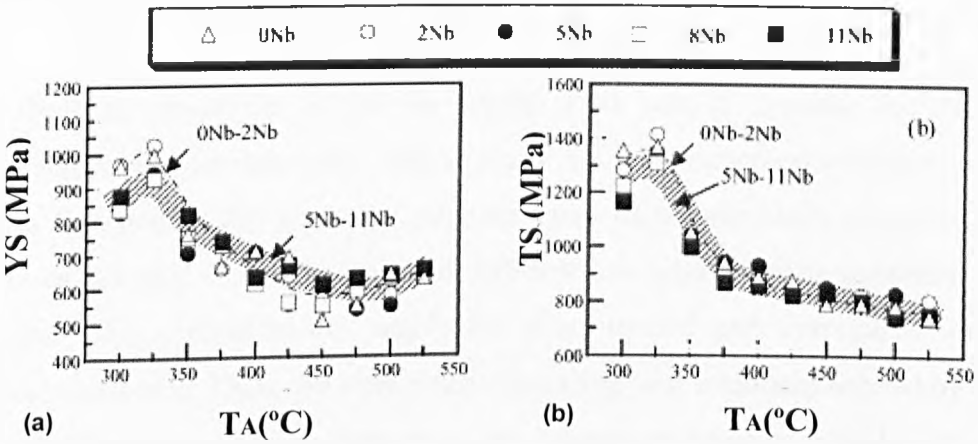

Fig. 2.29 Variations in (a) yield stress (YS) and (b) tensile strength (TS) as a function of austempering temperature for 0 Nb–11 Nb steels [63].

The stretch-formability was significantly improved by the addition of niobium of 0.08–0.11 mass%, in particular when the steels were austempered at low temperatures of 300–350 °C. It was considered that this was associated with refined microstructure and an increase in pro-eutectoid ferrite volume fraction [63].

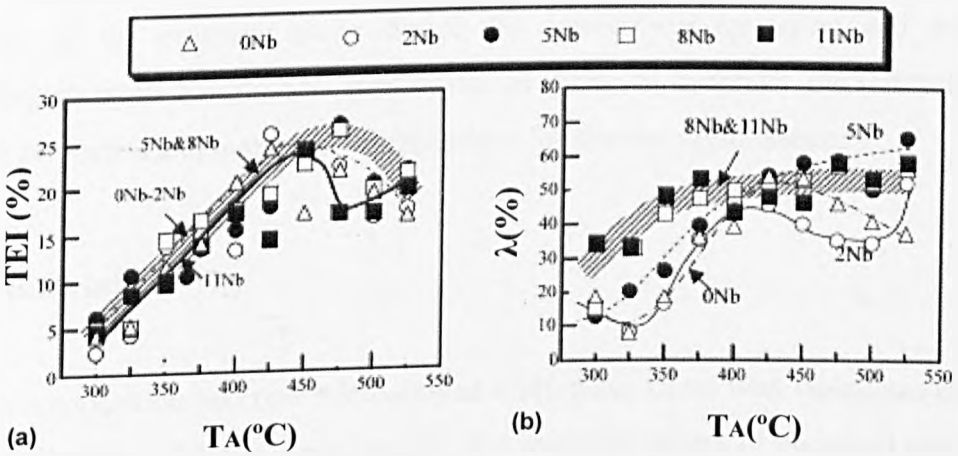

Fig. 2.30 Variations in (a) total elongation (TEl %) and (b) hole-expanding ratio (λ) as a function of austempering temperature for 0 Nb–1 [63].

Chapter 3 Experimental Procedure

3.1 Summary

One of the main objectives within the current work was to simulate the industrial thermal cycle within the laboratory and to study the microstructural evolution at each step. As a first part of the work, the microstructure of commercially produced steels with various vanadium contents and two different hot rolling coil temperatures were investigated. The microstructure was fully characterised and correlated with the mechanical properties. Then, the intercritical annealing heat treatment applied by Corus in their steel processing was adapted to the laboratory scale to simulate the real conditions. Three steels were investigated, namely a base composition and the same steel, but with vanadium contents of 0.06 wt % and 0.12 wt %. The steels were supplied in the hot and cold rolled condition, with two different coiling temperatures. The retained austenite plays a key role in the multiphase steel properties. At the same time, the martensite and the bainite transformation are influenced by the chemical composition and grain size of the austenite produced during the intercritical anneal. Thus, it is important to determine the vanadium effect on the volume fraction and stability of the austenite phase during the intercritical annealing and subsequent transformation to bainite and martensite, in order to correlate microstructure with tensile properties and make recommendations for process optimisation.

3.2 Materials

A base composition and two microalloyed multiphase steels with vanadium content of 0.06 wt % and 0.12 wt % were used in this research project of chemical composition given in Table 3.1. The steels were produced and supplied by Corus, IJmuiden.

The microalloyed steels were produced from a split cast of the base composition, and with the exception of the vanadium content, had very similar composition. The base composition and the vanadium microalloyed multiphase steels were hot rolled (finish roll temperature of 850°C) and coiled at two different temperatures: 640 °C and 550 °C, see Table 3.2. Tensile tests were performed on the finished steels at Corus IJmuiden using the standard procedure for testing thin (1 mm thick) sheet.

First, in order to characterise the multiphase steel microstructure, i.e. ferrite, bainite, martensite and retained austenite constituents, samples were supplied in the fully annealed condition for both the base composition and the vanadium microalloyed steels, which had been intercritically annealed by Corus, as shown in the Figure 3.1. Schedule details are shown in the Table 3.3. The size of the samples supplied was 20 mm (l) x 35 mm (w) with a thickness of 1 mm. From these, specimens were cut for X-ray diffraction (XRD), scanning electron microscopy (SEM) and transmission electron microscopy (TEM). The samples' nomenclature is given in Table 3.4.

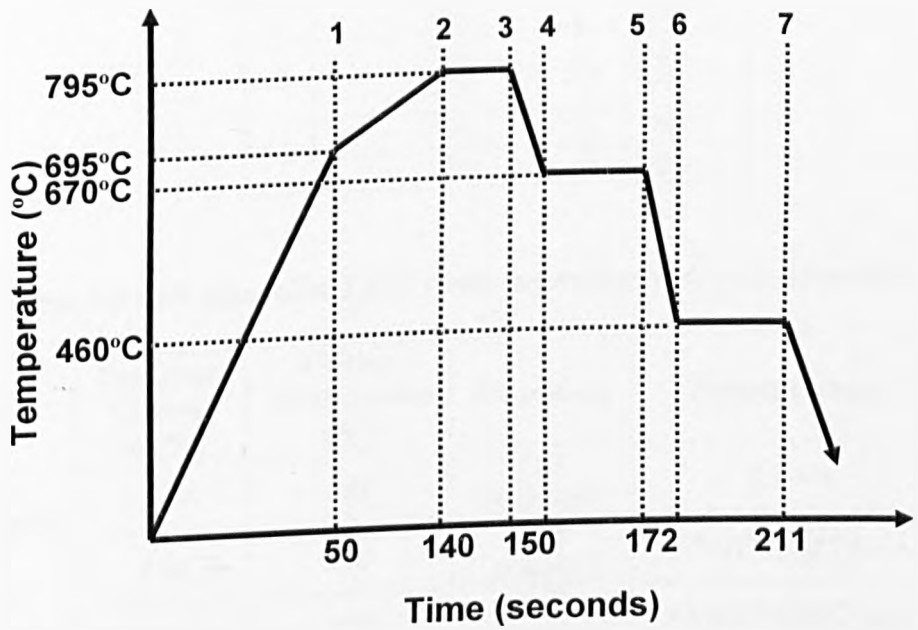

Fig. 3.1 Schedule of the full annealing process applied by Corus for the base composition and vanadium microalloyed multiphase steel.

Table 3.1 Chemical composition of the base composition and vanadium microalloyed steels.

Steel	Alloy	C	Mn	Si	Al	P	N	V	Ti
TRIP 700	Base composition	0.20	1.50	0.38	0.40	0.07	------	-----	----
TRIP 800	Low vanadium	0.21	1.50	0.37	0.33	0.028	0.0050	**0.06**	0.0014
	High vanadium	0.20	1.50	0.37	0.31	0.094	0.0070	**0.12**	0.0025

Table 3.2 Vanadium microalloyed steels hot rolling conditions.

Hot rolled samples	Vanadium content (wt %)	Final hot-rolling temperature (°C)	Coiling temperature (°C)
Low vanadium	0.06	850	640
	0.06	850	550
High vanadium	0.12	850	640
	0.12	850	550

Table 3.3 Schedule variables of the full annealing process applied by Corus, IJmuiden.

Stages	Temperature (°C)	Time (s)
1	695	50
2	795	140
3	795	150
4	670	160
5	670	172
6	460	206
7	460	211

Table 3.4 Full Annealed TRIP steels produced by Corus, IJmuiden.

Steel	Alloy	Vanadium Content (wt %)	Coiling Temperature (°C)	Condition	Nomenclature	Designation
TRIP 700	Base composition	--------	*583*	Full Annealed	BA-FA	FA-1
TRIP 800	Low vanadium	*0.06*	*640*	Full Annealed	LV6(CT640°C)-FA	FA-2
		0.06	*550*	Full Annealed	LV6(CT550°C)-FA	FA-3
	High vanadium	*0.12*	*640*	Full Annealed	LV12 (CT640°C)-FA	FA-4
		0.12	*550*	Full Annealed	LV12(CT550°C)-FA	FA-5

Table 3.5 Characteristics of the cold rolled steels and their nomenclature.

Steel	Alloy	Vanadium Content (%wt)	Coiling Temperature (°C)	Condition	Nomenclature	Designation
TRIP 700	Base composition	--------	583	Cold Rolled	BA-CR	A1
TRIP 800	Low vanadium (LV6)	0.06	640	Cold Rolled	LV6 (CT640°C)-CR	B1
		0.06	550	Cold Rolled	LV6 (CT550°C)-CR	B2
	High vanadium (LV12)	0.12	640	Cold Rolled	LV12 (CT640°C)-CR	C1
		0.12	550	Cold Rolled	LV12(CT550°C)-CR	C2

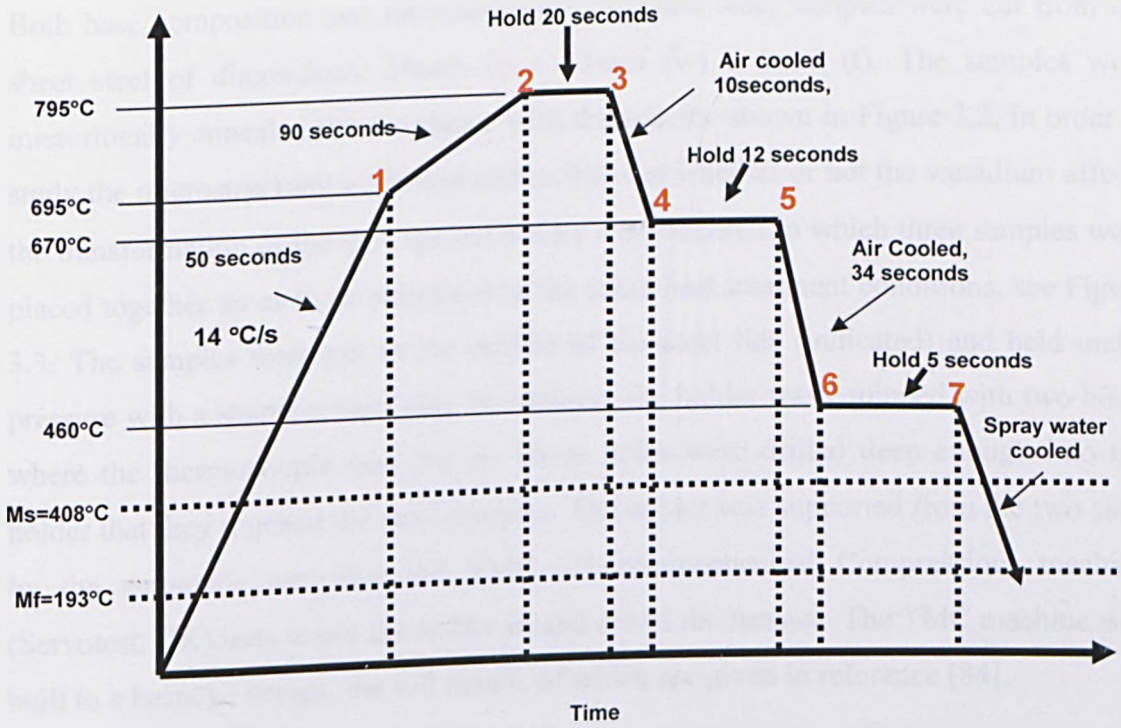

Fig. 3.2 Intercritical annealing process applied in the laboratory for the base composition and vanadium microalloyed steels in cold rolled condition.

In addition, the same steels were supplied in the cold rolled condition as the starting point for the simulated intercritical annealing treatments at Sheffield. The cold roll step is used primarily for gauge control, and only a small strain (~0.25%) is applied. The materials characteristics are listed in Table 3.5. The material was provided in sheet form with the following dimensions: 450mm (l) x 180mm (w) x 1mm thick. The schedule of the intercritical annealing process applied to the cold rolled steels is shown in the Figure 3.2.

3.3 Intercritical annealing process

3.3.1 Sample preparation

Both base composition and microalloyed multiphase steel samples were cut from the sheet steel of dimensions: 30mm (l) x 15mm (w) x 1mm (t). The samples were intercritically annealed in accordance with the scheme shown in Figure 3.2, in order to study the microstructural evolution and to find out whether or not the vanadium affects the transformation of the γ. A special holder was prepared in which three samples were placed together so as to be subjected to the same heat treatment conditions, see Figure 3.3. The samples were put in the middle of the steel lids (indicated) and held under pressure with a stainless steel clip. In addition, the holder was equipped with two holes where the thermocouple was put in. These holes were drilled deep enough into the holder that they touched the steel samples. The holder was supported from the two slots by the automatic arm that the TMC (Thermomechanical Compression) machine (Servotest, UK) uses to put the holder in and out of the furnace. The TMC machine was built to a bespoke design, the full details of which are given in reference [84].

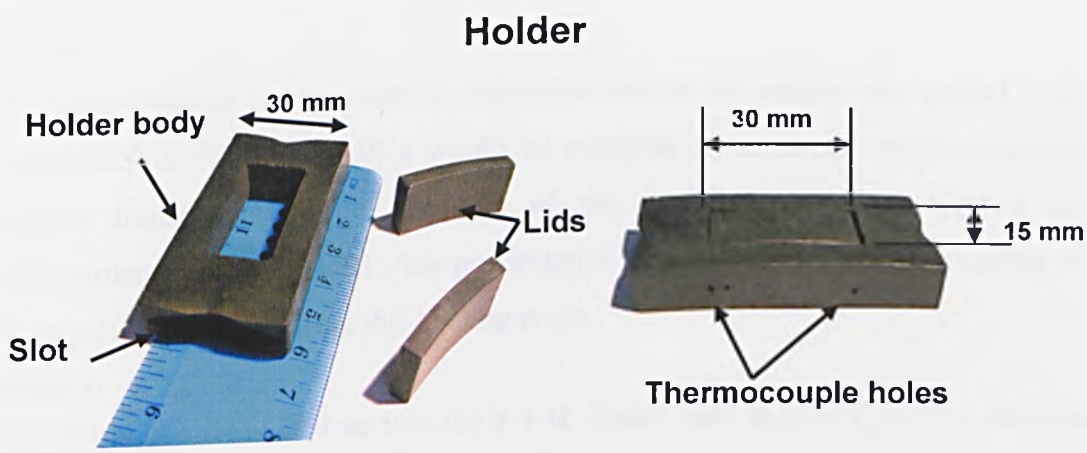

Fig. 3.3 Holder used in the heat treatments of the multiphase steels.

3.3.2. Annealing – heat treatment sequences

The intercritical annealing process was carried out in the rapid thermal treatment unit of the TMC machine. The furnace is designed to give accurate temperature control through active feedback. The heating of the sample is undertaken by induction, with the induction coil specifically designed for the holder geometry used in the current work. All the parameters were controlled by computer software. Also, calibrated thermocouple (Type K, Chromel - Alumel) was used to control and monitor the temperature in each heat treatment. The heating rate used for the heat treatments was set at 14 °C/s (on average) initially, from room temperature to 695°C and then reduced to 2 °C/s up to austenisation temperature, 795°C, in order to simulate the heating process applied by Corus. Both the base composition and the vanadium microalloyed steel samples in the cold rolled condition were heated and quenched, as indicated in Figure 3.2. The sequences of the heat treatments are described below. At the end of each stage a sample was water quenched in order to freeze in as much as possible of the high temperature structure. The sample was typically quenched to around room temperature in less than 2 seconds.

Stage 1:

The main changes produced in the microstructure as the sample was heated up to the temperature of 695 °C in 50 s would be expected to be ferrite recrystallisation and pearlite transformation, but the role of the vanadium-based precipitates on the microstructure is also crucial. Any precipitation that did not occur during coiling would be expected to occur during this heating stage.

Stage 2:

The samples were heated up into the $\gamma + \alpha$ phase field at 795 °C in 90 s and quickly cooled with water to room temperature. At this stage, austenite is formed and the ferrite recrystallised. Additionally, vanadium-based precipitation would have been completed by now.

Stage 3:

Once the samples were heated up to 795 °C in 90 s, they were held for 20 s for austenite formation. After that the samples were quenched down to room temperature. At this point, as well as the formation of austenite, grain growth would have occurred, the extent of which might depend on the ability of the vanadium based precipitates to pin the grain boundaries. However, coarsening of the precipitates would be expected.

Stage 4 and 5:

This step was included as it is inevitably produced by the Corus plant. Carbon repartitioning plays a key role in the retained austenite stabilization, thus a slow and controlled cooling is required, so at this point the samples were subjected to controlled cooling using only pressurized air from 795 °C to 670 °C; and in order to control and stabilize the retained austenite the samples were held for 12 s at this temperature. Again, the samples were water cooled to room temperature and analysed by XRD with the aim of evaluating the retained austenite content and its variation in carbon content.

Stage 6 and 7:

The samples were water mist cooled to the bainite transformation temperature of 460 °C. The bainitic transformation occurred isothermally during the 5 s hold. This is expected to result in stabilization of the retained austenite through growth of bainite laths and consequent carbon enrichment of the austenite.

Figure 3.4 gives a print-out of the temperature read out from the experimental annealing process used; note that temperatures were well controlled throughout the heat treatment which means that a very good temperature/heating accuracy was obtained (± 5 °C). On the other hand this indicates that the annealing heat treatment applied by Corus was well adapted to laboratory scale.

3.4 X–ray diffraction analysis (XRD)

Specimens of the fully annealed and heat treated steels from the laboratory were prepared for XRD to determine the volume fraction of the retained austenite. The samples were cut to an average size of 15 mm (l) x 10 mm (w) x 1 mm (t). Because the thickness of the samples was 1 mm, the analysis was carried out in a flat position. All the samples that were intercritically annealed in the laboratory were analysed by XRD to determine and compare the retained austenite evolution. All the samples were prepared metallographically in the conventional manner. The materials are relatively soft, so that the grinding operation with silicon carbide paper was carried out only with the 1200 grade under running water. The polishing operation was undertaken using cloths, with 6 μm and 1 μm diamond paste and water-based lubricant. Finally, the samples were polished with colloidal silica (Silco) having a polished surface of 0.04 μm. For the XRD test, the samples were slightly etched with 2% nital. XRD was undertaken on a Philips PW1710 reflection diffractometer, using Bragg-Brentano conditions, with monochromatic Co Kα radiation (1.78896 Å). The tube operating conditions were 40 kV and 30 mA. The samples were placed in a rotating holder to minimise the effects of preferential crystallographic orientation. The volume fraction of retained austenite was calculated by measuring the integrated intensities of the various diffraction peaks as such (200)γ, (220)γ and (311)γ. For accurate austenite determination a set of angles were scanned to get the appropriate integrated intensities. The recommended angles are showed in Table 3.6. Each side of each sample was examined.

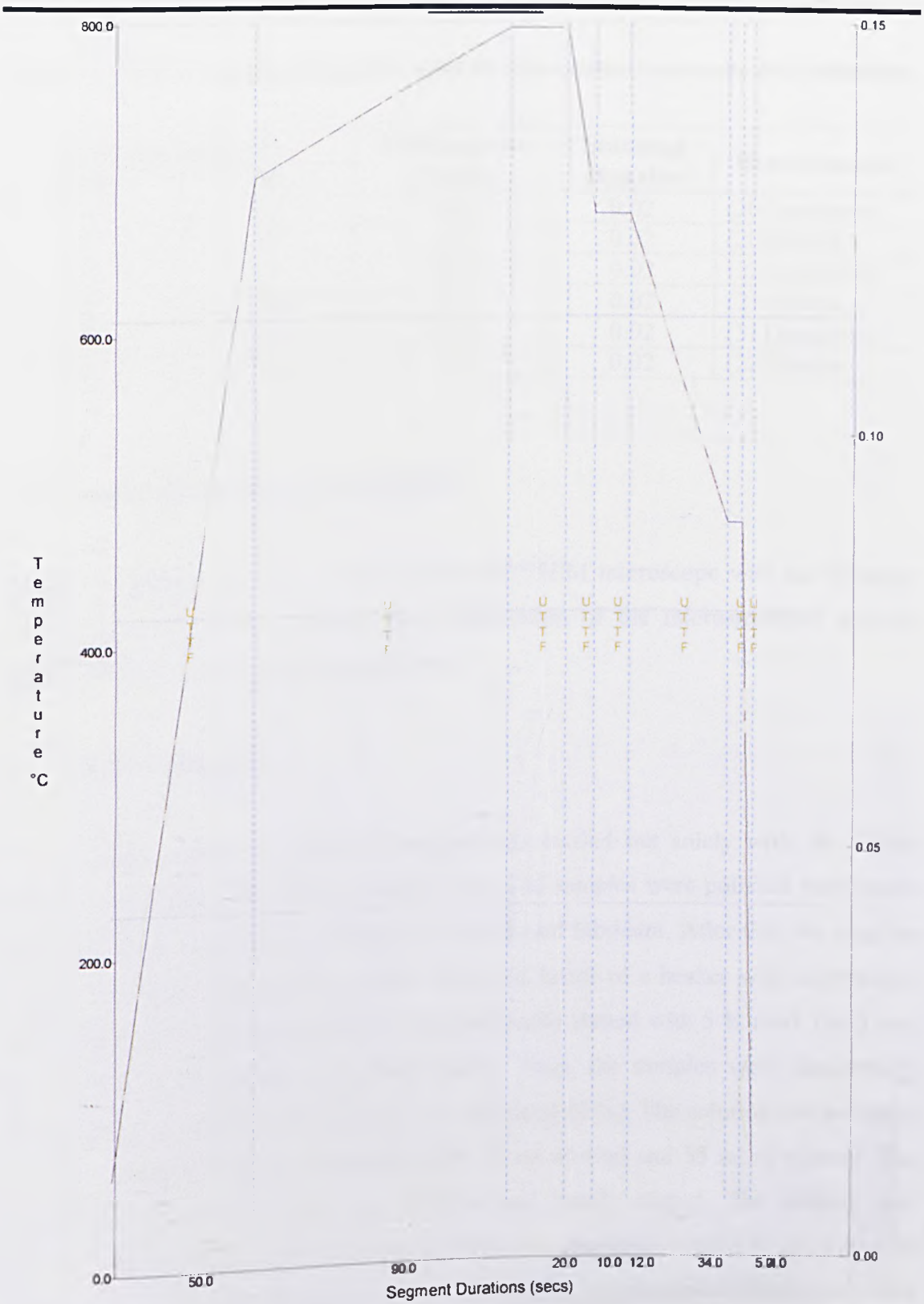

Fig. 3.4 Graph of the simulated annealing process.

Table 3.6 XRD scanning parameters used for the retained austenite determination.

Scanning angles (°)		Scanning rate (°/min)	Scanning step size	Phase scanned
From:	To:			
58	62	0.12	0.02	(200)austenite
75	79	1.2	0.02	(200)ferrite
87	92	0.12	0.02	(220)austenite
97	102	1.2	0.02	(211)ferrite
109	115	0.12	0.02	(311)austenite
121	126	1.2	0.02	(220)ferrite

3.5 Scanning electron microscopy (SEM)

For all the multiphase steels, a JEOL JSM 6400 SEM microscope with an operating voltage of 5~20 kV was used to gain information of the microstructural features between 5 000x and 15 000x magnification.

3.5.1 Sample preparation

The grinding process for the SEM samples was carried out solely with the silicon carbide paper 1200 grade under running water. The samples were polished with cloths using 6 μm and 1 μm diamond paste and water-based lubricant. After this, the samples were ultrasonically cleaned; the samples were put inside of a beaker with isopropanol for 8 minutes. Initially, the materials were chemically etched with 5 % nital, but it was not possible to distinguish each phase clearly. Thus, the samples were successfully etched with a mixed solution of nital (2 %) and picral (4 %). The solution was prepared at room temperature mixing 30 ml of picral, 15 ml of nital and 55 ml of ethanol. The samples were submerged into the solution and gently stirred. The etching was undertaken at 30 s time intervals. The best result was obtained between 90 and 120 s. In this way, the microstructure was well developed and it was possible to distinguish each phase.

3.6 Transmission electron microscopy (TEM)

3.6.1 Carbon extraction replicas

If the carbon replica is directly from a metal surface it can extract a particle from its surrounding matrix, thus allowing the phase alone to be analyzed without interference from electron scattering into the matrix as shown schematically in Figure 3.5 [68]. For the carbon extraction replicas, the samples were thoroughly polished, for approximately 10 minutes with 0.25 micron diamond paste and then lightly etched with 2% nital for 5 seconds. The samples were cleaned by putting a few drops of acetone on them and then carefully laying the acetate on the top, allowing the cellulose acetate to dry for a minimum of 30 minutes. They were removed when the carbon coater was ready. Once the sample was covered with carbon, it was scratched with a grid of ~ 2mm squares. To remove the carbon extraction replicas, the sample had to be put into 10% nital to soak until the carbon started to bubble. The sample was rinsed in methanol, then replaced into the nital and moved between the nital and methanol, keeping the sample in each solution for 30 seconds until bubbles appeared where the carbon was starting to lift off. The sample was carefully immersed at an angle in the de-ionised water, to use the surface tension to lift the carbon from it. Holding a 400 mesh copper grid by the rim, the carbon fragment was caught.

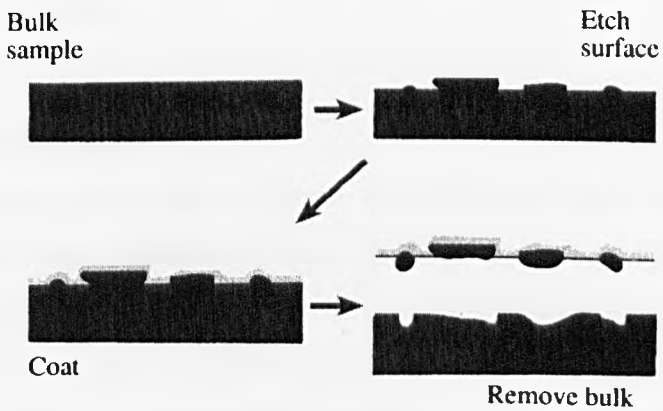

Fig. 3.5 Schematic steps of the carbon extraction replicas [68].

3.6.2 Thin foil sample preparation

TEM samples were prepared by mechanically thinning to 100 - 150 μm under running water. Disks of 3mm diameter were then punched and thinned into TEM foils up to 60 – 70 μm. Electropolishing was undertaken using 5% perchloric acid, 35% butoxyethanol and 60% methanol solution in a twin-jet electropolisher operating at 0.5 Amps and 38 V. The solution was freshly prepared each time and was cooled to -30 °C using liquid nitrogen. Immediately the foils were perforated they were cleaned in methanol, dried and stored in a dessicator.

3.6.3 TEM microscopes

A Philips 420 TEM microscope fitted with tungsten filament and operated with an accelerating voltage of 120 kV was used in this project. The microscope is fitted with a Link EDS (EDX) system. Both carbon extraction replicas and thin foils were examined in the Philips 420 TEM. For the precipitates size distribution the larger condenser aperture was used in combination with the medium size objective aperture. The optimal magnification to the precipitates quantification and measurement was of 52000x. At this magnification the precipitates were well distinguishable, but as large an area of the steel as possible was analysed.

3.7 Imaging analysis

3.7.1 Phases quantification

In order to estimate the volume fraction of the bainite and martensite phases, the micrographs that were obtained from the SEM were analysed using software SigmaScan Pro5. The contrast of the phases was increased in the image with the aim of facilitating measurement. The values from 15 SEM micrographs per sample were averaged. The analysis was undertaken both on the TRIP steels produced by Corus - IJmuiden in the plant and the materials processed on the laboratory scale.

Care was taken to compare like with like regions for the different sample conditions. In particular, regions were compared that would have been dominated by pearlite or by ferrite in the cold rolled condition were directly compared. However, it should be emphasised that such regions were not easy to identify in the final finished product, where the microstructure was much more homogenous.

3.7.2 Measurements precipitates and quantification

The particle diameter size distribution of the vanadium precipitates were measured from negatives of the TEM images taken from carbon extraction replicas, using the image analysis software SigmaScan Pro5. The images of the precipitates were taken from random areas on different samples to obtain representative precipitates size distribution data. The precipitates shape was mainly circular, so the mean diameter was measured. Between 800 and 1400 precipitates per composition were measured. The precipitation sequences were analysed in the multiphase steels in hot rolled conditions and on the stages 1, 2, 3 and 7 of the annealing process. Energy dispersive X-ray spectroscopy (EDS) was used to identify the precipitates. Indexing diffraction patterns was carried out using standard procedure. The software provided tabular values in pixels which were consequently converted to nanometres. The size distribution was plotted as a histogram.

Chapter 4 Results on the multiphase steels produced and provided by Corus

This chapter presents the results of the base composition and vanadium-microalloyed multiphase steels which were processed in plant trials by Corus. One of the objectives was to characterise the microstructure, in particular, the phase content, size and distribution to correlate with the observed mechanical properties.

4.1 Retained austenite content in the multiphase steels

The retained austenite, as pointed out earlier, plays a fundamental role in the balance between strength and ductility, so the first goal was to determine the austenite content in the base composition and vanadium microalloyed steels. Figure 4.1 shows XRD diffraction patterns of the multiphase steels (FA-1 and FA-5), which only exhibit peaks from bcc ferrite and fcc austenite. Retained austenite content was measured from the integrated intensities of austenite diffraction lines (200) fcc, (220) fcc and (311) fcc and ferrite diffraction lines (200) bcc, (211) bcc and (220) bcc. As expected, the austenite peaks are not as strong as the ferrite peaks. Table 4.1 shows the volume fraction of the retained austenite measured in the multiphase steels. The highest retained austenite was found in the samples with 0.12 wt % vanadium. The base composition steels had the lowest value of retained austenite. Thus, the retained austenite content increased with vanadium content.

Table 4.1 Retained austenite content of the multiphase steels produced by Corus.

Alloy	Steel	Vanadium Content(%wt)	Coiling Temperature (°C)	Retained Austenite (%)
Base composition	FA-1	N/A	583	4.8
Low Vanadium	FA-2	0.06	640	5.9
	FA-3	0.06	550	5.9
High Vanadium	FA-4	0.12	640	7.2
	FA-5	0.12	550	7.7

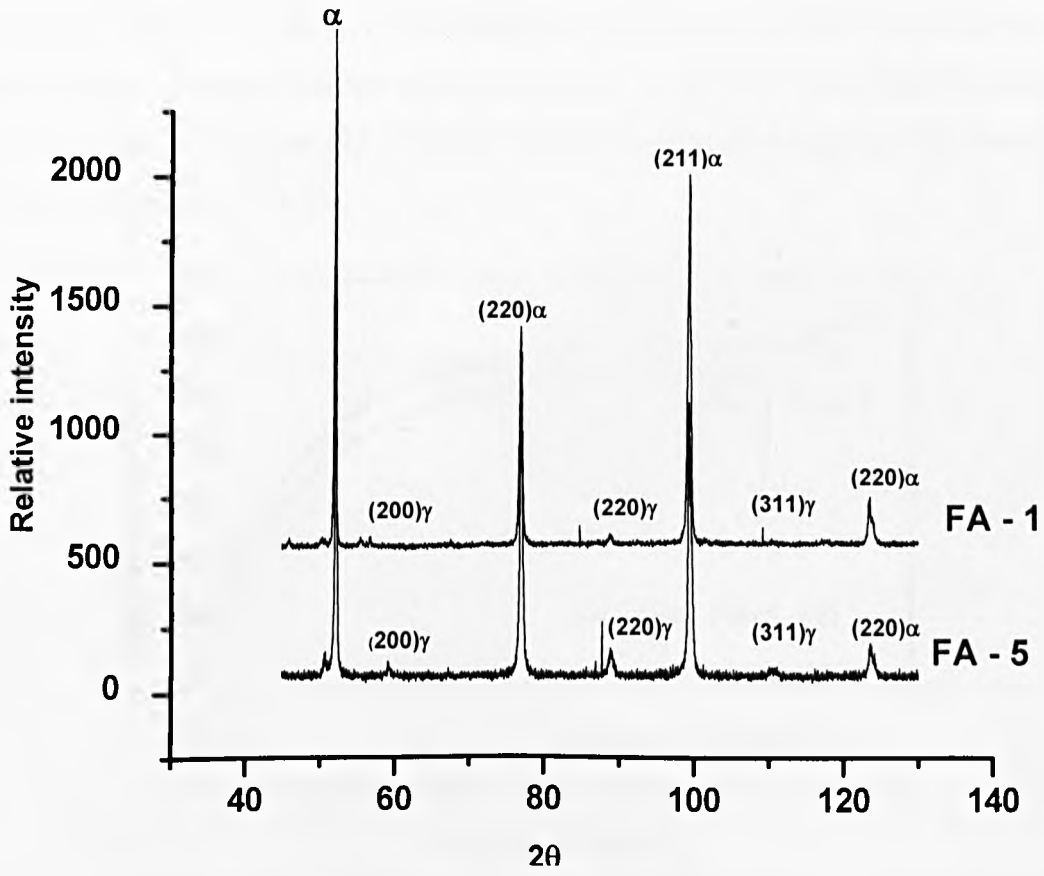

Figure 4.1 XRD diffraction patterns of the base composition (FA-1) and vanadium microalloyed steels (FA-5).

4.2 Tensile properties

Figures 4.2 and 4.3 show the stress – strain graphs of the multiphase steels, the tensile tests were carried out by Corus. Figure 4.2 shows the tensile results of the multiphase steel microalloyed with 0.06 wt % of vanadium (FA-2 and FA-3) and the base composition (FA-1); the highest UTS value corresponds to the low vanadium FA-3 steel with a coiling temperature of 550 °C. The base composition (FA-1) and the low vanadium FA-2 steel coiled at 640 °C have the same UTS value. Note that the base composition FA-1 shows a clear yield point that was not exhibited by the microalloyed steels. In the case of the steels microalloyed with 0.12 wt % of vanadium (FA-4 and FA5), Figure 4.3, the FA-5 sample with a coiling temperature of 550 °C has the highest UTS value, the lowest correspond to the base composition (FA-1) and the intermediate value was obtained by the FA-4 microalloyed steel coiled at 640 °C. Note that the highest retained austenite content also corresponds to the FA-5 steel which is consistent with the largest UTS value and similarly the lowest retained austenite was observed in the base composition (FA-1).

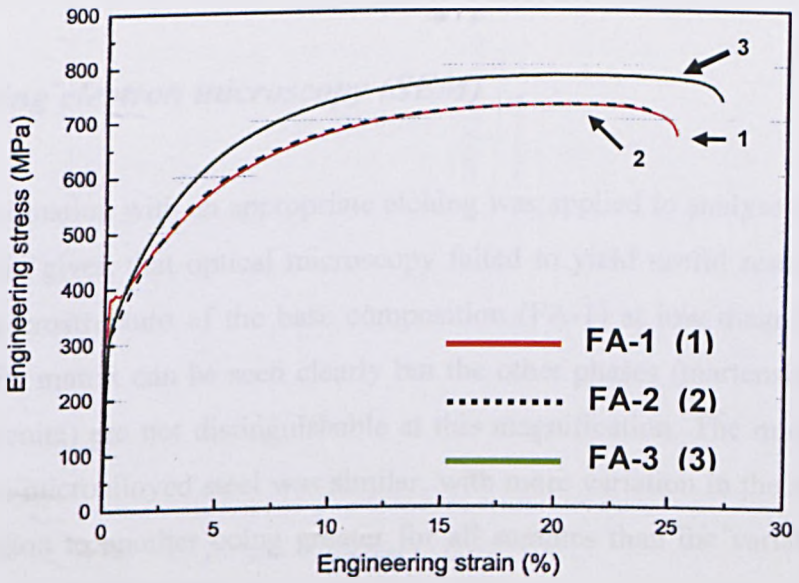

Fig. 4.2 Stress –strain graph of the multiphase steel microalloyed with 0.06 wt % of vanadium and coiling temperature of 640 °C (FA-2) and 550 °C (FA-3).

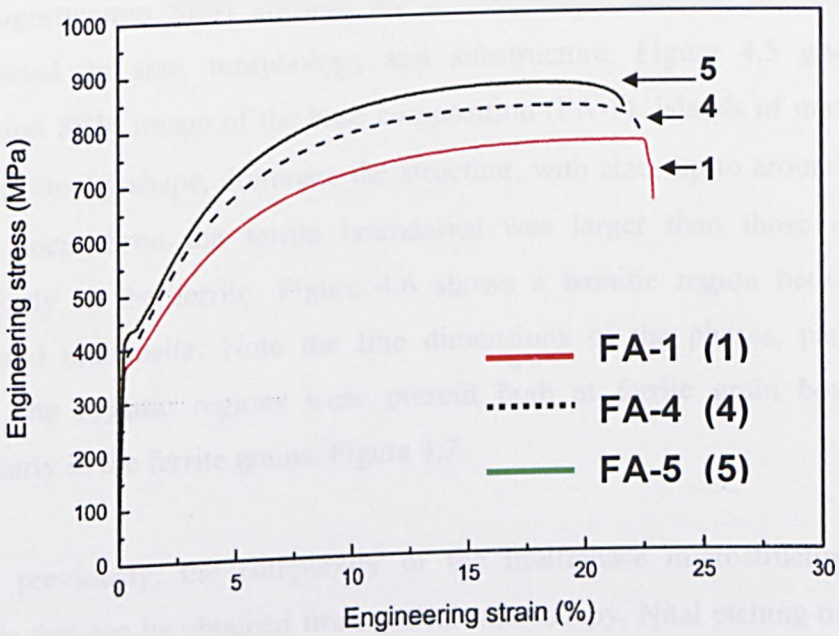

Fig. 4.3 Stress –strain graph of the multiphase steel microalloyed with 0.12 wt % of vanadium and coiling temperature of 640 °C (FA-4) and 550 °C (FA-5).

4.3 Scanning electron microscopy (SEM)

SEM in combination with an appropriate etching was applied to analyse the multiphase microstructure given that optical microscopy failed to yield useful results. Figure 4.4 shows the microstructure of the base composition (FA-1) at low magnification. Note that the ferrite matrix can be seen clearly but the other phases (martensite, bainite and retained austenite) are not distinguishable at this magnification. The microstructure of the vanadium microalloyed steel was similar, with more variation in the microstructure from one region to another being greater for all samples than the variations between different compositions.

4.3.1 Base composition (FA-1) multiphase steel

Higher magnification SEM allowed the differentiation between the various phases present, based on size, morphology and substructure. Figure 4.5 gives a higher magnification SEM image of the base composition (FA-1). Islands of martensite, with an irregular blocky shape, dominate the structure, with sizes up to around 4 μm. The martensite located on the ferrite boundaries was larger than those grains found intergranularly in the ferrite. Figure 4.6 shows a bainitic region between retained austenite and martensite. Note the fine dimensions of the phases, particularly the austenite. The bainitic regions were present both at ferrite grain boundaries and intergranularly in the ferrite grains, Figure 4.7.

As stated previously, the complexity of the multiphase microstructure limits the information that can be obtained from optical microscopy. Nital etching on its own did not adequately reveal the microstructure. A number of different etches were evaluated and the best was found to be a combination of nital and picric acid etching, which revealed both the ferritic grain structure and the substructure in the martensite and bainite, thereby allowing accurate determination of the phases present, see Figure 4.8 (a) and 4.9 (a). One commonly used etch, LePera, was unsuccessful for the current multiphase steels, as shown in Figure 4.10(a) where the full details of the microstructure were not developed. When the steel samples were etched with nital (5%) on its own, the second phases were differentiated from the ferrite matrix, but the etch failed to reveal which second phase was present i.e. the retained austenite could not be differentiated from martensite or bainite (Figure 4.10(b)). Equally, the nital etching failed to adequately reveal the ferrite grain structure. However, after a considerable investigation, the samples etched with a mixture of nital (5%) – picral (4%) and analysed by SEM developed a clear and distinguishable microstructure. Table 4.2 shows the amount of bainite and martensite present, measured by the Sigma-Scan Pro5 image analysis from an average of 15 SEM micrographs per composition (~ 2500 μm^2). Due to the complexity of the microstructure, the deviation and error standards were significant, Table 4.2.

4.3.2 Low (0.06%) (FA-2 and FA-3) and high (0.12%) (FA-4 and FA-5) vanadium steels

The main microstructural difference observed between the base composition and the vanadium microalloyed steels was the refinement in size of the different phases for the vanadium containing multiphase steels. Figures 4.11 and 4.12 show the finer and more uniform microstructure developed in vanadium steels compared to the base composition (FA-1) which was shown in Figure 4.4.

In the case of the low vanadium (0.06 wt %) (FA-2 and FA-3) steels, the bainitic colonies were around 2 μm on average (Figures 4.6, 4.13 and 4.14) and appear narrower than those developed in the base composition (FA-1) steel (Figure 4.6). The retained austenite was observed with a blocky shape and an average size of 1.5 μm (Figure 4.7 and 4.14). In addition, the RA was often located adjacent to the martensite, which some researchers refer to as the RA/M constituent (Figure 4.14 and 4.8). The retained austenite was also found in the centre and at the boundaries of the ferrite grains (15 SEM images on average per composition were analysed).

The martensite located at the ferrite boundaries had an irregular blocky shape (Figure 4.11). In Figure 4.8(a) a well defined martensite grain is shown, note that twinning can be observed, while in Figure 4.8(b) two martensite colonies are joined, indicating the morphology of the austenite during the intercritical annealing. The most uniform distribution of retained austenite was found in the high vanadium (0.12 wt %) (FA-4 and FA5) steel, Figure 4.12. The RA grain size was between 1 and 1.5 μm. In a similar manner to the low vanadium steels, it was observed that the martensite located at the ferrite grain boundaries was of an irregular blocky shape (Figure 4.15 and 4.9). The bainite formed was similar to the bainite observed in the base composition (FA-1) steel but its size was typically ~1 μm, which is smaller than the bainite developed in the base composition (FA-1) and low vanadium (FA-2 and FA-3) steel (Figures 4.16 and 4.9).

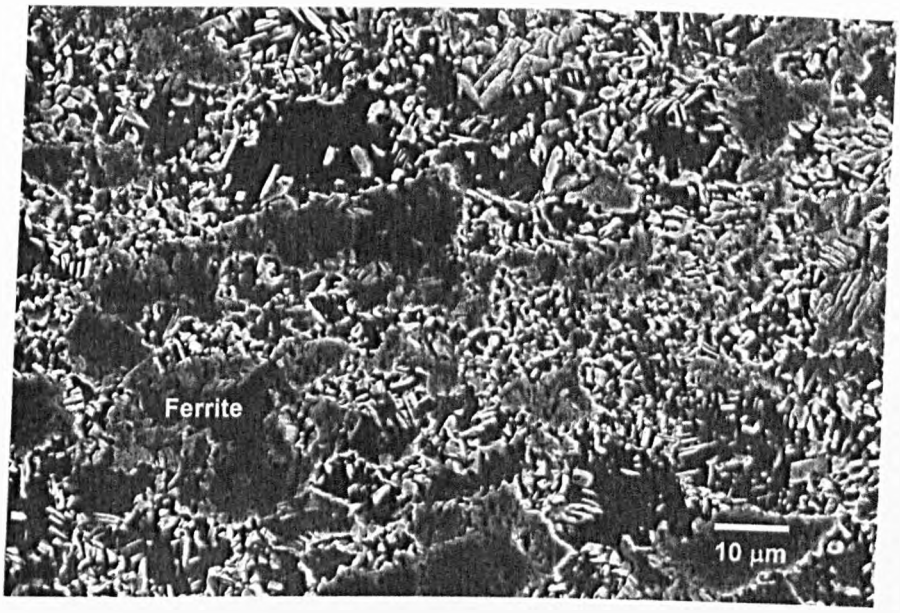

Fig. 4.4 SEM micrograph showing the rolling plane microstructure of the base composition (FA-1).

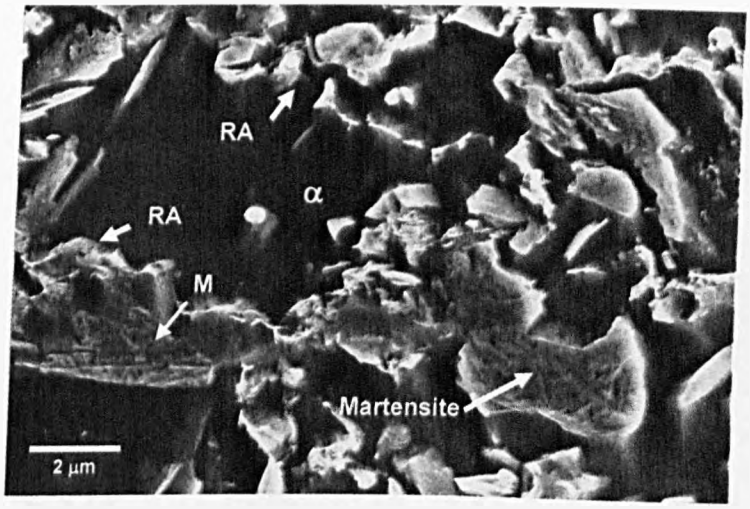

Fig. 4.5 SEM micrograph showing martensite and some retained austenite grains (arrowed), base composition (FA-1) steel.

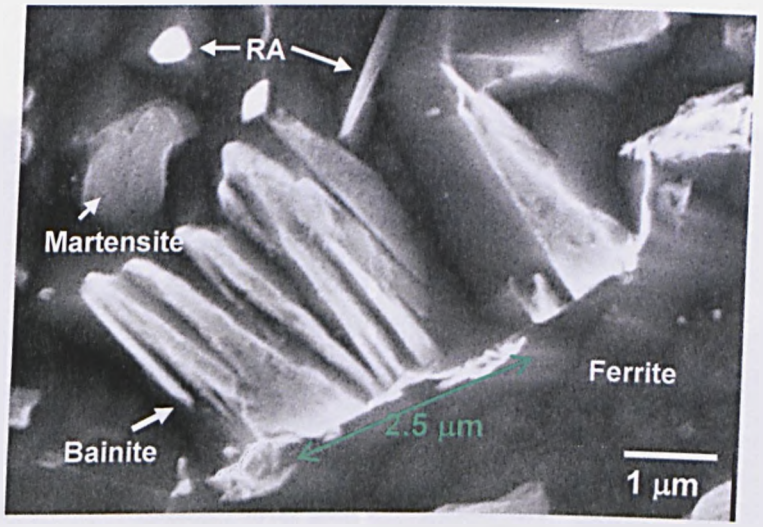

Fig. 4.6 SEM micrograph showing bainite between martensite and retained austenite, nital – picral etch, base composition (FA-1) steel, rolling plane.

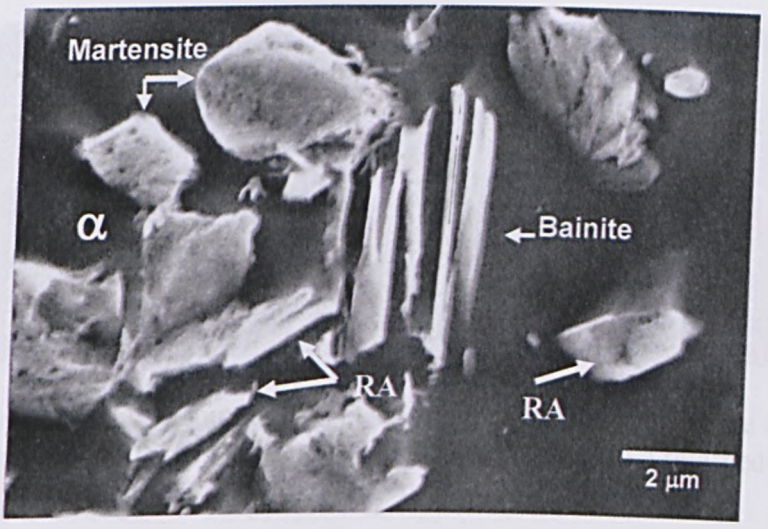

Fig. 4.7 SEM micrographs showing bainite, martensite and retained austenite, base composition (FA-1) steel.

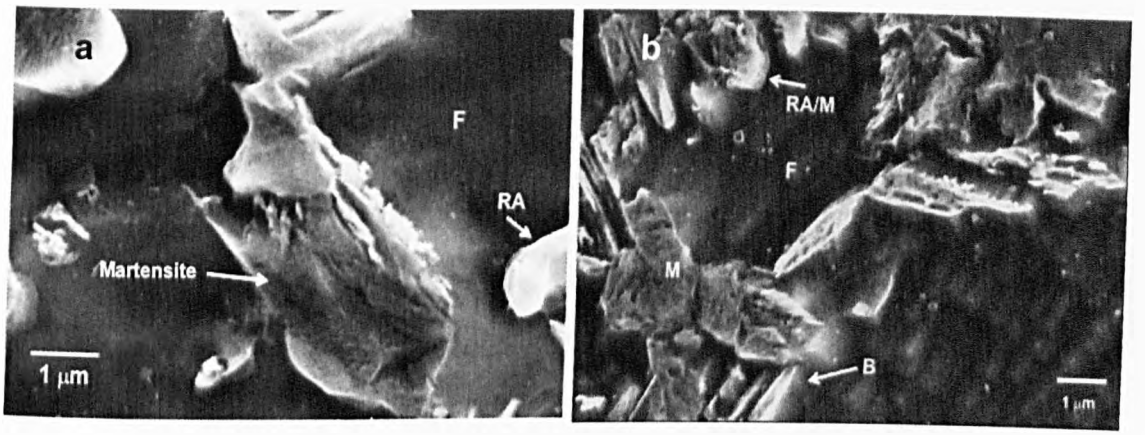

Fig. 4.8 SEM micrographs showing (a) martensite phase in the ferrite matrix, sample FA-2, longitudinal section, (b) retained austenite and martensite are mixed in the ferrite matrix and also martensite is close to a bainite grain, sample FA-3. nital – picral etch.

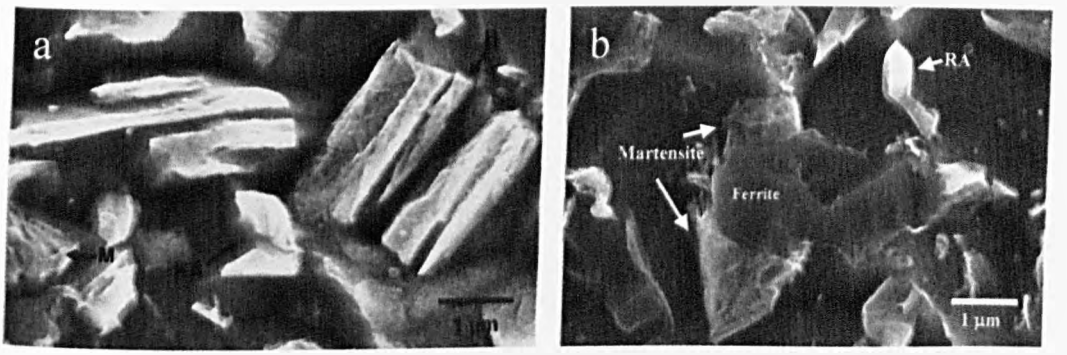

Fig. 4.9 SEM micrographs of sample FA-4 showing (a) bainite, martensite and retained austenite grains, (b) ferrite between martensite phases, close to a retained austenite grain, nital – picral.

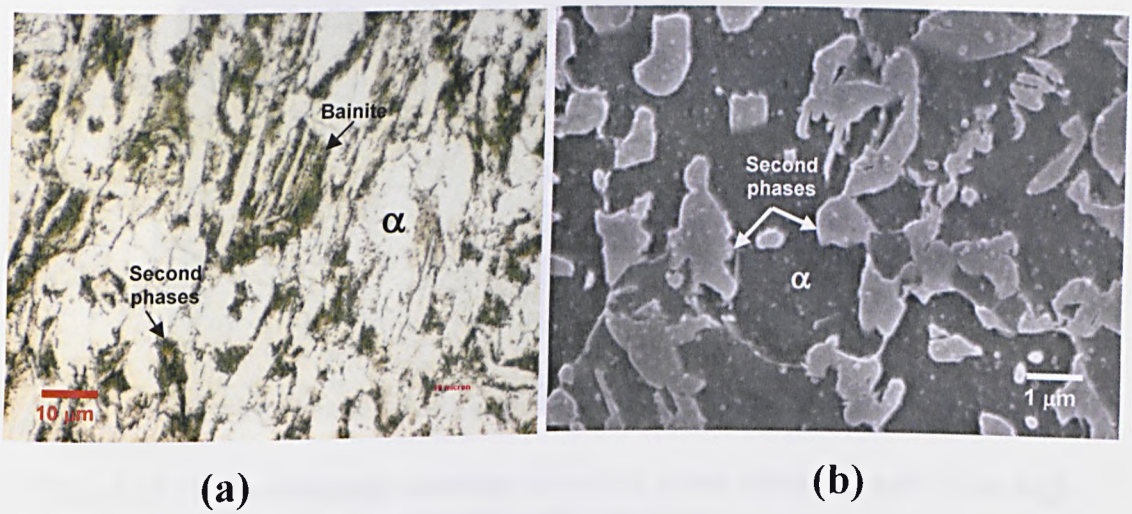

Fig. 4.10 Base composition (FA-1) microstructure etched with (a) LePera (optical micrograph) and (b) 5% nital (SEM micrograph).

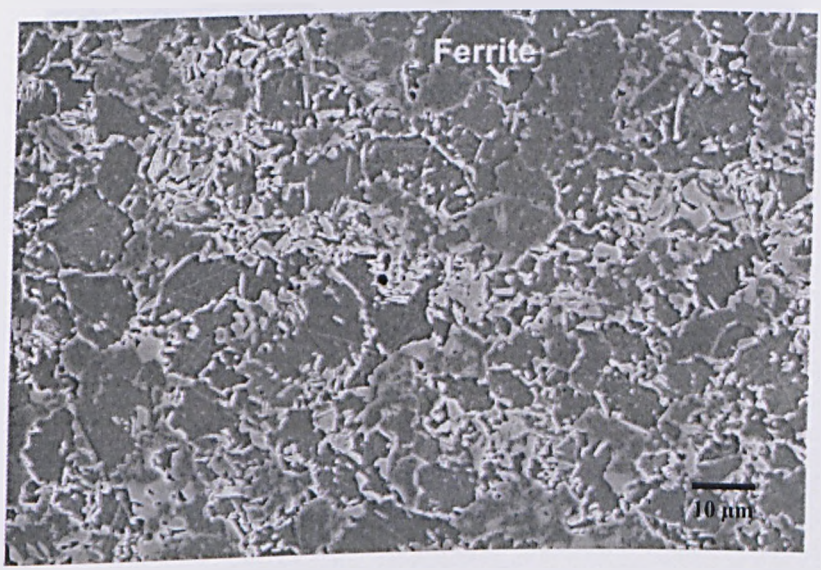

Fig. 4.11 SEM micrograph showing the rolling plane microstructure of the low vanadium (FA-2).

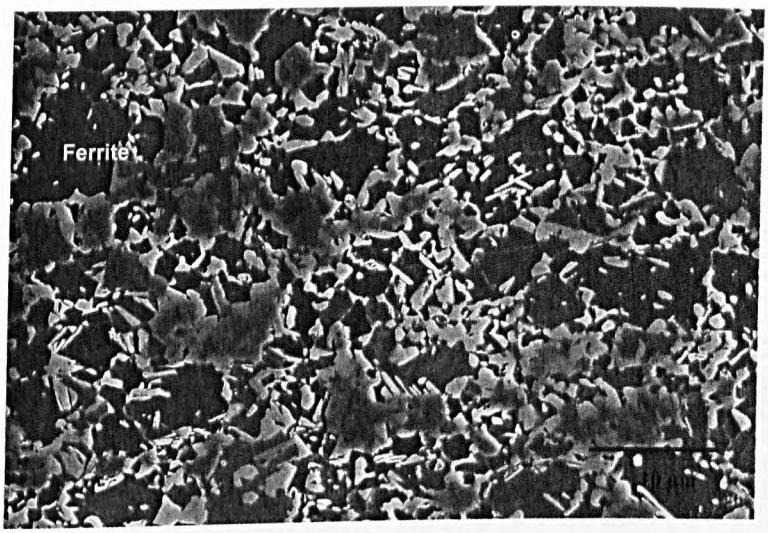

Fig. 4.12 SEM micrograph showing the rolling plane microstructure of the high vanadium (FA-5) steel.

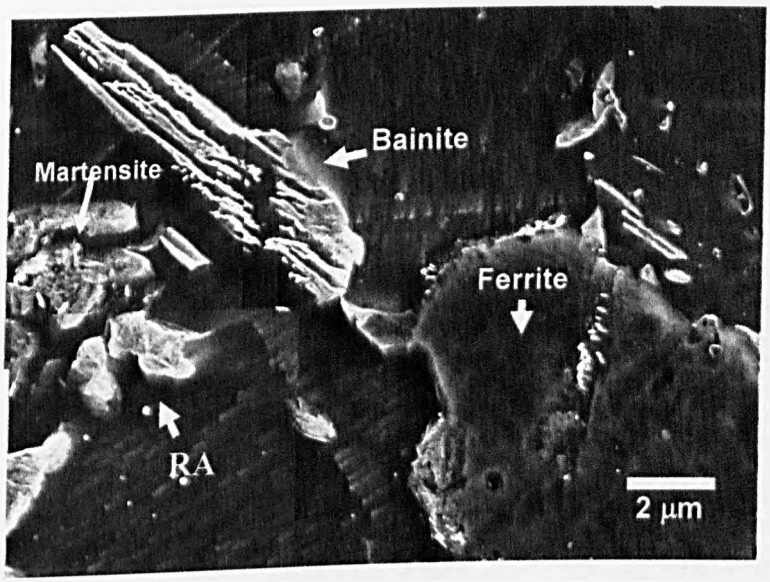

Fig. 4.13 SEM micrograph showing bainite, martensite and retained austenite and the ferrite matrix in the low vanadium (FA-2) steel.

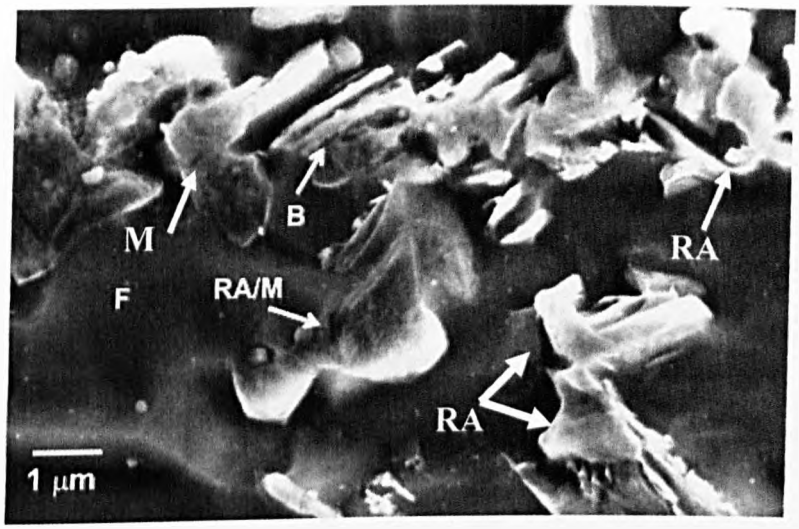

Fig. 4.14 SEM micrograph showing bainite surrounded by martensite and retained austenite grains, longitudinal section, low vanadium (FA-2) steel.

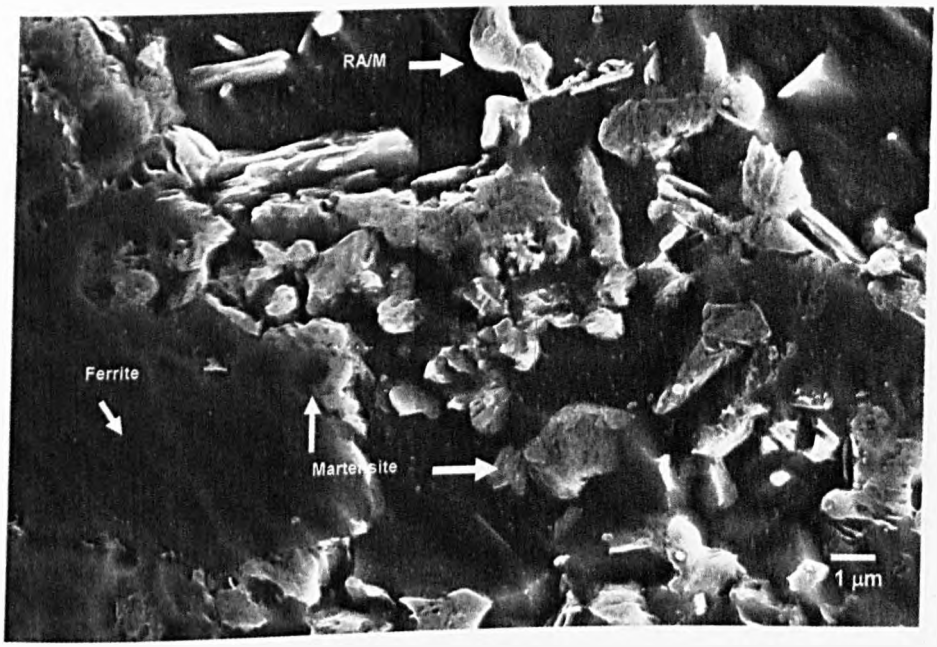

Fig. 4.15 SEM micrograph showing the microstructure of the high vanadium (FA-5) steel, martensite and RA/M are indicated in the ferrite matrix.

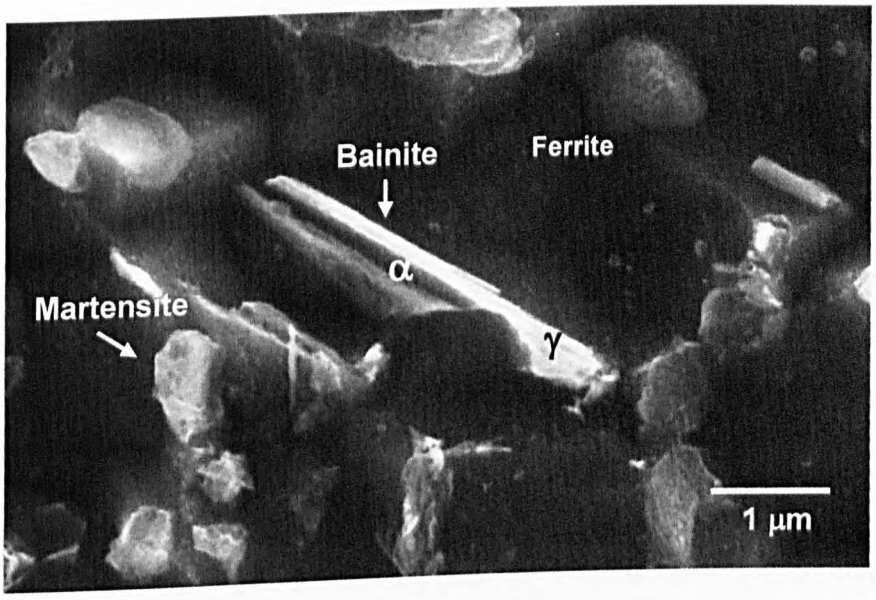

Fig. 4.16 SEM micrograph showing bainite and martensite in the high vanadium (FA-5) steel.

Table 4.2 Bainite and martensite content of multiphase (TRIP) steel.

Steel	Bainite (%)	Standard deviation of the bainite	Martensite (%)	Standard deviation of the martensite
FA-1	4.8	1.0	18	3.6
FA-2	3.5	1.4	20	3.4
FA-3	3.4	1.3	18	3.5
FA-4	3.2	0.7	18	3.7
FA-5	3.3	0.7	15	3.2

4.4 TEM examination

The shape and distribution of the different phases in the microstructure of the base composition and vanadium microalloyed steel were alike. Transmission electron microscopy (TEM) permitted the characterisation of each phase in a more accurate way. For example, the microstructures of the FA-1 steel shown in Figure 4.17 can be compared to the SEM image in Figure 4.6. Not surprisingly, they look similar but more detail can be observed in Figure 4.17, i.e. the form of bainitic laths, the locally increased dislocation density in the ferrite and evidence of retained austenite adjacent to the bainitic laths. The majority of the retained austenite was located intragranularly in the ferrite grains, Figure 4.18 (FA-2 steel). The RA was mainly rounded in shape, but in addition, elongated shaped retained austenite was also found in the centre of the ferrite grains, Figure 4.19 (FA-2 steel). The RA grains often contained fine twins, which were presumably recrystallisation twins. The martensite was found distributed at the ferrite grain boundaries and intragranularly in the ferrite and often associated with retained austenite, Figures 4.20 and 4.21 (FA-4 steel). Figure 4.22 shows a region of bainite in the low vanadium (FA-3) steel. Using dark field imaging, evidence of retained austenite was found at the lath interface, Figure 4.22(b). In addition, vanadium-based precipitates were found inside this phase, as shown in Figure 4.23 – in this case for the high vanadium (FA-4) steel. For the vanadium-bearing steels, the vanadium-based precipitates were found in all regions; throughout the ferritic matrix and within the austenite and bainite regions, see Figures 4.23-25 (FA-4 steel). Given the fine size of the precipitates and the complexity of the microstructure, it was not possible to quantify the size or fraction within each phase. Therefore, carbon extraction replicas in combination with EDS were used to determine the vanadium carbide precipitate distribution. The size distribution of the vanadium precipitates are shown in the histograms Figure 4.28. The number of particles quantified were between 600 and 1100 and for this measurement the average number of replicas were of 30 – 35 per composition.

As expected, in the high vanadium (FA-4 and FA-5) steels the precipitate number was higher than produced in the low vanadium (FA-2 and FA-3) steels, Figure 4.28. As shown in Figure 4.24, several precipitates were found inside and surrounding the retained austenite grains. The high vanadium (FA-4 and FA-5) steels exhibited a more homogenous size distribution of vanadium-based precipitates than observed in the low vanadium steels series FA-2 and FA-3 (Figures 4.26, 4.27 and 4.28). Figure 4.27 demonstrates how the precipitates were dispersed throughout the ferrite matrix and how some of them were located in the boundaries. Positive identification of precipitate type was made using the dark field imaging (Figure 4.27(b)). The precipitation behaviour developed by all the vanadium steels was quite similar, see Figure 4.28. This figure confirms the higher precipitate amount in the higher vanadium steels (See Table 4.3). In all cases, there was evidence of a bimodal size distribution, with finer precipitates approximately in the size range 6 to 17 nm and the coarser in the range 18 to 30 nm. Although difficult to compare, the size distributions appeared similar for the low vanadium steels (FA-2 and 3) and for the high vanadium steels (FA-4 and 5). In contrast, the coiling temperature did not appear to influence the size distribution (compare FA-3 and FA-5, or FA-2 and FA-4, which have the same coiling temperature, but have quite different size distributions).

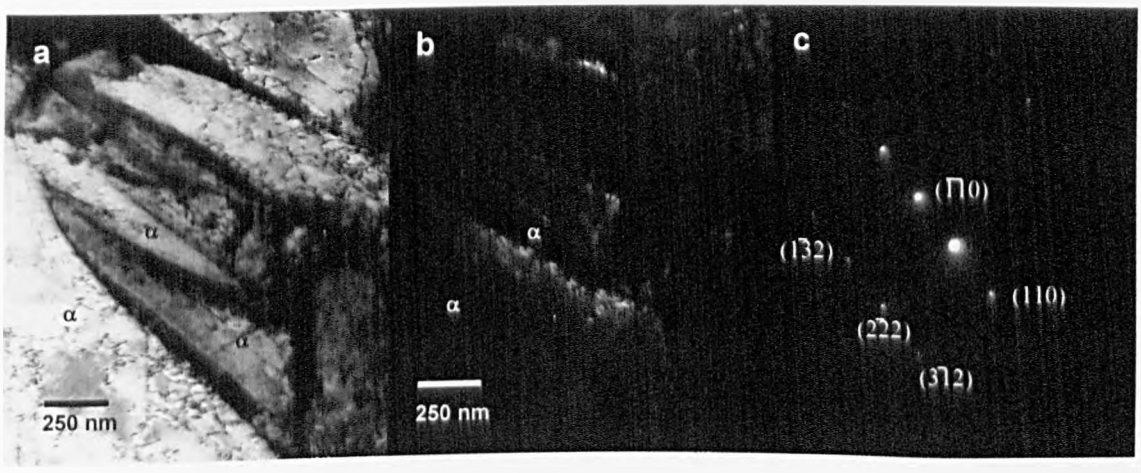

Fig. 4.17 TEM images showing a bainitic region; (a) bright field, (b) dark field and (c) diffraction pattern, sample FA-1(base composition multiphase (TRIP) steel).

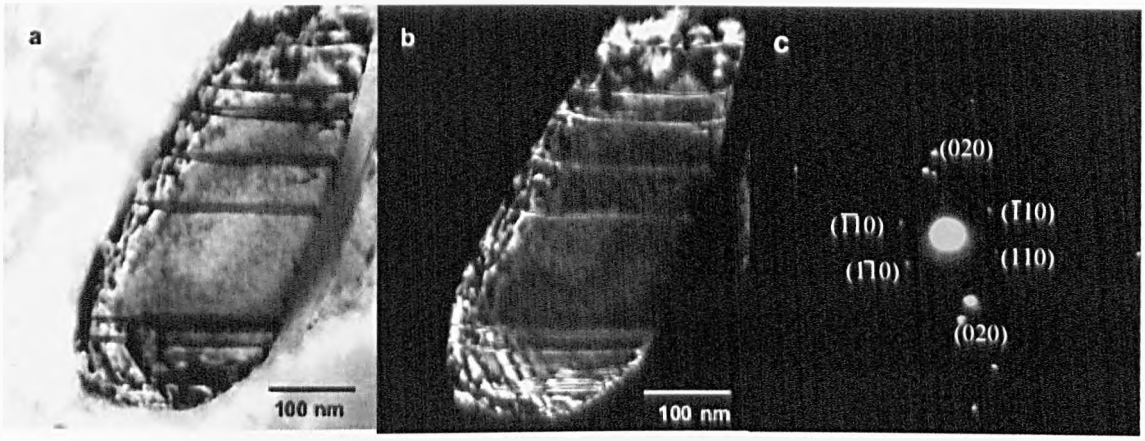

Fig. 4.18 TEM micrographs showing retained austenite located within a ferrite grain; (a) bright field, (b) dark field and (c) the diffraction pattern, sample FA-2 (low vanadium-0.06 wt %V (CT640 °C)).

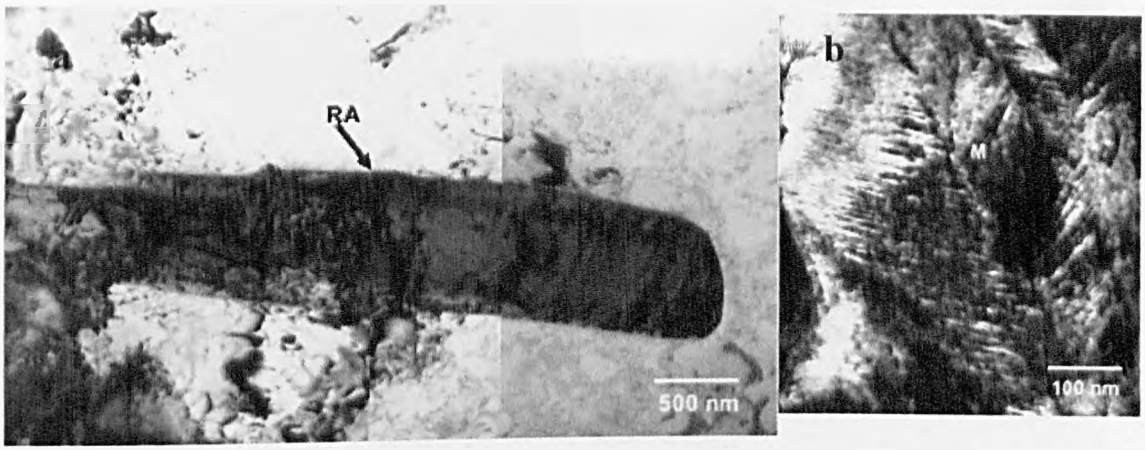

Fig. 4.19 TEM bright field micrographs showing (a) elongated retained austenite particle within a ferrite grain and (b) a martensitic region showing fine twins, sample FA-2 (low vanadium-0.06 wt %V (CT640 °C)).

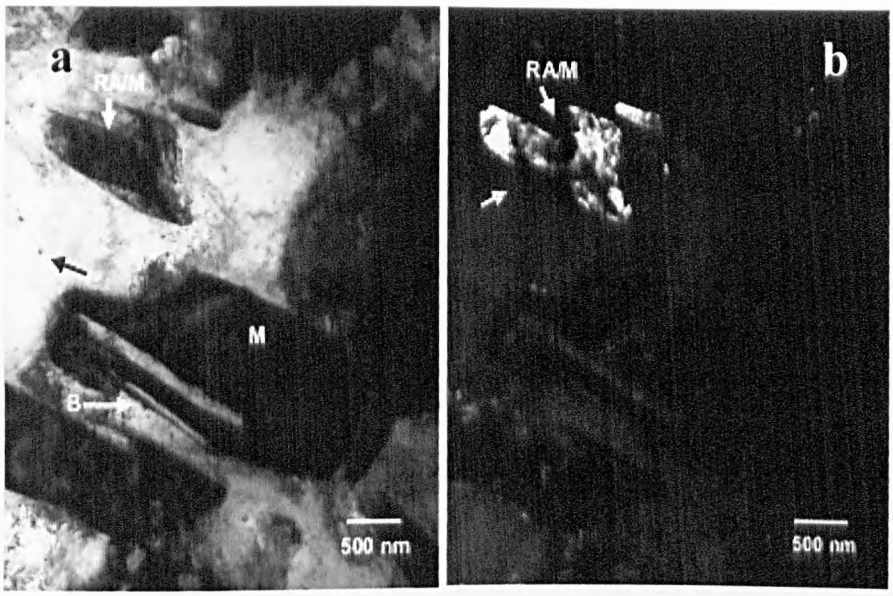

Fig. 4.20 TEM micrographs, (a) bright field image showing bainite, martensite and retained austenite and (b) dark field image showing retained austenite and some martensite. The arrows indicate the positions of the vanadium carbide precipitates, sample FA-4.

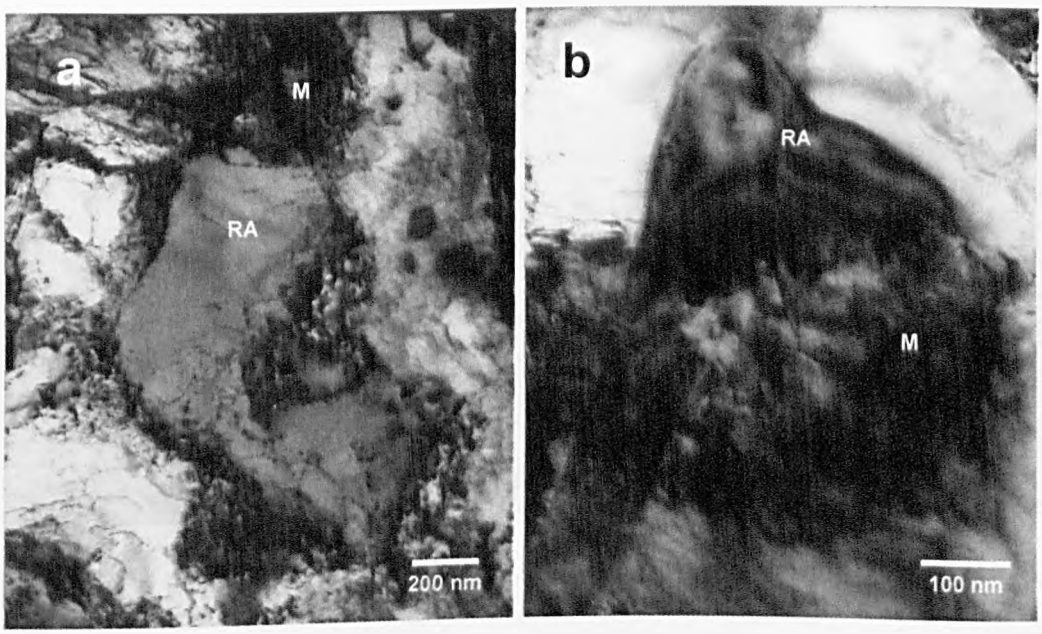

Fig. 4.21 TEM bright field micrographs showing retained austenite and a high local dislocation density in the ferrite in the base composition (FA-1) steel.

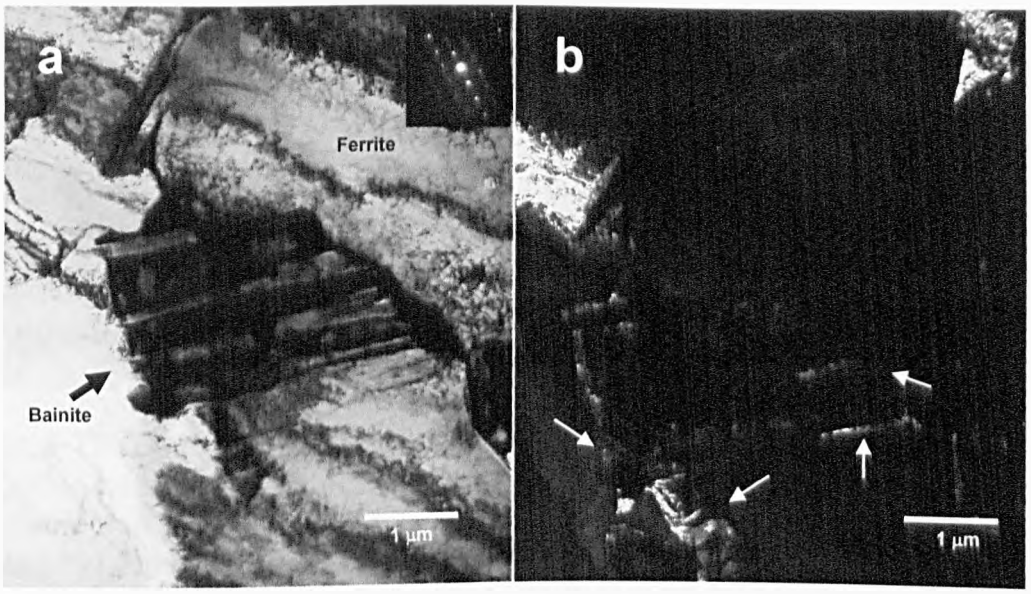

Fig. 4.22 TEM micrographs showing a bainitic region - (a) bright field and (b) dark field. The arrows indicate vanadium carbide precipitates close to the bainite, sample FA-3.

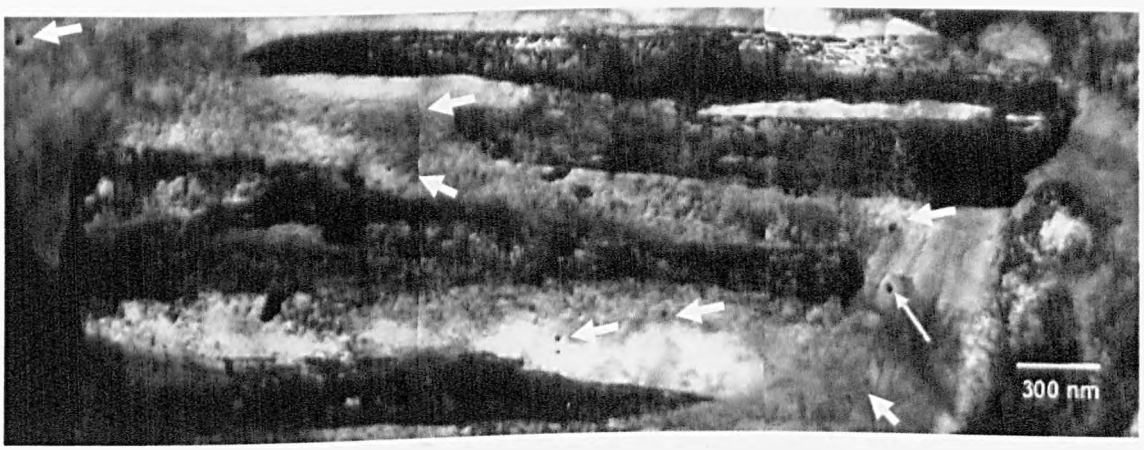

Fig. 4.23 TEM bright field micrograph showing a bainitic region. The arrows indicate vanadium carbide precipitates. Sample FA-4 (high vanadium – 0.12 wt %V (coiling temperature 640 °C)).

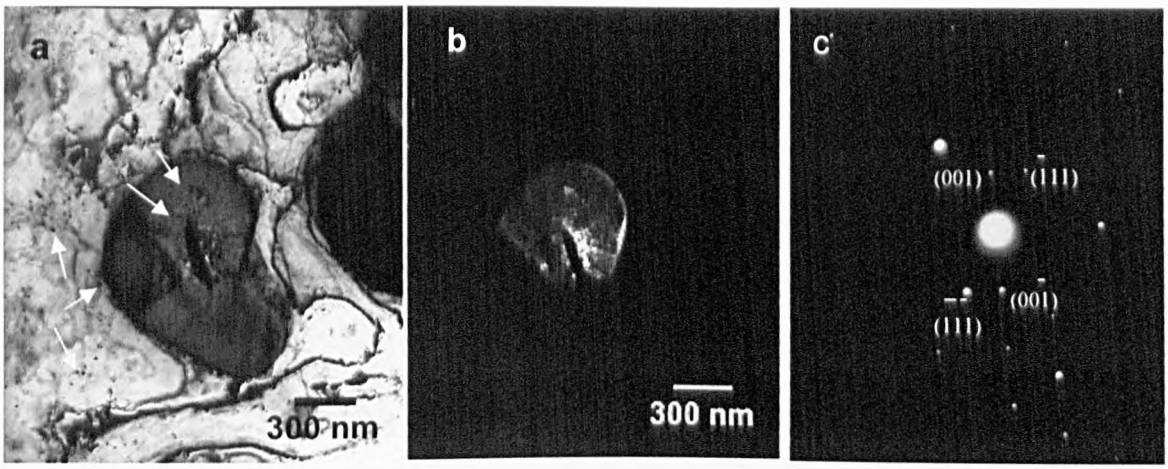

Fig. 4.24 TEM micrographs showing retained austenite located in a ferrite grain; (a) bright field image, (b) dark field image and (c) diffraction pattern. Vanadium carbide precipitates can be seen in both the ferrite and the austenite (indicated by arrows, sample FA-4 (high vanadium – 0.12%V (CT 640°C)).

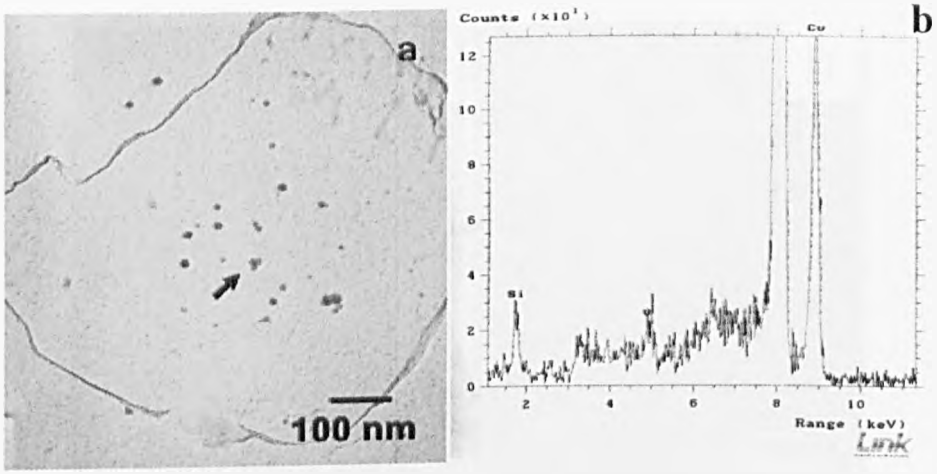

Fig. 4.25 Bright field TEM micrograph of a carbon extraction replica, showing (a) vanadium carbide precipitates inside grain and (b) EDS analysis, sample FA-4 (0.06 wt %V (CT 640 °C)).

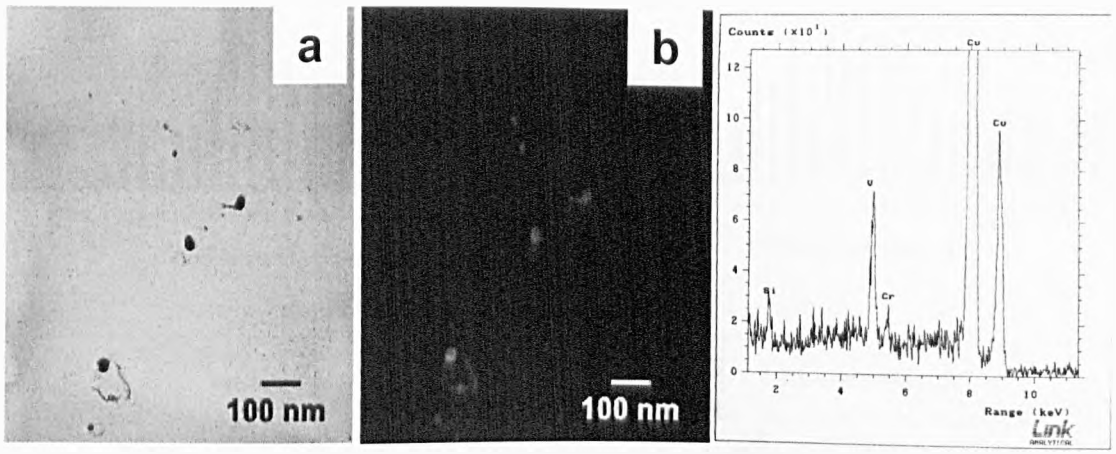

Fig. 4.26 TEM micrographs of a carbon extraction replica. (a) Bright field image showing vanadium carbide precipitates and (b) in the dark field, image, which shows a few more precipitates than (b) the bright field image. The EDS analysis confirmed that vanadium presence; sample FA-5 (0.06 wt %V (CT 550 °C)).

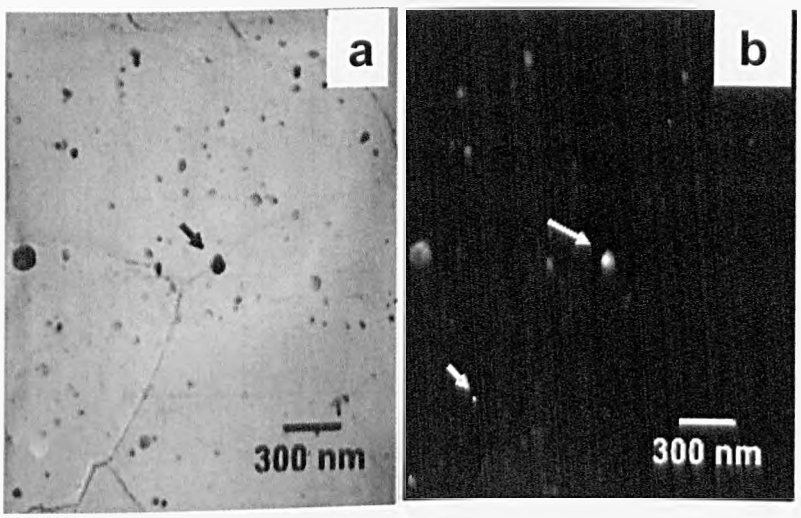

Fig. 4.27 Bright field TEM (a) and dark field (b) showing vanadium carbide precipitates, indicated by arrows, for sample FA-5 (0.12 wt %V (CT 550 °C)).

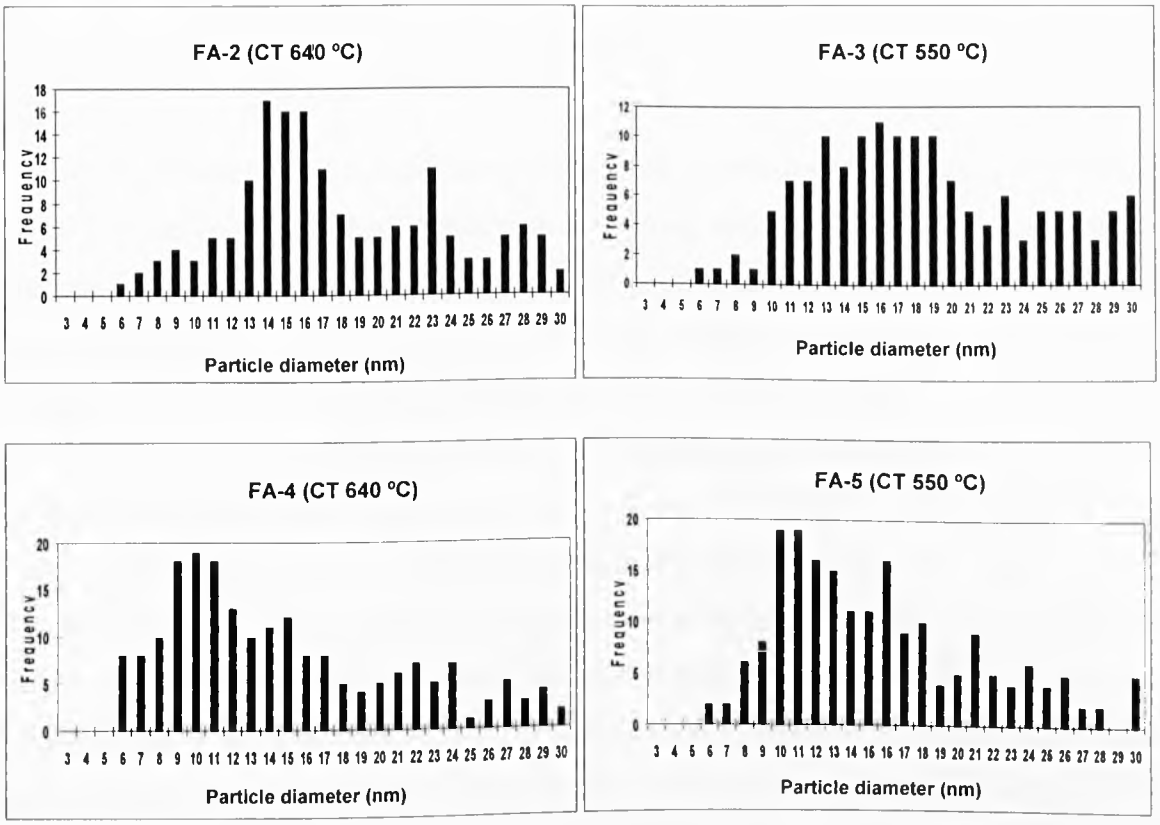

Fig. 4.28 Distribution and average diameter of the vanadium carbide for the microalloyed steels.

Table 4.3 Precipitates density for commercial multiphase steels

Steel	Precipitates/μm^2
FA-2	11.3
FA-3	11.7
FA-4	17.6
FA-5	18.6

4.5 Summary

The microstructure of the base composition and vanadium microalloyed multiphase (TRIP) steels consisted of a ferritic matrix, bainite, martensite and retained austenite. Retained austenite was found in the form of rounded and elongated crystals intragranularly in the ferrite grains and was also located with the bainite and martensite. A high dislocation density was observed in the ferrite adjacent to second phases, including austenite, bainite and martensite. Martensite was distributed in a random way in the ferritic matrix with an irregular blocky shape. The XRD results indicated higher values of retained austenite in the higher vanadium containing steel, FA-5 steel (7.7 wt %), the lowest value correspond to the base composition, FA-1 steel (4.7 wt %) and the intermediate values was obtained for the steels with intermediate vanadium composition, FA-2 and FA-3 (5.9 wt %). In a similar manner the highest UTS value was obtained for the FA-5 steel, while the FA-1 and FA-2 steels have the same UTS values, however the FA-1 shows a clear yield point that was not exhibited by the FA-2 microalloyed steel which showed a tensile curve similar to the developed by Dual Phase steels. According to the image analysis the base composition FA-1 steel has the highest bainite content (4.8 %); the vanadium microalloyed steel has a similar bainite content of between 3 and 3.5 %. The martensite content was very similar in all the multiphase steels at about 18 % on average. The data analysis of the precipitates suggested that mean size of the vanadium carbide precipitates was in the range of 6 – 17 nm for the FA-2 and FA-3 steels. In the case of the FA-3 and FA-4 steels the range was of 11 – 17 nm. No coiling effect on the vanadium carbide precipitation behaviour was observed, but the vanadium content did appear to affect the size distribution.

Chapter 5 Results on the intercritically annealed cold – rolled steels

This chapter presents the microstructural evolution and vanadium carbide precipitation behaviour of the base composition and microalloyed cold – rolled steels at the different stages of the intercritical annealing process, as simulated in the laboratory.

5.1 Retained austenite content

5.1.1 Variations of retained austenite content in the different stages of the annealing process

Retained austenite (RA) plays a fundamental role in the performance of the multiphase steels. The RA has a direct effect on mechanical properties such as strength and ductility; these properties are improved positively depending on the RA content. In addition, the bainite and martensite transformation is determined by the retained austenite properties such as thermal stability, carbon content, shape and size. For this reason it is important to perform the most precise characterization and quantification of the retained austenite.

The intercritical annealing process applied to the multiphase steels was described in Chapter 3, Figure 3.2. XRD analysis was carried out on all the intercritically annealed specimens to determine volume fraction of retained austenite and its carbon content. In order to follow the austenite evolution of the multiphase steel, XRD was applied in each stage of the annealing process.

Figure 5.1 corresponds to the base composition (A1) steel heated at 695°C where the X-ray diffraction pattern at the angle where (200) austenite peak is located, indicating that, as expected, the retained austenite content was below detectable levels at Stage 1.

Figure 5.2 shows the XRD diffraction pattern of the base composition (A1) and vanadium microalloyed (B1, C1) steels heated at 795 °C, corresponding to Stage 2 of the heat treatment, clearly showing the presence of austenite. The XRD diffraction pattern shows that the austenite peaks of the A1 steel look slightly less intense than the austenite peaks of vanadium microalloyed steels (B1 and C1). This difference in the intensity of peaks can be observed more clearly in Figure 5.3 where the individual $(220)_\gamma$ austenite peaks are present.

The austenite content was evaluated in the same manner for all samples at each stage of the annealing process. A summary of results from this is presented in Table 5.1.

The effect of vanadium on the retained austenite content is plotted in Figure 5.4. Note that despite vanadium being a stronger carbide former, the retained austenite content is increased as the percentage of vanadium increases. A similar result was found by Heller and Nuss [65] using Nb and Nb+Ti additions to similar base compositions.

The highest austenite content was produced at 795 °C; see Figure 5.5, and decreased with the decrease in the annealing temperature. Note that the vanadium microalloyed (B1, B2 and C1, C2) steels exhibited a higher retained austenite content compared to the base composition (A1) multiphase steel.

5.2 Variations of carbon content in the retained austenite at the different stages of the annealing process

The stability of the retained austenite below the A1 temperature is also controlled by its carbon content; thus it is important to measure the carbon content in the austenite. This cannot be measured directly, and therefore the standard indirect method was used, namely careful analysis of the lattice parameter of the austenite for each stage of the annealing process by means of XRD. The lattice parameter, a_γ, of the austenite was calculated by the Nelson-Riley method [69].

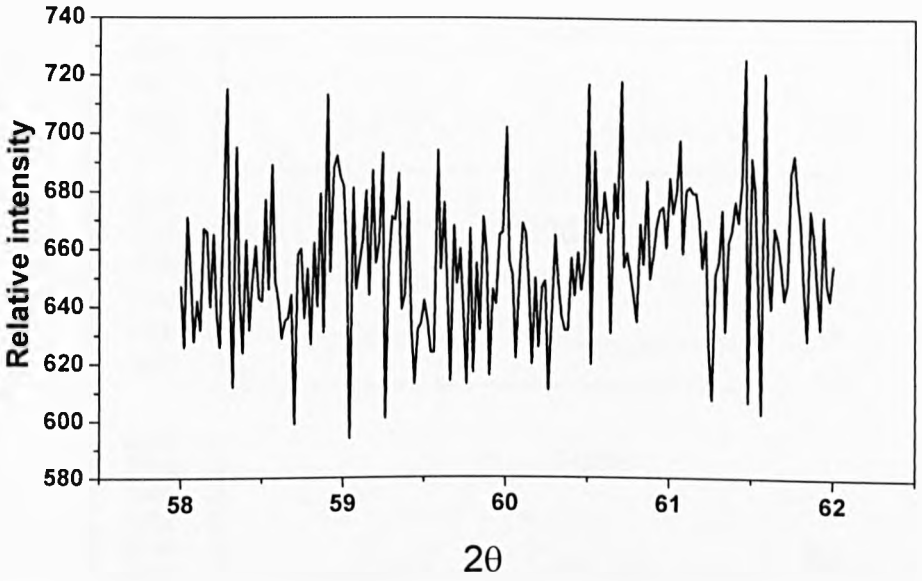

Figure 5.1 XRD diffraction pattern corresponding to the base composition (A1) steel heated at 695 °C – Stage 1, in the $(200)_\gamma$ angle.

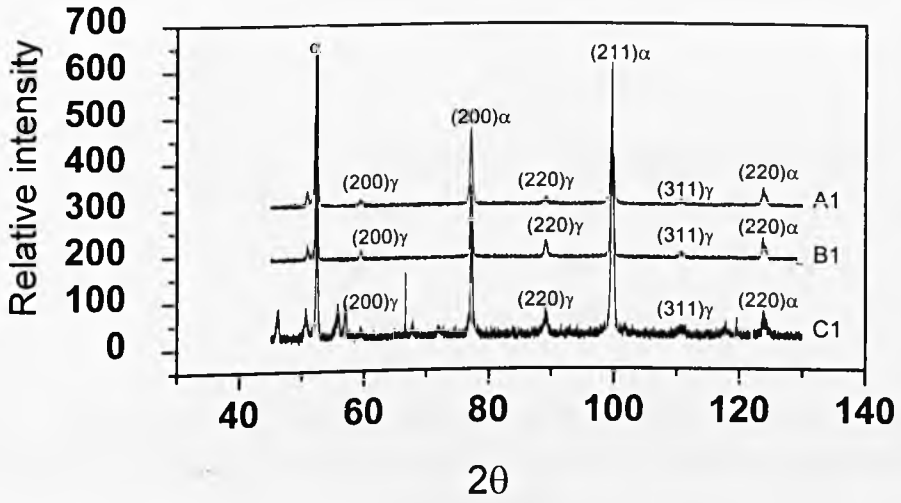

Fig. 5.2 XRD diffraction patterns of the base composition (A1), low vanadium (B1 - 0.06 wt %, CT 640 °C) and high vanadium (C1 - 0.12 wt %, CT 640 °C).

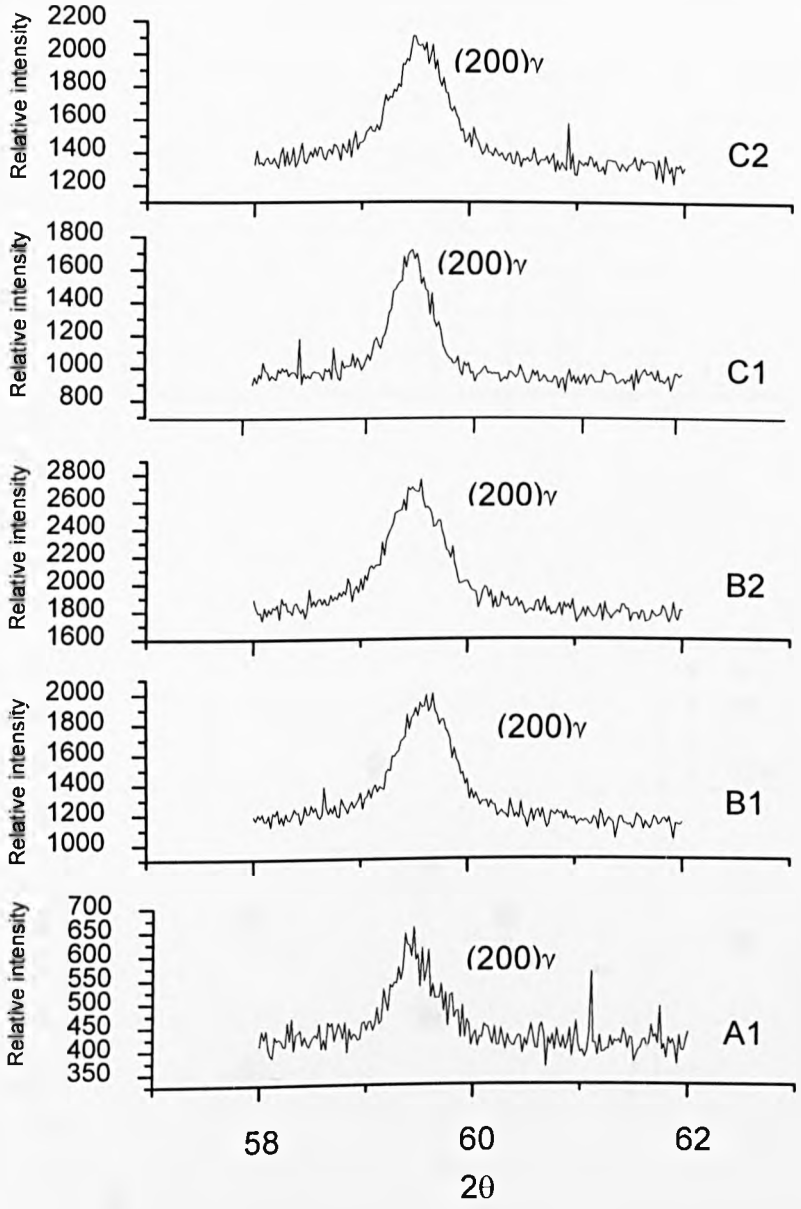

Fig. 5.3 Individual XRD diffraction patterns of the base composition (A1), low vanadium (B1 and B2) and high vanadium (C1 and C2) steels corresponding to the $(200)_{\gamma}$ angle.

Table 5.1 Variation in the retained austenite content for each stage of the annealing process.

	Retained austenite (%)						
Steel	**Stage 1**	**Stage 2**	**Stage 3**	**Stage 4**	**Stage 5**	**Stage 6**	**Stage 7**
A1	0.0	9.3	10.1	9.0	8.1	7.5	7.0
B1	0.0	11.2	13.0	12.7	12.3	12.0	11.3
B2	0.0	10.9	12.7	12.3	12.1	11.7	10.9
C1	0.0	13.0	14.3	13.8	13.0	12.7	11.9
C2	0.0	12.0	14.2	13.7	13.4	13.0	12.6

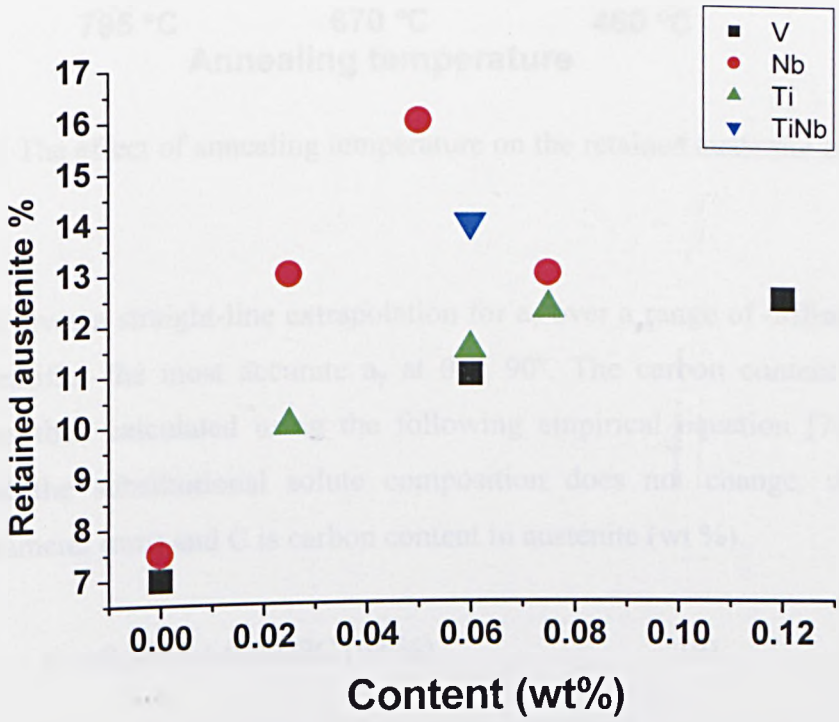

Fig. 5.4 The effect of vanadium on the retained austenite content (■=current data). Similar effect was found by Heller and Nuss using Nb, Ti and Ti+Nb [65].

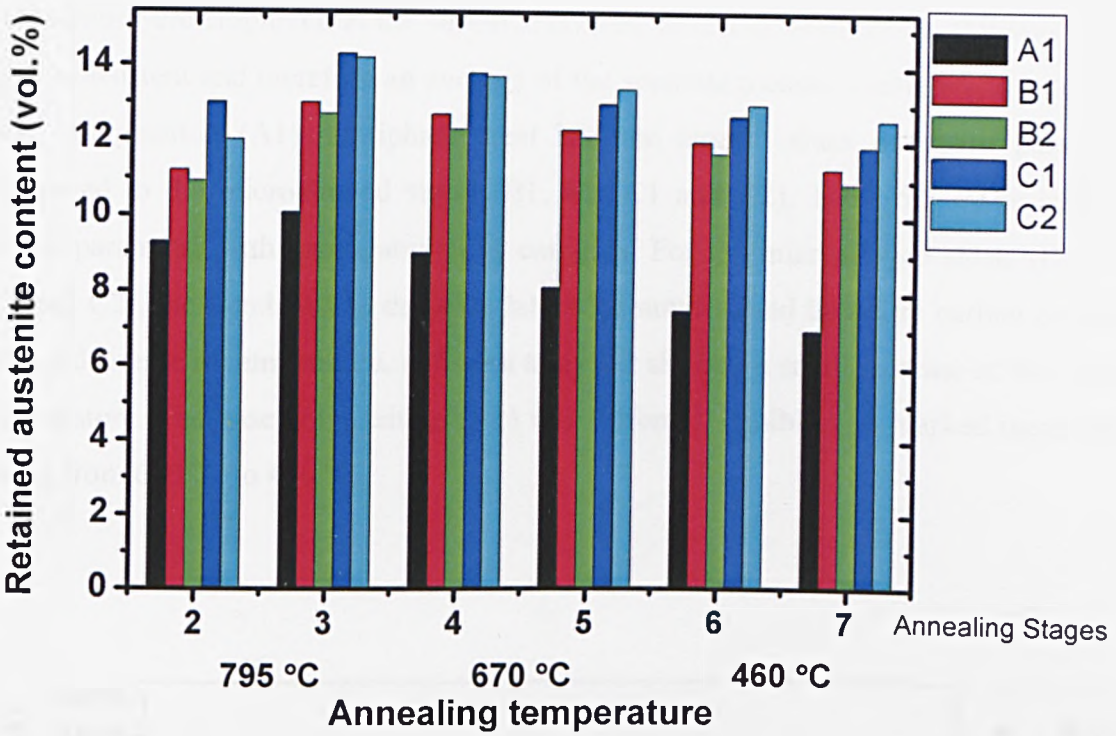

Fig. 5.5 The effect of annealing temperature on the retained austenite content.

This method gives a straight-line extrapolation for a_γ over a range of diffraction angles and then identifies the most accurate a_γ at $\theta = 90°$. The carbon content in retained austenite was then calculated using the following empirical equation [70,71] which assumes that the substitutional solute composition does not change, where a_γ, is austenite parameter (nm) and C is carbon content in austenite (wt %).

$$a_\gamma = 0.3572 + 0.0032C \text{ (wt \%)} \qquad (9)$$

Of course, this expression assumes that the austenite composition only changes through carbon content and that no other element diffuses in or out. The estimated carbon content for each stage of the annealing process is presented in Table 5.2. Figure 5.6 gives the change in lattice parameter with annealing temperature, while Figure 5.7 gives the corresponding changes in carbon content. Each datum represents the average from at least two separate measurements.

Where the value appeared to be at variance with the expected trend, repeat heat treatments were employed at the austenite content re-tested. In all cases, this was found to be consistent and therefore an average of the separate measurements was taken. The base composition (A1) multiphase steel had the larger values of lattice parameter compared to the microalloyed steels (B1, B2, C1 and C2), Table 5.3. The trend in lattice parameter with temperature was complex. For the microalloyed steels (B1, B2, C1 and C2), the trend was to decrease lattice parameter (and therefore carbon content) with a decrease in temperature, although alloy B2 showed a small increase at the lowest temperature. The base composition (A1) was different, exhibiting a marked increase in going from 670 °C to 460 °C.

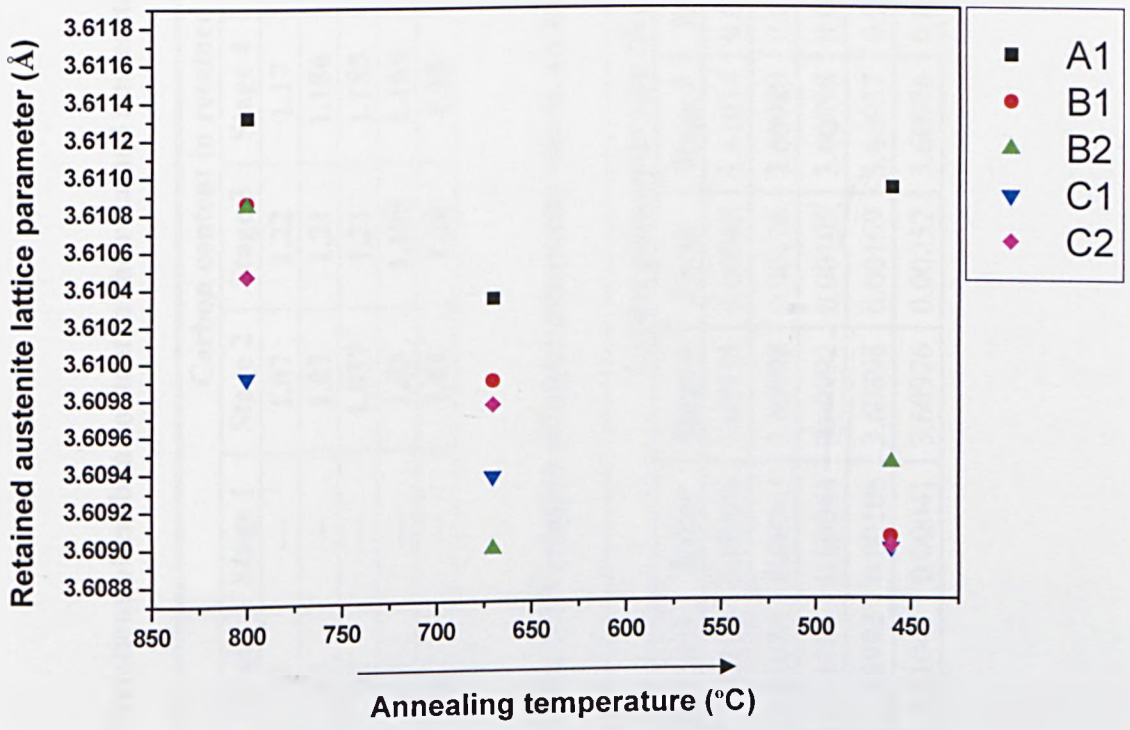

Fig. 5.6 Retained austenite lattice parameter variations with the annealing temperature.

Table 5.2 Variations of carbon content in the retained austenite in each stage of the annealing process.

	Carbon content in retained austenite (%)						
Steel	**Stage 1**	**Stage 2**	**Stage 3**	**Stage 4**	**Stage 5**	**Stage 6**	**Stage 7**
A1	---	**1.07**	**1.22**	**1.17**	**1.19**	**1.16**	**1.21**
B1	---	**1.07**	**1.21**	**1.186**	**1.18**	**1.125**	**1.157**
B2	---	**1.037**	**1.21**	**1.185**	**1.15**	**1.15**	**1.16**
C1	---	**1.03**	**1.185**	**1.155**	**1.16**	**1.14**	**1.155**
C2	---	**1.01**	**1.20**	**1.18**	**1.18**	**1.155**	**1.155**

Table 5.3 Variation of lattice parameter size in each stage of the annealing process.

	Lattice parameter size (Å)											
Steel	**Stage 2**	**Error**	**Stage 3**	**Error**	**Stage 4**	**Error**	**Stage 5**	**Error**	**Stage 6**	**Error**	**Stage 7**	**Error**
A1	3.60639	0.00209	3.61132	0.00106	3.60938	0.00042	3.61034	0.00276	3.60938	0.00042	3.61093	0.00047
B1	3.60639	0.00212	3.61086	0.00043	3.60998	0.00126	3.60989	0.00127	3.608	0.00106	3.60903	0.00169
B2	3.60521	0.00295	3.61085	0.00044	3.60992	0.00105	3.60898	0.00169	3.60898	0.00169	3.60943	0.00021
C1	3.60504	0.00021	3.60992	0.00106	3.60898	0.00169	3.60937	0.00041	3.60849	0.00085	3.60897	0.00063
C2	3.60447	0.00255	3.61047	0.00041	3.60976	0.00252	3.60976	0.00252	3.60898	0.0017	3.60898	0.0017

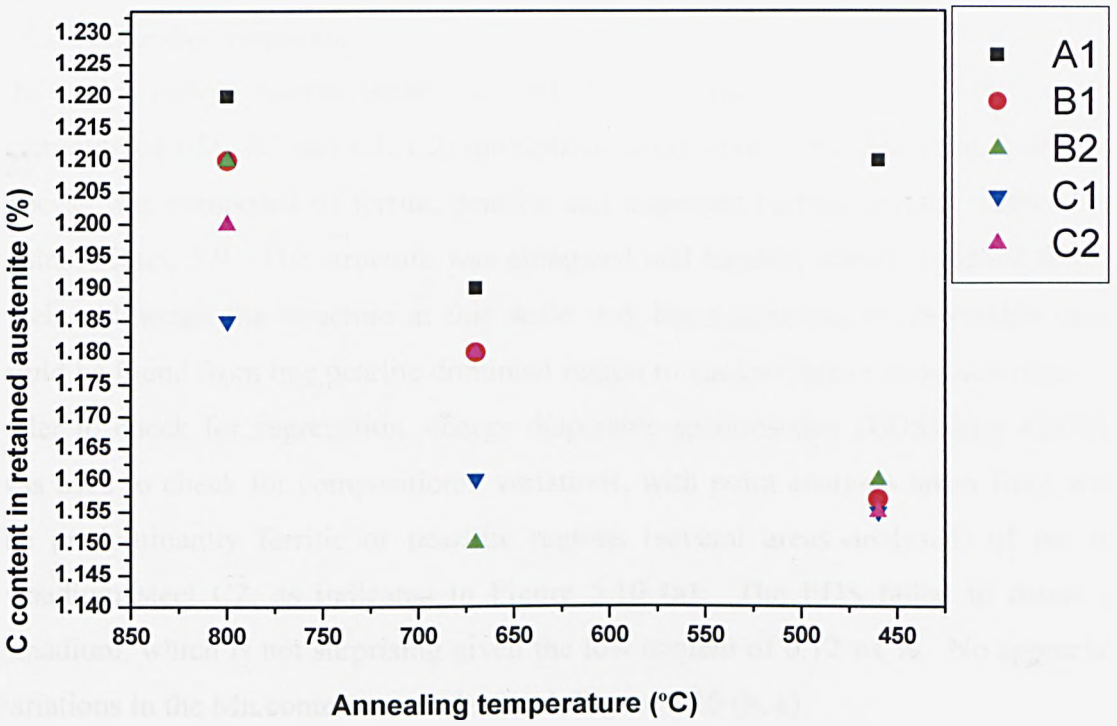

Fig. 5.7 Carbon variations with the annealing temperature.

5.3 Microstructural evolution of multiphase steels

5.3.1 Hot rolled condition

The hot rolled microstructure for the low vanadium B2 and high vanadium C2 is shown in Figure 5.8 (a) and (b) respectively which were composed of elongated ferrite and pearlite grains. No sample was available for the base composition in the hot rolled condition, it was supplied in the cold rolled condition.

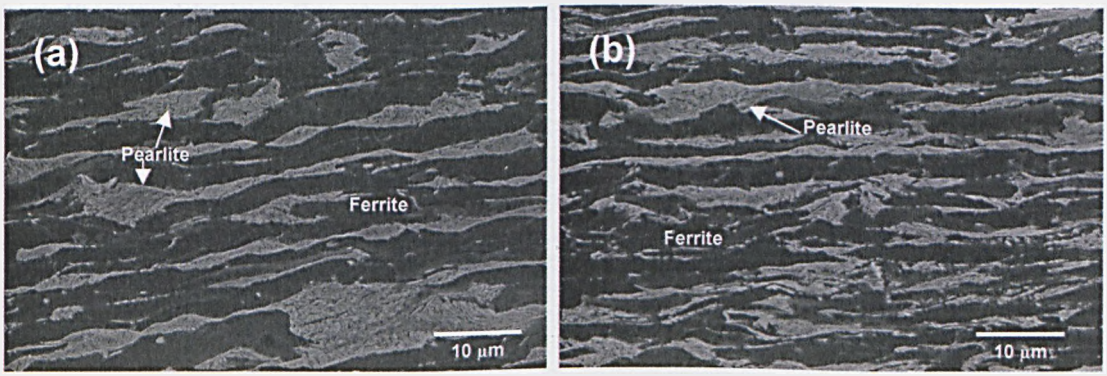

Fig. 5.8 Hot rolled microstructure (a) low vanadium B2 and (b) high vanadium C2 steels

5.3.2 Cold rolled condition

The cold rolled microstructure of the base composition (A1) and vanadium microalloyed (B1, B2 and C1, C2) multiphase steels prior to the intercritical annealing process was composed of ferrite, pearlite and dispersed carbide located within ferrite grains, Figure 5.9. The structure was elongated and banded, which is typical for such steels. Although the structure at this scale was heterogeneous, no detectable change could be found from one pearlite dominant region to another ferrite dominant region. In order to check for segregation, energy dispersive spectroscopy (EDS) in a FEGSEM was used to check for compositional variations, with point analyses taken from within the predominantly ferritic or pearlitic regions (several areas analysed) of the high vanadium steel C2, as indicated in Figure 5.10 (a). The EDS failed to detect any vanadium, which is not surprising given the low content of 0.12 wt %. No appreciable variations in the Mn content were observed, Figure 5.10 (b, c).

The small cold rolling reduction had broken up the lamellar pearlite such that some areas contained discrete carbides within ferrite grains (circled in Figure 5.11 (a) for steel B1, Figure 5.11 (b) for steel B2) while in others the pearlite eutectoid structure could still be clearly seen. Figure 5.11 (b) shows the B2 microstructure steel with similar features to the base composition and B1 steels.

Figure 5.12 compares the microstructure from the base composition with that from the high vanadium microalloyed steel, coiled at the lower temperature of 550 ^{o}C (steel C2). Differences were small and therefore the assessment was rather subjective. In some areas, the pearlite lamellar structure was easy to resolve, while in other areas it was difficult to differentiate individual lamellae. An example of the latter is given in Figure 5.13 for steel C1.

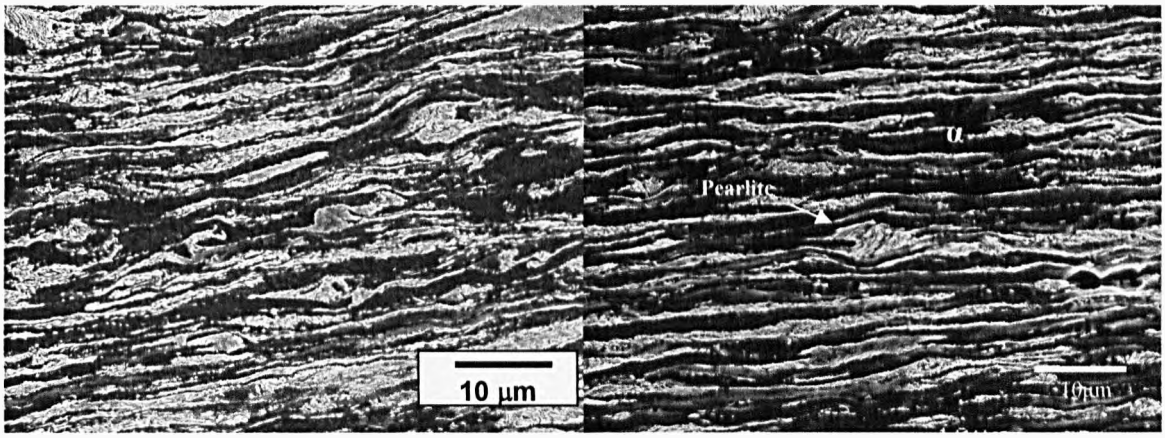

(a) **(b)**

Figure 5.9 Secondary electron SEM images of longitudinal sections of the cold rolled (a) base composition (A1), (b) high vanadium-C2-steel.

5.3.3 Intercritically annealed microstructure

Microstructural evolution of the base composition (A1) and vanadium alloy (B1, B2 and C1, C2) steel samples after being quenched from the main stages of the annealing process are given in this section. SEM micrographs were taken from numerous regions within one sample to determine the variation in microstructure. To determine the effect of composition and coiling temperature, areas with similar microstructural features were used to compare like with like, those that were predominantly pearlite and those that were predominantly ferrite.

However, this was not possible for the later stages of the heat treatment when the microstructure became much more uniform. Further microstructure observation was carried out by thin foil transmission electron microscopy (TEM). TEM of carbon extraction replicas were used to analyse and quantify the vanadium carbide precipitates. The microstructure produced in the different stages of the annealing process was complex and consisted of Fe_3C carbides (produced in Stage 1), martensite, bainite, and the martensite – austenite (MA) constituent in a ferritic matrix.

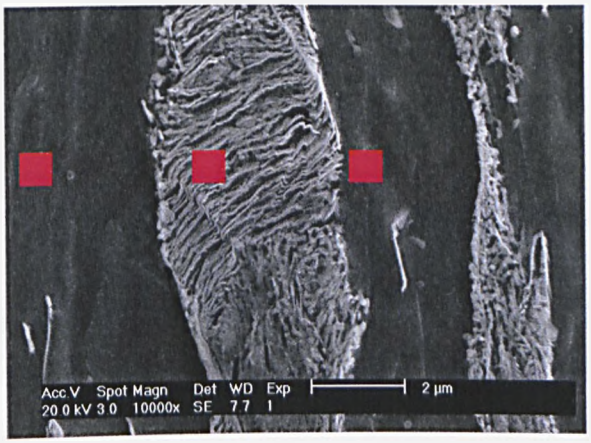

(a)

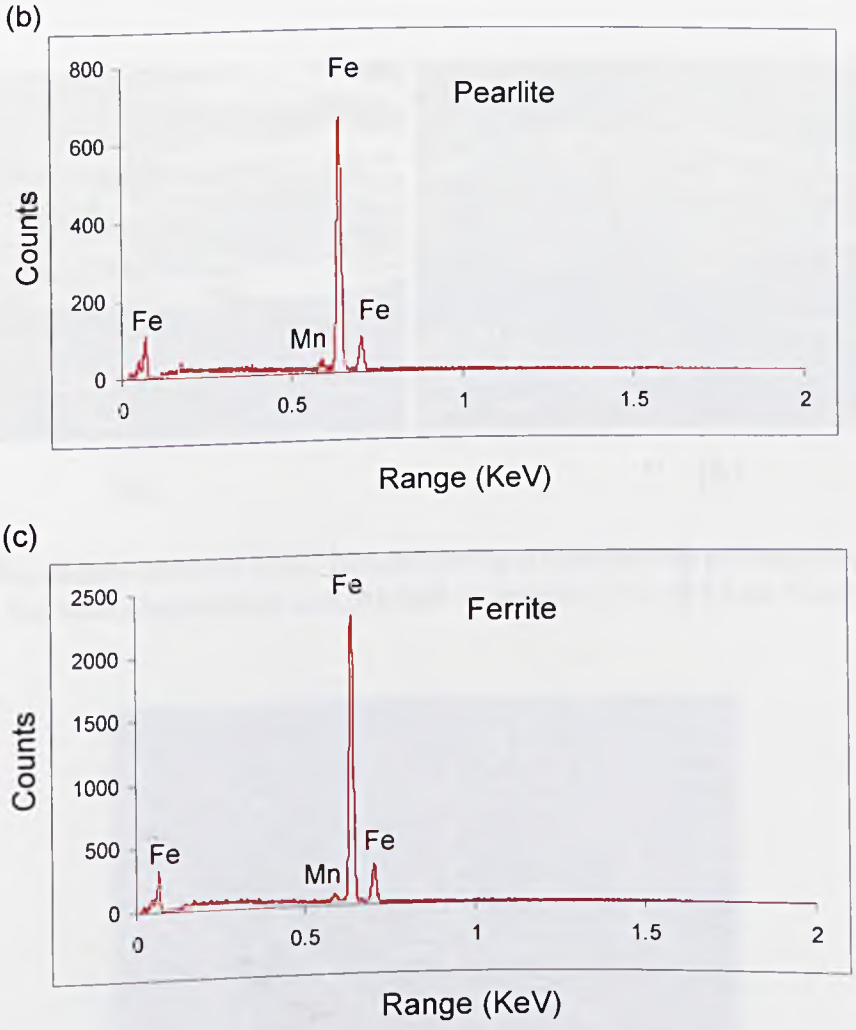

Fig. 5.10 Secondary electron SEM image of a longitudinal section of the cold rolled (a) detail showing ferrite and pearlite distribution in the high vanadium C2 steel, showing the location of point analysis by EDS, (b) EDS spectra from the pearlite and (c) ferrite taken from (a).

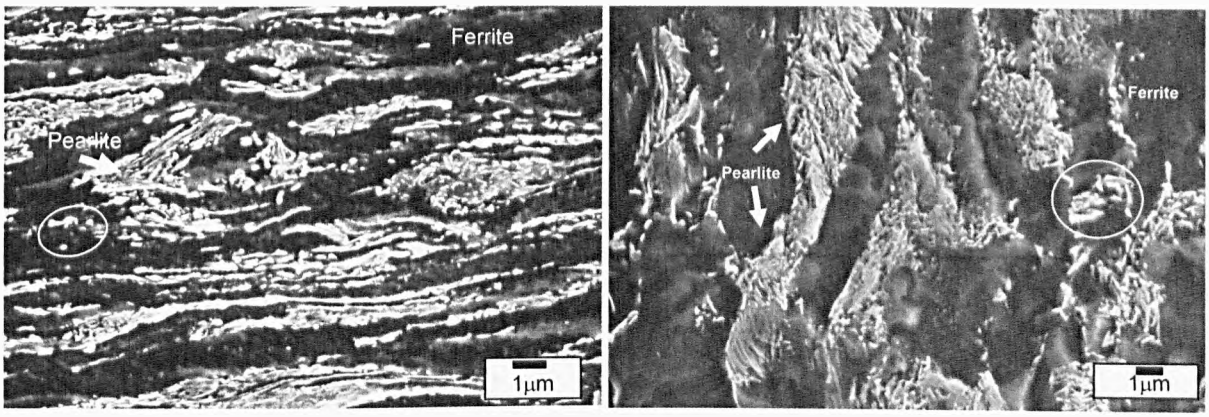

(a) **(b)**

Fig. 5.11 Microstructure of the (a) B1 and (b) B2 vanadium microalloyed steels in cold rolled conditions.

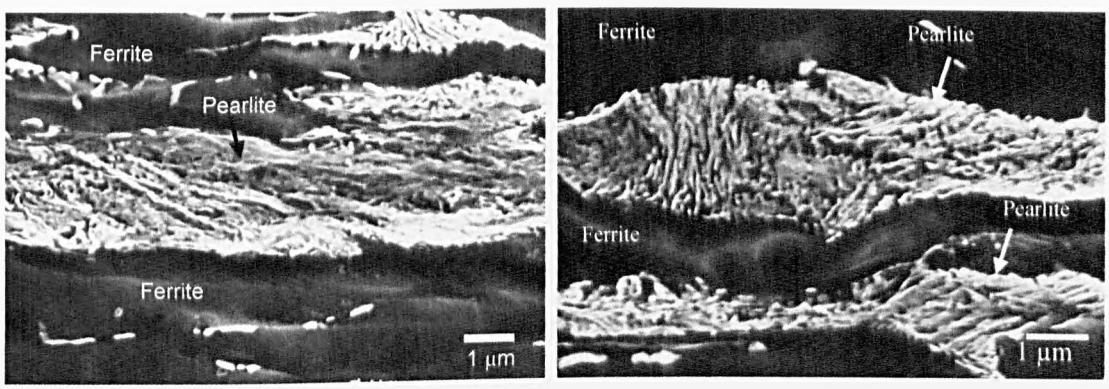

(a) **(b)**

Fig. 5.12 Secondary electron SEM images giving a comparison of the microstructure between (a) the base composition and (b) high vanadium – C2 (0.12 wt %) (CT 550 °C).

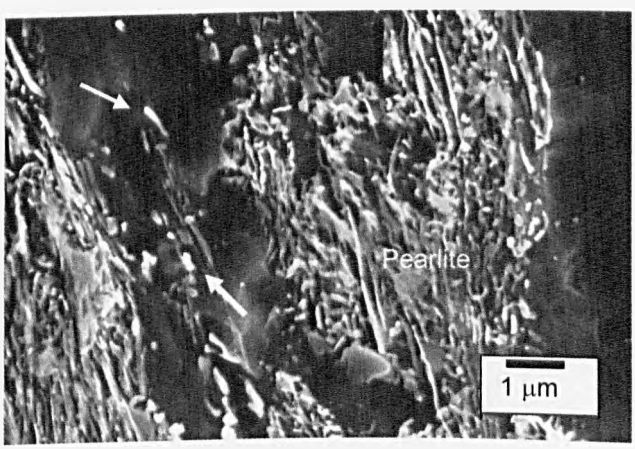

Fig. 5.13 Microstructure in cold rolled conditions of the vanadium-microalloyed C1 steel.

5.3.3.1 Heating effect at 695 °C (Stage 1)

The samples were heated to 695 °C with a heating rate of 14 °C/s and quenched with water to room temperature. At Stage 1 the microstructure consisted of banded polygonal ferrite (indicating recrystallisation), some elongated ferrite and lamellar pearlite which exhibited partial spheroidisation. Figure 5.14 (a) gives an example for the base composition microstructure (A1), showing discrete carbides located along the grain boundaries and within recrystallised ferrite grains. SEM indicated that most of the ferrite was equiaxed in the base composition, and therefore recrystallised. However, some grains retained the elongated morphology observed in the cold rolled condition.

These same general microstructural characteristics were observed in the vanadium microalloyed steels, Figure 5.14 (b). However, one important difference was that there were rather more ferrite grains that retained the elongated morphology, i.e. the extent of recrystallisation was less. In addition, the carbide particles appeared distinctly finer in the high vanadium microalloyed steel compared to the base composition, being difficult to resolve in SEM, Figure 5.14 (a, b). In general, the microstructure of the C1 and C2 steels appeared finer than the A1 base composition, but the heterogeneous nature of the microstructure made this difficult to quantify (but this was possible for later in the heat treatment schedule, see section 5.3.3.2).

A more detailed view of the cementite distribution is given in the TEM micrographs Figure 5.15 (a, b) for the base composition (A1). Figure 5.15 (a) appears to show a recrystallised ferrite grain (centre, with low dislocation density) growing into a region of ferrite with a high dislocation density (which presumably has only undergone recovery). Discrete, partially spheroidised carbides became entrapped within the ferrite grains. Figure 5.15 (b) shows a similar area of ferrite with low dislocation density surrounded by regions with high dislocation density, but in a region where the lamellar pearlite is only starting the spheroidisation process.

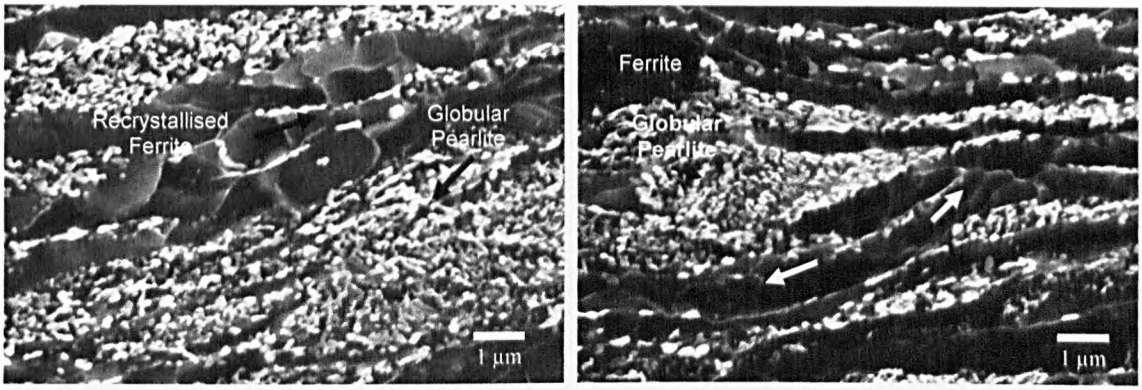

(a) **(b)**

Fig. 5.14 Secondary electron SEM images showing recrystallised ferrite produced after heating to 695 °C in (a) base composition (A1) and (b) high vanadium C2 steel where recrystallised ferrite grains are arrowed.

(a) **(b)**

Fig. 5.15 Bright field TEM micrographs from thin foil sections showing (a) partially spheroidised cementite within ferrite grain and (b) break-up of the lamellar structure in the pearlite, base composition (A1 steel) heated at 695 °C.

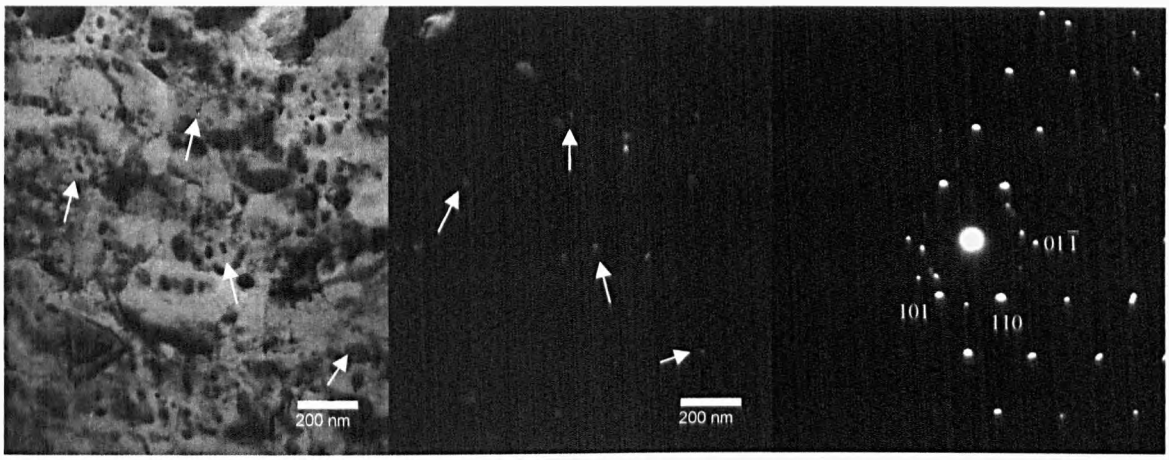

(a) (b) (c)

Fig. 5.16 TEM micrographs of the B1 steel heated at 695 °C, (a) bright field, (b) dark field, some vanadium carbide precipitates are arrowed and (c) diffraction pattern with ferrite peaks labelled.

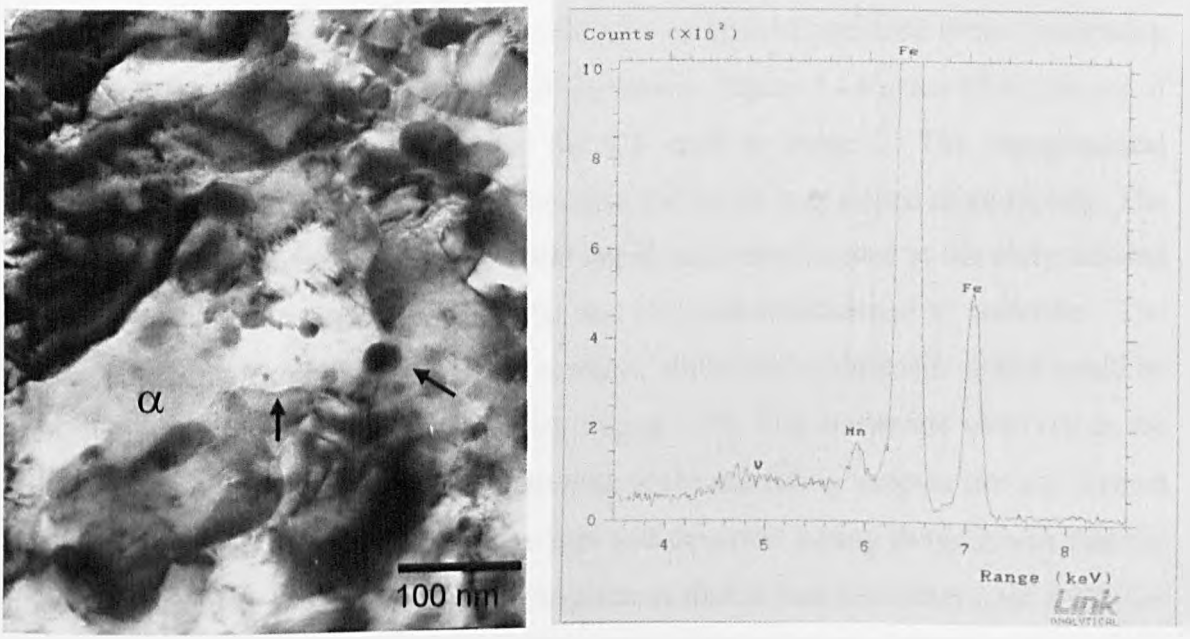

(a) (b)

Fig. 5.17 (a) Circular cementite inside of ferrite grain is arrowed and (b) EDS analysis, C2 high vanadium (0.12 wt %) steels heated at 695 °C.

TEM images, Figures 5.16 and 5.17 show examples of the fine scale structure from the microalloyed steels. Figure 5.16 shows relatively fine spherical carbides that are completely spheroidised, within a region of relatively dislocation-free ferrite. Note that the shape and size of the cementite looks more uniform than was found for the base composition. Vanadium carbide precipitates were identified by TEM using the dark field technique (Figure 5.16 (b)), the diffraction pattern is shown in Figure 5.16 (c). EDS analysis of the region in Figure 5.17 (a) is given in (b), and shows the presence of vanadium in the carbides (although the signal is weak because of the small proportion the carbide takes up in the sample thickness and the relatively coarse electron beam that had to be used in this microscope).

5.3.3.2 Microstructural changes at 795 °C (Stage 2)

Significant changes in microstructure were found to occur at Stage 2 (samples were heated at 795 °C with a heating rate of 14 °C/s and quenched quickly to room temperature with water). The microstructure now comprised equiaxed ferrite (indicating complete recrystallisation), austenite and martensite. Figure 5.18 gives SEM images of the base composition (A1) steel and the C2 steel at Stage 2. The topographical appearance of the SEM micrographs is because the ferrite was etched more rapidly. The distribution of the phases suggests that the initial cementite located at the recrystallised ferrite grain boundaries (Figures 5.18 (a) and (b)) had transformed to austenite. The retained austenite exhibits the brightest contrast, while some martensite grains could be identified by the fine substructure (twins), Figure 5.19. The martensite observed in the structure was presumed to have been austenite at the annealing temperature and formed during the quench. One marked change that had occurred during Stage 2 was that the microstructure was now much more homogeneous than it had been after cold rolling or Stage 1; for example, compare Figure 5.14 with Figure 5.18 (a) and (b). Indeed, after Stage 2 heat treatment, the original banding had become difficult to detect. Therefore, considerable diffusion of the carbon must have occurred. The majority of the austenite and martensite decorated the ferrite grain boundaries, although some intragranular austenite was also present, Figure 5.18.

The basic microstructure of the base composition and the low and high vanadium microalloyed steels was similar. However, the vanadium containing steels appeared to have a finer microstructure, and a more uniform distribution of ferrite grain size (Figure 5.20); compare Figure 5.18 (a) with (b). The size of the retained austenite + martensite for each condition is given in Table 5.3 (calculated using Sigma-Scan Pro images analysis from 15 SEM micrographs per material), which shows a general trend that the size decreased with vanadium addition, but there was not a statistically meaningful difference between the 0.06 wt % and the 0.12 wt % V steels.

Thin foil TEM micrographs of the Stage 2 specimens are shown in Figures 5.21 to 5.28. Although the XRD results indicated a significant RA content, the identification of the retained austenite was somewhat difficult. Figure 5.21 shows the distribution of the retained austenite and martensite, which have darker contrast than the ferrite. The second phase particles had a highly irregular shape. Dark field imaging in combination with the selected area diffraction pattern was useful in identifying the RA. In most cases, one region of second phase comprised both martensite and austenite, with rather irregular distributions, as shown in Figure 5.22 to Figure 5.25. It was more difficult to find retained austenite in the base composition than the vanadium microalloyed steels, although this could have been an error from sampling. However, discrete austenite crystals were found within ferrite grains; see Figures 5.26 and 5.28, in which case they tended to be entirely austenite, with no evidence of martensite.

For the microalloyed steels, vanadium carbides could be imaged both in bright and dark field, indicated by the arrows in Figure 5.24, 25 and 27. The full details of the vanadium carbide size distribution is presented and analysed later. The vanadium carbide was present in both the ferrite and in the retained austenite and martensite, as shown for example in Figure 5.27.

Table 5.4 Estimated austenite grain size produced at Stage 2

Steel	Austenite + martensite grain size (μm)
A1	2.4 ± 0.5
B1	1.8 ± 0.5
B2	1.9 ± 0.5
C1	1.6 ± 0.4
C2	1.7 ± 0.4

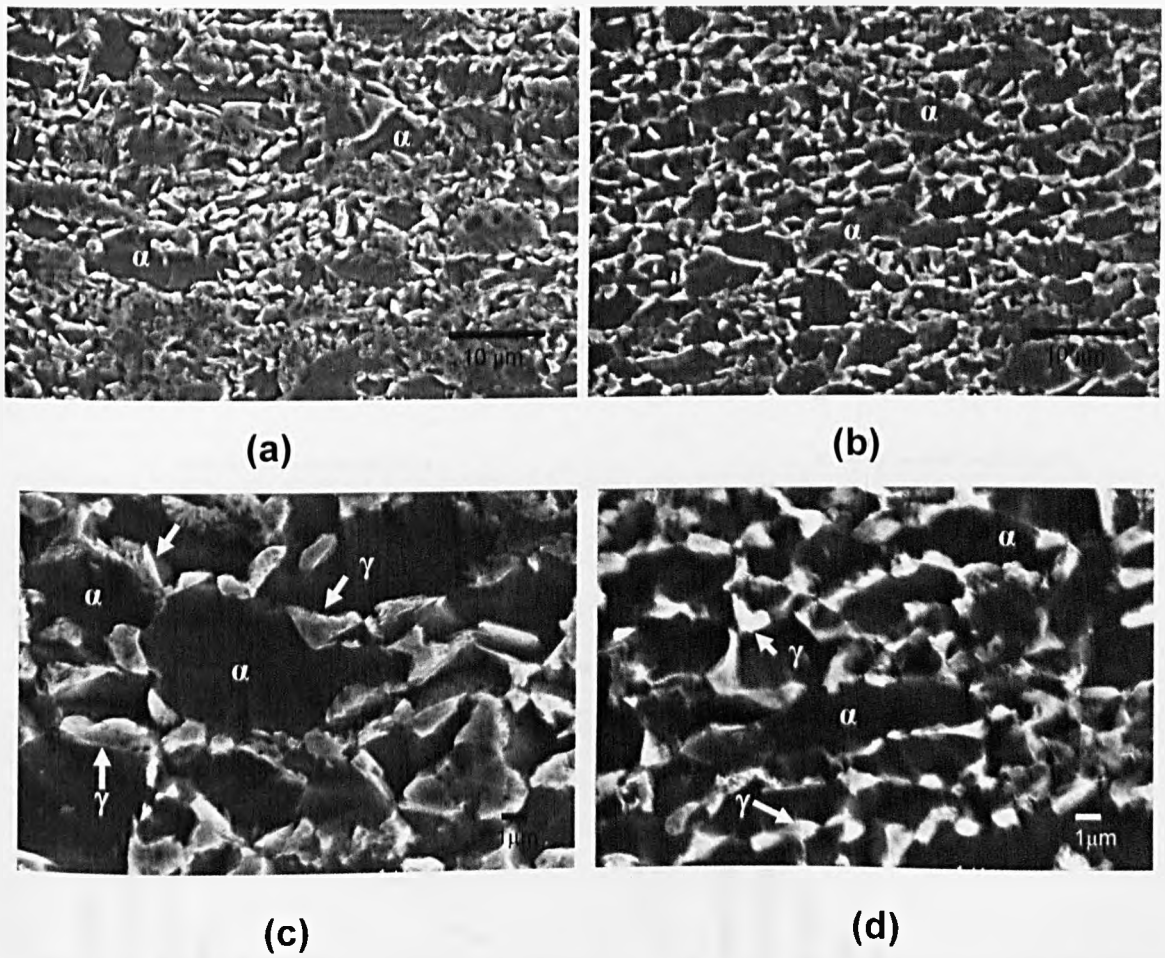

Fig. 5.18 Distribution of the austenite formed at 795 °C at low magnifications of the (a) base composition, (b) high vanadium – C2 steels. The austenite was formed in the ferrite grains boundaries both in (c) base composition and (d) high vanadium – C2 steel (0.12 wt %) (CT 550 °C).

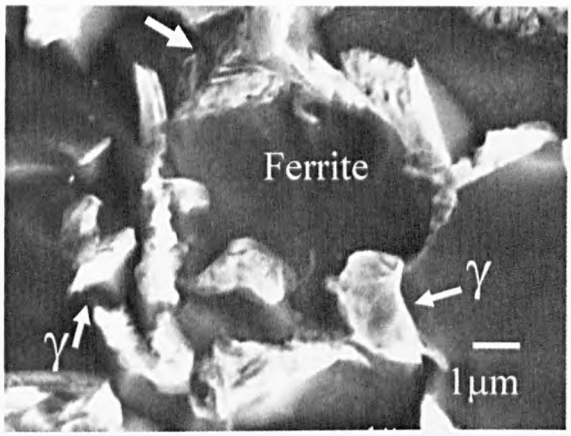

Fig. 5.19 SEM micrograph of the base composition (A1) steel, showing a ferrite grain surrounded by austenite and martensite.

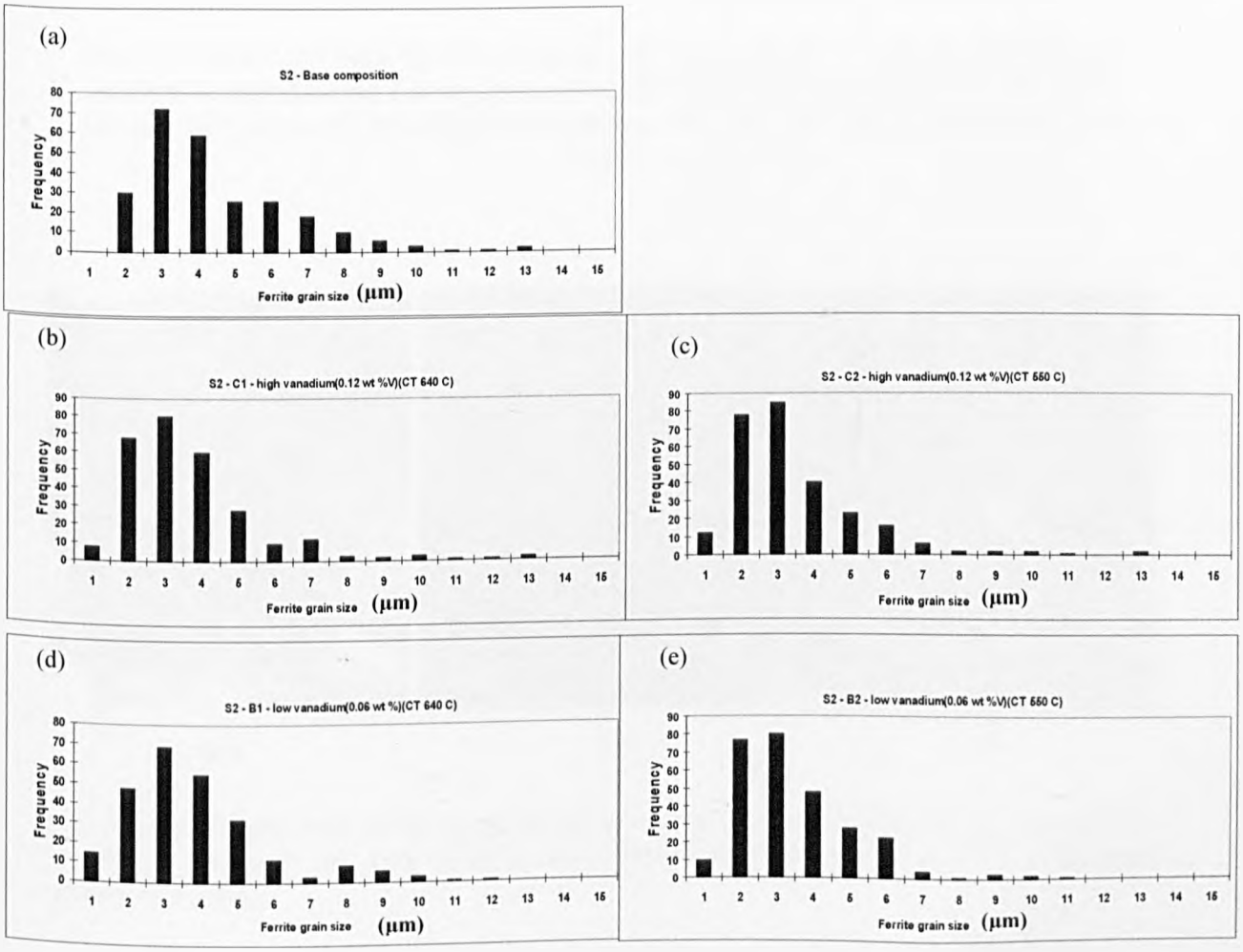

Fig. 5.20 Ferrite grain size of the base composition and vanadium multiphase steels produced at Stage 2.

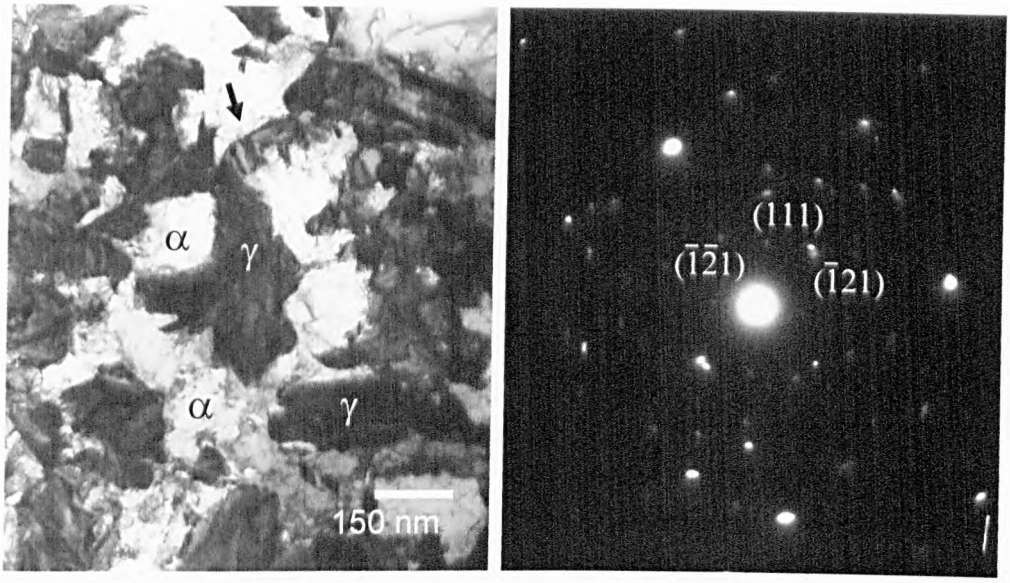

(a) **(b)**

Fig. 5.21 (a) Bright field TEM micrograph showing grains of retained austenite and martensite surrounding ferrite grains; note the austenite formed at the ferrite grain boundaries (arrowed), (b) diffraction pattern of this region. Base composition (A1) steel.

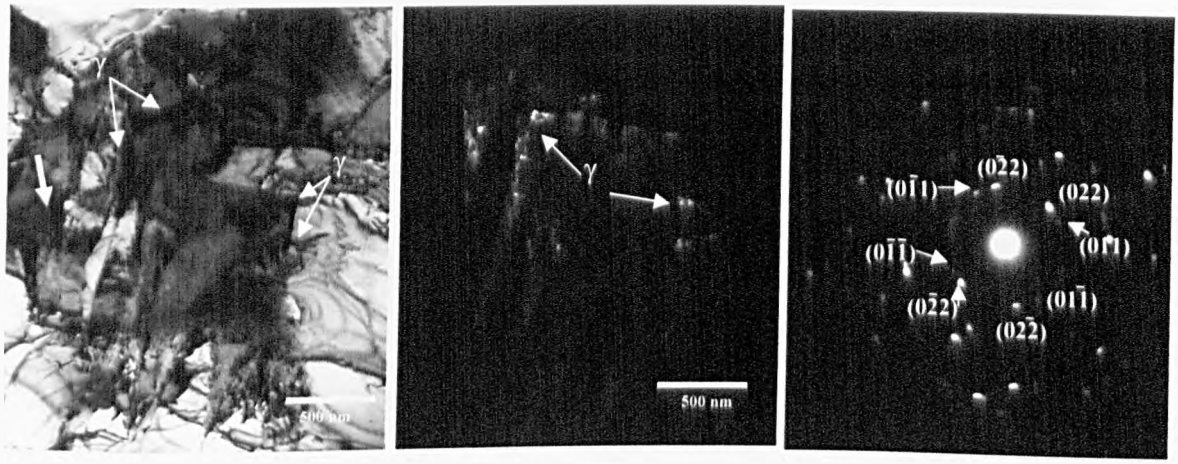

(a) **(b)** **(c)**

Fig. 5.22 (a) Bright field TEM image showing retained austenite and also dislocations in ferrite are arrowed; (b) dark field showing the retained austenite and (c) diffraction pattern. A1 steel.

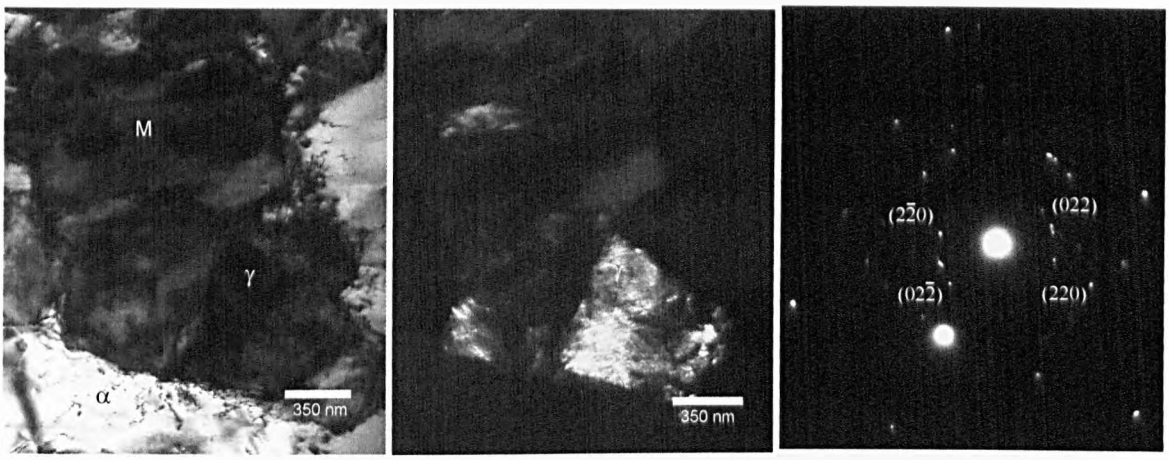

Fig. 5.23 TEM micrographs of the A1 steel showing retained austenite, (a) bright field, (b) dark field and (c) diffraction pattern.

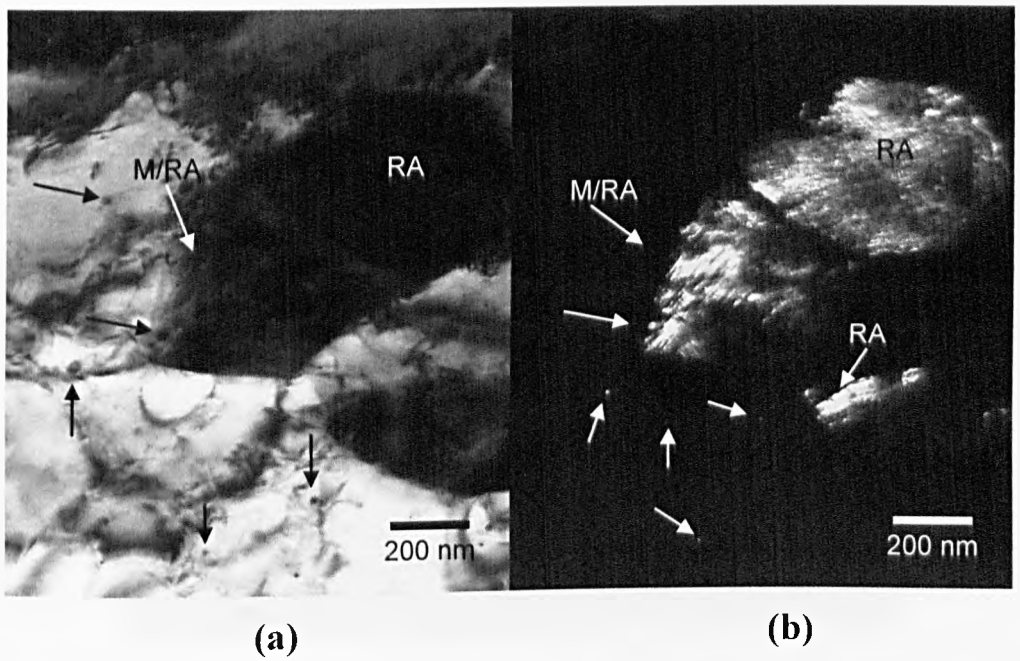

Figure 5.24 TEM micrographs of the B1 steel. (a) Bright field image showing an island comprising martensite and retained austenite, with fine vanadium carbide precipitates in the ferrite (arrowed) and (b) dark field using a retained austenite reflection.

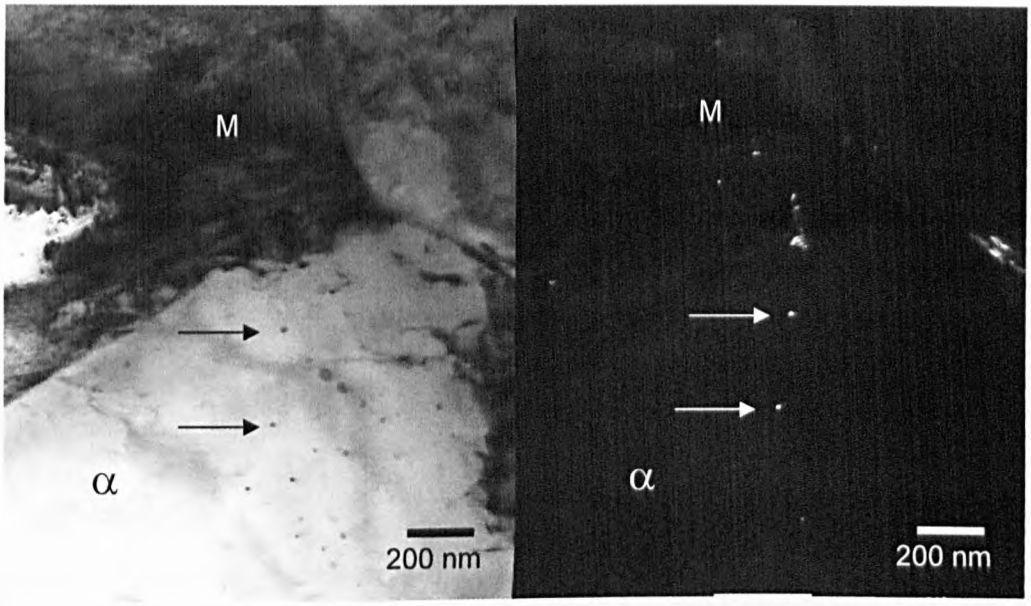

Figure 5.25 TEM micrographs of the B1 steel. (a) Bright field micrograph showing vanadium carbide precipitates (arrowed) and martensite (M) and (b) dark field image using a vanadium carbide reflection.

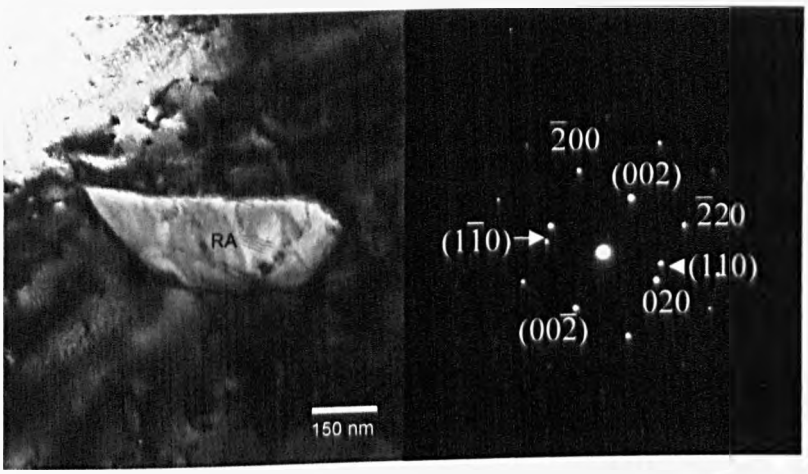

Fig. 5.26 (a) TEM bright field micrograph of an elongated retained austenite crystal and (b) associated diffraction pattern, B2 steel.

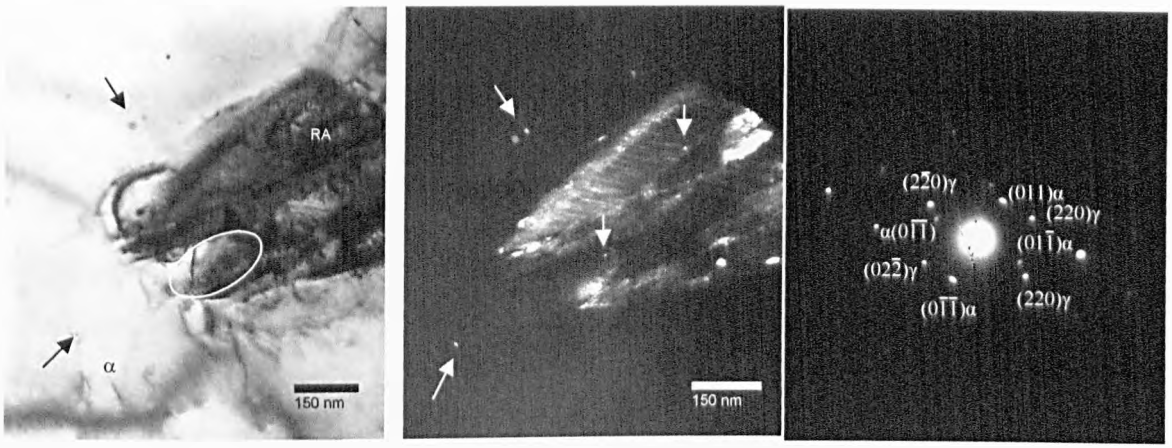

(a) (b) (c)

Fig. 5.27 TEM micrographs from the C2 steel. (a) Vanadium carbide precipitates (arrowed) within the ferrite, martensite and retained austenite grain (circled), (b) dark field image showing precipitates within the austenite grain, the diffraction pattern is shown in (c).

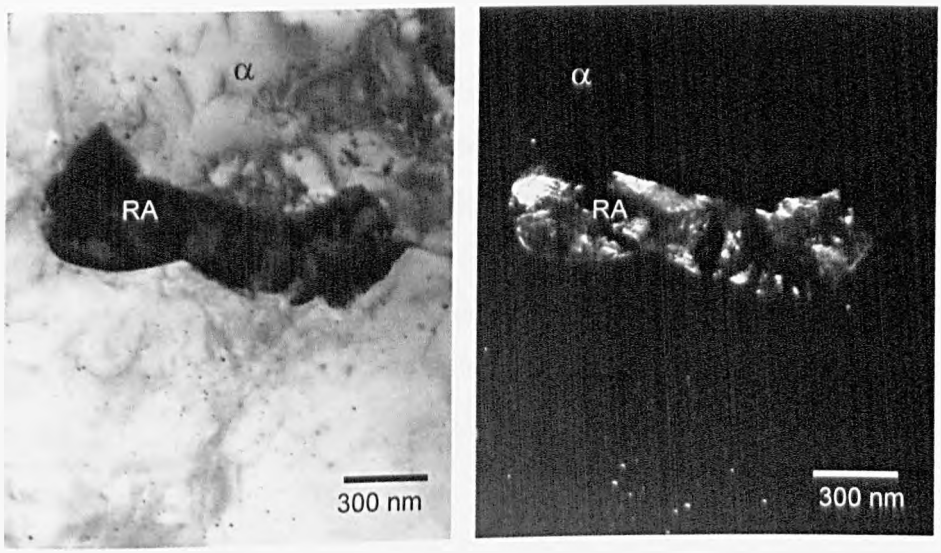

(a) (b)

Fig. 5.28 TEM micrographs of the C2 steel. (a) Bright field image showing an elongated retained austenite grain within and (b) dark field image.

5.3.3.3 Microstructural changes at 795 ℃ after being held for 20 s (Stage 3)

After heat treatment to Stage 3, the microstructure development was more homogeneous and the coarser scale banding observed in the cold rolled condition was no longer evident, Figure 5.29. The retained austenite was somewhat easier to differentiate from the martensite than had been the case at Stage 2, e.g. Figure 5.29 (c). This made it appear that the amount of retained austenite had increased, even though the actual increase was small (Table 5.1). The size of the austenite and martensite was measured in the same way as for Stage 2, the results of which are given in Table 5.5. This demonstrated a small increase in size for the vanadium containing alloys, and a larger increase for the base composition. This increase in grain size was also observed in the ferrite grain as shown in Figure 5.31. As with Stage 2, the microstructure of the vanadium containing steels was more homogeneous at Stage 3 than for the base composition, Figure 5.29. The austenite and martensite was irregular in shape, Figure 5.30 – 5.33, as was the case at Stage 2. Locally the amount of second phases was higher (e.g. Figure 5.33) in some areas than others, but as shown in Figure 5.29, this was just a local sampling effect. The increase in austenite grain size was confirmed by TEM analysis. Figure 5.34 (a) shows an RA grain, ~1.5 μm in diameter from the A1 steel and in (b) retained austenite exhibits bright contrast in the dark field image. Figure 5.36 corresponds to the B1 steel where the RA grain size is around 0.5 μm and also vanadium carbides are present close to the austenite grain. Figure 5.35 shows an isolated RA grain found in the centre of ferrite grain, which exhibited a central planar feature believed to be a twin. VC precipitation was relatively easy to identify in the ferrite, Figure 5.36, 5.37. In some areas, the martensite twinned structure was clearly seen, Figure 5.37.

Table 5.5 Estimated austenite grain size produced at Stage 3

Steel	Austenite grain size (μm)
A1	3.2 ± 0.3
B1	2.5 ± 0.2
B2	2.4 ± 0.2
C1	2.1 ± 0.1
C2	2.0 ± 0.1

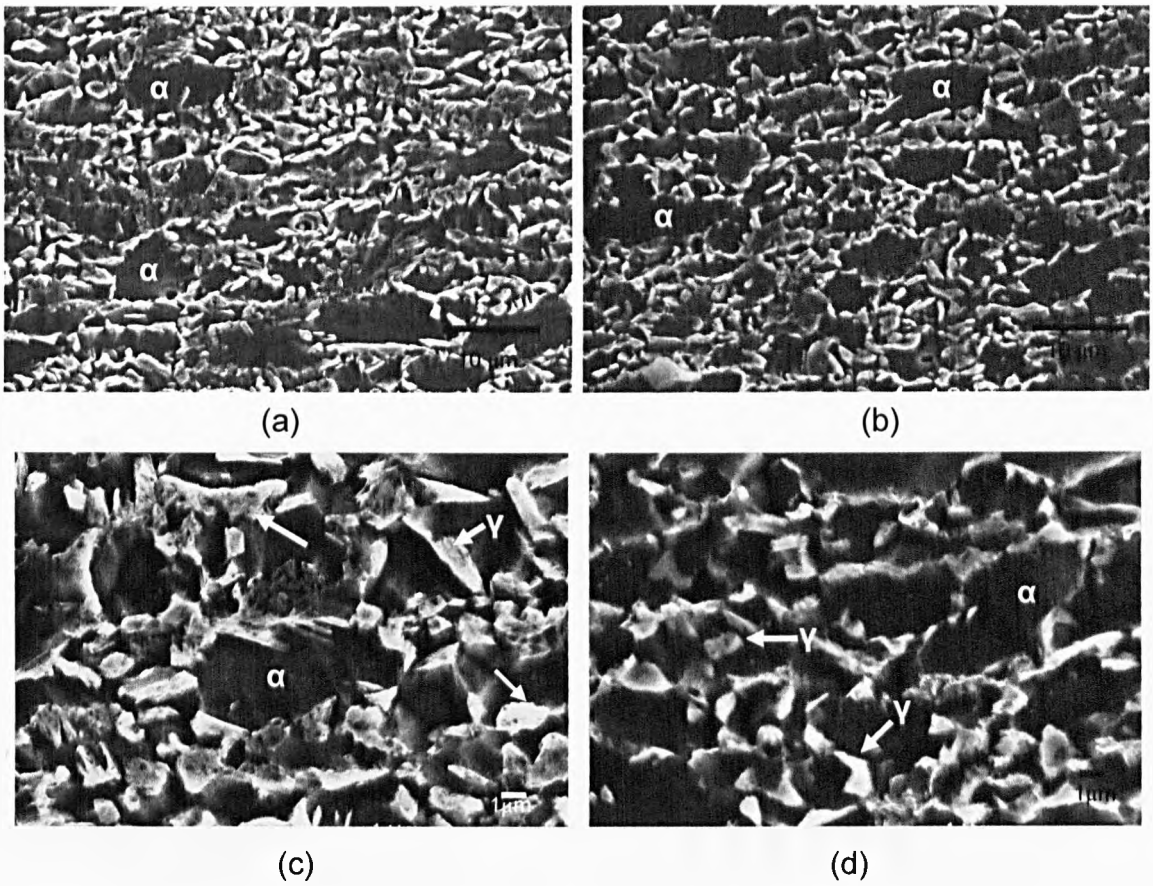

Fig. 5.29 Microstructure of the (a) base composition and (b) ferrite grains of high vanadium – C2 (0.12 wt %) (CT 550 °C) steel that looks smaller than of the (a) base composition, also the austenite grain of the (d) C2 steel appears finer than of the (c) base composition.

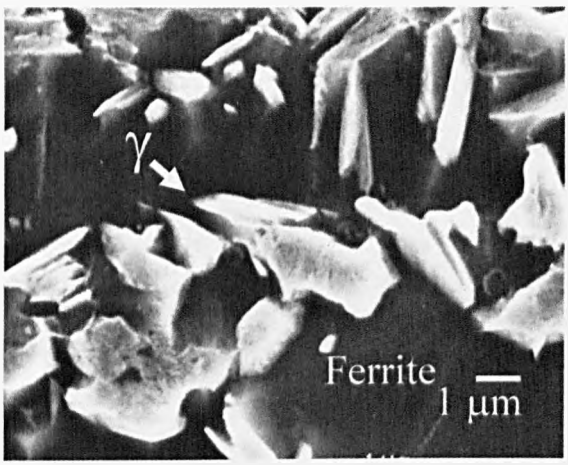

Fig. 5.30 SEM micrograph showing retained austenite grain size of the base composition (A1) steel.

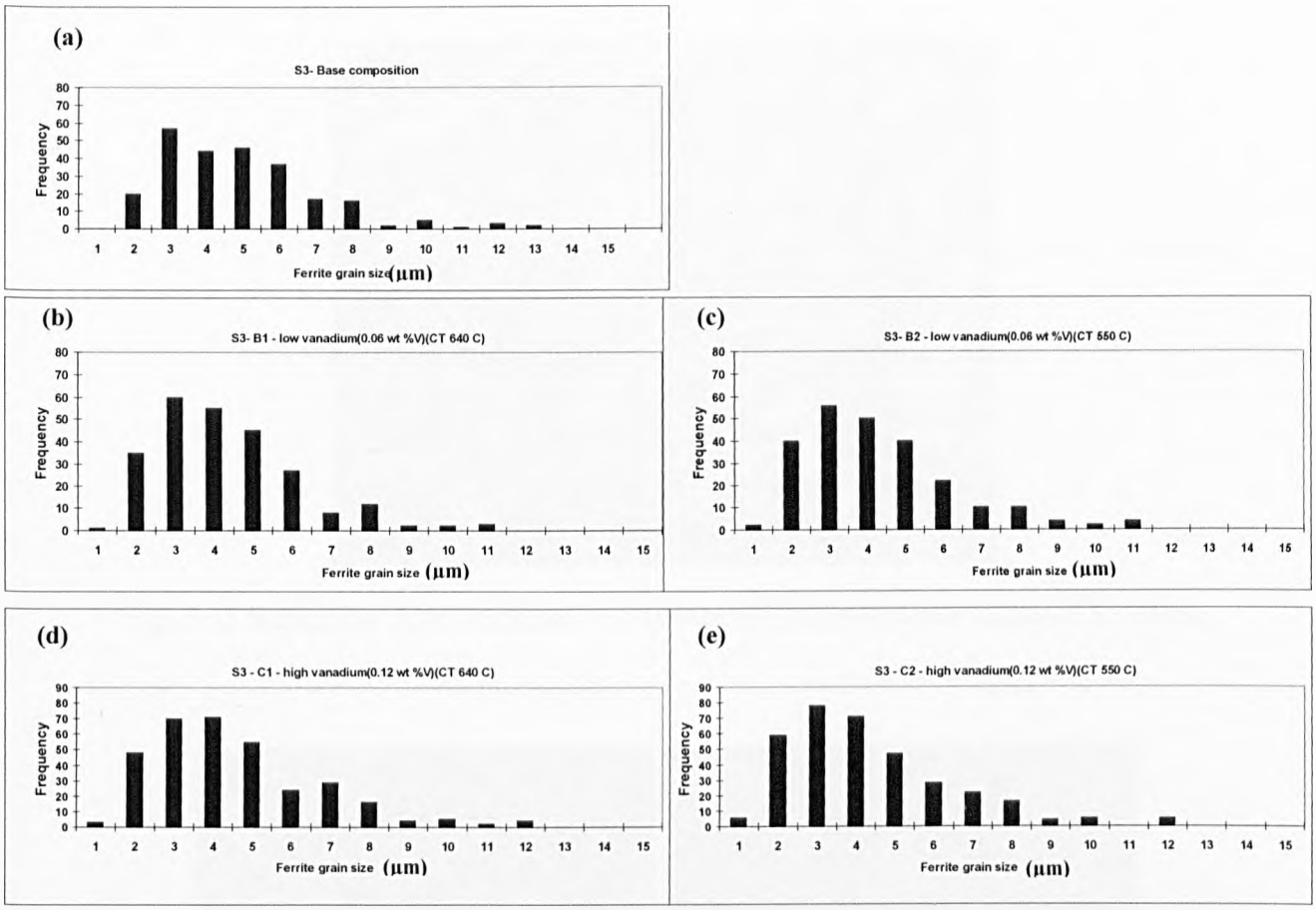

Fig. 5.31 Ferrite grain size of the (a) base composition A1, low vanadium (b) B1 and (c) B2, and high vanadium(d) C1 and (e) C2 multiphase steels produced at Stage 3.

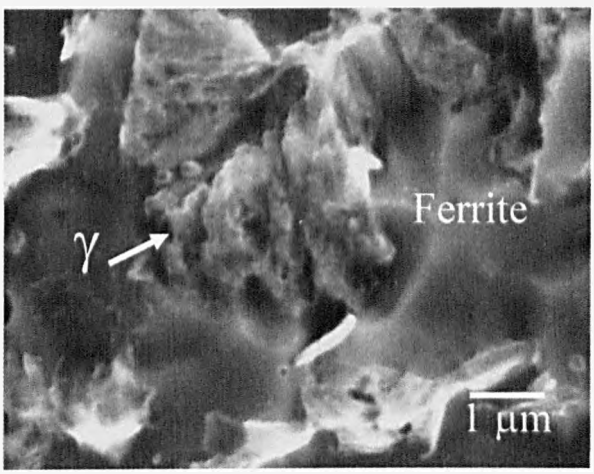

Fig. 5.32 Retained austenite and martensite developed in the B2 steel.

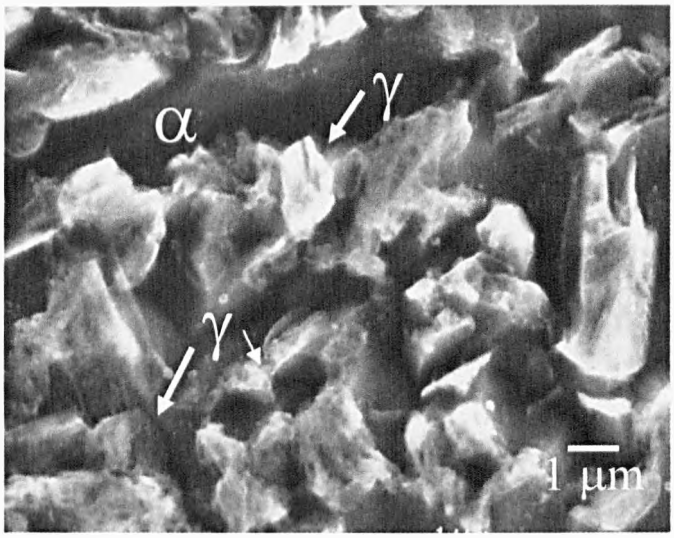

Fig. 5.33 Relatively finer austenite and martensite grains developed in the C2 steel.

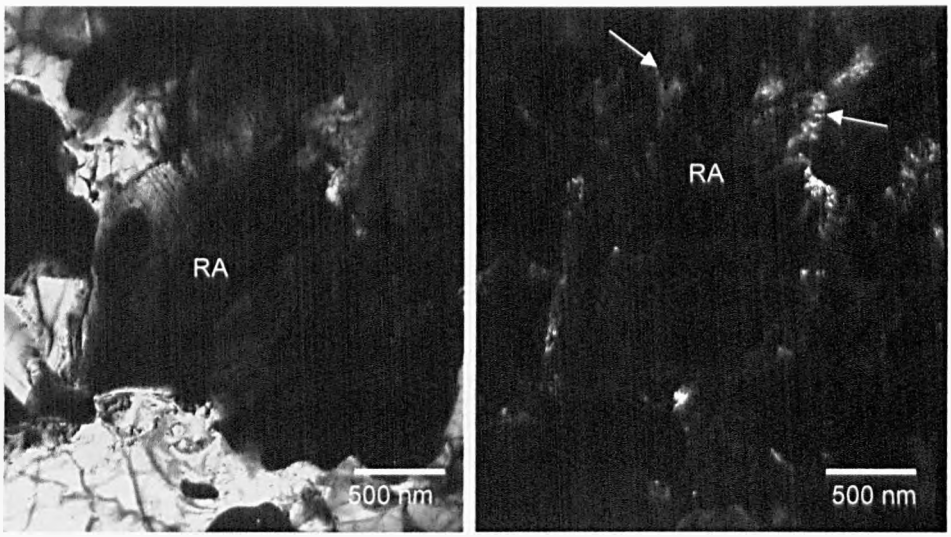

Fig. 5.34 TEM micrographs of the base composition (A1) steel (a) bright field showing a comparatively large grain of retained austenite with martensite present and (b) dark field, the RA is indicated.

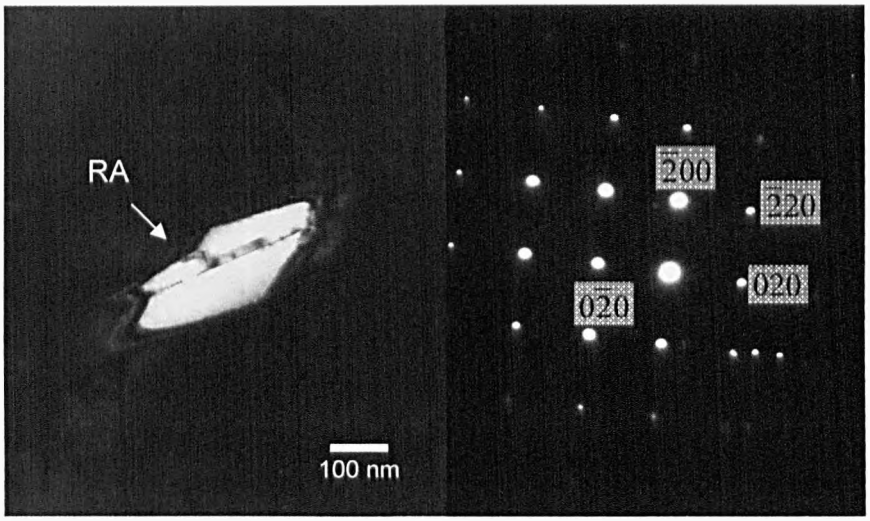

Fig. 5.35 (a) Dark field TEM micrograph; the bright region is retained austenite and (b) diffraction pattern, B1 steel.

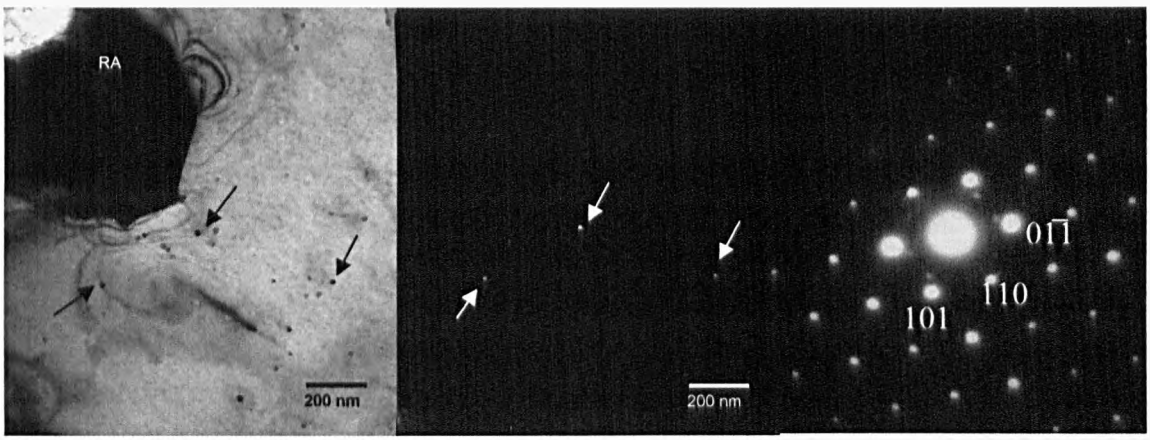

Fig. 5.36 (a) Bright field TEM micrograph showing VC dispersed in ferrite adjacent to a RA particle and (b) dark field image showing the VC distribution and (c) diffraction pattern, B1 steel.

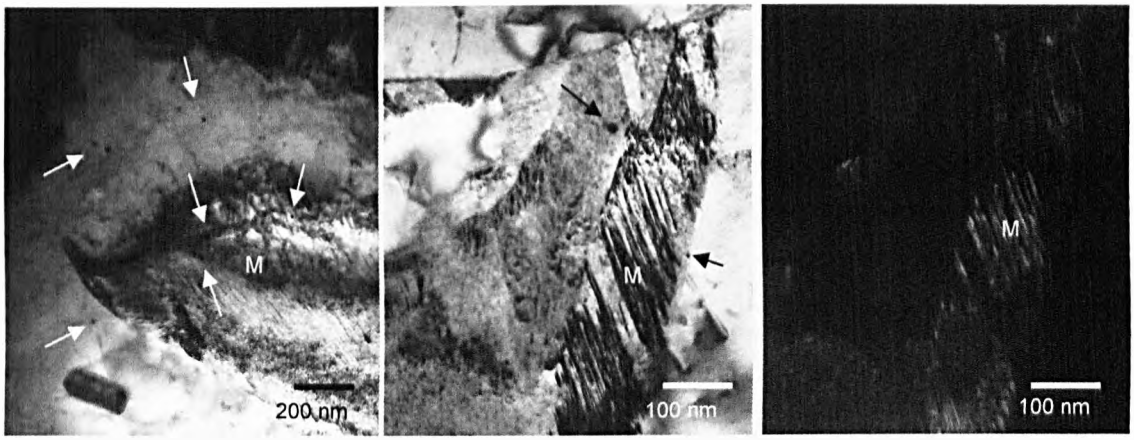

(a) **(b)** **(c)**

Fig. 5.37 TEM micrographs showing (a) martensite and vanadium precipitates, (b) martensite exhibiting twinned deformation, also VC were found in the boundaries and (c) dark field image, C2 steel.

5.3.3.4 Microstructural changes at 670 °C after being held for 12 s (Stage 5)

After slow cooling from 795 °C to a 12 second hold at 670 °C, the microstructure produced in all the multiphase steel samples consisted of retained austenite in a ferritic matrix with some martensite islands. The martensite could have been formed during this cool or during subsequent quenching. As with the earlier stages, the second phase particles were irregular in shape. The retained austenite was present as a more acicular shape, which tended to be associated with the ferrite grain boundaries, while that formed in the centre of ferrite grains tended to be smaller and more rounded; see Figure 5.38 (a).

In the base composition (A1) steel, in addition to the retained austenite and martensite, features were present that appeared bainitic, i.e. parallel sided lath like features growing away from an austenite/martensite island, as circled in Figures 5.38. However, it was difficult to differentiate such feature from elongated retained austenite, which is not surprising given that the bainite formed in these steels is a mixture of ferrite and austenite.

Irrespective of whether this was bainite or not, such features were only observed in the base composition and were not found in the alloys containing vanadium; for example, compares Figure 5.38 with Figure 5.39. Regions where the martensite appeared to be banded were observed, Figure 5.39, but this was not a common observation.

TEM largely confirmed the features that were observed in the SEM images. Subjectively, the base composition appeared to have a coarser structure than the vanadium microalloyed steels, for example, the retained austenite grains appeared to be larger in the base composition than vanadium steels, see Figure 5.41. Despite extensive examination, there was no evidence in the TEM foils of the bainitic regions that were observed in the SEM images. Vanadium carbides were found in the ferritic matrix and in the retained austenite/ferrite boundary, see Figures 5.42 and 5.43.

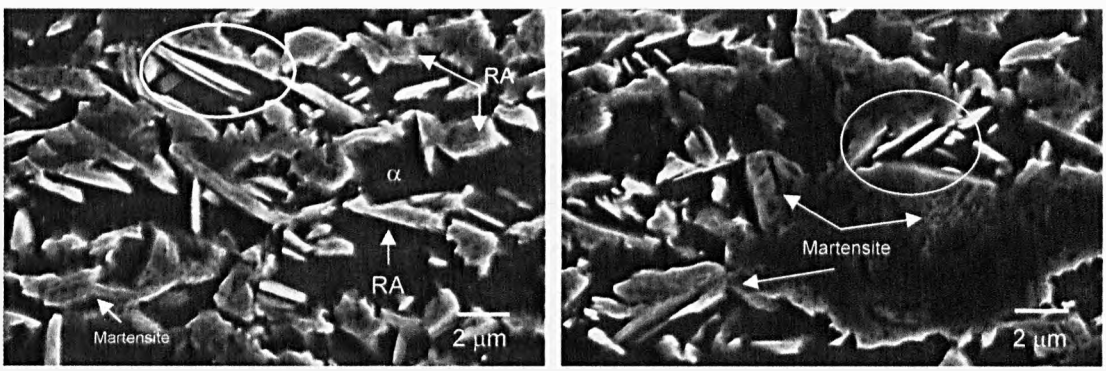

(a) **(b)**

Fig. 5.38 Ferritic matrix having: (a) retained austenite, (b) martensite islands, and also some regions that appeared to be bainite (circled) were found, base composition (A1) steel.

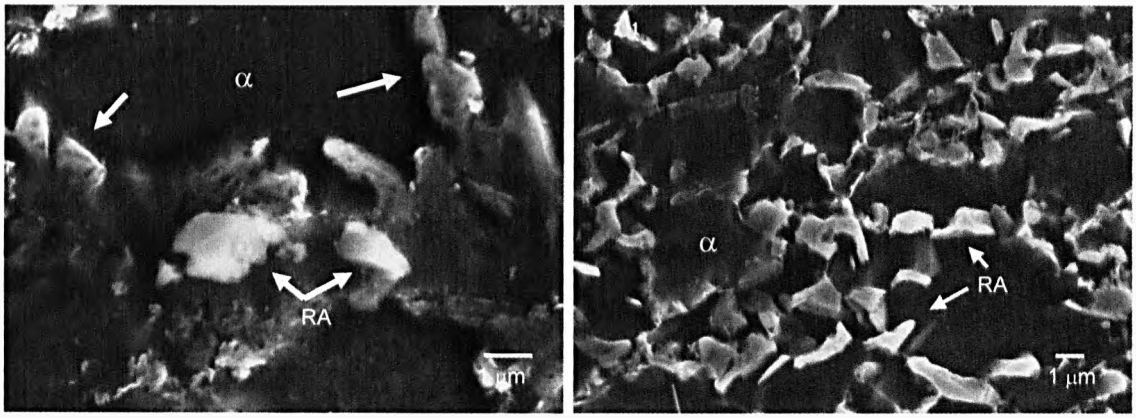

(a) **(b)**

Fig. 5.39 (a) Retained austenite in the middle of ferrite grain and (b) retained austenite – martensite distribution, high vanadium (C2) steel.

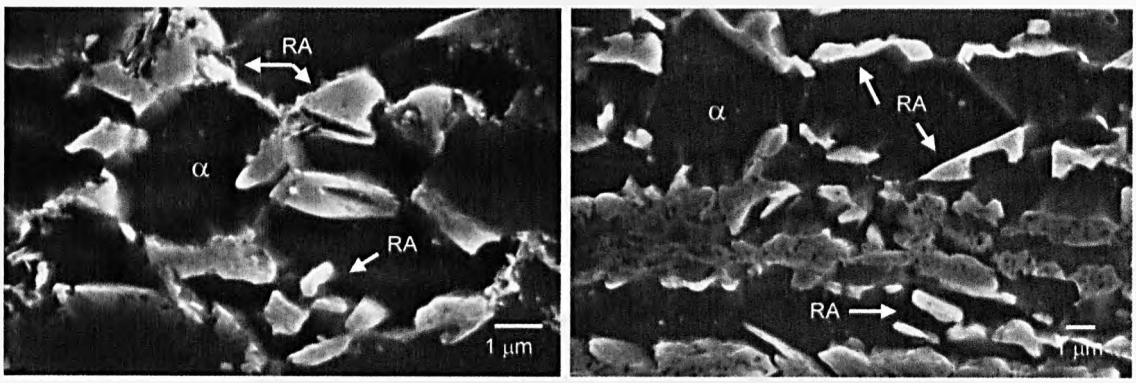

(a) **(b)**

Fig. 5.40 (a) Retained austenite and (b) martensite formed in a banded region in the low vanadium (B2) steel.

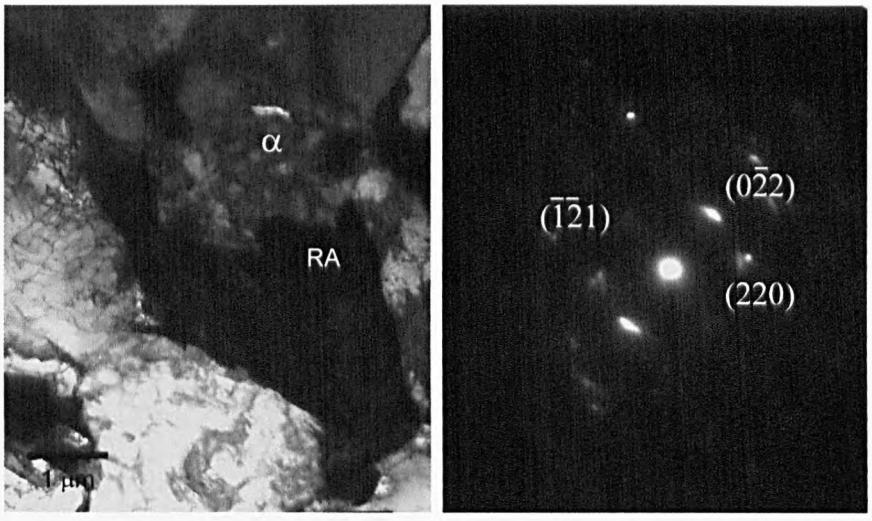

Fig. 5.41 (a) TEM bright field image showing retained austenite grain and (b) diffraction pattern, base composition (A1) steel.

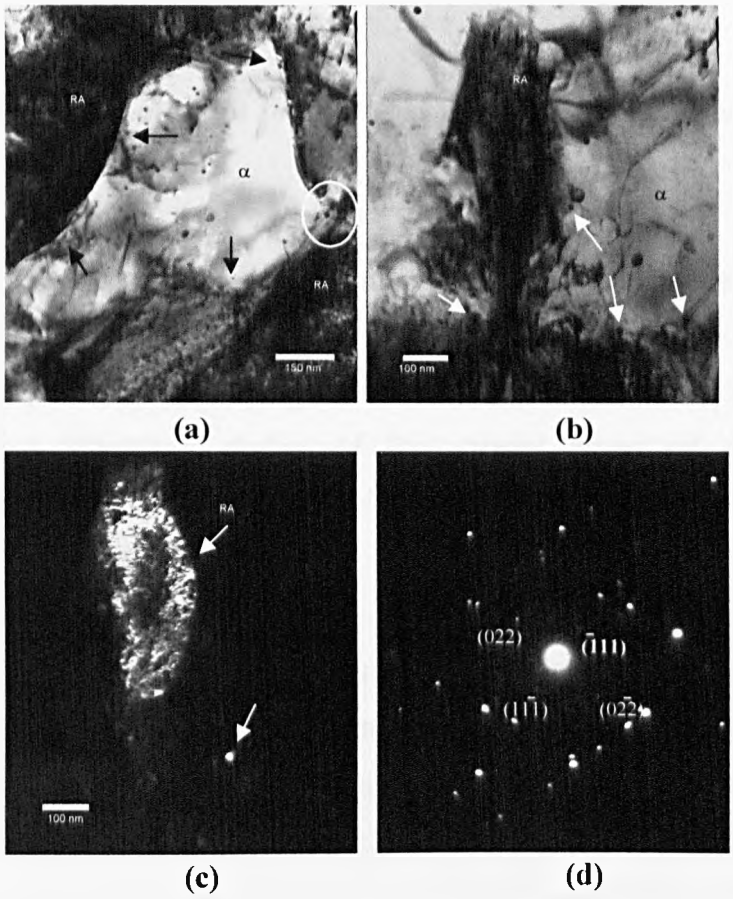

Fig. 5.42 TEM micrographs of (a) a ferrite grain with vanadium carbides and surrounded by retained austenite, (b) bright field showing retained austenite with some vanadium carbides at a ferrite/ferrite grain boundary, (c) dark field showing the vanadium precipitates and (d) diffraction pattern, high vanadium (C2) steel.

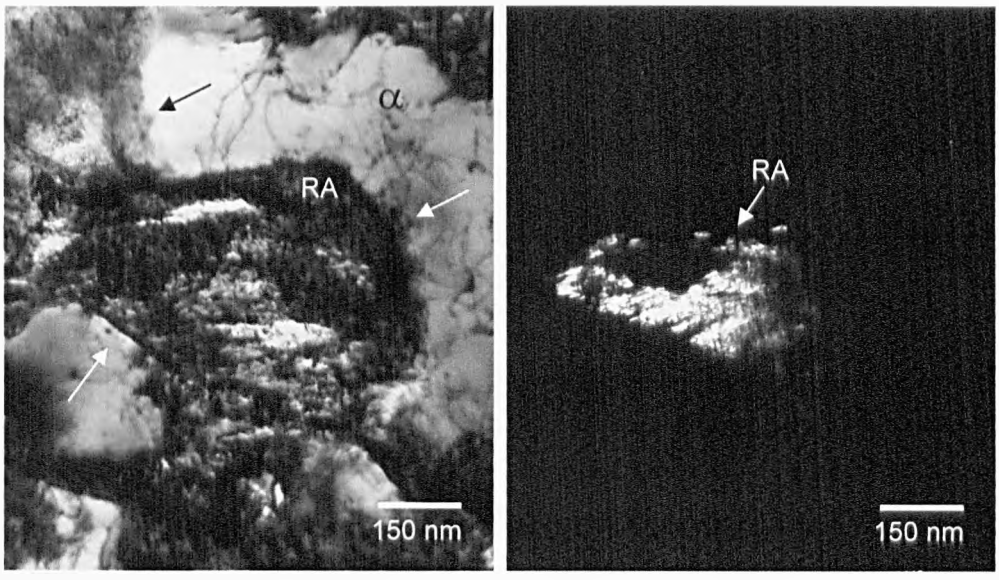

(a) **(b)**

Fig. 5.43 TEM micrographs of (a) vanadium carbides on the retained austenite/ferrite limit and (b) retained austenite found using dark field, low vanadium (B1) steel.

5.3.3.5 Microstructure produced in the isothermal bainitic transformation region at 460 °C (Stage 7)

The principal role of this stage of the heat treatment in the commercial process is to combine hot-dip galvanising with the isothermal bainite transformation. However, the short time of 5 seconds at 460 °C, which is dictated by commercial practice, is far less than used in most laboratory studies of this crucial aspect of microstructural development. This step determines the final size and volume fraction of each phase.

The microstructure developed consisted of one principal change, namely the formation of bainite at the expense of retained austenite. The microstructure still comprised martensite grains and the retained austenite – martensite constituent (RA/M), as-expected. Figure 5.45 gives low magnification views of the microstructure of the base composition (A1) and the high vanadium microalloyed steel (C2), comparing like with like areas of the samples. The main observed microstructural differences between the base composition (A1) and vanadium (B1, B2 and C1, C2) microalloyed steels were in the grain size, shape and homogeneity of the second constituents such as bainite, retained austenite, martensite and RA/M as shown in Figure 5.45.

As with Stages 3 and 5, the microstructure was generally homogeneous, although some residual banding effects could be seen, Figure 5.45 (b). One immediately obvious difference between the base composition and the microalloyed steel was the greater proportion of bainite in the former; compare Figures 5.45 (a) with (b). Not only did there appear to be a greater volume fraction of bainite in the base composition, but also the bainite was clearly coarser in the former, such that it often contained 3 austenite laths, while the microalloyed steel usually exhibited two. Bainite and martensite size measurements were carried out using image analysis of a minimum of 15 SEM images per steel and the values were averaged for each composition, following the procedure described in Chapter 3. The specimens were over etched in order to sufficiently differentiate the martensite and bainite. Table 5.6 presents a summary of the quantification of the amount of bainite and martensite. Figure 5.46 and Figure 5.47 shows this data plotted graphically, showing the effect of vanadium content on the amount of bainite and martensite. The increase in vanadium appears to give an approximately linear decrease in bainite content. The addition of 0.06 wt % vanadium reduces martensite content, but the further addition to 0.12 wt % appears to have no further effect.

The microstructure of the microalloyed steels was generally finer than that of the base composition. Table 5.7 gives the estimated grain size of the phases. Consistent with the size measurements made earlier in the process, the addition of vanadium decreased the size of all constituent phases. The ferrite grain size is shown in Figure 5.44.

Table 5.6 Summary of the quantification of the amounts of bainite and martensite of the multiphase steels fro Stage 7. SD= standard deviation.

Steel	Bainite		Martensite	
	(%)	SD	(%)	SD
A1	4.6	1.4	11	3.6
B1	3.7	1.4	9.7	1.2
B2	3.0	1.0	9.2	1.3
C1	2.9	1.0	9.9	0.9
C2	2.6	1.3	9.8	0.8

Table 5.7 Estimated grain size of the bainite, martensite and retained austenite in the multiphase steels.

Steel	Average grain size (μm)					
	Bainite	SD	Martensite	SD	RA	SD
A1	3.0	1.2	3.3	1.2	3.1	0.9
B1	2.1	0.6	2.4	0.7	2.3	0.4
B2	1.9	0.6	2.5	0.7	2.2	0.3
C1	1.5	0.4	2.0	0.6	1.8	0.4
C2	1.5	0.4	1.9	0.6	1.9	0.4

Note: RA=retained austenite, SD=standard deviation

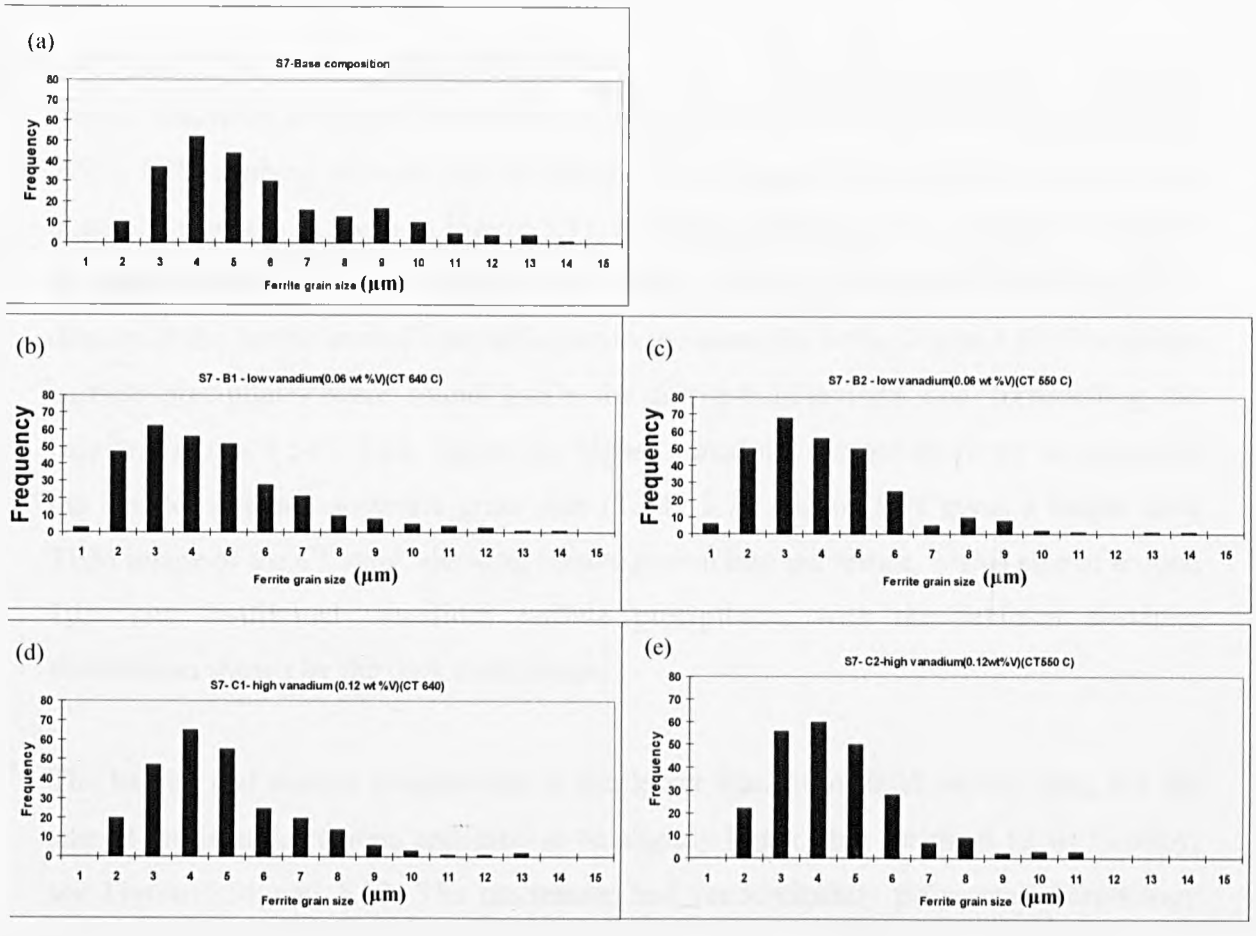

Fig. 5.44 Ferrite grain size of the base composition A1 and vanadium-microalloyed steels, Stage 7.

The morphology of the bainite is shown in Figures 5.48 through to 5.55 for steels A1, B2 and C2. The bainite in the base composition (A1) steel typically contained numerous laths, the example in the SEM micrograph in Figure 5.48 showing 6. The bainite observed in the vanadium microalloyed steels exhibited similar characteristics but typically only one or two laths were formed, as show in Figures 5.51 and 5.52 for B2 and C2 steels respectively.

The retained austenite was found mainly in a polygonal form but some RA was also found in elongated form in the centre of ferrite grains and, in addition, isolated crystals of RA were found in the centre of the ferrite grains. The polygonal austenite particles were similar for all the multiphase steels, the main difference was in their size, being smaller and more uniformly distributed in the microalloyed steels (Figure 5.45, 5.48 and 5.50). TEM analysis showed that the bainite generally grew from an austenite grain, an example of which is given in Figure 5.53, although SEM had given examples of where the phase appeared discrete, Figure 5.51. TEM generally showed a high dislocation density in the ferrite immediately adjacent to the austenite laths, Figure 5.53. Vanadium carbide precipitates were found inside the ferrite-bainite laths and surrounding the bainite, Figures 5.54 – 5.58. Again, the higher vanadium content (0.12 wt %) produced the smaller retained austenite grain size (Table 5.7). Figure 5.58 gives a bright field TEM image of the C1 steel, showing bainite grown into the ferrite, with a size of around 1μm and distributed vanadium carbide precipitates, with the retained austenite distribution shown by the dark field image.

The bainite had similar morphology in the lower vanadium (0.06 wt %) steel, but the size of the bainitic regions appeared to be slightly larger than for the 0.12 wt % alloy, see Figure 5.51 and 5.57. The martensite had predominantly polygonal morphology with a high density of dislocations, but many contained a fine twinned structure, see Figure 5.56. The particles frequently comprised a mixture of both martensite and retained austenite, Figures 5.56 and 5.59.

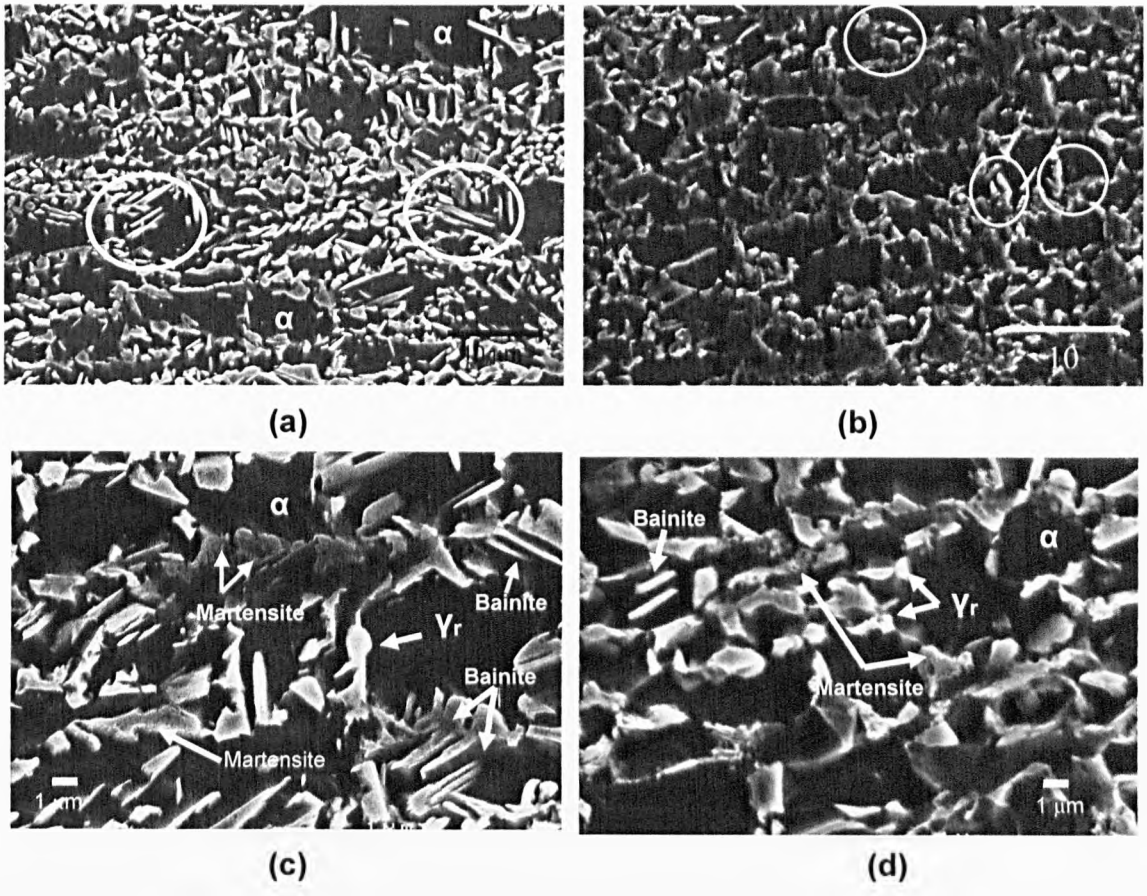

Fig. 5.45 general view of the final microstructure of (a) base composition and (b) high vanadium – C2 (0.12 wt %) (CT 550 °C) steel, bainite grains are circled also more bainite grains can be observed in the base composition (c) but the (d) high vanadium – C2 steel developed finer grains

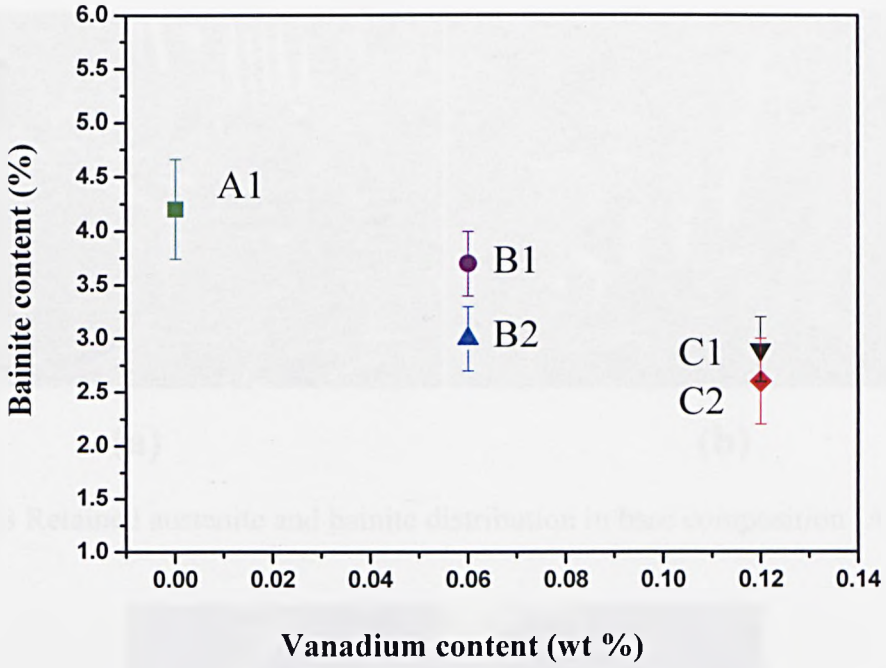

Fig. 5.46 Vanadium effect on the bainite content.

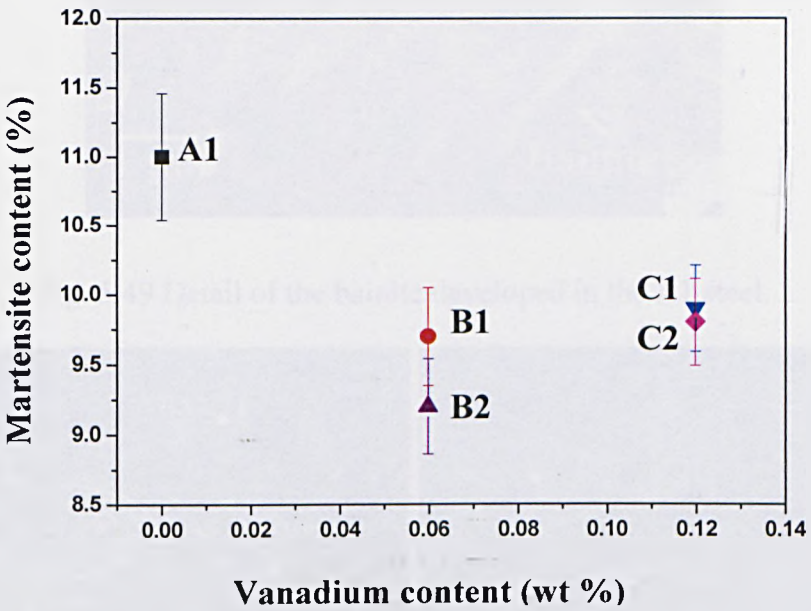

Fig. 5.47 Vanadium effect on the martensite content.

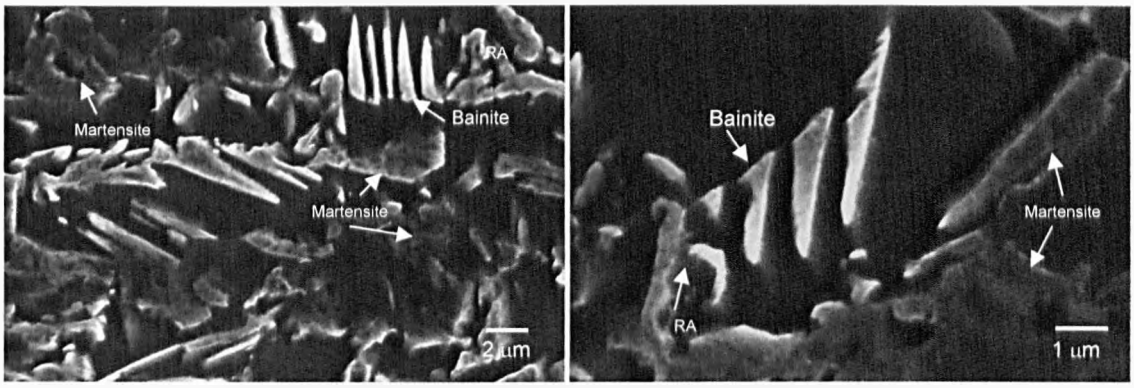

(a) **(b)**

Fig. 5.48 Retained austenite and bainite distribution in base composition (A1) steel.

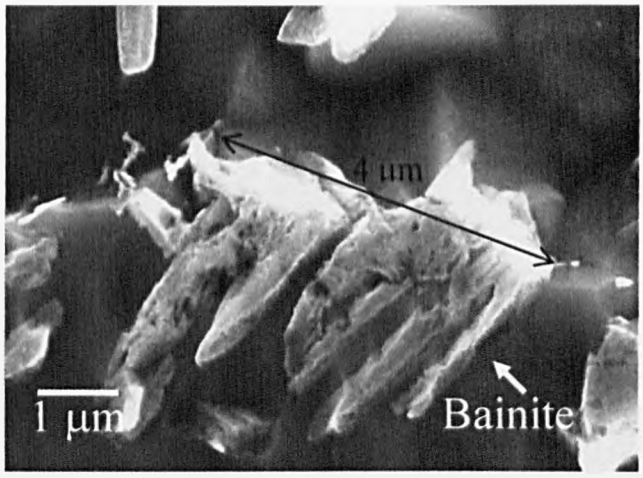

Fig. 5.49 Detail of the bainite developed in the A1 steel.

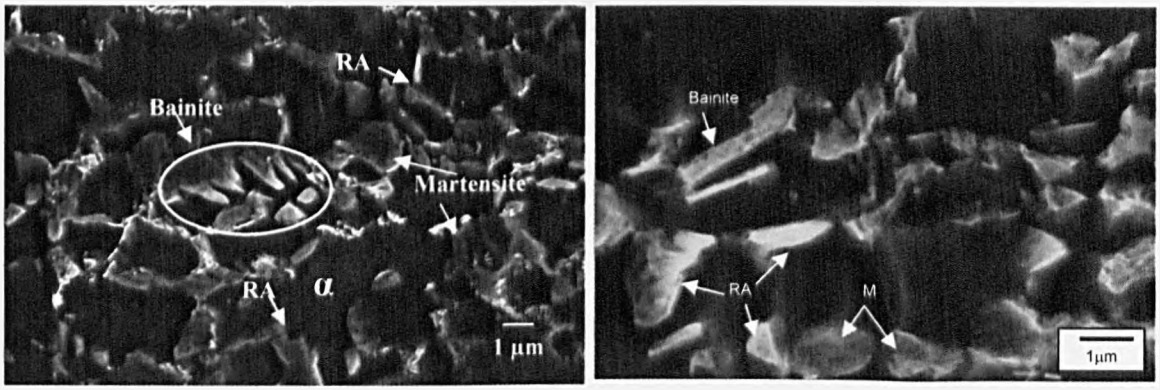

Fig. 5.50 Distribution of the phases in the high vanadium (C2) steel, showing only occasional bainite.

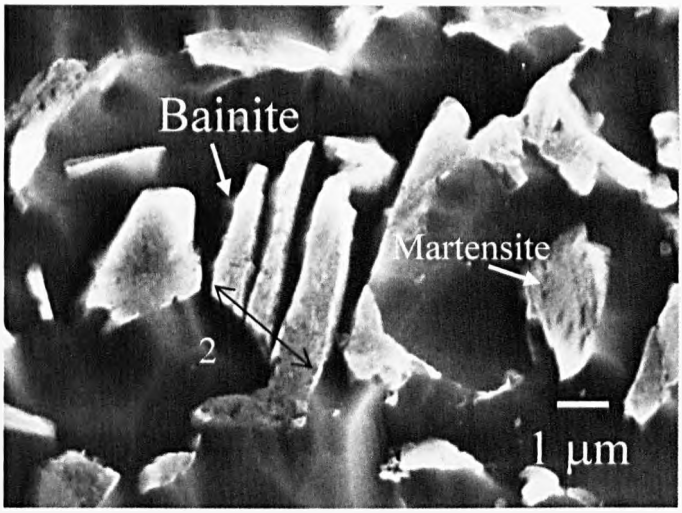

Fig. 5.51 Bainite grain developed in the B2 steel.

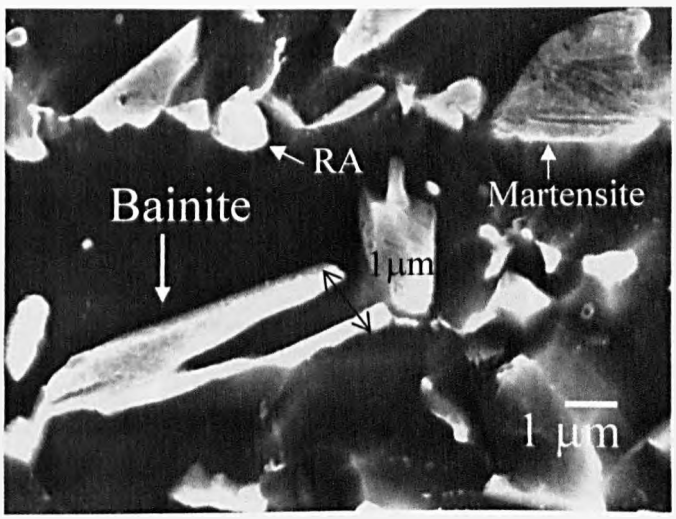

Fig. 5.52 The smaller bainitic grain size was produced in the C2 steel.

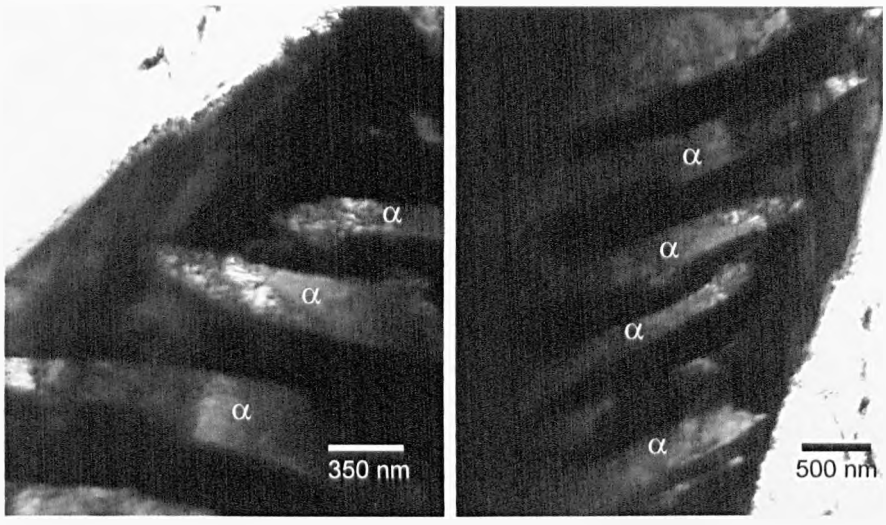

(a) **(b)**

Fig. 5.53 (a, b) TEM bright field micrographs showing the morphology of the bainite in the A1 steel.

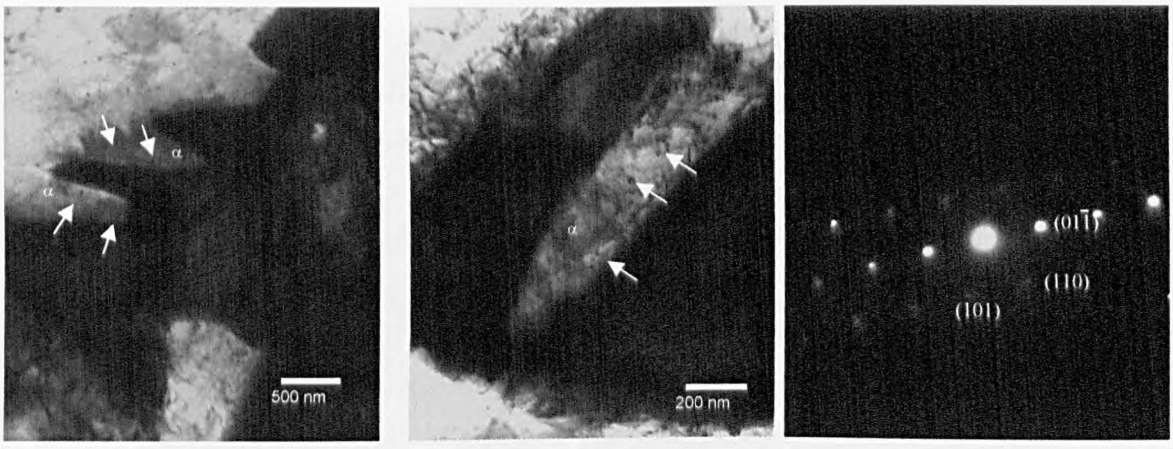

(a) **(b)** **(c)**

Fig.5.54 (a, b) TEM bright field micrographs showing the bainite and (b) vanadium carbides were found inside of the bainite, C2 steel. (c) Diffraction pattern from (b).

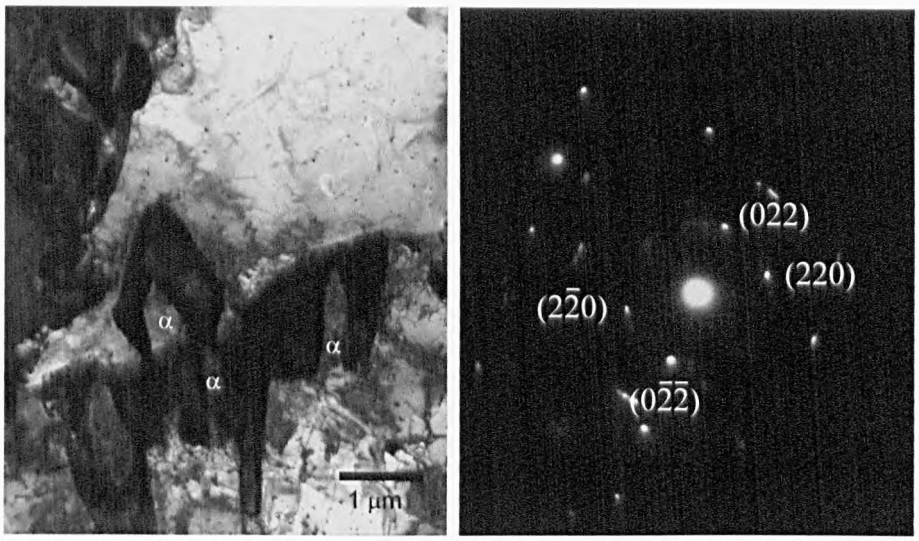

Fig. 5.55 (a) TEM bright field micrograph showing bainite and (b) diffraction pattern, C2 steel.

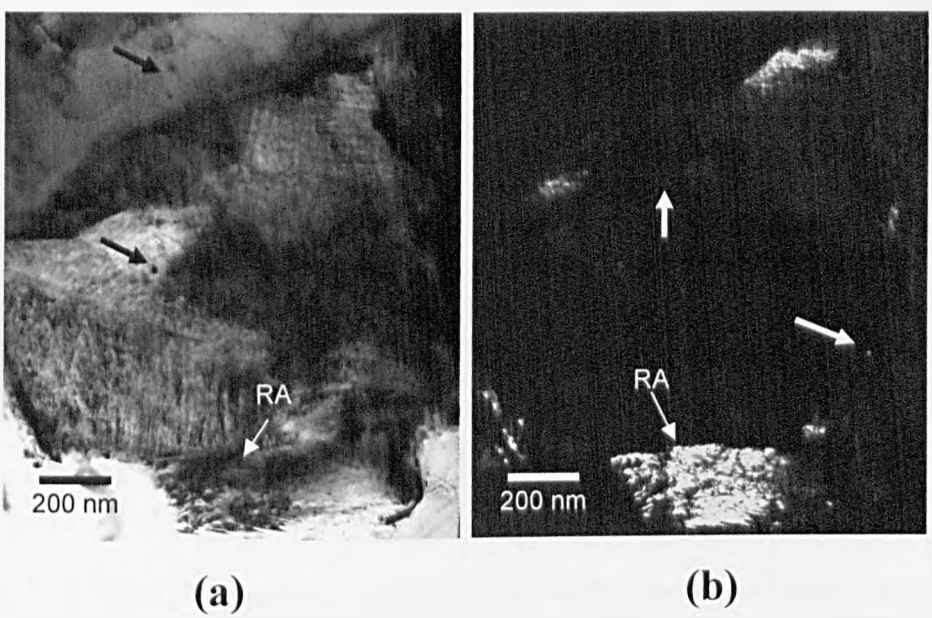

Fig. 5.56 TEM micrographs showing (a) retained austenite – martensite, bright field and (b) dark field, B1 steel.

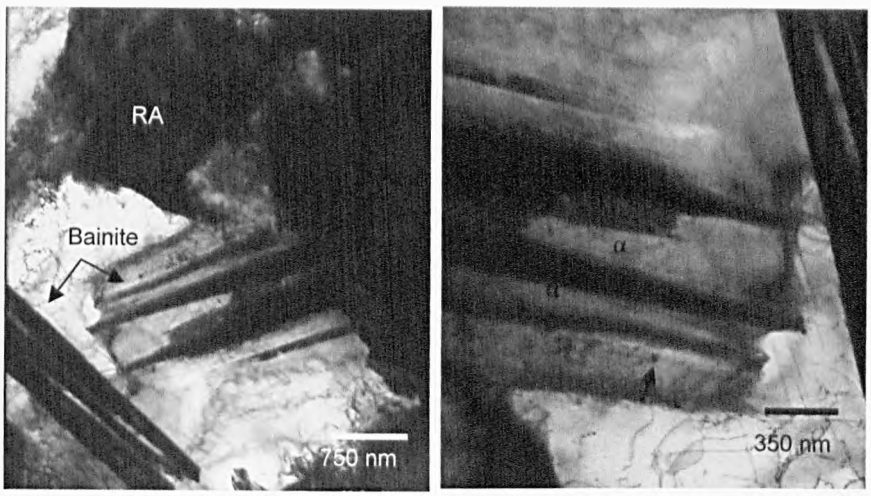

Fig. 5.57 TEM bright field micrographs showing (a) bainite and (b) at higher magnification showing vanadium carbides found within the bainite, B1 steel.

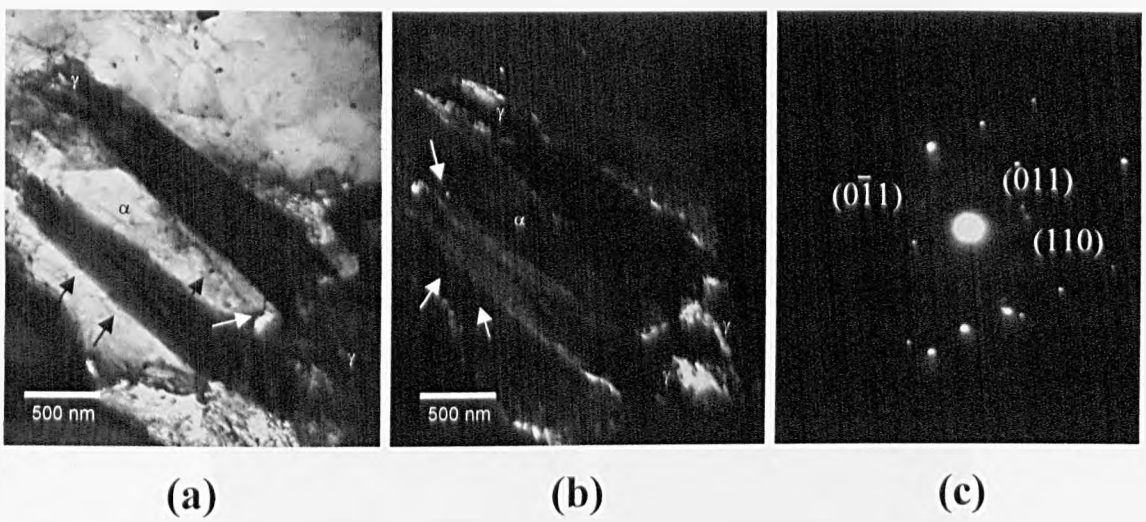

Fig. 5.58 TEM micrographs, (a) bright field image showing bainite with some vanadium carbides arrowed, (b) dark field showing the retained austenite at the interface between bainite laths and ferrite and (c) diffraction pattern, C1 steel.

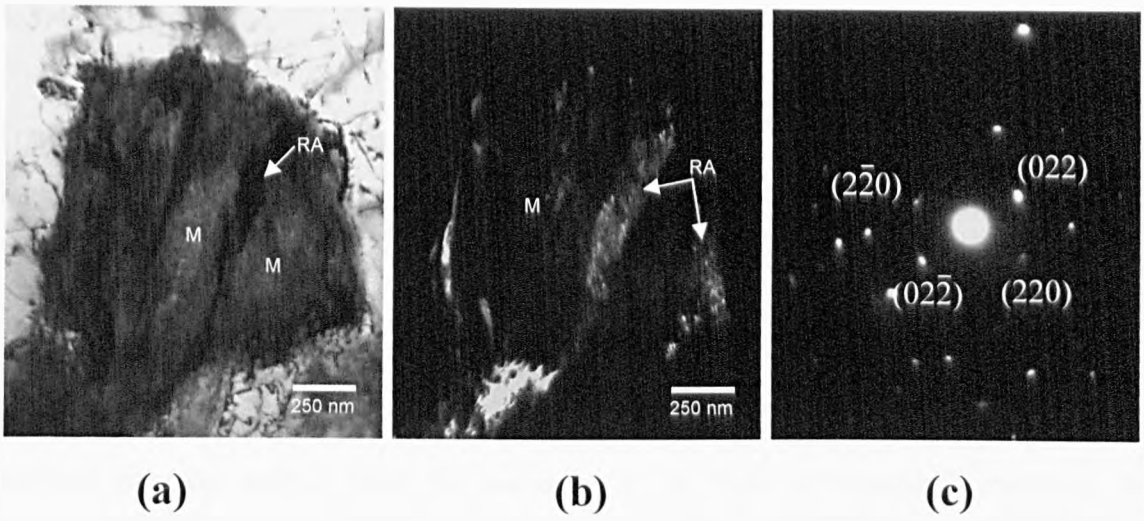

Fig. 5.59 TEM micrographs, (a) Bright field image showing retained austenite grain and martensite, (b) dark field image and (c) diffraction pattern, base composition (A1) steel.

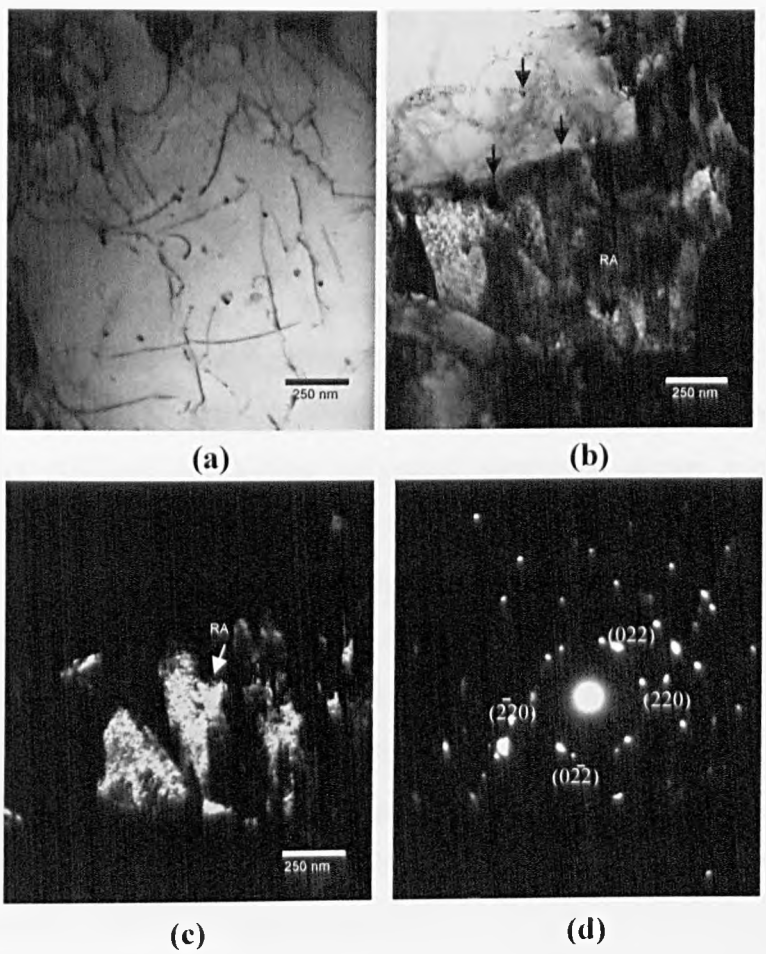

Fig. 5.60 TEM micrographs (a) Bright field image showing VC distribution in ferrite with dislocations, (b) bright field image showing retained austenite, some VC precipitates are indicated in the boundary, (c) dark field image from (b) and (d) diffraction pattern from (b). B1 steel.

5.3.4 Summary

The cold rolled starting structure was heavily banded, but no segregation of Mn or V was found. For the base composition (A1), low and high vanadium multiphase steel, the amount of retained austenite was determined by the austenite produced in the ferrite + austenite phase field which is influenced by the annealing temperature and holding time, e.g. the base composition (A1) steel was heated at 795 °C developing 9.3% of RA which was increased to 10% after being held for 20 seconds. Even though the vanadium addition removes carbon from the austenite in the form of vanadium carbides, the amount of retained austenite was higher in the vanadium microalloyed steels (12%) than the base composition (7%). The addition of 0.06 wt % V gave a substantial increase in the RA content, while the further addition up to 0.12 wt %V gave a further increase, but had less of an effect. The base composition (A1) had a higher carbon content in austenite than measured for the vanadium microalloyed (B1, B2 and C1, C2) steels but the results showed that having ~ 1.15% of carbon content in austenite is still enough to keep stable the RA at room temperature.

The microstructural transformations were similar for all the multiphase steels. The microstructure prior to the annealing process was composed of elongated ferrite grains and pearlite. The first transformation occurred on heating to 695 °C, where the ferrite was partially recrystallised developing polygonal elongated grains and the lamellar pearlite spheroidised. Retained austenite was not produced at this temperature. Significant transformation was observed at the annealing temperature of 795 °C, where austenite was formed and its content increased after being held for 20 seconds. From the microstructural analyses it is believed that the austenite formation took place firstly in the spheroidised cementite (produced at 695 °C) and secondly at the recrystallised ferrite grains boundaries. Interestingly, the strong banding observed in the cold rolled structure was not nearly so evident after heat treatment at 795 °C, when the microstructure became far more homogeneous.

The final microstructure was complex and consisted of a ferrite matrix plus retained austenite, bainite, martensite and the RA/M constituent. Vanadium additions reduced the bainite and martensite contents in the microalloyed steels, giving an increase in the retained austenite. This indicates that the vanadium addition led to a more stable austenite. In addition, the retained austenite and bainite grain sizes were decreased by the vanadium additions. The bainite size was determined by the retained austenite grain size. The origin of these observations will be discussed in Chapter 6.

5.4 Vanadium precipitation behaviour during the annealing process

To study the type, morphology and distribution of vanadium-based precipitates in detail, carbon extraction replicas were taken from specimens in hot rolled and intercritically annealed conditions. In the samples heated at 695°C, besides the coarse cementite, very fine Fe_3C carbides were also formed, which appeared similar to the vanadium-based precipitates making their identification difficult. After Stage 1, the size of precipitates was fairly uniform and easily distinguishable. One of the aims of this research work was to ascertain whether or not the coiling temperature affected the precipitation and therefore the properties. To investigate this, the vanadium-based precipitation was analysed in the different stages of the annealing process as follows:

- Characterisation in hot rolled conditions
- During the heating at 695 °C – Stage 1
- In the ferrite + austenite region (heated at 795 °C for Stage 2 and held for 20 seconds for Stage 3)
- In the isothermal bainitic transformation – Stage 7.

The first particular objective was to establish if the vanadium–based precipitates formed were carbides (VC) or carbonitrides (VCN). In order to determine the kind of vanadium–based precipitates formed, Electron Energy Loss Spectroscopy (EELS) was undertaken in the TEM using extraction replicas.

EELS is particularly sensitive to light elements and is therefore the most appropriate technique. Figure 5.61 shows the EELS spectrum obtained, where it can be seen that nitrogen was not found. The carbon observed could have come from the extraction replica substrate or from the carbide. However, the absence of nitrogen strongly suggests that the vanadium-based precipitates were vanadium carbides (VC). Substantial numbers (between 600 and 1200 particles) of VC with difference sizes were observed distributed throughout the ferrite matrix, along the RA/ferrite boundaries, in the martensite, and within the retained austenite and bainite.

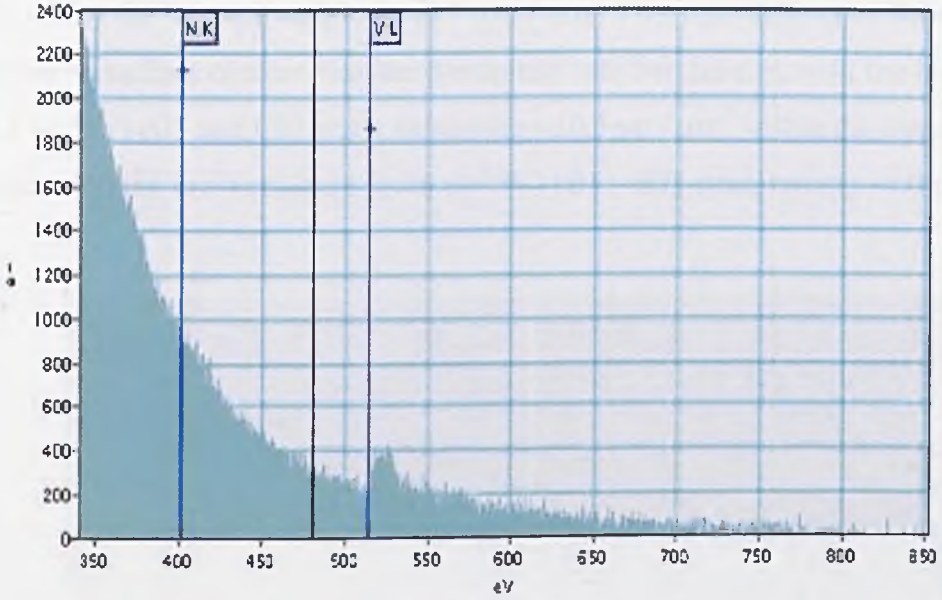

Fig. 5.61 EELS spectrum of a vanadium based precipitate showing the presence of vanadium but the absence of nitrogen, suggesting VC precipitates.

5.4.1 Vanadium carbide precipitate characterisation in hot rolled conditions

The vanadium carbides (VC) were found dispersed in the ferrite matrix and at the interface of the ferrite/pearlite grains. This VC distribution was similar for low vanadium (0.06 wt %) (B1 - B2) and high vanadium (0.12 wt %) (C1 – C2) steels. The distribution of vanadium carbides is shown in Figure 5.62 (a) and (b) which corresponds to the low vanadium (B1) steel.

Figure 5.62 (a) shows VC located in the ferrite (arrowed), while in (b) finer VC particles are located in ferrite/cementite boundary (indicated by arrows and circled). Figure 5.63 shows the VC distribution for the high vanadium (C2) steel, with the VC found in the matrix in Figure 5.63 (a), while (b) shows VC within the ferrite and at the ferrite/pearlite boundary, the VC being distinguished using dark field imaging (Figure 5.63 (c)). The average diameter and distribution of the VC are shown in the histograms given in Figure 5.64 for the low and high vanadium steels. The VC size distribution was quite similar for the low vanadium (B1, B2) steels, with a size range from 7 to 16 nm. Similar behaviour was observed in the high vanadium (C1, C2) steels; see Figure 5.64, where the VC size ranged from 7 to 17 nm. The main difference between the high and low vanadium content was the precipitate number density, with the high vanadium (0.12 wt %V) (C1 and C2) steels exhibiting ~10.5 pp / μm^2 within the same sample area compared to the low vanadium (0.06 wt %V) (B1 – B2) steel, having ~5.8 pp / μm^2.

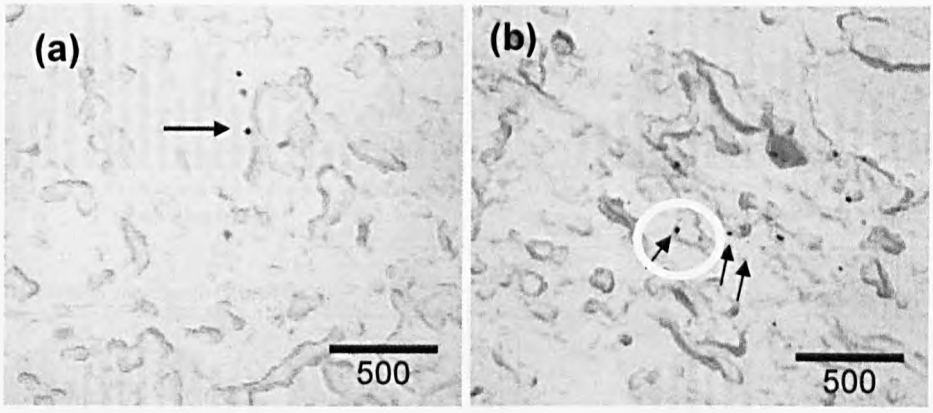

Fig. 5.62 TEM bright field micrographs of extraction replicas showing (a) Vanadium carbides in ferrite and (b) in the ferrite/pearlite boundary, B1 Steel in hot rolled conditions.

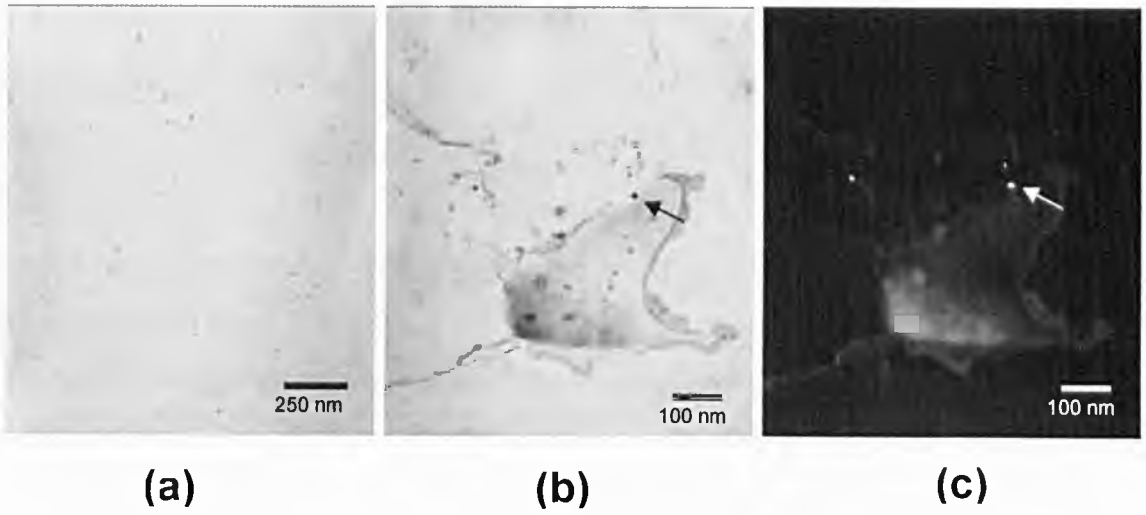

Fig. 5.63 TEM bright field micrographs of extraction replicas (a) VC precipitates, (b) VC in the ferrite and close to the boundaries, (c) dark field showing the VC, C2 Steel in hot rolled conditions.

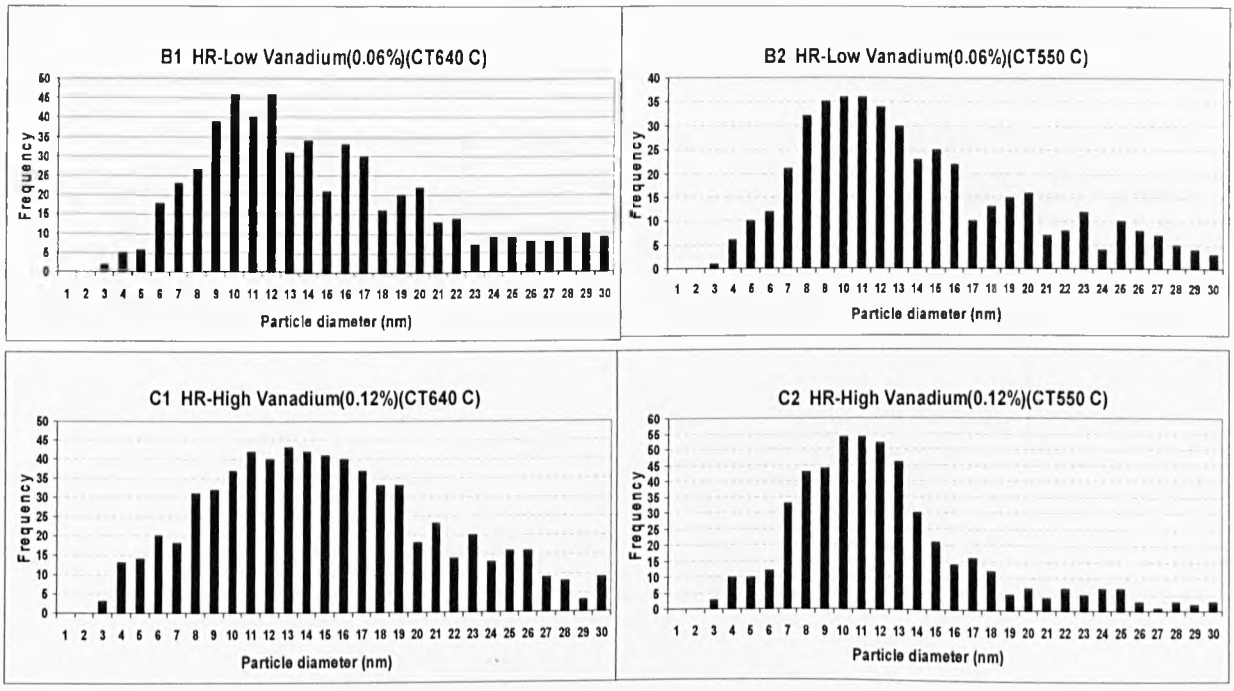

Fig. 5.64 Distribution and diameter of the vanadium carbides of the low (B1, B2) and high (C1, C2) vanadium steels in hot –rolled conditions with coiling temperatures of 640 °C and 550 °C.

5.4.2 Vanadium – based precipitate evolution during the heating at 695 °C – Stage 1

Precipitation of vanadium carbides was observed during Stage 1. The precipitate number density increased from 5.8 pp / μm^2 to 7.9 pp / μm^2 on average in the B1 and B2 steels, and from ~10.5 pp / μm^2 to 15 pp / μm^2 in the C1 and C2 steels. The dominance of fragmented pearlite at this stage made the observation of VC difficult, in particular some Fe_3C carbides from the pearlite were spherical shaped and finer than ~ 40 nm, appearing quite similar to the VC. Dark field was helpful in identifying the VC, as shown in Figures 5.65 and 5.66 for the B1 and C2 steels respectively. The VC carbides were found at the ferrite/cementite boundaries.

EDS analysis confirmed the VC identification (Figure 5.65 (c)). Even using the carbon extraction replicas for the quantification of precipitate distributions, it was necessary to use dark field imaging in order to distinguish the VC as shown in the Figures 5.67 (a) and (b) for the B1 and C2 steels respectively. The average diameter was broadly similar for both materials at this stage, see Figure 5.68, but such measurements inevitably suffer from sampling errors.

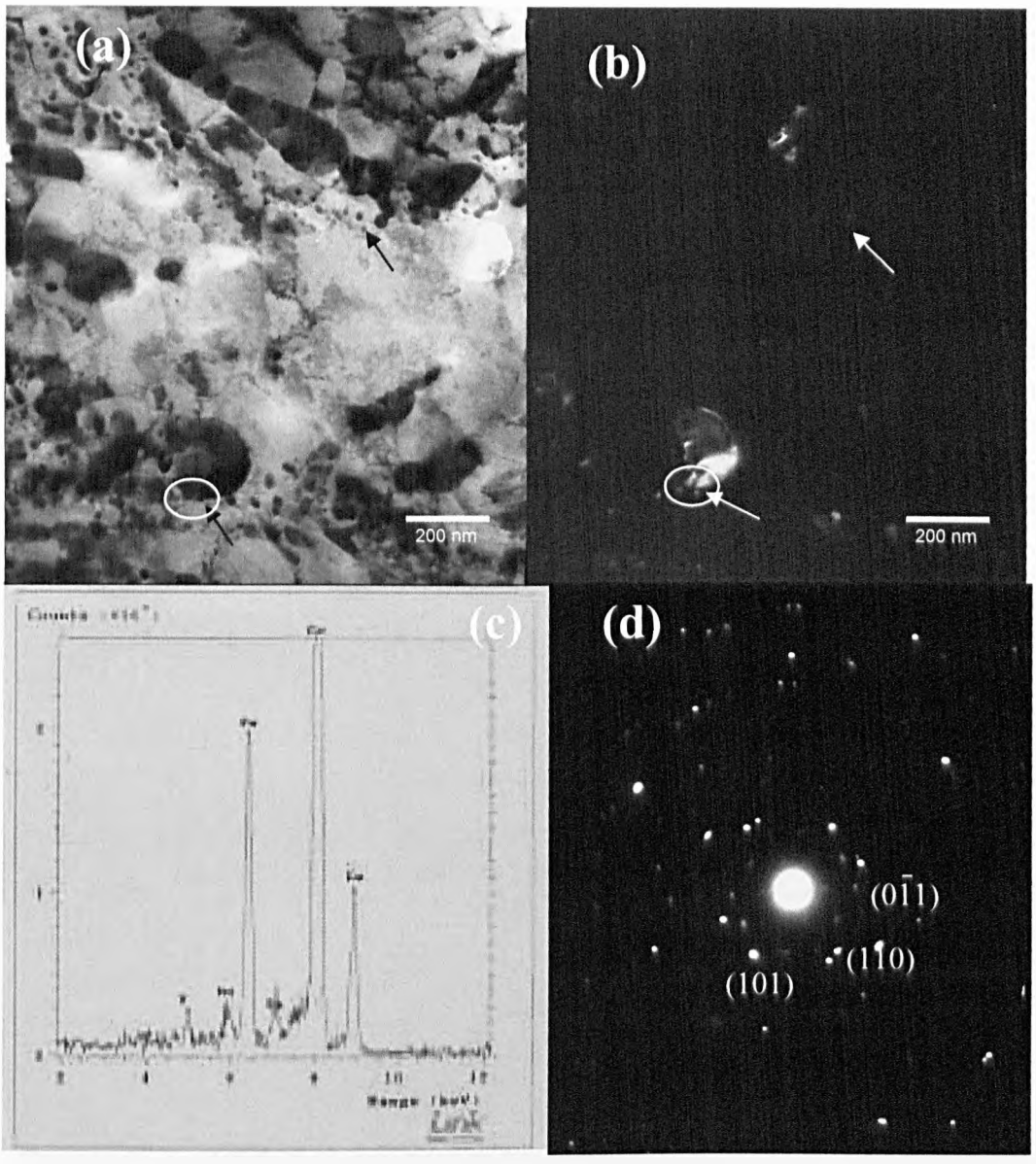

Fig. 5.65 (a) Bright field TEM micrograph of a thin foil showing VC found at the ferrite/cementite boundary and (b) dark field image of the same region with VC precipitates arrowed; (c) EDS confirming the presence of vanadium, and (d) the diffraction pattern. B1 steel.

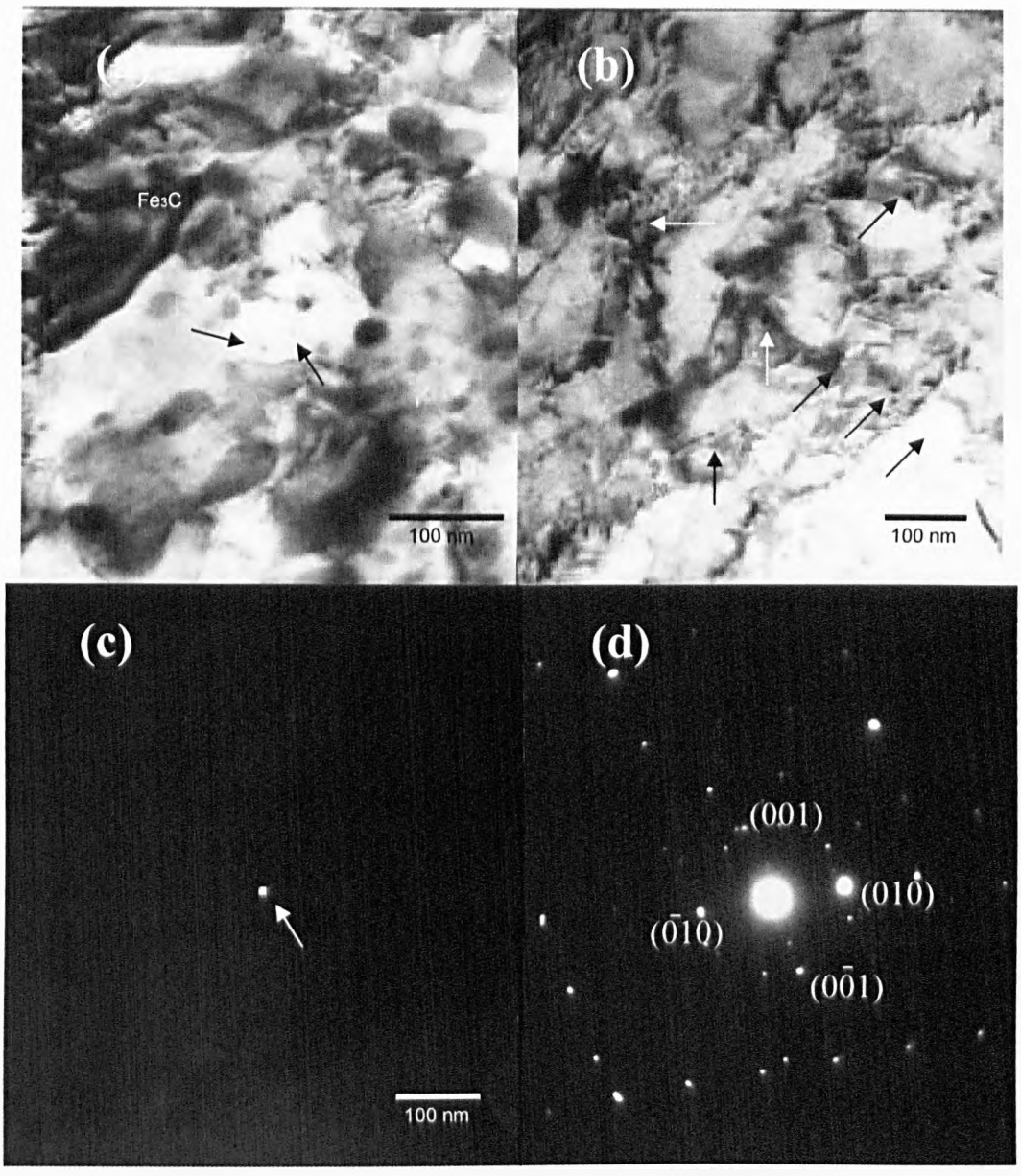

Fig. 5.66 (a) Bright field TEM micrograph of a thin foil showing vanadium carbide precipitates close to spherical cementite, (b) VC dispersed in ferrite, (c) precipitates found using dark field, the corresponding DP is shown in (d), C2 steel.

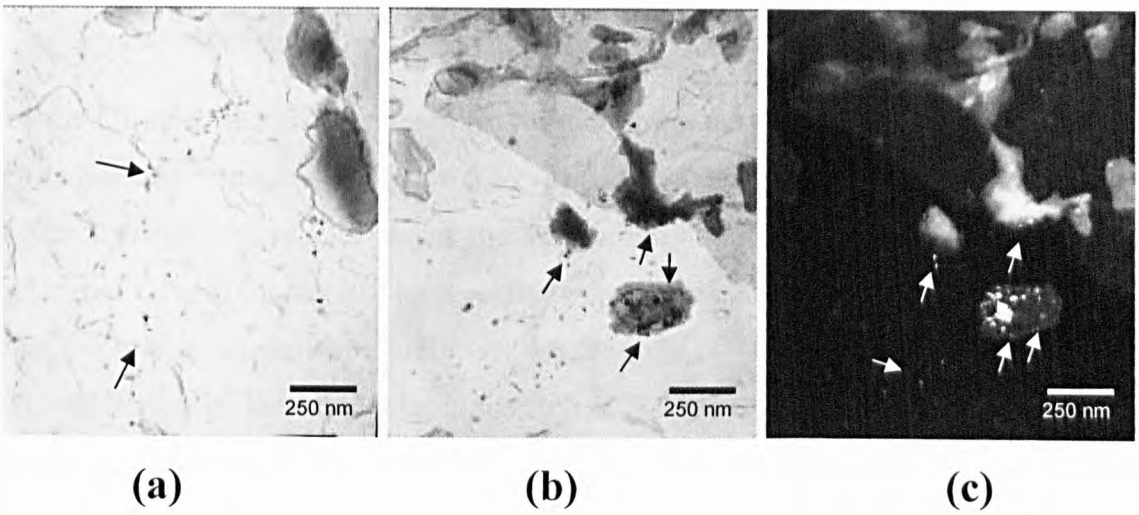

Fig. 5.67 (a) TEM bright field micrograph of a carbon extraction replica, showing VC precipitates found in ferrite grains boundaries, B1 steel, (b) precipitates found at the cementite boundary in steel C2, and (c) dark field of the same region as (b) showing the precipitates.

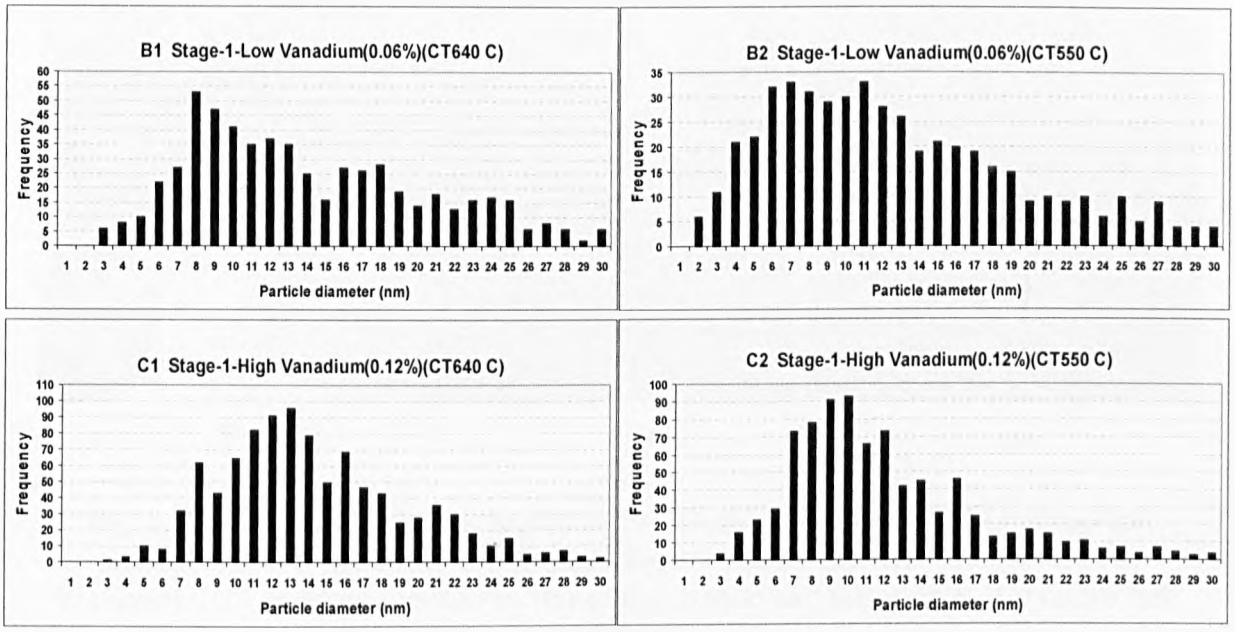

Fig. 5.68 Distribution and diameter of the vanadium carbides obtained from carbon extraction replicas of the low (B1, B2) and high (C1, C2) vanadium steels in Stage 1, with coiling temperatures of 640 °C and 550 °C.

5.4.3 Vanadium carbide precipitate evolution at 795 °C – Stage 2

For the C1 steel, the precipitates were located in the austenite, in the ferrite and at the ferrite/austenite boundaries (Figure 5.69 (a) (b)) and the diffraction pattern is shown in Figure 5.69 (c). Figure 5.70 shows the VC distribution as shown by carbon extraction replicas of C1 and C2 steels. The precipitates were located at the ferrite boundaries with what is possibly an austenite grain; see Figure 5.70 (a). Using dark field imaging, the VC was found in the same place; see Figure 5.70 (c). The EDS analysis showed a significant vanadium peak, Figure 5.71. An increase in the size of the VC was observed for all steels, see Figure 5.72. At Stage 2, for the B1 and B2 steel, the VC precipitate number density had increased from ~7.9 pp / μm^2 to ~11.3 pp / μm^2.

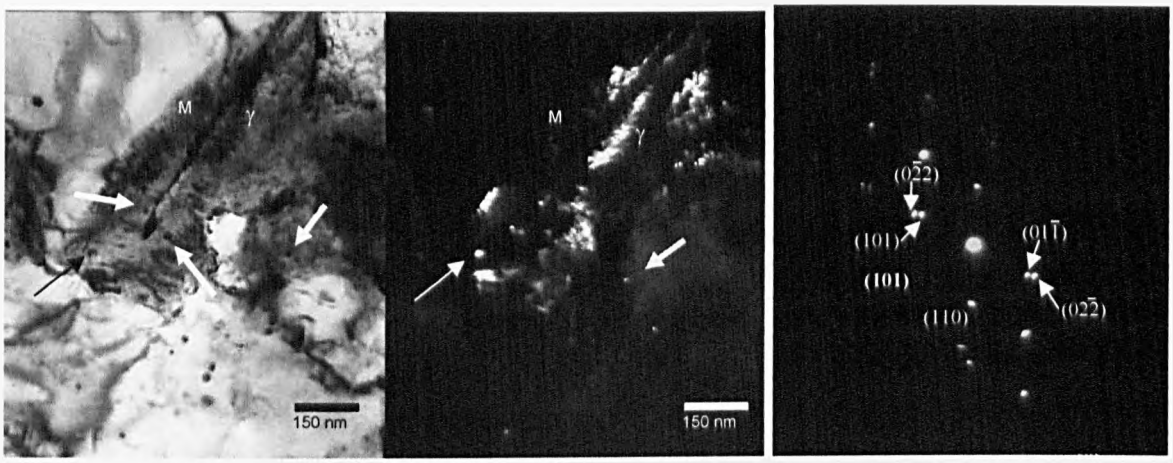

Fig. 5.69 C1 steel sample was heated at 795 °C. (a) Bright field TEM micrograph showing the VC located in the retained austenite phase partially transformed to martensite, (b) dark field shows the retained austenite and precipitates, (c) diffraction pattern.

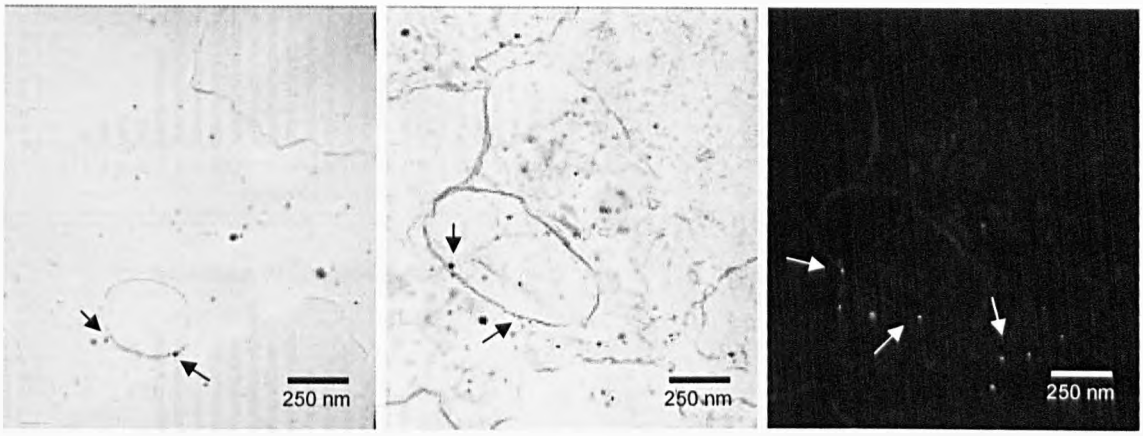

Fig. 5.70 (a) C1 steel, vanadium carbide precipitates were located in the ferrite/austenite interface, (b) C2 steel, VC dispersed in the ferrite and in the ferrite grain boundaries and (c) dark field showing the VC precipitates distribution C2 steel.

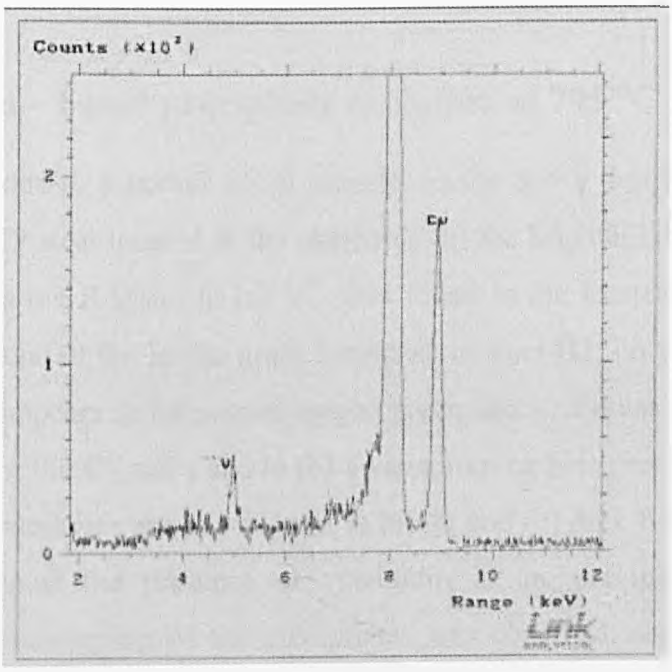

Fig. 5.71 EDS result showing a strong vanadium peak, C1 steel.

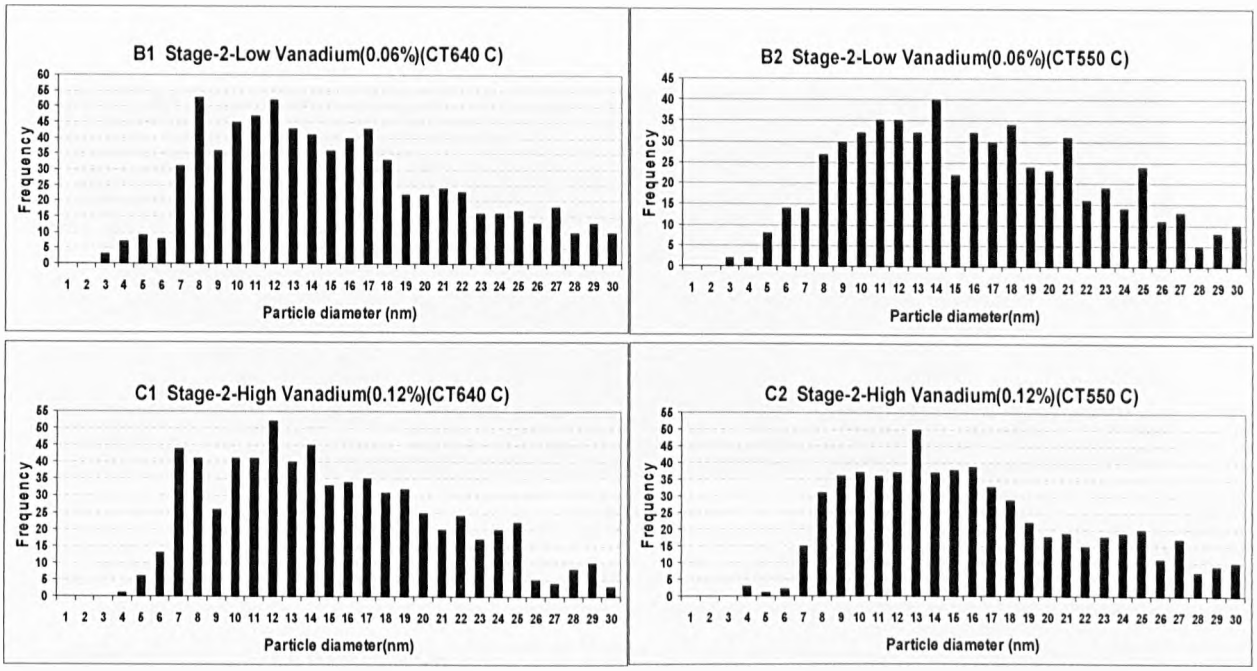

Fig. 5.72 Distribution and diameter of the vanadium carbides of the low (B1, B2) and high (C1, C2) vanadium steels at Stage 2, with coiling temperatures of 640°C and 550°C.

5.4.4 Vanadium – based precipitate evolution at 795 °C – Stage 3

Stage 3 corresponded to a period of 20 seconds in the $\alpha + \gamma$ domain. Figure 5.73 (a) shows VC in the C2 steel located in the austenite, (b) the brighter contrast region in the dark field image is the RA and in (c) VC was found in the martensite phase. Figure 5.73 shows VC found at the ferrite grain boundary in steel B1; note how the boundary looks curved and appears to be pinned by the precipitates. Figure 5.75 (a) shows the VC in the ferrite for the C1 steel, and in (b) a vanadium carbide precipitate in the ferrite and in the grain boundaries are shown both in bright and (c) dark field for the C2 steel. EDS again confirmed the presence of vanadium in the precipitates, Figure 5.74. Additional growth/coarsening of the precipitates was observed, see the histograms of the Figure 5.77. In the case of the B1 and B2 steels (Figure 5.77), the number of precipitates per unit area was basically the same, ~12 and 11.8 pp / μm^2 respectively. There was a small increase in the number of precipitates per unit area for the C1 and C2 steels which could be a sampling effect (18.7 and 19.9 pp / μm^2 respectively).

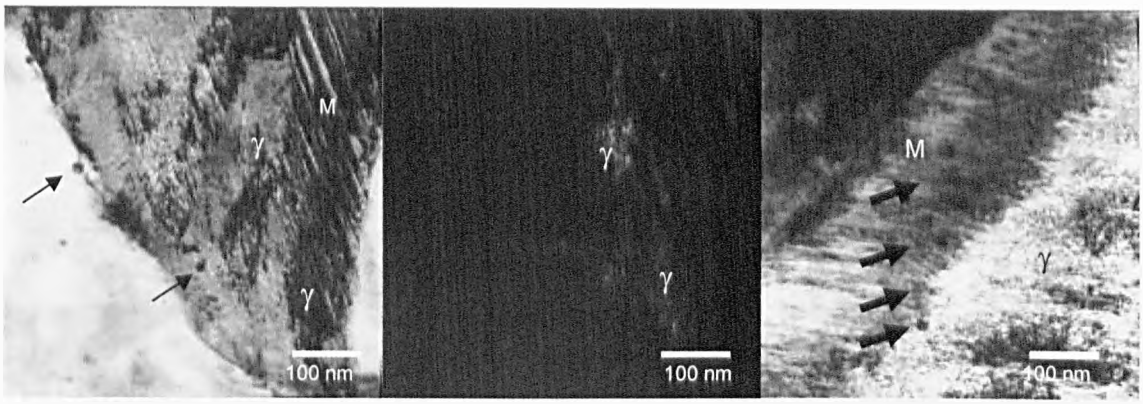

(a) **(b)** **(c)**

Fig. 5.73 C2 steel heated at 795 °C and held for 20 s. Bright field TEM micrograph of a thin foil showing (a) vanadium carbides located at the grain boundary and in the austenite, (b) dark field image showing the retained austenite, (c) twinned martensite with precipitates aligned in a stringer fashion.

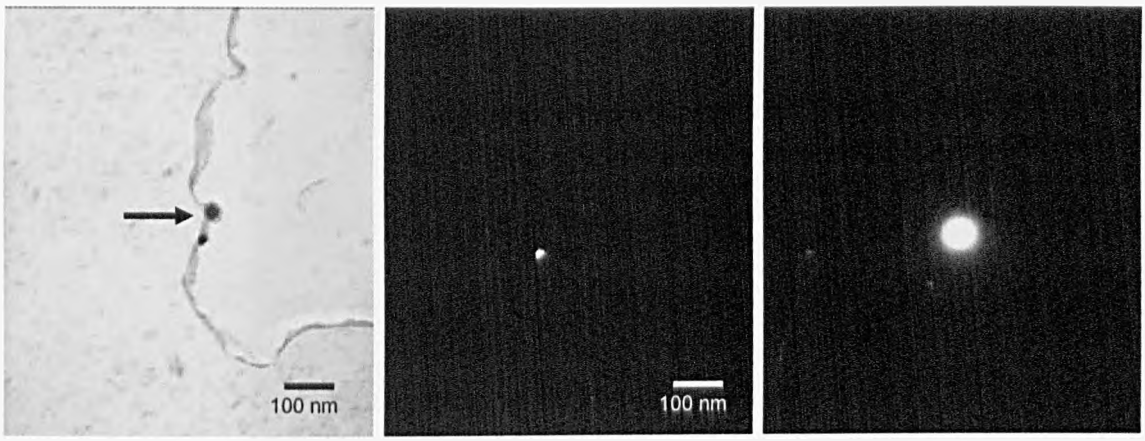

(a) **(b)** **(c)**

Fig. 5.74 (a) Bright field TEM micrograph a carbon extraction replica showing VC at the grain boundary, (b) dark field image of the same region and (c) diffraction pattern, B1 steel.

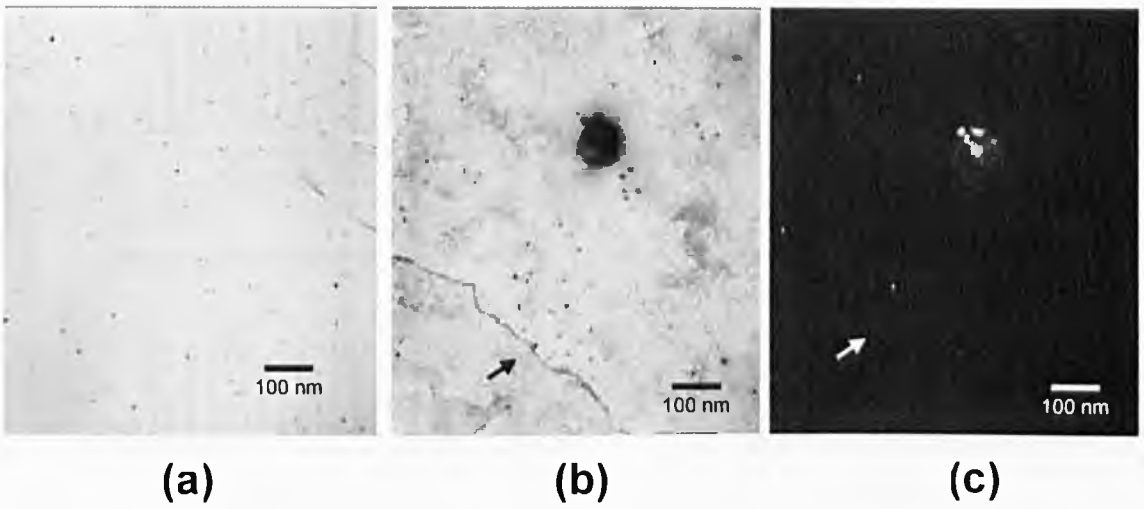

Fig. 5.75 (a) Bright field TEM micrograph a carbon extraction replica showing VC dispersion (C1 steel), (b) VC are arrowed close to a grain boundary, (c) dark field image of the same region as (b), C2 steel.

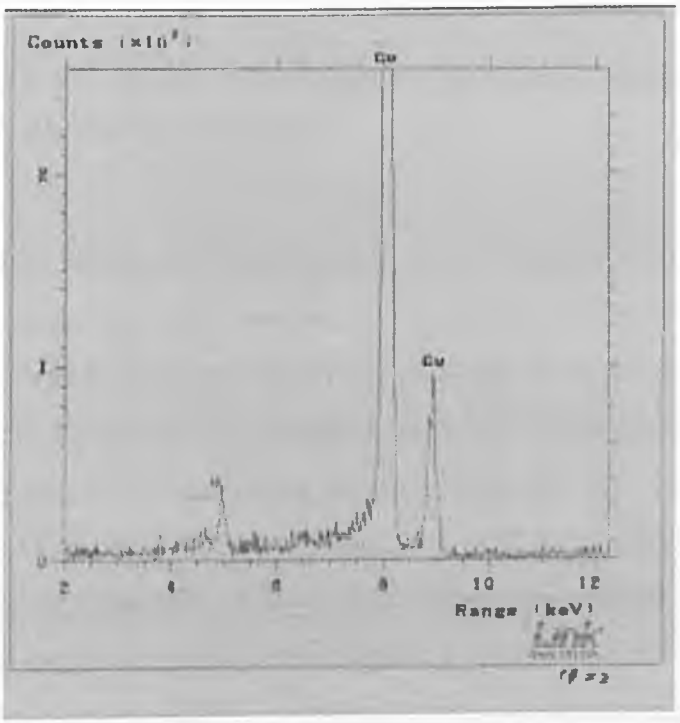

Fig. 5.76 EDS showing a clear and strong vanadium peak, C2 steel.

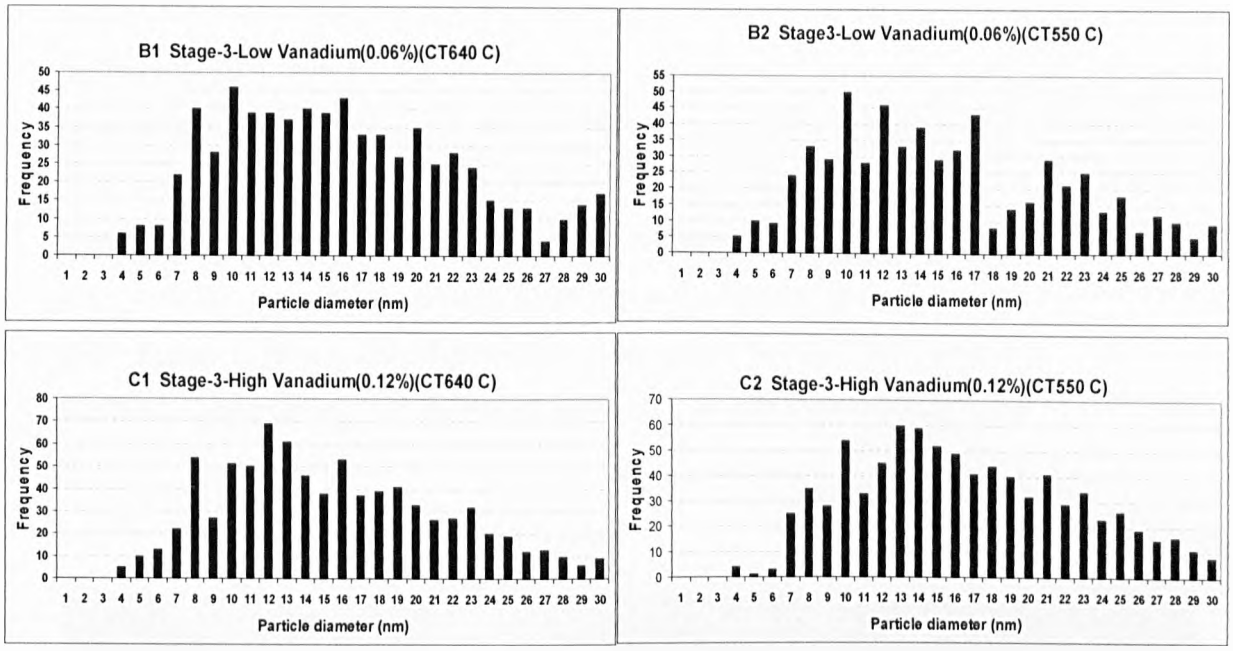

Fig. 5.77 Distribution and diameter of the vanadium carbides taken from carbon extraction replicas of the low (B1, B2) and high (C1, C2) vanadium steels at Stage 3, with coiling temperatures of 640°C and 550°C.

5.4.5 Vanadium – based precipitate evolution during isothermal transformation at 460 °C – Stage 7

This stage corresponded to a hold for 5 seconds at the isothermal bainitic transformation at 460 °C, following the intercritical anneal cycle. Figure 5.78 shows TEM micrographs from thin foil samples of the C1 and B1 steels, showing VC in the ferrite, sometimes as stringers, with some precipitates on dislocation lines. The micrograph in Figure 5.78 (a) and (b) also shows larger VC of ~30 nm diameter (arrowed). VC was also observed in the RA (circled in Figure 5.78 (b)) but the particles were quite difficult to observe. The RA appears bright together with VC in dark field image, Figure 5.78 (c). The VC distribution from a carbon extraction replica taken from the C1 steel is shown in Figure 5.79 (a) having a more homogenous appearance than was observed in the B1 steel, see Figure 5.79 (b). Again EDS was used to confirm the presence of vanadium Figure 5.80.

The vanadium carbide precipitation throughout the annealing process is shown in the histograms of Figures 5.81 and 5.82 that correspond to the low and high vanadium respectively. A more uniform size and homogenous distribution was developed by the high vanadium (0.12 wt %V - C1) steel, see Figure 5.82. Almost all precipitates measured were smaller than 30 nm, but there appeared to be a bimodal distribution of size, with two ranges, one from 7 to 16 nm and a second from 17 to 30 nm. For the B1 steel, Figure 5.79, the finer precipitates sizes were observed in a range from 4 to 16 nm, but the VC coarsening had produced an uneven distribution in the interval 17 – 30 nm.

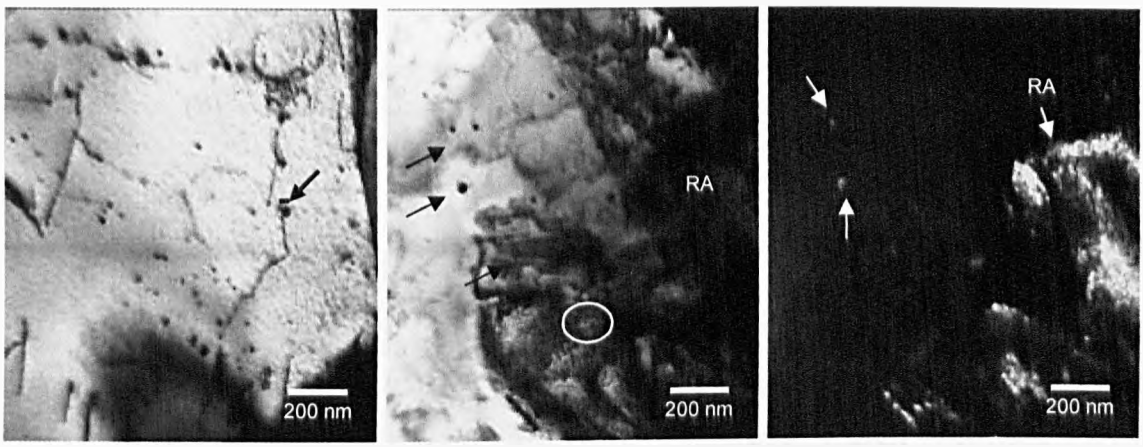

Fig. 5.78 (a) TEM bright field image from a thin foil showing VC dispersed in a ferrite grain, often associated with dislocations for the C1 steel, (b) VC within the RA, circled, and in the ferrite (arrowed) and (c) dark field image of RA and VC from the same region as (b), B1 steel.

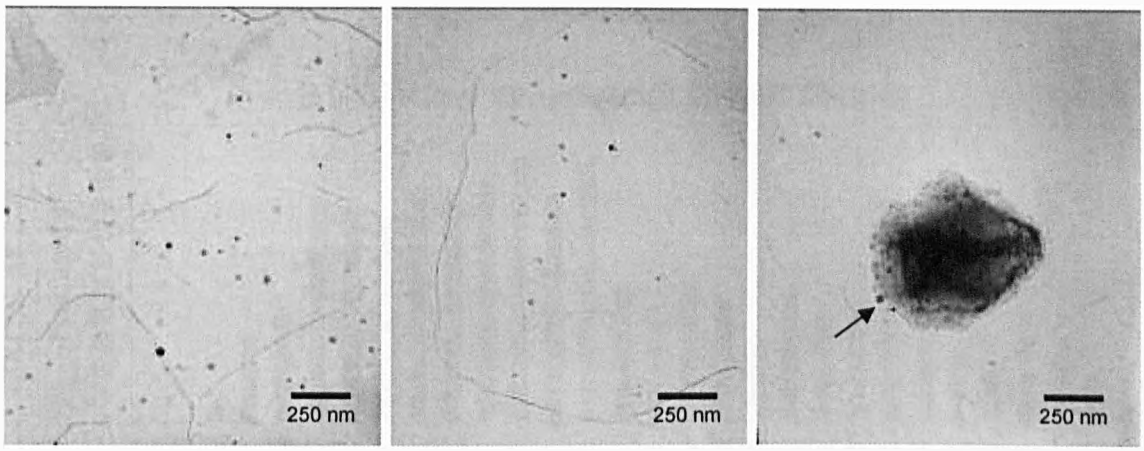

(a) **(b)** **(c)**

Fig. 5.79 TEM bright field images from carbon extraction replicas (a) VC distribution in C1 steel, (b) VC distribution within a ferrite grain for B1 steel and (b) VC in the ferrite/RA boundary, B1 steel.

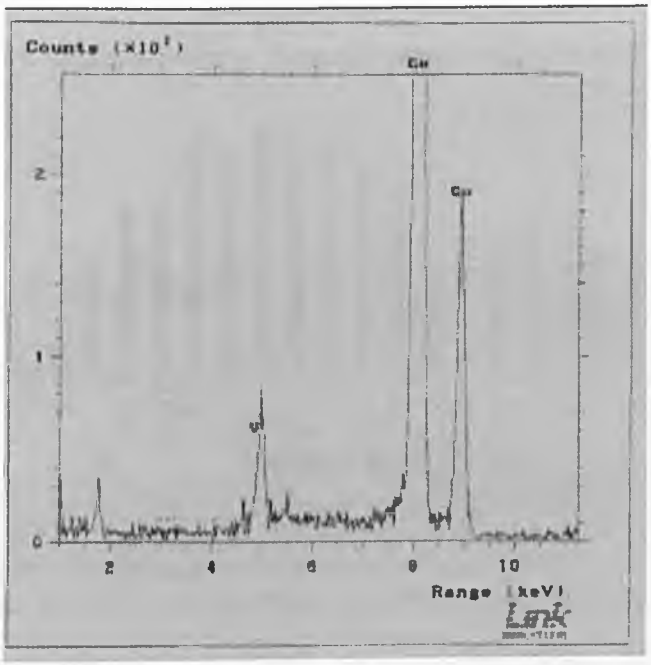

Fig. 5.80 EDS results of the C2 steel.

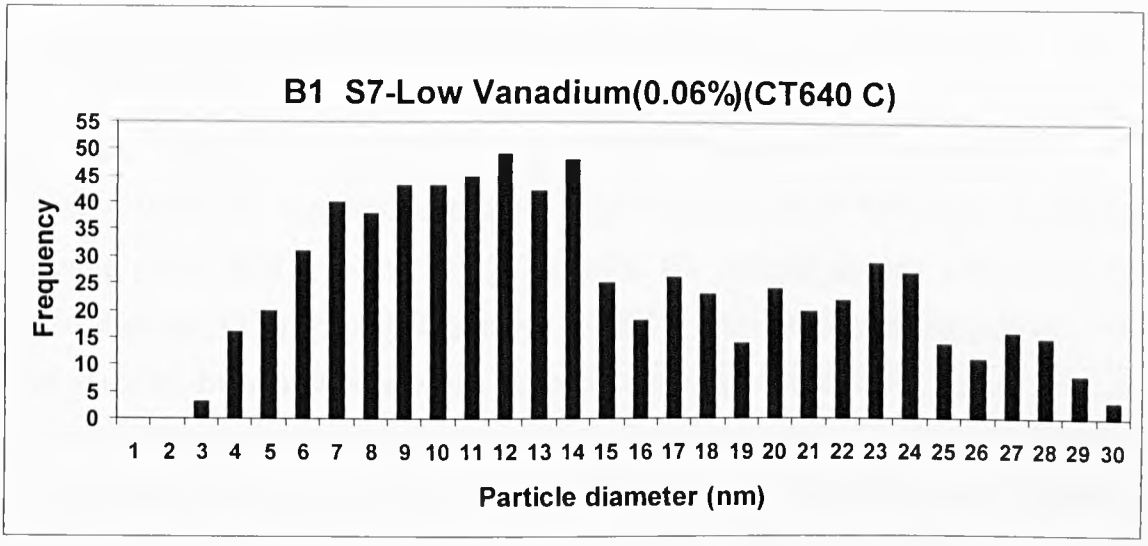

Fig. 5.81 Distribution and diameter of the vanadium carbides determined from a carbon extraction replica for the B1 steel Stage 7, with a coiling temperature of 640 °C.

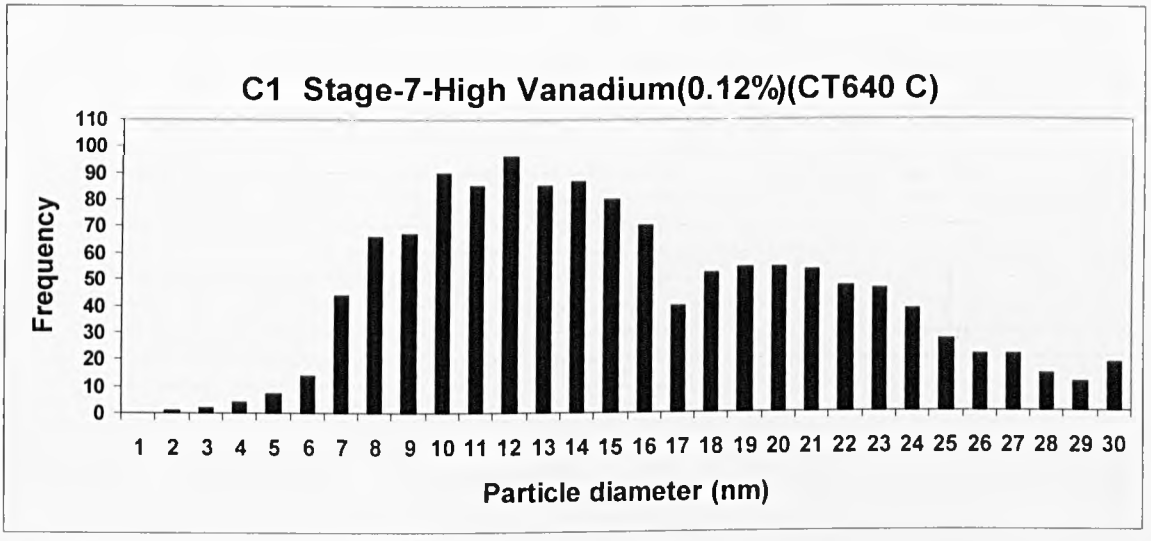

Fig. 5.82 Distribution and diameter of the vanadium carbides determined from a carbon extraction replica for the C1 steel Stage 7, with a coiling temperature of 640 °C.

5.4.6 Summary

The type of the precipitates formed by vanadium additions were predominantly VC and not V(C,N). In the hot rolled condition the vanadium carbides were found mainly dispersed within the elongated ferrite grains and some of them at the ferrite/pearlite interface. When the vanadium containing steels were heated at 795 °C, in the ferrite – austenite phase field and held for 20 seconds, the number density and the average diameter of the VC increased, suggesting fresh VC precipitation during heating. In the final stage of the annealing process, the steel samples were held for a short time of 5 seconds in the isothermal bainitic transformation area at 460 °C. VC was distributed within the ferrite matrix and also was found in the austenite and martensite. In addition, the vanadium carbides were observed inside and surrounding the bainite grains. Also vanadium carbides were observed at the ferrite/retained austenite boundaries. As expected, the high vanadium (0.12 wt %) steel developed a more uniform VC size distribution than precipitates developed in the low vanadium (0.06 wt %) steels.

Chapter 6 Discussion

6.1 Characterisation of the multiphase steels provided by Corus, IJmuiden

The need to reduce mass in the automotive industry is driving the production of multiphase steels with higher strength (>900 MPa) and improved ductility (>20%). This goal can be achieved through the use of precipitation in addition to the other strengthening mechanisms, such as a reduction in grain size. In the current research, vanadium was added to a base composition in order to study its effect on tensile properties and microstructure. The work was split into two parts: firstly, to characterise the microstructure of the base composition and vanadium microalloyed steels provided by Corus, to provide a base-line for material that had been processed through a commercial route and to correlate microstructure with the mechanical properties. The second part was to use the same steels to investigate microstructural evolution during the intercritical anneal.

6.1.1 Volume fraction of second phases

The retained austenite provides the balance between strength and ductility. A full scan of the XRD spectra of the base composition (FA-1) and high vanadium (FA-5) steels are shown in Figure 4.1. Table 4.1 gives an overview of the volume fraction of the retained austenite measured in the base composition FA-1 steel and vanadium microalloyed (FA-2, FA-3 and FA-4, FA-5) steels. The largest amount of retained austenite (7.7% on average) was found in the samples with 0.12 wt. % vanadium content (FA-4 and FA-5). The base composition (FA-1) steel had the lowest retained austenite (4.6%), and the low vanadium 0.06 wt. % content (FA-2 and FA-3) steels gave intermediate values (5.9 % on average). This result is perhaps the opposite to that expected, since vanadium should remove carbon in the form of vanadium carbides, thereby reducing the amount of carbon to stabilise the austenite.

In addition, the result is in contrast to that observed by Perrard and Scott [72], who found that a V+N addition did not modify the austenite fraction. However, Perrard and Scott investigated steels with a higher nitrogen content than those studied here and also they used a different heat treatment schedule, in particular a much lower coiling temperature of 400 °C, a lower bainite transformation temperature of 400 °C and a longer transformation time (300 s).

The effect of microalloy additions on the amount of retained austenite is not clear from the literature. For example, Timokhina et al. [73] investigated a TRIP steel with and without a Nb-addition and found the same retained austenite content in each, although there was considerable difference between the stability of the austenite, with the austenite in the Nb containing steel having lower carbon content and subsequently lower stability. In contrast, Sugimoto et al. [63] investigated a range of steels with systematic variations in Nb content and concluded that the high Nb content did increase the retained austenite content.

The differences between these two findings and the current work with that of Perrard and Scott are all likely to arise from differences in heat treatment cycle, which alters the carbon content in the austenite and also its size, morphology and the proximity of other phases. This issue will be discussed later, when the evidence of microstructural evolution during the intercritical anneal is also considered.

The estimated amounts of bainite and martensite are summarised in Table 4.2. Not surprisingly, the errors associated with these measurements were relatively large. The figures suggest that there may have been a slightly higher bainite content with the presence of vanadium, but if a real effect, which is debatable, the effect is small. The martensite content did not appear to be a function of the vanadium content. Therefore, the principal effect that the vanadium addition had was to increase the retained austenite content.

Table 6.1 gives the total fraction of second phases (retained austenite, martensite and bainite) for each alloy and coiling temperature. Given the errors involved, there is no measurable change in total second phase content with V addition or with coiling temperature, which is not surprising. Thus, the principal effect of the vanadium addition has been in the stabilisation of the austenite.

Table 6.1 Content of the phases presents the multiphase steel and their effect on the $R_m.A_g$ (the product of UTS and maximum uniform elongation).

Alloy	V (%wt)	Coiling T (°C)	RA (%)	M (%)	Bainite (%)	Total	$R_m.A_g$ ($x10^{-3}$) MPa %
Base	N/A	640/550	4.8	18	4.8	27.6	18.5
Low V	0.06	640	5.9	20	3.5	29.4	21.4
	0.06	550	5.9	18	3.4	27.3	18.5
High V	0.12	640	7.2	18	3.2	28.4	18.9
	0.12	550	7.7	15	3.3	26.0	18.5

6.1.2 Microstructural characterisation of the multiphase steels

The microstructure of the base composition (FA-1), low vanadium (FA-2, FA-3) and high vanadium (FA-4, FA-5) steels consisted of a ferritic matrix, retained austenite, bainite, martensite and retained austenite/martensite (RA/M) - see Figure 4.4. The size, volume fraction and distribution of each phase has a particular effect on the mechanical properties of these steels. Thus, a more accurate identification and quantification is necessary in order to evaluate their contribution to the performance of the multiphase steels.

6.1.2.1 Comment on the method for determination of the phase constitution and distribution

Several different methods and techniques exist to characterize the microstructure of multiphase steels. Optical microscopy is often used with a colour etching technique such as LePera. This etch tints each phase with a colour specific to that phase, for example the ferrite becomes slightly blue, bainite looks tan and retained austenite appears yellowish. However, three drawbacks were observed in the current work. Firstly, it was quite difficult to distinguish the martensite from the retained austenite /martensite constituent. Secondly, the phase mixture precluded homogenous etching, making the distinction between phases ambiguous. Thirdly, given that many constituents were present around the resolution limit of optical microscopy, which is of the order of 1μm, it becomes impossible to use the technique to characterise the microstructure. These problems are shown in Figure 4.10 (a) where the short comings are evident. However, other etches also failed, such as nital (5%), which showed the second phase distribution clearly, but could not differentiate martensite from austenite or bainite (Figure 4.10 (b)). However, an analysis based on samples etched with a mixture of nital (5%) – picral (4%) and analysed by SEM gave a clear and distinguishable microstructure, e.g. Figure 4.7 shows all the phases in the steel, which can be clearly differentiated. Table 4.2 shows the estimated amounts of bainite and martensite for each steel composition from SEM micrographs, which can be viewed in combination with Table 4.1 which gives the retained austenite values measured by XRD.

6.1.2.2 Microstructure of the base composition (FA-1) steel

A general view of the base composition (FA-1) microstructure is shown in Figure 4.4. The microstructure comprised a mixture of martensite, bainite and retained austenite in a ferritic matrix. It can be seen that some martensite grains are larger than 2 μm; these grains appear to have nucleated and grown in the middle of ferrite grains.

The martensite located at the ferrite grain boundaries was smaller than those grains found in the centre of a ferrite grain. The martensite grains were observed mainly with a polygonal shape (Figure 4.7). The bainitic grains were found at ferrite grain boundaries and in the centre of the grains. The bainite formed at the boundaries was composed of alternating ferrite and retained austenite needles, with an average size was of around 3 μm (Figure 4.6).

The bainitic regions located in the centre of the ferrite grains comprised bainitic ferrite laths with interspersed retained austenite laths that crossed the austenite grain, with an average size of around 2.5 μm (Figure 4.6).

6.1.2.3 Microstructure of the low vanadium steels

As with the base composition, in the case of the low vanadium (0.06 wt %) (FA-2 and FA-3) steels the martensite was located at the ferrite grain boundaries with an irregular shape (Figure 4.8). The nital – picral etching enhanced the finest features of the martensite as can be seen in Figure 4.8 (a), a very-well defined martensite grain is shown, and twinning deformation can be easily observed. Note that this martensite grain is linked to a region of retained austenite. A few grains of martensite adopted complicated forms as shown in Figure 4.8 (b). As expected, the austenite grains seem to have grown during the intercritical annealing which then transformed to martensite during subsequent cooling. The bainitic ferrite laths formed in the low vanadium steels appeared narrower than those formed in the base composition A1 steel (Figure 4.13). The size of the bainite grains were on average around 2 μm (Figures 4.7 and 4.9). The retained austenite was partly found at the ferrite grains boundaries but mostly in the middle of the ferrite grains. Its morphology was mainly polygonal with an average size of 1.5 μm (Figure 4.13 and 4.14). Additionally, RA was found mixed with martensite, which some researchers refer to as the RA/M constituent (Figure 4.9 and 4.10). This phase was not easy to see using the tint colour etching LePera, so phase quantification using this etching would give an incorrect estimation.

6.1.2.4 Microstructure of the high vanadium steels

For the high vanadium (0.12 wt %) (FA-4 and FA5) steel, the formation of the different phases was similar to the base composition and low vanadium steels. However, some differences were observed, for instance, the retained austenite had a more uniform distribution (Figure 4.12). An important feature was that the RA grain size was between 1 and 1.5 μm on average, i.e. similar to that in the low vanadium steel, but distinctly finer than in the base composition.

Similar to the base composition and low vanadium steels, the martensite was located at the ferrite grain boundaries with an irregular shape (Figure 4.12 and 4.15). Because of its fine retained austenite grain size (~1 μm), the bainite substructure, comprising alternative laths of bainitic ferrite and austenite, was finer than the bainite developed in the base composition (FA-1) and low vanadium (FA-2 and FA-3) steels (Figures 4.15 and 4.16).

Thus, while the SEM investigations did not reveal the fine scale substructure, it did indicate that the main difference between base composition and the vanadium microalloyed steels was the refinement in size of all the phases present. Clearly therefore, the precipitation of VC had a grain refining effect. Sugimoto et al. [63] report on their work that with niobium additions of 0.05 wt % or more, the prior austenite and retained grain size is refined, but grain size measurements are no reported. Heller and Nuss [65] found the similar niobium grain refinement effect for 0.19C-Mn-Si-Al multiphase steel, reporting for Nb free steel a retained austenite grain size of 1.9 μm which reduced to 1.8 μm for additions between 0.03 and 0.04 wt. % Nb, and 1.6 μm for a 0.07 wt. % of Nb addition.

6.1.2.5 Transmission electron microscopy (TEM).

The bainite observed in the base composition FA-1 was mostly formed from the retained austenite grains located at the ferrite grain boundaries. It has been reported that the bainitic ferrite laths grow towards the inside of the retained austenite grain [54], leading to a high dislocation density. This is consistent with the present observations, as shown in Figure 4.17 (a) where a high dislocation density was observed both within and surrounding the bainite. The retained austenite in the base composition was mainly an irregular shape which was always observed adjacent to martensite, as shown in Figure 4.21. The high dislocation density and micro twins always give the martensite a dark appearance in bright field TEM images.

A few bainitic regions observed in the vanadium steels had the morphology of parallel platelets, Figure 4.22 rather than the conventional lath shape that is normally expected. Such regions were adjacent to retained austenite - see Figure 4.20 (b). Additionally, some crystals of retained austenite, which exhibited twinning, were found mainly inside the ferrite grains, Figure 4.18 (FA-2 steel), which tended to have an elongated shape- see Figure 4.19 (low vanadium (FA-2) steel), and appear as small, bright, elongated grains in SEM images such as Figures 4.6 and 4.13. A typical martensite grain is shown in Figure 4.19 (b), formed mainly from the austenite located at the ferrite grain boundaries, as shown in Figure 4.8 (a). The martensite that was partially transformed from the retained austenite grains is presented in Figures 4.14 and 4.21. In the dark field image of the Figure 4.20 (b) the so-called retained austenite/martensite constituent can be seen. The martensite was mostly found at the ferrite grain boundaries having an irregular blocky shape, while the martensite found in the vanadium multiphase steels was blocky and rounded shaped.

6.1.2.6 Precipitation

As noted above, one of the main microstructural differences between the base composition and vanadium steels was the grain size, which was smaller in vanadium-containing steels. The vanadium grain refiner effect is well known but it is necessary to characterise the size, distribution and shape of the vanadium precipitates in order to have an idea of the mechanism of the grain refining effect and the likely effect on the TRIP effect. The precipitates were believed to be vanadium carbide, with no evidence of any nitrogen within the precipitates. The vanadium carbides were dispersed throughout the ferrite matrix, at the ferrite/ retained austenite boundaries, and within the bainite and retained austenite phases. Although difficult to image, there was evidence that they were also present within the martensite. The size distribution of VC was determined from carbon extraction replicas in the TEM, with between 25 and 35 replicas per composition being analysed, giving a total of 800 to 1,400 precipitates measured for the size distributions given in Figure 4.28. Thus, while the microstructure varied from one region to another, the VC size distribution should be a reasonable representation of the true precipitate size distribution.

Although the microstructure was somewhat heterogeneous, the microstructural characterisation undertaken suggested that the VC appeared to be relatively homogeneously distributed between phases (albeit rather heterogeneous within one particular phase), with no evidence of greater preference for VC precipitating in one particular phase. The majority of VC was randomly distributed within a particular phase, this effect being easiest to see within the ferrite (e.g. Figure 5.27). Occasional stringers of precipitates were also observed, suggesting strain-induced precipitation, although this effect could not be confirmed. Precipitates were also found inside and surrounding the retained austenite grains (e.g. arrowed in Figure 4.24(a) for the high V steel). Note here how the vanadium precipitates were well aligned on the ferrite/RA boundary.

The presence of precipitates inside the retained austenite, bainite and martensite suggests that precipitation had occurred before these phases had formed, i.e. during coiling and subsequent heating to the intercritical anneal. However, this point is considered further in Section 6.2 which looks in detail at the intercritical anneal. The high vanadium FA-4 and FA-5 steels developed a more homogenous phase distribution and narrower size distribution of VC than in the low vanadium FA-2 and FA-3 steels, as shown in Figure 4.2. Not surprisingly, the precipitate number density was higher in the high vanadium FA-4 and FA-5 steels (17.7 and 18.6 μm^{-2} precipitates respectively) than produced in the low vanadium FA-2 and FA-3 steels (11.3 and 11.7 precipitates μm^{-2} respectively). No significant effect of the coiling temperature (640 °C and 550 °C) was observed on precipitate size distribution in the commercially processed alloys. This suggests that the precipitate size distribution was formed on heat treatment after hot and cold rolling and that the size distribution arising from any precipitation that occurred during coiling was substantially changed during intercritical annealing. This point will be developed further when the laboratory intercritical annealing experiments are discussed. For all steels, the precipitate size distribution appeared to be bimodal, with a finer fraction in the approximate range 6 to 17 nm and a coarser interval was from around 18 to 30 nm. Comparing the size distributions given in Figure 4.28, the size distributions look similar for the low vanadium steel at the two coiling temperatures.

Equally, the size distributions appear similar for the high vanadium steel, irrespective of the coiling temperature. In other words, the size distribution did not appear to be determined by coiling temperature (compare Figure 4.28 (a) – (d)). Thus, the over-riding variable in determining the size distribution was the heat treatment schedule, with some effect of vanadium content,, but not the hot rolling/coiling conditions.

6.1.3 Mechanical properties

Figures 4.1 and 4.2 show the stress – strain graphs of the multiphase steels. The main driver for the current research was to increase the strength of the steel without compromising the ductility. As can be seen the higher vanadium content steel gave a distinct strength increment, with a UTS of ~870 MPa being obtained. Moreover, the coiling temperature clearly had a major influence on the resultant tensile properties. However, the increase in strength came at the expense of a loss in ductility of around 2-3%.

Quite a few studies have been carried out on multiphase steels in order to correlate mechanical properties with the microstructure. So far, the widely accepted conclusion is that the mechanical properties of the multiphase steels are influenced by the particular effect of each phase, with most focus on the retained austenite; but it has been difficult to isolate the effect of one phase on the properties of these steels. However, it has been found that the content, grain size, distribution and carbon content of retained austenite strongly influences the mechanical properties [6, 54].

As expected, the tensile strength was enhanced by vanadium additions of 0.06 wt % V and 0.12 wt % V through vanadium carbide precipitation. Although the 0.06 wt %V steel coiled at 640 °C exhibited almost identical tensile behaviour to the base alloy, except a small loss in ductility, the base alloy was coiled at 583 °C, suggesting that the finer structure associated with the lower coiling temperature was offset by the precipitation in the 0.06 wt %V alloy. Interestingly, the yield point for the 0.06 wt % V steels was lower than that for the base composition, irrespective of the coiling temperature, which is difficult to explain.

A higher yield point would be expected for the V bearing alloys as the V additions had resulted in a finer microstructure, while the presence of VC would also be expected to increase the yield strength. This was indeed observed for 0.12 wt %V alloys, but was not the case for the 0.06 wt %V alloys, Figure 4.2, which is difficult to explain.

One important difference is that the base alloy exhibited a yield point while the 0.06 wt % V alloys exhibited continuous yielding. Continuous yielding is normally associated with dual phase steels, where the residual mobile dislocation density is high, particularly in the ferrite adjacent to martensite islands. However, the TEM examinations and the phase constitution (Table 4.2) did not indicate any measurable differences.

The optimum performance of TRIP steel is associated with uniform work hardening, promoted by the continuous transformation of austenite during straining. This optimum is usually associated with the maximum in the product of the maximum tensile strength multiplied by the maximum uniform elongation. These data, along with the volume fractions of each phase in each alloy are presented in Table 6.1. The values of $R_m.A_g$ are similar to those in the literature, for example, presented by Zaefferer et al. [50], who obtained values between ~$12x10^3$-$23x10^3$ MPa as a function of bainite hold time. In comparison, the current values show virtually no change with V addition, with the exception of the 0.06 wt %V coiled at 550 °C, which exhibited the highest product, but this was out of line with the other values. Interestingly, the 0.06 wt %V coiled at 640 °C exhibited the highest volume fraction of second phases and the highest value of $R_m.A_g$, although not the highest retained austenite. However, it must be reiterated that the errors on the measurements were inevitably high, such that the differences in total volume fraction of second phases was not necessarily significant.

Table 6.1 shows that the increase in volume fraction of retained austenite did not systematically change the product of $R_m.A_g$. If $R_m.A_g$ was not increased, but the volume fraction of retained austenite was larger, the logical conclusion is that the retained austenite was much less transformable in the vanadium bearing steels. As further discussed in Section 6.2, this was believed to be primarily a result of the reduction in dimensions of the austenite particles, which is known to reduce transformability [73].

The coiling temperature clearly had a measurable effect on the flow curves, Figs. 4.1 and 4.2. However, the coiling temperature had less effect on the precipitate size distribution compared to the V content. The coiling temperature will have had two principal effects. Firstly, precipitation can occur at these temperatures given that for a hot rolling finish temperature above 900 °C should minimise precipitation during rolling [72]. A coiling temperatures as low as 400 °C is recommended in order to avoid precipitation [72], which of course is a much lower temperature than the ones used in this study (550-640 °C). The second effect is that the lower the coiling temperature the finer the structure. In the current work, the absence of an effect of coiling temperature on precipitate size distribution suggests that the principal effect of coiling temperature was on the size of the microstructure, with 550 °C producing a finer structure than 640°C. The lower coiling temperature would be expected to increase work hardening rate.

Hodgson et al. [73] investigated an Nb-containing TRIP steel which had the same retained austenite content as the equivalent Nb-free steel. The austenite in the Nb-containing steel had lower carbon content (in-line with the current results) and consequently the austenite was less stable, and therefore it transformed more easily at small strains, giving less contribution to the overall strain hardening. The transformation of the austenite also depended on its size, morphology and the proximity to other phases. The austenite present between the polygonal ferrite grains tended to transform first at lower strains because it tends to have a lower carbon content. The best elongation behaviour was associated with the austenite present as films between the subunits of bainite, since these have the higher carbon, rather than the blocky austenite. In the current study, the V addition was believed to reduce the size of all types of austenite (i.e. blocky and within the bainite), as examined in detail in Section 6.2. The two effects will have countered each other, with the size reduction making the austenite more stable, while the reduced carbon would make it less stable. The observation that the values of $R_m.A_g$ were almost identical for the base composition and the 0.12 wt %V steel, Table 6.1, indicates that the two effects did indeed appear to cancel each other out.

6.2 Intercritically annealed cold-rolled multiphase steels

Before examining the results from the heat treatment experiments, it is appropriate to firstly review the expected microstructural changes, undertaken in relationship to the diagrammatic representation of the thermal cycle, reproduced in Figure 3.2. 5 steels were examined, namely the base composition alloy (A1, coiled at 583 °C), low (B1, B2) and high (C1, C2) vanadium microalloyed steels, with coiling temperatures of 550 and 640 °C, as detailed in Table 3.1. The compositions of the steels were basically the same, with only the vanadium content changed (0.06 wt% to 0.12 wt %), and were from the same cast as reported in Chapter 4 and discussed in Section 6.1. Thus, the microstructural changes produced during the intercritical annealing process could be analysed in terms of vanadium content and the coiling temperature applied (640 °C and 550 °C) only.

The solubility product for VC and VN in austenite are given by [83]:

VC (γ): $\log_{10}Ks = -9500/T + 6.72$

VN (γ): $\log_{10}Ks = -7840/T + 3.02$

Figure 6.1 shows an equilibrium calculation of V(C,N) precipitation using a similar steel to the one in the current study, being Fe - 0.2C-1.5Mn-1.5Si-0.22V-0.015N (all wt%), taken from a study that was run in parallel with the current work [83]. The differences in composition will have given a different result for the current work, but those differences would have been comparatively small. In any event, it shows that the precipitation of VN would occur at higher temperature than VC, starting at > 1100 °C for the steel used by Scott et al. [83]. Virtually all the available nitrogen would be precipitated by 920 °C so that below this temperature, further precipitation only involves carbon, either as pure VC or by increasing the carbon content of pre-existing V(C,N). At equilibrium, all the vanadium has precipitated out at 700°C. However, the extent of precipitation during rolling will have depended on the hot rolling schedule, in particular interpass times and finishing temperatures.

Thermocalculations were undertaken in a parallel study at Arcelor to determine the effect of vanadium content on phase constitution [83]. This study concluded that the additions of vanadium and nitrogen should have no effect on the phase changes during heat treatment and continuous annealing. Scott et al. [83] showed that the experimentally determined phase fractions (austenite, martensite and bainite) were in good agreement with the equilibrium calculations.

Stage 1 involved a rapid (18 °C/s) heat to 695 °C. During this stage, recrystallisation of the ferrite would be expected as a result of the cold work. To a large extent, this will determine the final ferrite grain size and therefore the effect that the V additions have on this recrystallisation. During this time, significant spheroidisation of the cementite should occur. In addition, as described above, vanadium that remained in solution after the hot rolling process would be expected to precipitate as VC.

Stage 2 involved a slower heat to 795 °C, i.e. into the intercritical region. Clearly, at this stage, the cementite is dissolved and the austenite starts to form. As with Stage 1, the location and pinning force from the V-based precipitates is important in determining the size and location of the austenite. According to Figure 6.1, all the VCN will have precipitated by this temperature, with perhaps some dissolution occurring, and certainly coarsening expected to occur.

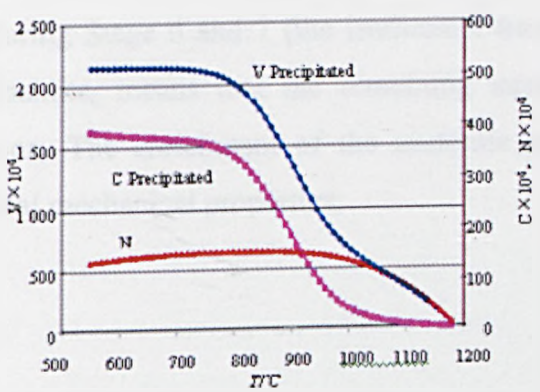

Fig. 6.1 Scott et al.'s equilibrium calculation (Arcelor CEQSCI software was used) of V(C,N) precipitation [83].

Stage 3 would be expected to essentially extend the changes that occurred in Stage 2, except that some coarsening of the austenite would also be expected. In addition, the solute partitioning should approach equilibrium, although it should be noted that this is not an issue that has not been fully explored in the literature. In addition, the V-based precipitates would be expected to coarsen.

Stage 4 is a cool from the intercritical region to Stage 5, while Stage 5 is a hold at 670°C. This part of the heat treatment was introduced to simulate the commercial plant. During Stage 5 some re-transformation from austenite to ferrite is inevitable, and therefore the volume fraction of retained austenite in the room temperature structure should decrease. This transformation is believed to be nucleation-less as the ferrite simply grows into the austenite. There is the potential for pearlite to form, although this is time dependent, the time depending on the composition. TRIP compositions are usually carefully formulated to ensure that the time is insufficient to give transformation to pearlite. However, further solute repartitioning would be expected, in particular enrichment of austenite with carbon rejected from the growing ferrite, which is important in determining the amount of retained austenite. Some further precipitate coarsening would be expected, although the extent should not be large given that the time was only 12 seconds.

Stage 6 was an air cool down to Stage 7, which was the important bainite transformation phase. During Stage 6 and 7 (the isothermal transformation), residual austenite transforms to bainite, means that the remaining austenite is expected to become enriched in carbon. The enrichment of the austenite increases its stability, directly influencing the final mechanical properties.

6.2.1 Base composition and vanadium (0.06 and 0.12 wt. %) microalloyed steels in the as-rolled condition

6.2.1.1 Microstructure in hot rolled condition

The hot rolled microstructure comprised a banded structure of pearlite rich and ferrite rich regions, making the microstructure microscopically heterogeneous. It was important, therefore, to compare like with like areas (Figure 5.8 (a) (b)). The vanadium carbide precipitates were analysed in the hot rolled condition in order to determine a) the extent of precipitation in the hot rolled condition and b) the effect of coiling temperature on microstructural scale and precipitate size distribution.

The EELS result of the precipitates removed on a carbon extraction replica failed to find nitrogen in the precipitates (Figure 5.61); therefore the precipitates formed in the microalloyed steels were most probably vanadium carbides (although absolute identification was not made and it was possible that some V(C,N) was present). Determination of the location of the VC in the hot rolled microstructure was straightforward in the ferrite, but clearly difficult in the pearlitic regions. The VC precipitates were firstly identified by EDS and supported by dark field imaging in order to find and distinguish them with more certainty (Figure 5.63 (c)). The vanadium carbides were located mainly along the elongated ferrite grains as seen in Figure 5.63 (a). Also some were observed in the ferrite/pearlite boundaries as shown in Figure 5.62. In Figure 5.63 (b) vanadium carbide was found on the boundary between ferrite and pearlite.

According to Honeycombe [74] the alloy carbides are not usually precipitated in direct association with pearlite because they are formed during the austenite/ferrite transformation, but on a much finer scale, as their nucleation and growth depends on the diffusivity of the alloying element in addition to that of carbon. The present study appears to be in accord with this. However, no interphase precipitation was detected.

The mean size of the precipitates is shown in Figure 5.64. In all cases, a bimodal size distribution was observed. The histograms of the low vanadium (0.06 wt %) steels, series B1 and B2, which were coiled with two different temperatures, 640 °C and 550 °C respectively, were similar. The higher coiling temperature produced a slightly larger precipitate size distribution, but this maybe experimental error.

The smaller precipitate size group ranged approximately between 7 and 17 nm. This is consistent with Fourlaris et al. [75] who reported for a Fe-0.4C-0.15V steel isothermally transformed at 600 °C, that the vanadium precipitates ranged from 5 to 10 nm with a spheroidal shape, and that some of them were located in the ferrite/pearlite interface. Equally, it is consistent with Scott et al. [83] who observed an average precipitate size of 7.5 nm for a hot rolled steel of similar composition, coiled at 540 °C.

The precipitate number density measurements from carbon extraction replicas showed that the coiling temperature had no effect on precipitate numbers for the B1 steel (both 640°C and 550 °C gave ~6 precipitates μm^{-2}, see Table 6.2). For the C1 and C2 steels (Figures 5.63 and 5.64), the higher coiling temperature gave a distinctly larger precipitate size distribution, as expected. A higher precipitate number density was observed for the high vanadium (0.12 wt%) steel compared to the low (0.06 wt%) steel, as expected, but again there was no effect of coiling temperature (10 and 11 precipitates μm^{-2} for the 0.12 wt% V steel coiled at 640 °C and 550 °C, respectively). Thus, the absence of a coiling temperature effect on the precipitate number density suggests that no significant precipitation occurred during coiling. This is in contrast to the suggestion of Perrard and Scott [72] who suggest that a coiling temperature as low as 400 °C is required in order to avoid precipitation. It is interesting that there appears to be a clear effect of coiling temperature on precipitate size distribution for the hot rolled state (which is not surprising), but the coiling temperature had no effect on final precipitate size distribution after heat treatment (discussed in Section 6.2.6 for Stage 7 and already shown for the commercial steel, Figure 4.28).

Rather surprisingly, the final precipitate size distribution appeared to be controlled by the V content. In any event, it is clear that the final precipitate size distribution was determined by the intercritical anneal schedule and not by the coiling temperature.

Table 6.2 Precipitate number density for the low and high vanadium-based multiphase steels

Steel	Precipitate number density (precipitates / μm^2)				
	Hot Rolled	Stage 1	Stage 2	Stage 3	Stage 7
B1	5.8	8.6	11.7	12.0	12.5
B2	5.8	7.2	11.0	11.8	----
C1	10.2	16.8	17.7	18.7	19.9
C2	11.0	14.6	18.7	19.9	----

6.2.1.2 Microstructure prior to the annealing heat treatment in the cold rolled conditions

The microstructure of the base composition (A1), low vanadium (0.06 wt %) (B1 and B2) and high vanadium (0.12 wt %) (C1 and C2) microalloyed steels in the cold rolled conditions was composed by elongated ferrite and pearlite grains, Figure 5.9 (a), giving the microstructure a banded appearance. These microstructure characteristics were the same for both base composition and high vanadium C2 steels as shown in Figure 5.12 (a) and (b) respectively.

The deformed nature of the microstructure made measurement of the ferrite grain size extremely difficult, as the ferrite boundaries were obscured by the etching of the deformation substructure, e.g. Figure 5.11 (b). However, vanadium carbides were identified, located in the middle of the elongated ferrite grains, Figure 5.11 and 5.13. The pearlite observed was of a typical lamellar form as can be seen in Figures 5.12 (a) but in several areas the pearlite had become broken up by the cold deformation, see Figure 5.13.

The smaller the Si:Mn ratio, the more powerful the banding in cold rolled steels [76]. The formation of elongated grains of ferrite and pearlite is accelerated as the manganese content is increased or the silicon content is decreased. The areas where manganese and carbon are concurrently segregated during casting are not fully homogenized. Thus, they are elongated in a band-type manner in which pearlite grains are intensively formed [76]. In order to know whether or not there is any significant segregation in cold rolled conditions, EDX analysis was applied in different points of the cold rolled microstructure as shown in Figure 5.10 (b) (c). The result shows that there was no significant variation Mn content, but that the vanadium content was below detectable levels and therefore no comment can be made on segregation of this element. Such a heterogeneous microstructure makes it more difficult to compare the differences between samples. However, considerable care was used to ensure that comparisons came from like with like areas. Moreover, as discussed in later sections, the heterogeneities decreased significantly during the intercritical anneal.

6.2.2 Microstructure transformation at 695 °C (Stage 1)

Stage 1 comprised the steel samples being analysed after heating to 695 °C, just ~30 °C below the A_1 temperature, followed by an immediate quench. The main changes that occurred at this stage were the partial recrystallisation of the ferrite and the spheroidization of the Fe_3C. Cementite was located at the grain boundaries of the recrystallised ferrite. There were interesting differences in these first changes between the base composition (A1) and vanadium microalloyed (B1, B2 and C1, C2) steels, as detailed below. As expected, retained austenite was not found in samples heat treated at this temperature (30 °C below the A1 temperature), as can be seen in Figure 5.1, which presents the singular XRD spectrum corresponding to the base composition at the angle (200) where no austenite peak was registered.

The ferrite recrystallisation produced in the base composition (A1) is shown in Figure 5.14 (a), which shows polygonal ferrite grains formed within a much larger elongated ferrite grain. The grain boundaries of these fine polygonal ferrite grains appear to be pinned by Fe_3C carbides, although some spheroidised carbides were also found in the centre of the polygonal grains. Thus, one of the first processes to occur was the recrystallisation of the cold deformed ferrite grains, with the resultant ferrite grain size limited by grain boundary pinning by spheroidised carbide particles (Figure 5.14 (a)). However, ferrite grain size was not measured at this stage because of the mixed structure of recrystallised and elongated grains.

In the base composition steel a significant fraction of ferrite grains were recrystallised. However, in the case of the microalloyed steels, the extent of ferrite recrystallisation was much less, indicating that the vanadium carbide present after hot rolling delays recrystallisation, as would be expected. This finding is consistent with the observations of Perrard and Scott [72]. The extent of ferrite recrystallisation also depends on the heating rate, as reported by Huang et al. [77]. They found that for sufficiently high heating rates, ferrite recrystallisation can be delayed. For example, for a Fe-C-Mn-Mo steel heated at 10 °C/s, the ferrite was about 50% recrystallised, while using a heating rate of 100 °C/s the ferrite recrystallisation was only 10 %. The heating rate applied in the current study was ~14 °C/s, such that the partial recrystallisation in the base alloy is consistent with the work of Huang et al. [77].

The main effect of the heating at 695 °C on the pearlite was the spheroidisation of the lamellar cementite (Figure 5.14). Coarsening and coalescence within the grain was seen, Figure 5.15 (b). A number of the cementite islands were located at the boundaries of the recrystallised ferrite in the middle of the new ferrite grains (Figure 5.15 (a)). For the case of the vanadium microalloyed steels, the microstructure changes in the pearlite rich regions produced at Stage 1 were similar to the base composition steel. Vanadium carbides were located at the ferrite/cementite boundary as well as in the ferrite grains as seen in Figure 5.62 and 5.63.

The VC precipitation produced in the low vanadium (0.06 wt %) B1 and B2 steels at 695 °C was similar to the particle size distribution observed in the hot rolled condition of these steels (Figure 5.64). It might be argued that there were more fine precipitates in the size range up to ~15 nm after Stage 1 for steels B2, C1 and C2, but this difference was not replicated in steel B1 (Figure 6.2). For all steels, precipitate number density increased after Stage 1 compared to the hot rolled condition, (48% for steel B1, 24% for B2, 65% for C1 and 33% for C2, Table 6.2). The combination of an increase in the number density and an increase in the proportion of finer precipitates suggests that precipitation of new VC occurred during heating to 695 °C.

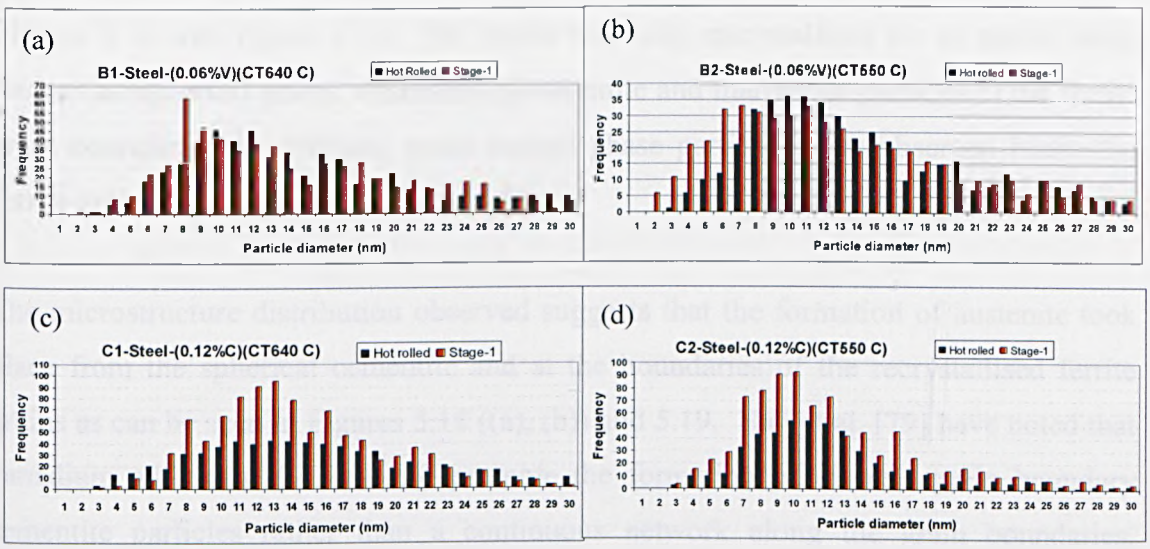

Fig. 6.2 Comparison of the precipitation behaviour of the low and high vanadium steels in hot rolled and Stage 1 condition.

6.2.3 Microstructural transformation on heating to 795 °C (Stage 2)

Significant microstructural changes of the base composition and vanadium microalloyed steels occurred for the Stage 2 heating to 795 °C, in which austenite had formed. The XRD results presented in Figure 5.2 confirm that the austenite had formed, although the austenite peaks in the XRD patterns were relatively weak. The difference in the retained austenite content is presented in Table 5.1; the base composition shows the lower value (~9 %) and the vanadium steels show higher values (~10 % – 12 %).

Other than the formation of austenite, one of the other major changes observed was that the structure had become significantly more homogeneous, for example, compare Figures 5.18 with Figure 5.14. The ferrite was fully recrystallised for all steels, being present as equiaxed grains, decorated by austenite and martensite particles at the ferrite grain boundaries. In addition, some second phase particles were observed inside the ferrite grains (see Figure 5.18 (c) and (d)).

The microstructure distribution observed suggests that the formation of austenite took place from the spherical cementite and at the boundaries of the recrystallised ferrite grains as can be seen in Figures 5.18 ((a), (b)) and 5.19. Han et al. [79] have noted that vanadium additions (0.15 wt %) promote the formation of discrete grain boundary cementite particles rather than a continuous network along the grain boundaries, although these observations were made for much higher carbon steels (0.94-1.15 wt %). In Figure 5.14 it can be seen how, in the base composition (A1), the initial cementite formed along the recrystallised ferrite grain boundaries transformed to austenite as shown in Figure 5.18 (a) and (c).

The main microstructural changes promoted by the addition of vanadium were a reduction in microstructural scale and the promotion of a more homogeneous structure. Figure 5.20 gives the ferrite grain size for the five steels at the end of Stage 2. This shows a small, but reproducible reduction in ferrite grain size with vanadium addition.

The values obtained are similar to those reported by Perrard and Scott [72] who observed a reduction in mean ferrite grain size from 3.2 ± 0.2 μm for the base composition reducing to 2.4 ± 0.2 μm for their V + N microalloyed steel after continuous annealing at 790°C. Table 5.4 gives the estimated austenite grain size for base composition and vanadium-based microalloyed steels. The austenite grain size for the base composition (A1) averaged 2.4 ± 0.3 μm (see Figures 5.21 to 5.23) which is relatively larger than the value obtained by the high vanadium C2 between of 1.7 ± 0.2 μm (Figures 5.27 and 5.28). Intermediate values were obtained by the low vanadium B1 and B2 steels (1.9 ± 0.3 μm, see Figures 5.24 and 5.25). Thus, the VC that precipitated out during hot rolling and during the Stage 1 heating appears to have had a grain refining effect. In addition, the addition of vanadium also appears to have promoted a greater uniformity to the structure, with the austenite in the microalloyed steels being more rounded in shape (compare Figures 5.18 (a, c) with 5.18 (b, d).

The carbon content of the retained austenite was measured at each stage of the heat treatment for all the multiphase steels, with the estimated values given in Table 5.2. The base composition A1 steel exhibited a 1.07 % C content at Stage 2 (795 °C). However, it was not enough to stabilise the austenite as the relatively larger retained austenite grains transformed, or partially transformed (Figure 5.23) to martensite at room temperature. De Cooman et al.'s [80] found that the Ms^{σ} (σ = stress needed to initiate the martensitic transformation) temperature decreased as the carbon content in the retained austenite increased in the range ~ 1 – 1.8 % C. They also found that the retained austenite grain size had a strong effect on the Ms^{σ}, concluding that both these variables contribute to the retained austenite stabilisation. For the current vanadium-containing steels, the austenite grains apparently were more stable (Figures 5.24, 5.27 and 5.28) since more was retained at room temperature. The number density of precipitates measured at the end of this Stage exhibited a small increase over that observed at the end of Stage 1, Table 6.2, suggesting that precipitation was still occurring during the heating from 695 to 795 °C. This is consistent with the thermodynamic predictions of Scott et al. [83], reproduced in Figure 6.1.

Heating to 795 °C resulted in measurable changes in the size distribution of the VC, in particular, the bimodal size distribution present in the hot rolled material was far less pronounced at this temperature. It would appear that this was a result of the coarsening of the precipitates, which resulted in dissolution of the finest particles and a shift in the average precipitate diameter to larger sizes, particularly in the size range 18 – 30 nm. Only a few precipitates larger than 30 nm were found, with no more than five vanadium precipitates with sizes between 40 and 50 nm were observed and these were located in the ferrite matrix. These results suggest that, in contrast to the number density measurements, that coarsening was dominant over further precipitation. The size of the VC measured in the current work is in agreement with those reported by Maropolus et al. [81] who studied a carbon steel alloyed with 0.2 wt % of vanadium. The material was austenitized at 830 °C, developing fine vanadium carbides (17 - 35 nm) and a few large particles (40 – 45 nm) that remained un-dissolved and a certain amount of vanadium was dissolved in austenite.

6.2.4 Effect of holding for 20 s at 795 °C on microstructure and precipitation progress (Stage 3)

The characteristics of the austenite formed at the intercritical temperature will determine the final microstructure properties of the multiphase steels at room temperature. The carbon content of the austenite is the main feature that chemically controls its stability at room temperature. The estimated carbon content for all the multiphase steels at each stage of the annealing process is presented in Table 5.2. Also, Figure 5.6 gives the change in lattice parameter with annealing temperature, while Figure 5.7 gives the corresponding changes in carbon content.

The base composition (A1) steel exhibited the highest carbon content in the retained austenite of 1.22 wt% C (Figure 5.7), but the B1 and B2 steels were similar at 1.21 % C. In the case of the C2 (1.20 wt% C) steel the difference of 0.02 wt% C to the base steel, which is not statistically significant. The lowest content was measured for the C1 steel with 1.19 wt% C having a difference of 0.03 wt% C in comparison to the A1 steel.

Thus, the main effect of the holding time at this stage was to increase the carbon content in the austenite, for example in the C2 steel from 1.01 ± 0.04 wt% C to 1.20 ± 0.02 wt% C. Similar values are reported by Emadoddin et al. [44] who worked with a TRIP-assisted steel with 0.27C, 1.48Mn and 1.08Al (all contents in wt %). The steel was heated at 810 °C and soaked for 5 min. The retained austenite volume fraction was ~ 1.01 with a carbon content of 1.35 % C. However, lattice parameter measurements are not reported. Similarly, Seong et al. [31] reported a carbon content of ~ 1.20 wt% C for 4.7 % retained austenite.

As expected, Stage 3 produced an increase in the retained austenite content, Table 5.1. The highest content was observed in the high vanadium (C1 and C2) steels having an average of ~14 %. In contrast, the base composition (A1) steel had the relatively low value of 10 % RA, while the low vanadium (B1 and B2) steels were intermediate at ~12 %. In addition, the size of the austenite also increased, Table 5.7. The coarsening of the austenite grain size appeared greater in the base composition (A1) steel than produced in vanadium steels (Figures 5.29). The austenite grain size for the base composition A1 was 3.2 ± 0.3 μm (Table 5.5) while the high vanadium C2 steel averaged 2.0 ± 0.1 μm (Figure 5.33). The low vanadium composition (B1 and B2) exhibited an average grain size of 2.5 ± 0.2 μm (Figure 5.32). Thus, the V addition had a measurable effect in refining the size of the austenite during the intercritical anneal. Moreover, the higher vanadium content (C1 and C2) appears to have been associated with a more homogenous size distribution, as shown in Figure 5.29 (b). Some of these austenite grains grew along the ferrite grain boundaries forming a necklace structure surrounding the ferrite grains, Figure 5.29 (c) (d) and 5.30. Also, the austenite grains formed in the centre of the ferrite grains keep its polygonal shape, Figure 5.34.

The intercritical anneal resulted in a small increase in average precipitate size. The bimodal precipitation distribution observed after hot rolling had disappeared, and there was no longer an effect of the coiling temperature on precipitation size distribution.

Furthermore, there was no difference in precipitate size between the two different alloy compositions. While the increase in size is not statistically clear cut, it was found to systematically occur for all four microalloyed steels, and is in-line with what is expected at this temperature. Moreover, the finest precipitates of between 1 to 3 nm were not found, consistent with the expectation that coarsening would occur rather than fresh precipitation. However, the number of extracted precipitates per unit area exhibited a slight increase, Table 6.2, the opposite of what would be expected from coarsening. As noted before, measurements of particle density from carbon extraction replicas is subject to significant errors, and therefore this change is not believed to be significant. Nevertheless, there was the expected difference in precipitate number density as a function of alloy composition. Perrard and Scott [72] made measurements of precipitate number density based on dissolution studies, and found that the number density decreased after 90 s at 775 °C. However, these measurements were made by dissolution studies, which fail to pick up the finer precipitates (because of the minimum size of the pores in the filter used). In addition, they did not present any data for shorter times than the 90 s they used, and therefore a transition from precipitation to coarsening may have taken place during this time frame.

6.2.5 Controlled cooling from 795 °C to 670 °C (Stage 4- 5)

Following the intercritical annealing, the samples underwent a controlled cool from the ferrite –austenite phase field (795 °C) to 670 °C and were held at this temperature for 12 seconds. The microstructural transformations observed were the following:

- For all steels, the retained austenite content decreased in-line with the initial predictions. This RA reduction was higher in the base composition (A1) than in the vanadium containing steels.
- The RA that transformed did so mainly into martensite; more martensite was observed in base composition (A1) steel than in vanadium steels.
- A few bainite grains were formed, but solely in the base composition (A1) steel.

As Table 5.1 shows, for the base composition (A1), the retained austenite after Stage 3 (795 °C) was 10.1 % and this decreased at to 9.0 % Stage 4 (670 °C) and then down to 8.1 % after a hold for 12 seconds. The reduction in retained austenite content was associated with a significant reduction in lattice parameter of the retained austenite (measured at room temperature), Figure 5.6, corresponding to a change in the carbon content. Thus, the conclusion is that this stage of the heat treatment resulted in a reduction in retained austenite because of a reduction in carbon content and therefore its stability. Of course, the inevitable increase in size of the retained austenite particles would have also decreased its stability. It is interesting to note that this controlled cooling stage had a similar general effect on the V containing steels as the base composition, even though the carbon contents of each was appreciably different. However, there were interesting differences. The base composition exhibited a reduction in retained austenite content of 2 %, which was associated with a reduction in carbon content of ~0.05 %. In contrast, the V-containing steels, which appeared to give the same behaviour whatever the coiling temperature or V content, exhibited a smaller reduction in retained austenite content of 0.6-0.8 %, associated with a fall in carbon content of 0.06 %. As discussed earlier, the amount of retained austenite did not correlate with carbon content in the austenite when all alloys and conditions were considered (although there was a correlation when one particular alloy composition was considered). This will be discussed further later, when all stages of the heat treatment have been considered.

The vanadium carbide distribution was similar at this Stage to Stage 3. Vanadium carbides were found along the ferrite/RA boundary (indicated by arrows and circled in Figure 5.42(a) (b)) and some of them were located in the ferrite grain (Figure 5.43). In contrast, in Figure 5.41 a retained austenite grain is shown which belongs to the base composition (A1) steel that has an irregular form and is larger than observed in the vanadium steels.

The martensite was mostly located at the ferrite grain boundaries, as shown in Figure 5.38 (b) (which corresponds to the base composition (A1) steel). Thus, the grain boundary austenite appeared to be more unstable than that located in the middle of the ferrite grains. This is probably because the austenite formed from the spherical cementite was richer in carbon than the grain boundary RA which required diffusion of carbon along ferrite grain boundaries to be enriched. The same behaviour was observed in the low and high vanadium steels. Thus, the vanadium addition does not appear to have affected the relative stability of the grain boundary and grain centre RA.

A few grains of bainite were observed in the base composition (A1) steel, but not in the vanadium microalloyed steels, e.g. Figure 5.38 (a) which shows the characteristic bainitic shape, formed by three alternative needles of ferrite/retained austenite. The bainitic areas were formed mostly at the ferrite grain boundaries, consistent with the comments above about RA stability being related to its location. In contrast, bainite was not observed in the low and high vanadium steels. Similar phase transformations were found by Rocha et al. [20] for a steel that was slowly cooled from 820 °C to 710 °C. The microstructure consisted of ferrite with a few carbides, martensite formed at grain boundaries of the recrystallised ferrite grains and the martensite – austenite constituent. They observed that a small amount of granular bainite was formed. They identified the granular bainite as a combination of equiaxed ferrite grains having high dislocations density and martensite/retained austenite islands. They explain that during slow cooling, part of the austenite is transformed to ferrite by diffusion controlled phase transformation, whilst the remaining austenite, with a minimal carbon content, transforms to granular bainite and martensite following quenching.

6.2.6 Isothermal bainitic transformation at 460 °C (Stage 6 and 7)

The final microstructure transformation is undertaken isothermally at a temperature that gives the bainitic transformation. During the bainite formation the carbon is believed to diffuse into the adjacent austenite. The carbon enhancement of the austenite increases its thermal stability and consequently the austenite can be retained during cooling at room temperature [46].

The austenite to bainite transformation of the base composition (A1) and vanadium steels was carried out at 460 °C where the steel samples were held for 5 seconds. The final microstructure developed consists of a ferritic matrix plus retained austenite, bainite, martensite grains and the retained austenite – martensite (RA/M) constituent.

6.2.6.1 Microstructural homogeneity

The final microstructure shown in Figure 5.45 was similar to that seen in the commercial steel, although the exact phase constitution differed slightly, Table 6.3 and 6.4, the details of which are discussed below. One of the striking changes that occurred during the heat treatment cycle was a substantial improvement in the microstructural homogeneity. The banding that was obvious in the hot rolled (Figure 5.8 (a) (b)) and cold rolled (Figure 5.9 (a) (b)) had largely disappeared in the final product (Figure 5.45), although the structure did retain a degree of directionality. Although subjective, the addition of vanadium appeared to promote a more homogeneous structure. This is in-line with other observations on similar TRIP steels [72] and higher carbon vanadium microalloyed steels [79].

6.2.6.2 Retained austenite

Stages 6 and 7 produced a reduction in retained austenite content by just over 1% for all alloys studied, with no apparent difference between the base composition and the V containing steels, Table 5.1. The values of retained austenite, bainite and martensite obtained in the current work are compared to those obtained in the commercial steel in Table 6.3. Generally, the retained austenite content was greater in the laboratory simulations than the commercial steel, but the total volume fraction (retained austenite + martensite + bainite) was greater in the commercial steel compared to the laboratory trials. Nevertheless, the differences were relatively small. The important point is that the trend in phase constitution as a function of composition was the same for both commercial steel and laboratory trials.

The amount of retained austenite increased with the vanadium increment as shown in Figure 5.4. A similar effect was found by Heller and Nuss [65] using Nb and Nb + Ti additions. They reported that for a C-Mn-Si microalloyed with 0.049 wt % Nb the retained austenite content was of 15 % on average. The same steel microalloyed with ~0.08 % of titanium yielded 12 % RA and a combination of Nb+Ti produced 14 % retained austenite. The Nb+Ti containing alloy showed a linear increase in the retained austenite with alloy addition, consistent with the current observations presented in Figure 5.4 for the vanadium additions. The retained austenite grain size produced in these steels studied by Heller and Nuss [65] was between 1.6 and 1.9 μm and the carbon content of the retained austenite was of ~1%. However, they were unable to explain why the retained austenite increased with the Nb and Ti additions.

In contrast, Sugimoto et al. [63] reported for a multiphase steel with additions of niobium between 0.05 and 0.8 mass %, the carbon content of the retained austenite is decreased, but that the volume fraction of retained austenite was slightly increased at low austempering temperatures. They explain that this high retained austenite volume fraction may be caused by the niobium in solid solution which suppresses the cementite precipitation during the isothermal bainitic transformation.

It is well known that carbon is the main austenite stabilizer and therefore a reduction in carbon content will reduce its stability. In addition, the stability of austenite is also influenced by its grain size and distribution in the matrix.

The bainite transformation is widely believed to result in enriching the adjacent retained austenite with carbon and therefore enhancing its stability [72]. The change in carbon content is shown in Table 5.2 and graphically in Figure 5.7. It is clear that the measured carbon content did not change in the expected manner, except, perhaps for the base composition, A1. With the exception of steel B2, the remaining three microalloyed steels all exhibited a decrease in carbon content.

Table 6.3 Comparison of the second phase content of the commercial and laboratory based steels.

Alloy	V (%wt)	Coiling T (°C)	Commercial				Laboratory Simulation			
			RA (%)	C (wt %) in RA	Bainite (%)	Martensite (%)	RA (%)	C (wt %) in RA	Bainite (%)	Martensite (%)
Base composition	N/A	640/550	4.8	*1.25*	*4.8*	*18*	7.0	1.00	*4.6*	*11*
Low Vanadium	0.06	640	5.9	*1.14*	3.5	20	11.3	0.97	*3.7*	*9.7*
	0.06	550	5.9	*1.14*	3.4	18	10.9	0.97	*3.0*	*9.2*
High Vanadium	0.12	640	7.2	*1.10*	3.2	18	11.9	0.97	*2.9*	*9.9*
	0.12	550	7.7	*1.12*	3.3	15	12.6	0.97	*2.6*	*9.8*

Table 6.4 Comparison of the total second phase content (austenite + martensite + bainite) for the commercial and laboratory based steels.

Alloy	Total Commercial (%)	Total lab (%)
Base	27.6	22.6
B1	29.4	24.7
B2	27.3	23.1
C1	28.4	24.7
C2	26	25

However, it should be noted in the alloy steels that only 2.6 – 3.7 % bainite was produced at this stage, and so the amount of carbon available from this for enrichment into the austenite would have been small. Given that the XRD gives an average value from all the retained austenite, it would have been difficult to detect the enrichment in the fraction of austenite where transformation to bainite occurred. However, as shown by Jacques et al. [55], and reproduced in Figure 2.21, the carbon content in the austenite does not change much during the initial stages and is only measurable after at least 40 seconds transformation [55]. Therefore, a measurable change would not be expected in the current study where the transformation time was very short (5 s).

It has been reported that among the main parameters determining the stability of retained austenite is the austenite particle size. The stability is increased as the particle size of the retained austenite decreases. Also, it has been proposed that the grain size of retained austenite should be in the range of 0.01 to 1 μm to ensure the TRIP effect. Larger retained austenite particles are unstable and transform quickly to martensite at small strains, while smaller particles are too small to transform [80]. The mean size of the retained austenite grains was as ~3.1 ± 0.3 μm for the base composition (A1) steel, ~1.9 ± 0.1 μm for the high vanadium steel and ~2.2 ± 0.2 μm and for the low vanadium steel, which are values somewhat larger than the proposed range of 0.01 to 1 μm.

The retained austenite was located in two main places, namely at the ferrite grain boundaries, or in the centre of the ferrite grains. In both cases, it was found on its own or in the vicinity of bainite and martensite. The two different types of retained austenite had different morphologies and carbon concentrations, both of which influence its stability. The morphology of the retained austenite that was formed at the ferrite grain boundaries was somewhat similar in both base compositions (A1), low, and high vanadium steels. The retained austenite nucleated and grew along the ferrite boundaries forming a necklace like structure that surrounded the ferrite grain as seen in Figures 5.39 (b) and 5.40 (a).

The only difference was that in the vanadium steels the size of the austenite was reduced by the vanadium based precipitates. The retained austenite formed in the centre of the ferrite grains of the base composition steel was observed with two morphologies: polygonal and irregular blocky form. In contrast, the retained austenite nucleated in the ferrite grains of the vanadium steels was mostly polygonal and rounded. Other forms of retained austenite found alongside the bainite included a needle morphology (Figure 5.57 and 5.58) and the retained austenite located close to the martensite was of an irregular blocky form and also a few laths of retained austenite were found. Thus, the laboratory trials confirmed the observations of the commercial trials that the principal role of the vanadium-based precipitates was to reduce the size of the austenite at the heat treatment temperature, thereby controlling its stability.

6.2.6.3 Bainite

During the bainite transformation, the carbon is ejected from the bainite towards the austenite. Alloy elements, such as the Si or Al, inhibit the carbide formation allowing the C content of the remaining austenite to increase and eventually the bainite transformation stops when the austenite C content has reached its limit.

The type of bainite observed here is similar to that observed by other researchers [50,54], namely alternative laths of ferrite and retained austenite. There was no difference in this transformation between the base composition and the microalloyed steels. The main difference observed was that the bainite grain size and the thickness of bainitic laths in some grains. For example, the bainite produced in the base composition is shown in Figure 5.49, which shows the formation of five needles of retained austenite, which appear bright. The average grain sizes was 3.0 ± 0.5 μm. Similar bainite grains were observed by TEM as seen in the micrographs of Figure 5.53, which confirmed the alternative laths of ferrite and retained austenite. In this case, the base of the grain which exhibits dark contrast and contains a high dislocation density is austenite, which indicates that the bainitic ferrite grew into the austenite grain, as expected.

Not surprisingly, the number of bainitic ferrite laths that form depended on the size of the austenite grain from which they grew. One effect of the vanadium was to reduce the size of the austenite laths and so the greater the vanadium content the lower the number of bainitic laths (compare Figures 5.51, 52 and 54). Not only did the number of bainite laths change with vanadium content, but also the thickness of the lath also appeared to be a function of the vanadium addition, with vanadium appearing to reduce the lath thickness. Examples of this are shown in Figures 5.57 for the B1 steel that can be compared with Figure 5.53 for the base composition. However, the lath thickness was not quantified in a statistically meaningful way and so this observation is subjective.

The current work is consistent with the observations of Jacques et al. [54] who observed that the bainite transformation starts earlier in small retained austenite grains (~2 μm) than in the large grains (~8 μm) but transformation progresses at a slower rate. Indeed, the reduction of the retained austenite grain size produces an increase in the grain boundary area that accelerates the rate of transformation as a result of an enhanced nucleation rate. Thus, the kinetics of bainite transformation in small retained austenite grains is consequently controlled solely by the grain boundary nucleation rate.

The addition of vanadium had a marked effect on the amount of bainite produced, Table 5.6, Figure 5.46. The base composition (A1) steels had the highest bainite content, ~4.6 %, while the high vanadium (C1 and C2) steels exhibited the lowest value of ~2.9 %, giving what appeared to be a linear decrease in bainite with vanadium addition. Bainite was produced at higher temperature for the base composition (A1) than the microalloyed steels, as shown by the results from Stage 5. Jacques et al. [54] indicates that shorter bainite transformation times, such as those used in the current study, leads to no change in carbon content, but to less bainite, in-line with the current results.

van der Zwaag and Wong [82] argue that the mechanism of the bainite transformation is still a controversial issue, however they report that substitutional alloying elements such as Cr, Si, Mn, Mo, Al, etc, or carbide forming (Nb, V and Ti) decrease the bainite start temperature.

In agreement with van der Zwaag, Heller and Nuss [65] presented a time-temperature-transformation diagram (Figure 6.3) showing the effect of the alloying elements that control the transformation performance in the steel. It can be seen that the elements mentioned by van der Zwaag tend to reduce the bainite area transformation moving the peak of the nose to the right.

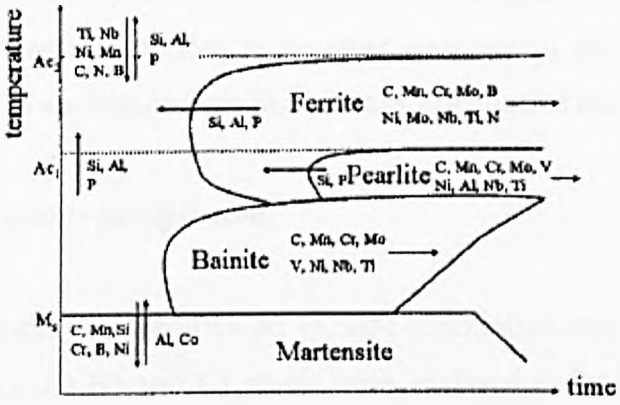

Fig. 6.3 Influence of the alloying elements on transformation behaviour of steel [65].

6.2.6.4 Martensite

The amount of martensite formed was greater in the base composition compared to the V microalloyed steels, Table 5.7, which is consistent with the higher retained austenite content in the latter. This was not a result of the carbon content of the austenite as the retained austenite in the base composition contained higher carbon than the V microalloyed steels. The principal difference appears to have been as a result of differences in size of the retained austenite, Table 5.7, with the base composition exhibiting a larger size for the martensite and the retained austenite. The low vanadium (B1 and B2) steels had the lowest martensite content of ~9.2%, Figure 5.47. This is clear evidence that the principal effect of the vanadium addition was the reduction in growth/coarsening rates during intercritical annealing by the VC precipitates, but not a chemical effect of the vanadium on austenite stability.

The martensite formation was determined by the retained austenite stability. As mentioned previously, the austenite formed both at the ferrite boundaries and in the centre of the ferrite grains. It was observed that the martensite was more easily formed from the austenite located at the ferrite grains boundaries as seen in Figures 5.48 (A1 steel) and 5.50 (C2 steel). This was believed to be because the austenite formed from the FeC_3 located within the centre of the recrystallised ferrite grains was richer in carbon than those austenite particles formed at the ferrite grain boundaries. In addition, the grain boundary austenite tended to be more irregular in shape and consequently likely to provide more nucleation sites for the transformation to martensite.

6.2.6.5 Vanadium carbide precipitation

Since the effect of coiling temperature on VC size distribution was lost early in the heat treatment cycle, only the B1 and C1 steels were analysed at Stage 7. The precipitate size distribution of the B1 steel at stage 7 was bimodal, see Figure 5.77. The average particle diameter produced at this stage was of 13.9 nm and the number of precipitates per unit area was 12.5 precipitates/ μm^2. A similar trend was observed for the high vanadium C1 steel. At Stage 7, the average precipitate diameter was 15 nm compared to 14.6 nm at Stage 3. Similarly, the precipitate number density was little changed being 19.9 precipitates/ μm^2 at Stage 7 and 18.7 precipitates/ μm^2 at Stage 3. While errors are always present for extraction replicas, the current data was obtained from 860 precipitates at Stage 3 and 1400 at Stage 7. Comparing these results with those obtained at Stage 3, it can be seen that very little change has occurred, both in precipitate number density and in size distribution. This implies that little coarsening occurred after the intercritical anneal - i.e. during the short times at 670 °C and 470 °C. The current work shows certain agreement with Scott et al. [83] who investigated steels with composition 0.19C-1.47Si-1.5Mn and 0.10 – 0.21V (wt. %). However Scott et al. employed different annealing temperatures with one of them at 795 °C with relatively long holding times of 90 and 180 seconds. They observed that nucleation and growth of the vanadium based precipitates occurs during the heating stage, followed by coarsening during the intercritical anneal, as found here.

6.3 Summary

A base composition, 0.2C-1.5Mn-0.38Si (wt %) and vanadium microalloyed with 0.06 and 0.12 wt. % vanadium were investigated after production from the commercial plant and after laboratory simulations of the intercritical anneal.

The commercial material contained retained austenite contents in the range 4.6 – 7.7 %, which is at the low end for TRIP steel. However, it should be noted that most TRIP steels reported in the literature with higher retained austenite were produced in the laboratory and not commercially. Irrespective of this, the addition of vanadium led to an almost linear increase in the retained austenite content. It did not increase the total fraction second phases, Table 6.3, and therefore promoted more austenite at the expense of martensite and bainite. Thus, the high temperature austenite was more stable with the vanadium addition than without. This was counter intuitive as the precipitation of vanadium carbide or carbo-nitrides would have removed the interstitial elements responsible for stabilising the austenite. Simply by viewing the final microstructure, the reasons for the enhanced retention of austenite could not be evaluated. Thus, the laboratory simulations were essential, discussed below.

The addition of vanadium broadly had the expected effect on the tensile properties, namely an increase in tensile strength and a reduction in ductility, Figures 4.2, 4.3. The increase in tensile strength is consistent with an increase in the retained austenite content that should promote higher work hardening rates as it transforms during the test. However, the addition of vanadium and the resultant increase in volume fraction of retained austenite did not systematically change the product of $R_m.A_g$ (maximum tensile strength times the maximum uniform elongation). If more retained austenite was transforming on straining, the higher work hardening should give greater ductility.

However, the absence of a change in $R_m.A_g$ implies that the increase in tensile strength arose from either a precipitation hardening effect or a reduction in microstructural scale, rather than additional austenite transforming during the test. It was unfortunate that the tensile test specimens could not be released by Corus to evaluate the retained austenite content in the strained specimens. Superimposed on the effect of the vanadium was the effect of the coiling temperature. As expected, the lower coiling temperature gave a higher tensile strength. This effect was believed to be primarily the effect of the microstructural scale, which would be finer the lower the coiling temperature. The observation that the 0.06 wt %V steel coiled at 640 °C had the same tensile behaviour as the base composition coiled at 583 °C, Figure 4.2, suggests that precipitation hardening was not a very substantial effect.

The laboratory simulations were successfully developed to simulate the entire intercritical anneal, including the rapid heating rates in Stage 1. The laboratory simulations did not produce exactly the same phase constitution, giving higher retained austenite at the expense of martensite, although bainite contents were similar (Table 6.2). In addition, a slightly lower total volume fraction second phase was obtained in the laboratory simulations (Table 6.3). The differences were probably as a result of small differences in time/temperature during the intercritical annealing. It would appear that the main difference was probably during Stage 3, the intercritical anneal, with the laboratory having slightly lower temperature or time, resulting in less austenite forming (and hence less total volume fraction second phase) and finer austenite (resulting in less austenite transforming on cooling). In contrast, the bainite transformation appears to have been replicated extremely well.

A comparison of the hot rolled steel and the steel at Stage 2 suggested that substantial vanadium carbide precipitation occurred during hot rolling prior to coiling and that some additional precipitation occurred during the heating stages to the intercritical anneal temperature. Thus, the precipitation prior to coiling would have implications for the final precipitate size distribution and for the scale of the microstructure formed after hot rolling.

In addition, it was shown that the vanadium addition significantly affected the rate of ferrite recrystallisation that occurred during the stage 1 and 2 heating programmes. The reduction in recrystallisation kinetics and the pinning of ferrite grain boundaries resulted in a finer ferrite grain size, which was probably one of the most significant factors in determining the yield strength of the material.

The intercritical anneal resulted in coarsening of the vanadium carbides such that the size distribution present after coiling was lost and replaced by a new, larger size distribution. However, it is interesting to note that the extent of coarsening was not great and many precipitates remained remarkably fine after the entire heat treatment process. It was particularly interesting to see that the final size distribution appeared to be determined more by the vanadium content than the coiling temperature. In Figure 4.28, the precipitates appeared to be finer for the high vanadium compared to the low vanadium additions. However, this difference was not replicated in the laboratory simulations, Figure 5.81 and 5.82, perhaps suggesting that sampling errors were important. In any event, it is difficult to explain how an increase in vanadium content could decrease the precipitate size distribution.

There was no doubt that the vanadium addition reduced the size of all phases present. As noted above, the recrystallised ferrite grain size reduced with vanadium addition. In addition, there was clear evidence that the VC precipitates pinned the austenite and reduced the grain growth rate during the intercritical anneal. This led to a reduced amount of transformation to martensite on cooling, resulting in the increase in retained austenite with vanadium content. This result is at variance with other studies, for example, Timokhina et al. [73] investigated a TRIP steel with and without a Nb addition and found the same retained austenite content in each, and Perrard and Scott [72] found that a V+N addition did not modify the austenite content, but for much longer intercritical anneals, and for a microstructure with a finer retained austenite.

In contrast, the present results are consistent with other studies, namely Heller and Nuss [65] who found increased retained austenite with the addition of Nb and Nb+Ti, Figure 5.4. However, differences between studies are hardly surprising where the principal effect appears to be the size of the austenite rather than any inherent stability factor. Each study used a different hot rolling finish temperature, coiling temperature and heat treatment cycle, which would have strongly affected precipitate size distribution and therefore Zener pinning potential. It is clear that for the conditions used here, the precipitates had a measurable effect on austenite grain size and therefore its stability. Unfortunately, the increased stability may also mean that less austenite transforms on subsequent straining, therefore not giving any benefits to the work hardening rate and therefore the total ductility. A clear opportunity for future work will be to look at the effect to the heat treatment cycle to see whether the austenite size can be optimised to give a high content but also highly transformable austenite.

The bainite content was relatively small in both laboratory and commercial steels, in both cases because of the short times employed. The reason for the short time is that the bainite transformation coincides with the hot dip galvanising, and therefore the time is defined by the thickness of the Zn coat required. The current work demonstrated that such short times gave no benefit in enhancing the carbon content of the remaining austenite, in-line with the observations of [55]. Again, it would be interesting to investigate the effect of longer transformation times on the austenite stability.

Chapter 7 Conclusions

The work presented in this thesis was concerned with the microstructural and precipitation evolution during the intercritical annealing of a multiphase steel microalloyed with vanadium (0.06 and 0.12 wt %). In particular, the investigation was carried out in order to know the effect of the vanadium content on the microstructure compared to an equivalent base composition multiphase steel. The laboratory based simulated intercritical anneal and hot dip galvanise cycle was compared to 5 commercially produced steels in finished form, for which the microstructure was related to the mechanical properties. Based on the discussion of the results presented in Chapters 4 and 5, the following conclusions can be drawn:

7.1 Commercially Produced Steels

1. The addition of 0.12 wt % V gave an increase in tensile strength (UTS) over the base alloy irrespective of the coiling temperature following hot rolling. For a 0.06 wt %V addition, a coiling temperature of 640 °C gave no increase in UTS, compared to the base alloy coiled at 583 °C, while a coiling temperature of 550 °C did increase UTS. However, in all cases the addition of vanadium reduced ductility.

2. The addition of vanadium increased the retained austenite content in an almost linear manner. However, the results shown in Table 6.1 indicate that this increase in the retained austenite content did not systematically change the product of $R_m.A_g$. This implies that the increase in retained austenite was not accompanied by an increase in the amount of austenite transforming during the tensile test (which regrettably could not be verified in the absence of suitable specimens).

3. The addition of vanadium decreased the size of all microstructural features. Thus, the increase in tensile strength with vanadium addition was probably a result of grain size refinement or precipitation hardening rather than the increase in retained austenite.

4. The vanadium carbide precipitate size distribution appeared to be controlled more by the vanadium content than the coiling temperature.

5. The addition of vanadium led to a decrease in the carbon content in the retained austenite. Given that a higher carbon content leads to greater retained austenite stability, this result strongly suggests that more austenite was retained in the vanadium bearing steels because of the size of the austenite, and not the composition.

7.2 Laboratory Trials

1. A laboratory simulation of the commercial route intercritical anneals and hot dip galvanise was successfully developed.

2. The precipitates were shown to be vanadium carbides, with no evidence that they contained nitrogen. However, such precipitates are known to be complex and therefore the presence of carbonitrides cannot be totally ruled out.

3. In the hot rolled condition, the microstructure comprised ferrite and pearlite with fine VC precipitates. The precipitate size distribution was bimodal, with a finer distribution being observed for the lower coiling temperature. Not surprisingly, the higher vanadium addition gave a larger precipitate number density (~ 5 precipitates/μm^2 for the low vanadium and ~ 11 precipitates/μm^2 for the high vanadium alloy).

4. Following cold rolling, the first microstructural change produced during the heating was the recrystallisation of the cold deformed ferrite grains. In the base composition A1 steel a significant fraction of ferrite grains were recrystallised by 695 °C, yielding a recrystallised grain size of ~3 μm.

However, in the case of the low (B1, B2) and high (C1, C2) vanadium steels, recrystallisation was limited, indicating that the vanadium addition delays recrystallisation, presumably through pinning of the grain boundaries by VC. The extent of recrystallisation is also a function of heating rate. The extent of recrystallisation in the base alloy with the heating rate of ~14 °C/s are consistent Huang et al. [77] who reported that for a heating rate of 10 °C/s, the ferrite was ~ 50 % recrystallised, and for 100 °C/s the ferrite recrystallisation was of ~ 10 %.

5. During the intercritical anneal, austenite appeared to form from the spherical cementite and also at the boundaries of the recrystallised ferrite grains. The morphology of the retained austenite formed at the ferrite grain boundaries was somewhat similar in both the base composition (A1), low, and high vanadium steels. This retained austenite formed a necklace structure surrounding the ferrite boundaries. The main difference observed in the vanadium steels was the size of the austenite which was limited by the vanadium carbides. The addition of vanadium appeared to change the morphology of the austenite within the grains, with vanadium giving finer and more rounded austenite compared to that observed in the base composition, where it had an irregular blocky form.

6. After heating to 795 °C (Stage 2), the precipitate number density was measured as ~ 8 precipitates/μm^2 for the low vanadium steel and ~14 precipitates/μm^2 for the high vanadium steel. This is a small increase in precipitate density compared to the hot rolled condition (~ 5 precipitates/μm^2 – low vanadium and ~ 11 precipitates/μm^2 – high vanadium) suggesting that most of the vanadium carbide precipitation had occurred hot rolling and coiling, with only a small fraction produced during heating to the intercritical anneal temperature. By the end of the intercritical anneal, no effect of coiling temperature on precipitate size distribution was observed.

7. The cool from the intercritical anneal temperature to 670 °C and subsequent short hold resulted in a reduction in retained austenite, but minimal coarsening of the phases present. In the base composition, martensite and a small amount of bainite was present, while in the vanadium bearing steels, the only transformation product other than ferrite was martensite, with no bainite observed. The carbon content of the austenite also fell at this stage.

8. The isothermal hold at 460 °C resulted in the formation of around ~2.6 – 4.6 % bainite. The amount of bainite was small because of the short hold times, used to simulate the hot dip galvanise of the commercial process. The vanadium addition appeared to suppress the formation of bainite, believed to be because vanadium tends to reduce the size of the bainitic transformation area in the TTT diagram, and moves the peak of the nose of the transformation to the right [65]. The transformation failed to enhance the carbon content in the retained austenite for any of the alloys, believed to be because the amount of transformation was small and the times too short.

9. The VC was mainly located in the ferrite, but was also found in all other phases. This again indicates that much of the VC precipitation occurred prior to coiling. The average VC precipitate diameter of the high vanadium C1 steel at the final stage was of ~ 15 nm while for the low vanadium B1 the diameter averaged ~ 14 nm. The precipitate size distribution was mainly governed by the vanadium content rather than the coiling temperature. As was expected, more precipitates per unit area were produced in the high vanadium C1 steel having ~ 19 precipitates/μm^2 while the low vanadium B1 averaged 14 precipitates/μm^2. Although the heat treatment cycle did change the precipitate size distribution, removing the original size distribution at coiling, the average size did not change greatly on annealing, indicating that the hot rolling/coiling conditions which determined the initial size distribution were therefore important in determining the final precipitate size distribution.

10. At the end of the laboratory simulation, the total volume fraction second phases (which reflects the total austenite fraction produced during the intercritical anneal) was slightly smaller for the laboratory simulation compared to the commercial practice. The bainite fraction was similar after both processes, but the retained austenite content was much higher for the laboratory simulation, while the martensite content was lower. This suggests that the difference in phase constitution and total volume fraction second phases was a result of the laboratory simulation using slightly lower temperature or shorter time than the commercial practice during the intercritical anneal itself (Stage 3).

11. The amount of retained austenite increased with the vanadium addition, in-line with the commercially produced steels.

12. The main effect of the vanadium addition appears to have been in the reduction in size of all the phases present and the reduction in carbon content of the retained austenite. For example, the high vanadium C1 and C 2 steels developed a RA grain size of ~ 1.9 ± 0.1μm while the base composition A1 steels averaged 3.1 ± 0.3 μm. Similar reductions were observed in the ferrite, martensite and bainite (e.g. the bainite grains in the vanadium steels contained one or two ferritic laths, while the base composition exhibited bainite composed of three of five ferritic laths). The vanadium did not appear to have any direct effect on austenite stability, the main effect being through control of the austenite grain size, and a change in morphology (the retained austenite nucleated in the ferrite grains of the vanadium steels was mostly polygonal and rounded).

Chapter 8 Future work

1. The bainite content (~4%) produced in the commercial steels provided by Corus and the material processed in laboratory was small. Both materials were held for just 5 seconds during the isothermal transformation, which is a very short time dictated by the galvanising process applied by Corus for these materials. In contrast, most of the current literature employs holding times over 50 seconds. Thus, it would be helpful to investigate the effect of longer bainitic transformation times for these materials. The times suggested for this investigation is shown in the graph below. This would also allow the effect of vanadium addition on the enhancement of the carbon content in the austenite by the bainitic transformation to be investigated.

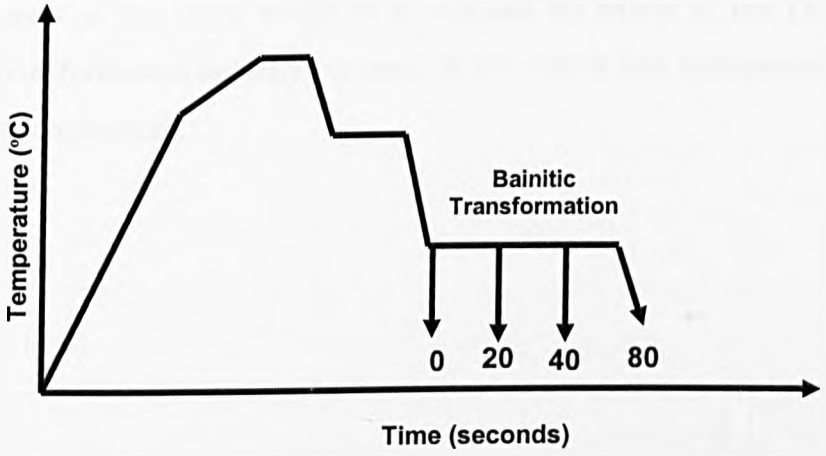

2. In this work, the retained austenite grain size was refined by vanadium additions resulting in enhanced stability. However, improved stability of the retained austenite by a reduction in size probably means less transformation to martensite during the straining, i.e. a smaller TRIP effect. Thus, further investigations can be addressed to evaluate the effect of retained austenite size, controlled by VC precipitation on the work hardening. Given that the retained austenite produced in the vanadium microalloyed steels contained less carbon than the austenite of the base composition, it would be interesting to understand the relationship between size and carbon content on transformability during straining. This could be evaluated using small changes to the temperature/time during the intercritical anneal.

3. Following on from the above, there is clearly disagreement as to the effect of microalloying elements on the retention of austenite. In the current work this is believed to be a result of the control of the austenite size. In a similar manner to (2) above, changes in the coiling temperature should yield differences in precipitate size distribution and therefore differences in microstructural scale at the start of the intercritical anneal. In combination with differences in the intercritical anneal temperature/time, a range of microstructural scales could be produced that would allow a more systematic understanding of the inter-relationship of microalloy addition, heat treatment conditions and austenite grain size. By producing a base composition microstructure with the same size as that in the microalloyed steel, the true effect of microalloy addition on retained austenite stability could be evaluated. A particularly important aspect of this work would be to evaluate the extent of the TRIP effect, i.e. how much transformation actually occurred in the tensile test specimens as a function of starting microstructure.

Chapter 7 References

[1] J. King (2004) *ULSAB-AVC Advanced vehicle concepts*, Corus-Automotive, http://www.corusautomotive.com/en/design_and_innovation/collaborative_development/ULSAB_AVC accessed on 20.06.2004.

[2] C. D. Horvath (2004) *The future revolution in automotive high strength steel usage* - Body structures and closures group - General Motors Corporation, http://www.autosteel.org/pdfs/gdis_2004_horvath.pdf, accessed 20.06.2004

[3] D.J. Schaeffler (2004) *Introduction to advanced high strength steels Part I : Grade overview,* The Fabricator.com, http://www.thefabricator.com/MetalsMaterials/MetalsMaterials_Article.cfm?ID=113 , accessed 20.06.2004.

[4] ThyssenKrupp Stahl – Automotive (2003) *High – Strength steel for lightweight auto body manufacture,* Thyssen Krupp Stahl AG http://www.thyssenkruppstahl.de/upload/binarydata_tkscsauto/3693auto.pdf, accessed 15.12.2004.

[5] Rautaruukki – Automotive Solutions (2003) *Using extra and ultra high strength steels sheets and tubes,* Rautaruukki – Group, http://www.rautaruukki.com, accessed 15.12.2004.

[6] H. K. D. H. Bhadeshia *TRIP-Assisted steels?* ISIJ International, 2002, 42 No. 9, pp. 1059–1060.

[7] B. Mintz *Hot dip galvanising of transformation induced plasticity and another intercritically annealed steels*, International Materials Reviews, 2001, 46 No.4, pp. 169 – 197.

[8] C.M. Sellars *Options and constraints for thermomechanical processing of microalloyed steels,* HSLA steels - Metallurgy and Applications, Proceedings of an International Conference on HSLA Steels, 1985, pp.73 – 82.

[9] M. Cohen and S.S. Hansen *On the fundamentals of HSLA steels*, HSLA steels-Metallurgy and Applications. Proceedings of an International Conference on HSLA Steels, 1985, pp.61 – 71.

[10] A.K. Sinha *Physical metallurgy of the microalloyed high strength low alloy steels,* Proceedings of the Emerging Technologies for New Materials and Product-mix of the steel industry, 1991, pp. 195 – 205.

[11] E.E. Fletcher *High strength low alloy steels,* 1979, Battelle Press, Columbus Ohio.

[12] A.J. DeArdo *New developments in the alloy design of microalloyed and other modern HSLA steels*, HSLA steels, Metallurgy and Applications. Proceedings of an International Conference on HSLA Steels, 1985, pp.21-32

[13] F. J. Humphreys *Recrystallization and related annealing phenomena*, Pergamon, Oxford, 1995.

[14] T. Gladman *Grain refinement in multiple microalloyed steels,* HSLA steels, Metallurgy and Applications. Proceedings of an International Conference on HSLA Steels, 1985, pp. 3 – 14.

[15] T. Gladman *Grain size control*, Maney Publishing, London, 2004.

[16] L.J. Cuddy *The effect of microalloy concentration on the recrystallization of austenite during hot deformation,* Thermomechanical Processing of Microalloyed Austenite – Conference Proceedings / The metallurgical Society of AIME. 1982, pp. 52 – 60.

[17] S. Yamamoto, C. Ouchi and T. Osuka *The effect of microalloying elements on the recovery and recrystallization in deformed austenite*, Thermomechanical Processing of Microalloyed Austenite – Conference Proceedings / The metallurgical Society of AIME. 1982, pp .40 – 52.

[18] W. M. Rainforth, M.P. Black, R.L. Higginson, E.J. Palmiere, C.M. Sellars, I. Prabst, P. Warbichler and F. Hofer *Precipitation of NbC in a model austenitic steel*, Acta Materialia, 2002, 50, pp. 735 – 747.

[19] A.M. Sage *An overview of the use of micro-alloys in HSLA steels with particular reference to vanadium and titanium*, HSLA steels, Metallurgy and Applications. Proceedings of an International Conference on HSLA Steels, 1985, pp.51 – 60.

[20] R.O. Rocha, T.M.F. Melo, E.V. Pereloma and D.B. Santos *Microstructural evolution at the initial stages of continuous annealing of cold rolled Dual Phases steel*, Materials Science and Engineering, 2004, 391,296 – 304.

[21] G. Thomas, *New cold formable Fe/Al/C Dual phase steels*, HSLA steels, Metallurgy and Applications. Proceedings of an International Conference on HSLA Steels, 1985, pp. 801 – 808.

[22] M. Erdogan, *Effect of Austenite dispersion on phase transformation in Dual Phase steel*, Scripta Materialia, 2003, 48, pp. 501 – 506.

[23] S. Sun and M. Pugh *Properties of thermomechanically processed Dual-Phase steels containing fibrous martensite*, Materials Science and Engineering, 2002, 335 pp. 298–308.

[24] A. Bayram, A. Uguz, and M. Ula *Effects of microstructure and notches on the mechanical properties of Dual-Phase steels*, Materials Characterization, 1999, 43, pp. 259–269.

[25] Y. L. Su and J. Gurland *Strain partition, uniform elongation and fracture strain in Dual-phase Steels*, Materials Science and Engineering, 1987, 95, pp. 151 – 165.

[26] A. K. Jena and M. C. Chaturvedi *On the effect of the volume fraction of martensite on the tensile strength of Dual-phase steel*, Materials Science and Engineering, 1988, 100, pp. 1 – 6.

[27] P. Deb and M. C. Chaturvedi, *Influence of thermomechanical treatment on the structure-property relationship of a microalloyed Dual-Phase high strength, low alloy steel*, Materials Science and Engineering, 1986, 78, pp. 7 – 13.

[28] S. S. Hansen and R.R. Pradhan *Structure – properties relationships and continuous yielding behaviour in Dual Phase steels*, Conference and Proceedings of the Fundamentals of Dual – Phase Steels, 1981, pp. 113 – 114.

[29] S. S. Hansen and R.R. Pradhan *Structure – properties relationships and continuous yielding behaviour in Dual Phase steels*, Conference and Proceedings of the Fundamentals of Dual – Phase Steels, 1981, pp. 113 – 114.

[30] A.A. Fallahi 1990. *Processing of Dual Phase steels by controlled rolling.* Thesis (PhD). University of Sheffield.

[31] B.S. Seong, E.J. Shin, Y.S. Han, C.H. Lee, Y.J. Kim and S.J. Kim *Effect of retained austenite and solute carbon on the mechanical properties in TRIP steels*, Physical B, 2004, 350, pp. 467 - 469.

[32] T. De Cock, J.P. Ferrer, C. Capdevila, F.G. Caballero, V. Lopez and C. Garcia de Andres *Austenite retention in low Al/Si multiphase steels*, Scripta Materialia, 2006, 55, pp. 441 – 44.

[33] Key-to-steel (2007) *High strengths steels: TRIP Steels*, Key-to-steel.com http://www.key-to steel.com/default.aspx?ID=CheckArticle&LN=EN&NM=194 accessed on 20.06.2004.

[34] M. Takita and H. Ohashi *Application of high-strength steel sheets for automobiles in Japan*, La Revue de Métallurgie – CIT, 2001.

[35] VF. Zackay, ER. Parker, D. Fahr and R. Busch *The enhancement of ductility in high-strength steel*, Transactions of the ASM, 1967, 60, pp. 252 – 259.

[36] O. Matsumura, Y. Sakuma and H. Takechi *Enhancement of elongation by retained austenite in intercritical annealed O.4C-1.5Si-O.8Mn Steel*, Transactions ISIJ, 1987, 27, pp. 571 – 579.

[37] Ch. M. Parish 2000 *Fundamental study of phase transformations in Si-Al-TRIP steels*, Thesis (BS). University of Pittsburgh.

[38] B.C. De Cooman *Structure–properties relationship in TRIP steels containing carbide-free bainite*, Current Opinion in Solid State and Materials Science, 2004, 8, pp. 285 – 303.

[39] A. Wasilkowska, P. Tsipouridis, E.A. Werner, A. Pichler and S. Traint *Microstructure and tensile behaviour of cold rolled TRIP-aided steels*, Journal of Materials Processing Technology, 2004, 157-158,pp. 633 – 636.

[40] M.H. Saleh and R. Priestner *Retained austenite in dual – phase silicon steels and its effect on mechanical properties*, Journal of Materials Processing Technology, 2001, 113, pp. 587 – 593.

[41] W. C. Jeong and C. H. Kim *Formation of austenite from a ferrite-pearlite microstructure during intercritical annealing*, Journal of Materials Science, 1985, 20, p.p. 4392 – 4398.

[42] M. C. Chaturvedi and A. K. Jena *Effect of intercritical annealing temperature on equilibrium between ferrite and austenite*, Materials Science and Engineering, 1987, 94, pp.1 – 3.

[43] F. Silva, N.I.A. Lopes, D.B. Santos *Microstructural characterization of the C–Mn multiphase high strength cold rolled steel*, Materials Characterization, 2006, 56, pp. 3 – 9.

[44] E. Emadoddin, A. Akbarzadeh and Gh. Daneshi *Effect of intercritical annealing on retained austenite characterization in textured TRIP-assisted sheet steel*, Materials Characterization, 2006, 57, pp. 408 – 413.

[45] W. Shi, L. Li, C. Yang, R. Fu, L. Wang and P. Wollants *Strain-induced transformation of retained austenite in low-carbon low-silicon TRIP steel containing aluminium and vanadium*, Materials Science and Engineering A,2006, 429, pp. 247 – 251.

[46] A. K. Srivastava, G. Jha, N. Gope and S.B. Singh *Effect of heat treatment on microstructure and mechanical properties of cold rolled C–Mn–Si TRIP-aided steel*, Materials Characterization, 2006, 57, pp. 127 – 135.

[47] A. K. Srivastava, D. Bhattacharjee, G. Jhab, N. Gope and S.B. Singh *Microstructural and mechanical characterization of C–Mn–Al–Si cold-rolled TRIP-aided steel*, Materials Science and Engineering A, 2007, 445–446, pp. 549 – 557.

[48] K. Hulka (2004) *The role of niobium in multi-phase steel,* Niobium Products Company GmbH-Germany, http://www.us.cbmm.com.br/english/sources/techlib/report/novos/pdfs/the_role2.pd accessed on 15.05.2004.

[49] D.A. Porter and K.E. Easterling 1992, *Phase transformations in metals and alloys*. Chapman and Hall, London, UK.

[50] S. Zaefferer, J. Ohlert and W. Bleck *A study of microstructure, transformation mechanisms and correlation between microstructure and mechanical properties of a alloyed TRIP steel*, Acta Materialia, 2004, 52,pp. 2765 – 2778.

[51] S.B. Singh and H.K.D.H. Bhadeshia *Quantitative evidence for mechanical stabilisation of bainite*, Materials Science and Technology, 1996, 12, pp. 610 – 612.

[52] P.H. Shipway and H.K.D.H. Bhadeshia *Mechanical stabilisation of bainite,* Materials Science and Technology, 1995, 11, pp. 1116 – 1128.

[53] A. Basuki and E. Aernoudt *Influence of rolling of TRIP steel in the intercritical region on the stability of retained austenite*, Materials Processing Technology, 1999, 89-90, pp. 37 – 43.

[54] P.J. Jacques *Transformation – induced plasticity for high strength formable steels*, Current Opinion in Solid State and Materials Science, 2004, 8, pp. 259 – 265.

[55] P. Jacques, E. Girault, T. Catlin, N. Geerlofs, T. Kop, S. Vander Zwaag and F. Delannay *Bainite transformation of low carbon Mn–Si TRIP-assisted multiphase steels: influence of silicon content on cementite precipitation and austenite retention*, Materials Science and Engineering A, 1999, 273 – 275, pp. 475 – 479.

[56] S.M.K. Hosseini, A. Zarei-hanzaki, M.J.Y Panah and S. Yue *ANN model for prediction of the effects of composition and process parameters on tensile strength and percent elongation of Si-Mn TRIP steels*, Materials Science and Engineering A, 2004, 374, pp. 122 – 128.

[57] Evans P. J, Crawford L. K and Jonesa A. *High strength C-Mn steels for automotive applications*, Iron making and steelmaking, 1997, 24, No.5, pp. 361 – 367.

[58] High strength structural and high strength low alloy steels. Metals Handbook - Properties and selection, Vol. 1, ed. ASME International, 1990, USA, pp. 389 – 423.

[59] J. Lis, J. Morgiel and A. Lis *The effect of Mn partitioning in Fe-Mn-Si alloy investigated with STEM-EDS techniques*, Materials Chemistry and Physics, 2003, 81, pp. 466 – 468.

[60] Q. Furnemont, M. Kempf, P.J. Jacques, M. Goken and F. Delannay *On the measurement of the nanohardness of the constitutive phases of TRIP-assisted multiphase steels*, Materials Science and Engineering A, 2002, 328, pp. 26 – 32.

[61] J. Maki, J. Mahieu, B.C. de Cooman and S. Claessens *Galvanisability of silicon free C-Mn-Al TRIP steels,* Materials Science & Technology, 2003, 19, pp. 125 – 131.

[62] T. Gladman 1997. *The physical metallurgy of microalloyed steels*. The University Press, Cambridge, UK. The Institute of Materials.

[63] K. Sugimoto, T. Muramatsu, S. Hashimoto and Y. Mukaid *Formability of Nb bearing ultra high-strength TRIP-aided sheet steels*, Journal of Materials Processing Technology, 2006, 177, pp. 390 – 395.

[64] E.J. Drewes and E.F. Walker *Niobium bearing steels in the automotive Industry*, Proceedings of the International Symposium Niobium 2001, TMS, Warrendale, PA, 2001, pp. 873 – 888.

[65] T. Heller and A. Nuss *Effect of alloying elements on microstructure and mechanical properties of hot rolled multiphase steels*, Iron-making and Steelmaking, 2005, ***32- No. 4***, pp. 303 – 308.

[66] S. Oliver, T.B. Jones and G. Fourlaris *Dual phase versus TRIP strip steels: comparison of dynamic properties for automotive crash performance*, Materials Science and Technology, 2007, 23 – 4, pp. 423 – 431.

[67] H.Y. Yu, Z.Q. Lin, G.L. Chen and S.H. Li *Overall stress–strain relationship of cold rolled transformation induced plasticity multiphase steels*, Materials Science and Technology, 2005, 21, No. 3, pp. 311 – 315.

[68] D.B. Williams and C. Barry Carter *Transmission electron microscopy*, 1996, 1 ed. Springer Science, New York pp. 168.

[69] B.D. Cullity *Elements of x-ray diffraction* – second edition, 1978, Addison – Wesley publishing, Reading Massachusetts pp. 355 – 357.

[70] N. Ridley, H. Stuart and L. Zwell *Lattice Parameter of Fe-C austenites at Room Temperature*, Transaction Metallurgical Society. AIME, 1969, 245, pp. 1834 – 1836.

[71] R. Ruhl and M. Cohen *Splat Quenching of Iron-Carbon Alloys*, Transaction Metallurgical Society. AIME, 1969, 245, pp. 241 – 251.

[72] F. Perrard and C. Scott *Vanadium precipitation during intercritical annealing in cold rolled TRIP steels*, ISIJ International, 2007, 47, No. 8, pp. 1168 – 1177.

[73] I.B. Timokhina, E.V. Pereloma and P.D. Hodgson *Microstructure and Mechanical properties of C – Si – Mn(-Nb) TRIP steels after simulated Thermomechanical processing*, Materials Science and Technology, 2001, 17, pp. 135 – 140.

[74] R.W.K. Honeycombe *Fundamentals Aspects of Precipitation in Microalloyed Steels*, HSLA steels, Metallurgy and Applications. Proceedings of an International Conference on HSLA Steels, 1985, pp. 243 -250.

[75] G. Fourlaris, A. J. Baker and G. D. Papadimitriou *A Microscopic investigation of the precipitation phenomena observed during the pearlite reaction in vanadium alloyed carbon steels*, Acta Metallurgica, 1995, 43, No. 10, pp. 3733 – 3742.

[76] S. Kim, C. G. Lee, I. Chol and S. Lee *Effects of heat treatment and alloying elements on the microstructures and mechanical properties of 0.15 Wt Pct C transformation-induced plasticity–aided cold-rolled steel sheets*, Metallurgical and Materials Transactions A, 2001, 32, pp. 505 – 514.

[77] J. Huang, W.J. Poole and M. Militzer *Austenite formation during intercritical annealing*, Metallurgical and Materials Transactions A, 2004, 35, pp. 3363 – 3375.

[78] D. H. Shin, Y. S. Kim and E. J. Lavernia *Formation of fine cementite precipitates by static annealing of equal - channel angular pressed low – carbon steels*, Acta Materiallia, 2001, 49, pp. 2387 – 2393.

[79] K. Han, T.D. Mottishaw, G.D.W. Smith, D.V. Edmonds and A.G. Stacey *Effects of vanadium additions on microstructure and hardness of hypereutectoid pearlitic steels*, Materials Science and Engineering A, 1995, 190, pp. 207 – 214.

[80] L. Samek, E. De Moor, J. Penning, and B.C. De Cooman *Influence of alloying elements on the kinetics of strain-induced martensitic nucleation in low-alloy, multiphase high-strength steels*, Metallurgical and Materials Transactions A, 2006, 37, pp. 109 – 124.

[81] S. Maropoulos, S. Karagiannis and N. Ridley *The effect of austenitizing temperature on prior austenite grain size in a low-alloy steel*, Materials Science and Engineering A, 2008, 483–484, pp. 735 – 739.

[82] S. Vander Zwaag and J. Wang *A discussion on the atomic mechanism of the bainitic reaction in TRIP steels*, Scripta Materialia, 2002, 47, pp.169 – 173.

[83] C. Scott, F. Perrard and P. Barges *Microalloying with Vanadium for Improved Cold Rolled TRIP Steels*, International Seminar on Application Technologies of Vanadium in Flat – Rolled Steels, 2005, pp.15 – 25.

[84] A.J. Lacey, M.S. Loveday, G.J. Mahon, B. Roebuck, C.M. Sellars and M.R. vander Winden, *Measuring good practice guide No. 27: Measuring Flow Stress in Hot Plane Strain Compression Tests*, 2002